Triggered Drug Release from Thermosensitive Liposomes

by

Ludger Markus Ickenstein

M.Sc. (Pharm. Sc.), University of British Columbia, Vancouver, Canada

Diplom Biologist, Friedrich-Alexander-Universität Erlangen-Nürnberg, Germany

A THESIS SUBMITTED IN PARTIAL FULFILLMENT OF
THE REQUIREMENT FOR THE DEGREE OF
DOCTOR OF PHILOSOPHY

in

THE FACULTY OF GRADUATE STUDIES

The Faculty of Pharmaceutical Sciences
Division of Pharmaceutics and Biopharmaceutics

We accept this thesis as conforming to the required standard

THE UNIVERSITY OF BRITISH COLUMBIA

December 2003

© Ludger Markus Ickenstein

ABSTRACT

Targeted delivery of anticancer drugs by delivery devices such as thermosensitive liposomes promises to increase the efficacy of drugs while decreasing their side effects. The objectives of the present thesis were to characterize a lysolipid-containing thermosensitive liposomal formulation (LTSL) of the antineoplastic agent doxorubicin (DOX) and to determine its drug release mechanisms and efficacy in mice bearing multidrug resistant (MDR) tumors. It was hypothesized that lysolipids accumulate at membrane grain boundaries leading to physical alterations of the membrane and rapid drug release at the liposome's phase transition temperature (T_C). This property was hypothesized to be beneficial in the use of LTSL encapsulated with DOX (LTSL-DOX) in combination with tumor hyperthermia against MDR tumors overexpressing P-glycoprotein (PGP) by overcoming PGP-mediated drug efflux from tumor cells.

At temperatures of 41 and 42 °C, drug release rates of LTSL were approximately 100-times faster than those of traditional thermosensitive liposomes. Membrane redistribution patterns of a fluorescent label resembling lysolipid and the membrane retention of radiolabeled lysolipids indicated that lysolipids accumulated in LTSL membrane regions over time and lysolipids did not dissociate from LTSL after phase transition *in vitro*. Cryogenic electron microscopy images revealed the formation of membrane discs in heated LTSL and this process was dependent on the degree of phospholipid hydrolysis. The mean plasma half-life of DOX in mice after LTSL-DOX administration was 0.67 h and lysolipids dissociated rapidly from LTSL after *in vivo* exposure. In mice bearing MDA435/LCC6^{MDR1} tumors, the efficacy of LTSL-DOX in combination with hyperthermia was similar to that of free DOX with or without tumor

hyperthermia treatment.

It was concluded that the velocity of drug release from LTSL at temperatures close to their T_C was unsurpassed by any other known triggered drug release mechanism. After intravenous administration however, DOX retention in LTSL was insufficient to allow for tumor drug accumulation and the rapid dissociation of lysolipids from LTSL compromized their superior drug release properties observed *in vitro*. These shortcomings of the LTSL-DOX formulation and the choice of the DOX-insensitive tumor model were considered responsible for the lack of improved efficacy of the LTSL-DOX treatment in mice bearing MDA435/LCC6^{MDR1} tumors as compared to free DOX administration.

TABLE OF CONTENTS

LIST OF TABLES

LIST OF FIGURES

Page

Background

Page

Experimental

Results

Page

Page

Page

LIST OF ABBREVIATIONS

α	Tilt angle
a	Monomer size
A	1) Frequency factor or 2) total liposome surface area
ANOVA	Analysis of variance
AUC	Area under the curve
Balb	Bragg albino
CF	Carboxyfluorescein
ΔC	Drug concentration gradient
CMC	Critical micelle concentration
cryo-TEM	Cryogenic transmission electron microscopy
[^{14}C]-MPPC	[^{14}C]-1-Palmitoyl-2-hydroxy-*sn*-glycero-3-phosphatidylcholine
D	1) Diffusion coefficient or 2) distance
DAPC	1,2-Darachidoyl-*sn*-glycero-phosphatidylcholine
DHPC	1,2-Dihexadecyl-*rac*-glycero-phosphatidylcholine
DHPE	1,2-Dihexadecyl-*rac*-glycero-phosphatidylethanolamine
DMEM	Dulbecco's modified eagle's medium
DMPC	1,2-Dimyristoyl-*sn*-glycero-phosphatidylcholine
DMPE	1,2-Dimyristoyl-*sn*-glycero-phosphatidylethanolamine
DMPS	1,2-Dimyristoyl-*sn*-glycero-phosphatidylserine
DOX	Doxorubicin
DPPC	1,2-Dipalmitoyl-*sn*-glycero-phosphatidylcholine
DPPE	1,2-Dipalmitoyl-*sn*-glycero-phosphatidylethanolamine
DPPG	1,2-Dipalmitoyl-*sn*-glycero-phosphatidylglycerol
DSC	Differential scanning calorimetry
DSPC	1,2-Distearoyl-*sn*-glycero-phosphatidylcholine
DSPE	1,2-Distearoyl-*sn*-glycero-phosphatidylethanolamine
DSPE-PEG$_{2000}$	1,2-Distearoyl-*sn*-glycero-3-phosphatidylethanol-amine-N-[methoxy (polyethylene glycol)-2000]
E_a	Activation energy
E_0	Incoming light electrical field amplitude

E_S	Scattered light electrical field amplitude
G	Gibbs free energy
η	Shear viscosity
h	Planck's constant
H	Enthalpy
HBS	HEPES buffered saline
HBSS	Hank's balanced salt solution
HDL	High-density lipoprotein
HEPES	N-[2-hydroxyethyl]piperazine-N'-[2-ethanesulfonic acid]
HPLC	High performance liquid chromatography
HSPC	Hydrogenated soy *sn*-glycero-3 phosphatidylcholine
[^{3}H]-CHE	[^{3}H]-Cholesterol hexadecyl ether
I_0	Incoming light intensity
I_S	Scattered light intensity
i.m.	Intramuscular
i.p.	Intraperitoneally
i.v.	Intravenous
IS	Internal standard
J	Drug flux
k	Rate constant
k_d	Dissociation rate constant
K	Boltzmann's constant
λ_{ex}	Excitation wavelength
λ_{em}	Emission wavelength
L	Polymer length extension
$L_{\beta'}$	Gel phase
L_α	Liquid-crystalline phase
LTSL	Lysolipid-containing thermosensitive liposomes
LUV	Large unilamellar vesicle
MLV	Multilamellar vesicle
m.p.	Melting point

MDR	Multidrug resistance
MPS	Mononuclear-phagocyte system
MPPC	1-(mono) Palmitoyl-2-hydroxy-*sn*-glycero-3-phosphatidylcholine
MSPC	1-(mono) Stearoyl-2-hydroxy-*sn*-glycero-3-phosphatidylcholine
MW	Molecular weight
ν	Frequency
n	Number of samples
n_p	Refraction index of particles
n_s	Refraction index of solvent
N	Degree of polymerization
N_A	Avogadro's number
NMR	Nuclear magnetic resonance
NTSL	Non-thermosensitive (cholesterol-containing) liposomes
OGP	n-Octyl β-D-gluco-pyranoside
p	Probability of a type I error
$P_{\beta'}$	Ripple phase
PEG	Polyethylene glycol
PGP	P-glycoprotein
PHDA	Pyrene hexadecanoic acid
POPS	1-Palmitoyl-2-oleoyl-*sn*-glycero-phosphatidylserine
QELS	Quasi-elastic light scattering
R	1) Radius or 2) universal gas constant for ideal gases
Rag2	Recombinase activating gene 2
RES	Reticulo-endothelial system
R_F	Flory dimension
RT	Room temperature
S_0	Ground state
S_1	Relaxed singlet excited state
S_1'	Singlet excited state
S	Entropy
SDS	Sodium dodecyl sulfate

s.c.	Subcutaneous
SEM	Standard error of the mean
SUV	Small unilamellar vesicle
T	Temperature
T_C	Main gel-to-liquid-crystalline phase transition temperature
T_C'	Pre-transition temperature
T_C^*	Gel phase-to-liquid micellar phase transition temperature
TSL	Thermosensitive liposomes
UV	Ultraviolet
V	Volume
V_g	Molar volume of the lipid in the gel phase
Vis	Visible
V_l	Molar volume of the lipid in the liquid-crystalline phase
W	Width

ACKNOWLEDGMENTS

I have received most valuable support, guidance, and an abundance of stimulating ideas from my supervisor, Dr. Lawrence D. Mayer, during my time in his laboratory, which I much enjoyed. I am very thankful to Dr. Helen M. Burt, my co-supervisor from the Faculty of Pharmaceutical Sciences at the University of British Columbia (UBC), for her critical supervision of my Ph.D. research project, which saved me from numerous pitfalls. I owe a large debt of gratitude to my committee members, Dr. Peggy Olive (BC Cancer Research Center, Department of Medical Biophysics), Dr. Mary Ensom (Faculty of Pharmaceutical Sciences at UBC/BC Women's Hospital), and Dr. John McNeill (Faculty of Pharmaceutical Sciences at UBC) for valuable discussions, helpful advice, and encouragement at different stages of my work. I thank Dr. Marcel Bally, head of the Department of Advanced Therapeutics at the BC Cancer Research Center, for his intellectual challenge and his many most valuable suggestions and ideas during the work on my Ph.D. thesis. I also appreciate the critical review of my thesis by Dr. Pieter Cullis (Faculty of Biochemistry and Molecular Biology at UBC), Dr. Don Brooks (Faculty of Pathology and Laboratory Medicine at UBC), and Dr. Mats Almgren (Department of Physical Chemistry at Uppsala University, Uppsala, Sweden), who served on my examining committee as the University Examiners and the External Examiner, respectively.

I am very grateful to my collaborator Dr. Katarina Edwards at the Department of Physical Chemistry, University of Uppsala, Uppsala, Sweden for the warm hospitality I received in her laboratory, her contribution to this thesis, many stimulating discussions, and for her encouragement when I needed it most. I am also thankful to Ms. Maria C.

Arfvidsson and Mr. Göran Karlsson (Department of Physical Chemistry, University of Uppsala, Uppsala, Sweden) for their valuable help and great expertise with generating cryo-TEM images. I thank my collaborators Dr. David Needham, and Dr. Gopal Anyarambhatla, both from the Department of Mechanical Engineering and Material Sciences, Duke University Durham, NC, for many stimulating discussions.

I gratefully acknowledge my debt to my excellent summer students Ms. Amanda Wolfe (University of British Columbia) and Mr. Niels Hagenaars (University of Utrecht, Utrecht, The Netherlands) for their help with *in vitro* and *in vivo* assays, to Ms. Rebecca Ng and Ms. Dana Masin (BC Cancer Research Center, Department of Advanced Therapeutics) for their help with animal experiments, to Ms. Norma Hudon and Ms. Linda Zhang (BC Cancer Research Center, Department of Advanced Therapeutics) for their aid with HPLC analyses, and to Dr. Christine Allen (Celator Technologies Inc.) for her help with DSC analyses. Thanks to all my colleges and dear friends in the Department of Advanced Therapeutics and everyone at Celator Technologies for their great support and friendship. I am only too aware of the many imperfections, which remain in this thesis, but without all the help, which has been given me so generously, there would be many more and entire sections of this thesis could not have been completed.

Funding for this project has been provided by an industry-sponsored studentship from the Canadian Institutes of Health Research (CIHR) and Celator Technologies Inc. (200-604 West-Broadway, Vancouver, BC, Canada, V5Z 1G1), Grant #: ZU9-44169, and a research grant from the Lotte & John Hecht Memorial Foundation.

DEDICATION

I dedicate this thesis to my wife Susanne for her immense support and to my daughters Tessa and Mara for their great cooperation during the time of writing this thesis. Thanks to all of you girls.

INTRODUCTION

Solid tumors occur in approximately 85% of all cancer patients and half of these patients die because of their disease [3]. The main treatments for cancer are surgery, radiation, and chemotherapy, which are often combined in treatment strategies [4]. The paradox of treating tumors with chemotherapeutic agents is that many anticancer drugs are cytotoxic and carcinogenic themselves. Therefore, physicians treating patients with chemotherapeutic agents with narrow therapeutic indices are challenged to choose the right therapeutic dose of a drug or several drugs that can also induce severe side effects to their patients. Dose-limiting acute toxicities of many anticancer drugs are primarily bone marrow suppression and mucositis (inflammation of the gastrointestinal mucosa) producing severe immune suppression and pain, respectively. Other serious drug-specific side effects include cardiac-, neuro-, and nephro-toxicity as well as secondary malignancies, mainly leukemias, particularly with topoisomerase inhibitors or alkylating agents [5, 6]. In an escalating dosing regime, these side effects often prevent therapeutic drug levels being reached at the tumor site.

In view of these challenges, much effort has been spent on pharmaceutical research and development of drug delivery systems that can change the pharmacokinetics and biodistribution of anticancer drugs. These drug delivery systems are designed to increase drug concentrations locally at the disease site, thus enhancing their efficacy, while decreasing drug exposure of non-target tissue, thus minimizing dose-limiting side effects. The goal of targeted drug delivery is to decrease side effects of chemotherapy drugs, as well as to increase the patient's tolerance and compliance with the dosing regime [7].

One approach for site-specific drug delivery is to encapsulate drugs within small (100 nm) biocompatible, membrane-bound vesicles, named liposomes, designed to circulate in the blood stream without interacting with non-target tissues and subsequently accumulate at tumor sites where they release their contents in the tumor interstitium. Liposomal anticancer drug formulations have been investigated in clinical trials for over two decades [8] but to date, only three liposomal anticancer drug formulations and two liposomal antifungal formulations are used clinically [9]. These liposomal anticancer drug formulations are the two liposomal formulation of doxorubicin Caelyx® (= Doxil® in the USA) (Sequus/Alza) and Myocet® (The Liposome Company/Elan), and DaunoXome® (Nexstar/Gilead), a liposomal daunorubicin formulation. The main advantage of using liposomal anticancer drug formulations is the reduction in dose-limiting side effects but skin toxicities (mucositis and palmar-plantar erythema) are associated particularly with administration of Doxil®. In many instances, liposomal formulations of anticancer drugs have failed to increase the drug's efficacy in solid tumors as compared to free drug administration [10]. In some cases, the lack of increased efficacy was evident despite the fact that tumor drug concentrations were theoretically sufficiently high to eradicate all tumor cells. For example, in a variety of tumor models, administration of liposomal cisplatin enhanced tumor drug delivery compared to free cisplatin without increasing its efficacy [2]. This incongruity may be explained by the fact that the drug is not available to tumor cells because it is not released from its carrier. Thus, the ability to trigger drug release from liposomes in a controlled manner would be expected to significantly enhance the therapeutic benefits of liposomal anticancer drug formulations, over those achieved within current liposomal drug formulations.

Several triggered release mechanisms have been proposed and investigated for liposomal delivery of anticancer drugs [11]. One of those mechanisms is the use of thermosensitive liposomes, which release of their contents at temperatures above the T_C of the membrane. When used in combination with local hyperthermia, administration of most thermosensitive liposomal drug formulations to mice improve tumor drug uptake and result in an approximately 2 to 9-fold increase in tumor growth delay as compared to controls (no hyperthermia or administration of free drug) [12]. However, tumor drug uptake and tumor growth delay often do not correlate, which may be explained by the fact that drug release from traditional thermosensitive liposomes is slow and often incomplete.

A novel approach for temperature triggered drug release from liposomes was achieved by incorporation of small amounts of lysolipid in the liposome membrane, which enhanced both the release rate of encapsulated drug [13] and efficacy in a mouse tumor model [1]. Increasing the release rate of encapsulated drug was thought to be the reason for the increased efficacy, which appeared to destroy the tumor vasculature as well as to increase the intracellular drug concentration in tumor cells [14]. This new liposomal doxorubicin formulation is currently being tested in a Phase I clinical trial but to date, the mechanism by which these liposomes release their contents so rapidly upon heating is not fully understood.

Goals of the present thesis were to elucidate the drug release mechanism of lysolipid-containing thermosensitive liposomes (LTSL), to characterize a LTSL formulation of DOX *in vitro* and *in vivo* and to test the efficacy of this formulation in a multidrug resistant (MDR) tumor model. It was hypothesized that the drug release

mechanism was based on structural changes in the cholesterol-free liposome membrane and these changes were regarded as a feature that can be exploited as a tool to control triggered drug release more effectively.

1. BACKGROUND

1.1. Liposomes as drug delivery systems

Liposomes are small membrane bound vesicles ranging in size from approximately 50 nm to several micrometers, encapsulating an aqueous volume. Liposomes consist of a phospholipid double layer composed of a single or a few phospholipid species and may contain cholesterol up to 50 mol%. Phospholipid double layers are a major structural component of procaryotic and eucaryotic cells and can therefore be regarded as one of the basic building blocks of life. The lipid membrane of eucaryotes consists of 150-200 different lipid molecules and at least twenty different species of phosphatidylcholine [15]. This complexity of the membrane's composition may be necessary to provide the correct physical structure and microenvironment for the proper function of membrane-bound proteins and other complex membrane functions such as mitosis.

Liposome research evolved out of many disciplines. One of the first mentions of the liposome concept can be traced back to the late nineteenth century when the German chemist F. Krafft speculated on the idea of creating artificial "protocellular vesicles" from amphiphilic molecules [16]. Thirty years later in 1924, red blood cells (chromocytes) were proposed to consist of a double layer of "lipoid molecules" [17]. It took another forty to forty-five years, however, until the existence of the first artificial "phosphatidylcholine vesicle" was convincingly demonstrated [18] and suggested that phosphatidylcholine vesicles could serve as a model for biological membranes [19-21]. Later, the term "liposome" was established for these vesicles, which stems from the Greek words λίπος (lipos) for fat and σώμα (soma) for body. In the late 1970s the

potential of liposomes as drug carriers was realized and liposomal drug formulations were investigated with the aim to alter the pharmacokinetic behavior and biodistribution of drugs. Liposomes were found particularly useful for delivering anticancer drugs with narrow therapeutic indices, because by encapsulating drugs into liposomes, drug concentrations could be increased at tumor sites and decreased at sites where they could cause serious side effects. Therefore, the drug's potency can be increased. In fact, drug concentrations at tumor sites can be increased up to 100-fold over free drug [22] after *i.v.* injection of liposomal drug formulations and the exposure time of tumor cells to drug can be extended [23].

The major limitation of early phospholipid/cholesterol liposomes was their tendency to aggregate and their relatively short blood circulation half-life [24]. A major improvement in prolonging the blood circulation time of liposomes was achieved in the mid 1980s by covalently attaching the hydrophilic polymer polyethylene glycol (PEG) to a portion of the phospholipids (see section 1.5.2.2.). These so-called sterically stabilized phospholipid/cholesterol/PEG-lipid liposomes display prolonged blood circulation lifetimes, which allows for accumulation at extravascular sites such as solid tumors due to increased vascular permeability through discontinuous endothelia [25]. Discontinuous or sinusoidal endothelia possessing interendothelial cell junctions of up to 300 nm and a discontinuous basal membrane are found in the liver, spleen, and bone marrow. The vasculature in solid tumor is generally considered discontinuous [26, 27] and often chaotic in its organization with numerous venal-arterial shunts [28, 29]. Thus solid tumors have become the primary target of liposomal drug formulations (Figure 1).

Liposomal drug formulations possess limitless compositional flexibility that can

be adjusted to the drug, the target tissue, and the targeted disease. Currently, numerous liposomal drug formulations varying greatly in their phospholipid composition, physical structure, drug content, and their target tissue are investigated for their use in cancer chemotherapy.

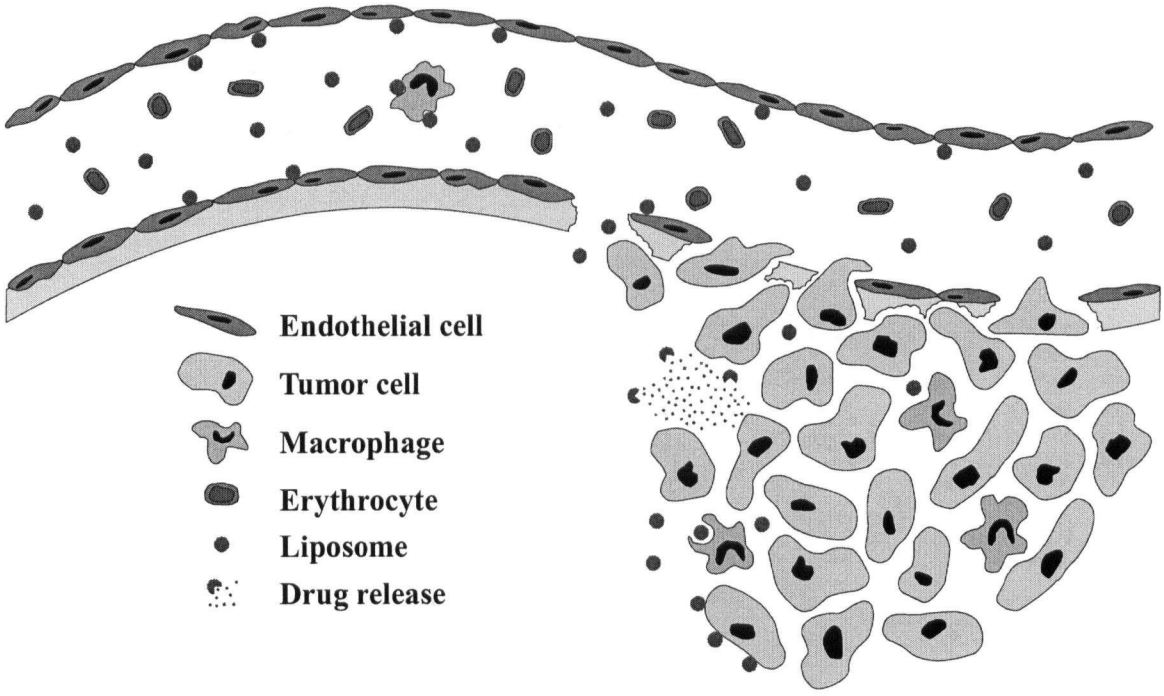

Figure 1: Schematic diagram of liposomes leaving a discontinuous vasculature through endothelial junctions at a tumor site.

1.2. Chemical and physical properties of liposome components

Most biological and liposomal membranes consist of three components, phospholipids, sphingolipids, and cholesterol. Phospholipid and sphingolipid molecules can be divided into four moieties: the tail region consisting of two hydrophobic hydrocarbon acyl chains of variable length, a glycerol backbone, a phosphate group, and a variable head group. Two carbon atoms of the glycerol backbone are bound to two fatty acid molecules by ester bonds (one amide bond for sphingolipids), the third carbon atom of the glycerol backbone is bound to the phosphate group, which in turn is bound to a hydrophilic head group, often choline or ethanolamine (Figure 2). The chain length of commonly used phospholipids ranges usually from 10-22 carbon atoms and acyl chains may contain up to three double bonds (Table 1) [8, 30]. At physiological pH, the phosphate group of the phospholipid molecule is negatively charged. This negative charge is neutralized in phospholipids possessing a positively charged headgroup, e.g. phosphatidylcholine and phosphatidylethanolamine. In phospholipids possessing a neutral headgroup, e.g. phosphatidylserine, phosphatidylglycerol, or phosphatidylinositol, the phospholipid molecule bears an overall negative charge [30].

Table 1: Phospholipid acyl chain moieties. Notation = number of carbon atoms and double bonds in both acyl chains.

Prefix	*Notation*	*Molecular formula*
Laureoyl-	12:0	$CH_3(CH_2)_{10}COOH$
Myristoyl-	14:0	$CH_3(CH_2)_{12}COOH$
Palmitoyl-	16:0	$CH_3(CH_2)_{14}COOH$
Stearoyl-	18:0	$CH_3(CH_2)_{16}COOH$
Arachidoyl-	20:0	$CH_3(CH_2)_{18}COOH$
Behenoyl-	22:0	$CH_3(CH_2)_{20}COOH$
Palmitoleoyl-	16:1	$CH_3(CH_2)_5CH=CH(CH_2)_7COOH$
Oleoyl-	18:1	$CH_3(CH_2)_7CH=CH(CH_2)_7COOH$
Linolenoleoyl-	18:2	$CH_3(CH_2)_4CH=CHCH_2CH=CHCH_2(CH_2)_6COOH$
Arachidonoleoyl-	20:4	$CH_3(CH_2)_4(CH=CHCH_2)_4(CH_2)_2COOH$

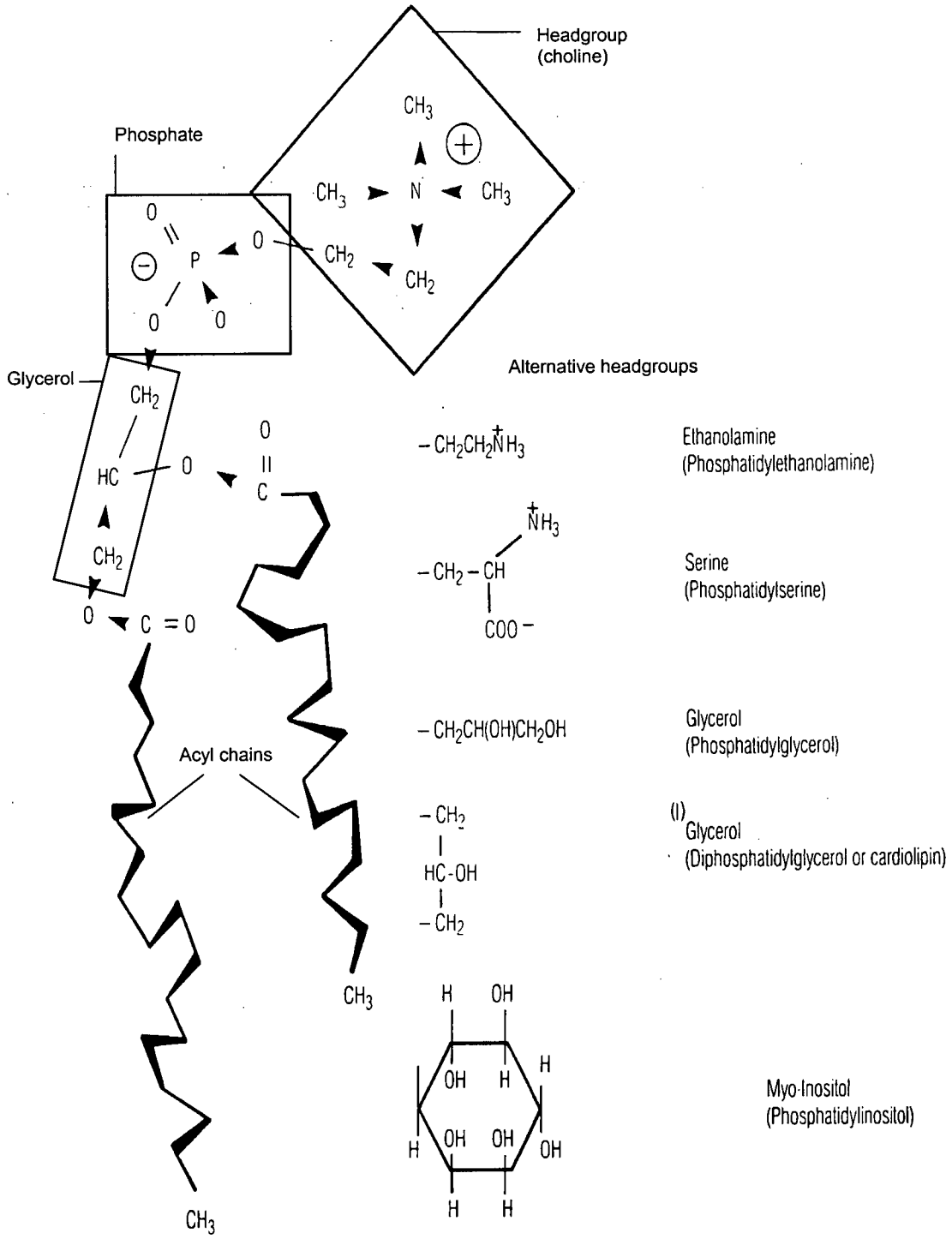

Figure 2: Molecular structure of a phosphatidylcholine molecule and different phospholipid headgroups (modified from [30]).

Sphingolipids represent a separate class of lipids. The central unit of the sphingolipid molecule is the sphingosine molecule, a long-chain amino alcohol. Addition of a fatty acid by an amide-link gives rise to a ceramide. Addition of phosphatidylcholine to ceramide yields sphingomyelin, and the addition of one or more sugar moieties yields cerebrosides and gangliosides [31] (Figure 3). Sphingolipids are very similar in structure to phospholipids but are synthesized biochemically from different precursors. Sphingomyelin is an ubiquitous component of animal cell membranes and can comprise as much as 50% of the lipids in certain tissues in particular nervous tissue. It is the single most abundant lipid in erythrocytes of most ruminant animals, where it replaces phosphatidylcholine entirely [8]. Sphingolipids are involved in signal transduction pathways mediating cell growth, differentiation, and cell death [32, 33]. Ceramides have been found to be intracellular second messengers for tumor necrosis factor α, IL1-β, and other cytokines [34-36].

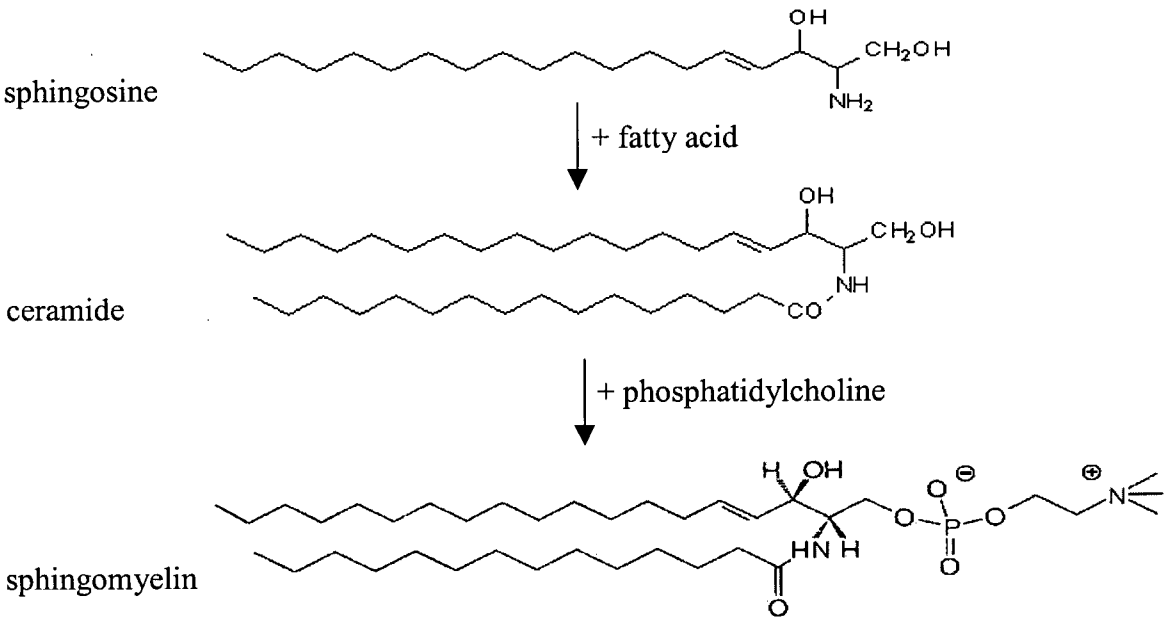

Figure 3: Chemical structures of sphingosine, ceramide, and sphingomyelin.

One synthetic phospholipid present in all liposome formulations used in experiments of the present thesis but not in biological membranes is a phospholipid onto which a PEG molecule is grafted at the headgroup (PEG-lipid). PEG is a $[CH_2CH_2O]_n$-polymer with n = 45 for a molecular weight (MW) of 2000 (PEG_{2000}). PEG-lipids are used to modulate a variety of liposome characteristics and PEG-lipid was found to play a major role in the drug release mechanism in liposome formulations described in the present thesis (see section 1.5.2.2.).

Lastly, steroid molecules are common components of biological membranes, which can make up to 45% of the total membrane content. In membranes of mammals, plants, bacteria, and fungi, the steroid molecules are cholesterol, stigmasterol, ergosterol, and lanosterol, respectively [8]. The molecular structure of these membrane components is different from phospholipids and sphingolipids and consists of apolar planar heterocycles with a hydroxyl group at the third carbon of ring A. Cholesterol and related molecules integrate into phospholipid membranes with the 3-β-hydroxyl group facing the polar headgroup moiety of phospholipid molecules and the rigid steroid ring system facing the acyl chains [37] (Figure 4).

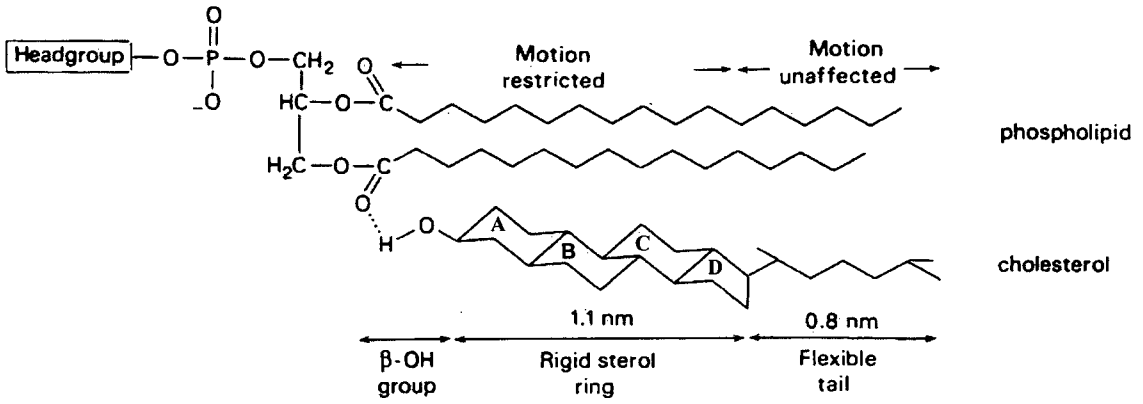

Figure 4: Schematic representation of the interaction between cholesterol and phospholipid molecules (adapted from [37]).

1.2.1. Phospholipid aggregate structures

In aqueous solution, phospholipid molecules are surrounded by approximately 20 water molecules per molecule to shield hydrophobic interactions between phospholipids and thereby reducing the mobility of the hydrocarbon chains [37]. This ordering gives rise to a large overall decrease in entropy (ΔS). When small hydrophobic molecules are dissolved in water at a temperature (T) of 25°C, the enthalpy (ΔH) of the system increases by approximately 2-6 kcal/mol but the entropy decreases by 10-20 cal/(gram °C). Since the free energy of the system (ΔG) is given by

$$\Delta G = \Delta H - T\ \Delta S \qquad \textit{(Equation 1)}$$

the free energy of the system remains positive and the process is thermodynamically not favored [37]. In aggregates, water molecules are excluded from the bulk phospholipids and their rise in motional freedom increases the entropy of the system to such an extent that the free energy of the system becomes negative and the process proceeds spontaneously [37].

Liposomes form spontaneously when a dried phospholipid film is hydrated in an aqueous solution. However, liposomes are not the only aggregate structure of phospholipids. The most commonly adopted phospholipid aggregates are the spherical micelle, the bilayer, and the hexagonal phase (Figure 5). According to the shape concept [38, 39] the thermodynamically favoured aggregate of phospholipid molecules depends on the ratio between their molecular volume (v) and the product of the optimal molecular surface area (a_0) and tail length (l_c), which calculates a shape factor (N_s):

$$N_s = v / a_0\ l_c \qquad \textit{(Equation 2)}$$

For lipids such as PEG-lipids and lysolipids, which possess a small headgroup relative to the tail length, the shape factor value is less than $^1/_3$. The thermodynamically favoured aggregate in aqueous solution for those phospholipid molecules is the spherical micelle. For the lysolipid MPPC, the critical micelle concentration (CMC) in water is 0.02 mM [8].

Phospholipids with intermediately sized head groups and a N_s value between ½ and 1, such as dipalmitoylphosphatidylcholine (DPPC) aggregate into two-dimensional bilayers. In bilayers, the hydrophobic acyl chains of the molecules are unfavourably exposed to water at the rim of the bilayer. Thus, phospholipid bilayers tend to expand or to close themselves into vesicles (liposomes), which are kinetically stable, but thermodynamically metastable aggregates.

Phospholipids such as phosphatidylethanolamines possess relatively large head groups relative to the tail length. Molecules with a shape factor greater than 1 aggregate into a so-called hexagonal HII phase, which can form tubular structures and expand into complex three-dimensional networks. The value of N_s and thus the aggregate structure of phospholipid molecules further depends on environmental factors such as solvent, salt concentration, pH, hydration state, temperature, and interactions with other molecules [30].

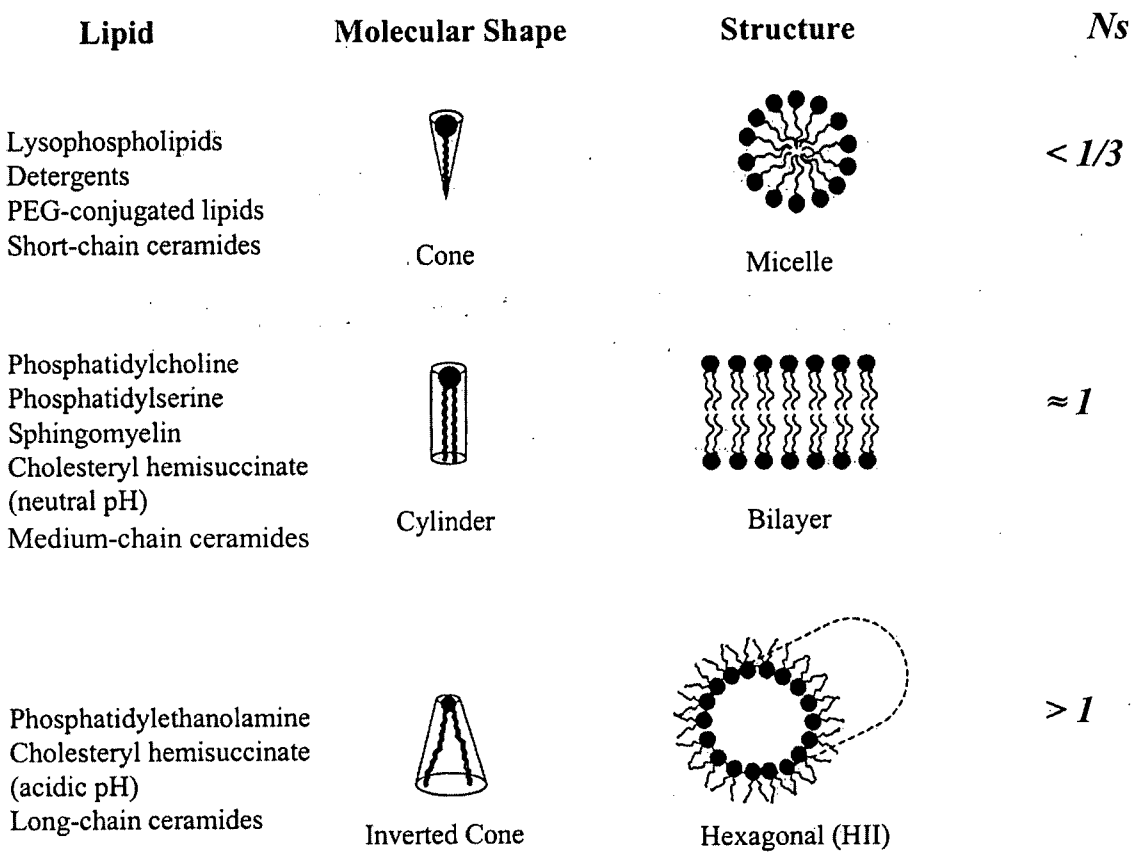

Figure 5: Molecular shape of phospholipid molecules and their aggregate structures (modified from [40]).

1.2.2. Liposome species (MLVs, SUVs, and LUVs)

All liposomes used in the present thesis were large unilamellar vesicles (LUVs). Besides LUVs, two other liposome species exist, small unilamellar vesicles (SUVs) and multilamellar vesicles (MLVs) [41].

Upon hydration, phospholipid bilayers tend to stack on top of each other and form MLVs [42]. MLVs are heterogenous in size with diameters between 0.5 μm and 10 μm [43, 44]. The trapped volume is typically low at approximately 0.5 μl/μmol lipid but

can be increased to as high as 10 μl/μmol lipid by increasing the interlamellar spacing by repetitively freezing and thawing the sample above its T_C [44].

When MLVs are extruded through filters with a pore size between 30 nm and 200 nm, the MLV membrane layers can be shed presumably by budding or blebbing as they are forced through the narrow filter pores. This process gives rise to either large unilamellar vesicles (LUVs) with a diameter greater or equal than 100 nm or small unilamellar vesicles (SUVs) with a diameter smaller than 100 nm (Figures 6 and 7). Other methods of generating SUVs include sonication [20], French press extrusion [45], and ethanol injection [46]. SUVs are of lesser importance as a drug delivery device since the encapsulation volume is small and the membrane stress is high, which can lead to an asymmetric distribution of membrane components [20, 45] and liposomes tend to fuse to release their bending pressure [47].

Generally, LUVs are the liposomes of choice for therapeutic drug delivery purposes because of their relative physical stability, their relative high encapsulation volume, and favorable tumor accumulation properties [44]. LUVs can be prepared by several methods including detergent dialysis [48] and reverse phase evaporation [49]. However, the most widely employed and most versatile method is the extrusion method [50-52]. In this method, MLVs are forced usually by nitrogen gas pressure of 200-800 psi repetitively at temperatures above their phase transition temperature (T_C) through polycarbonate filters with variable pore sizes, depending on the desired liposome diameter. The advantage of this method is that it is reliable, reproducible, can be scaled-up, the size distribution of liposomes is narrow, and liposomes do not come in contact with detergents, solvents, or other potential impurities.

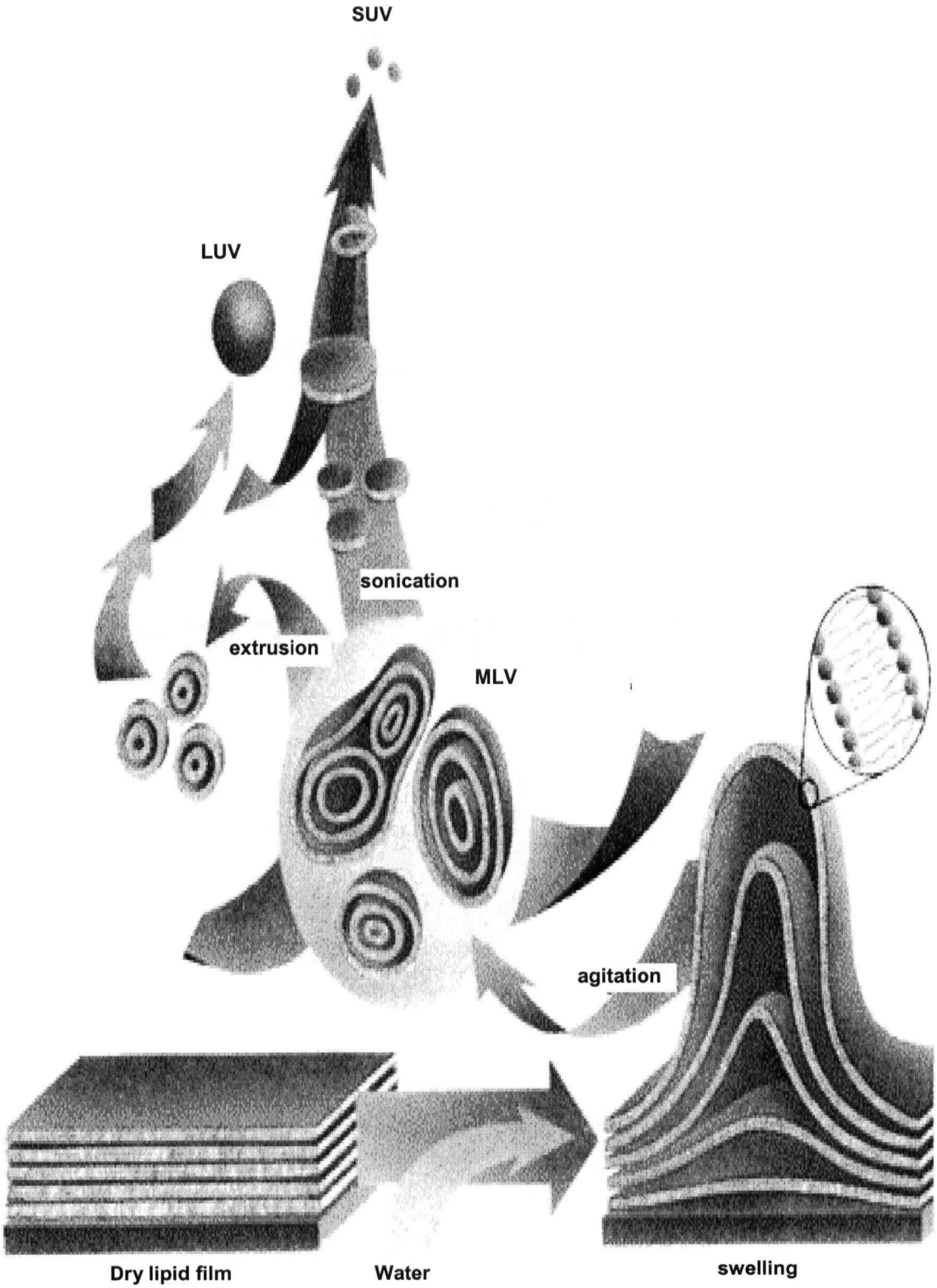

Figure 6: Schematic representation of liposome preparation (modified from http://www.avantilipids. com/PreparationOfLiposomes.html).

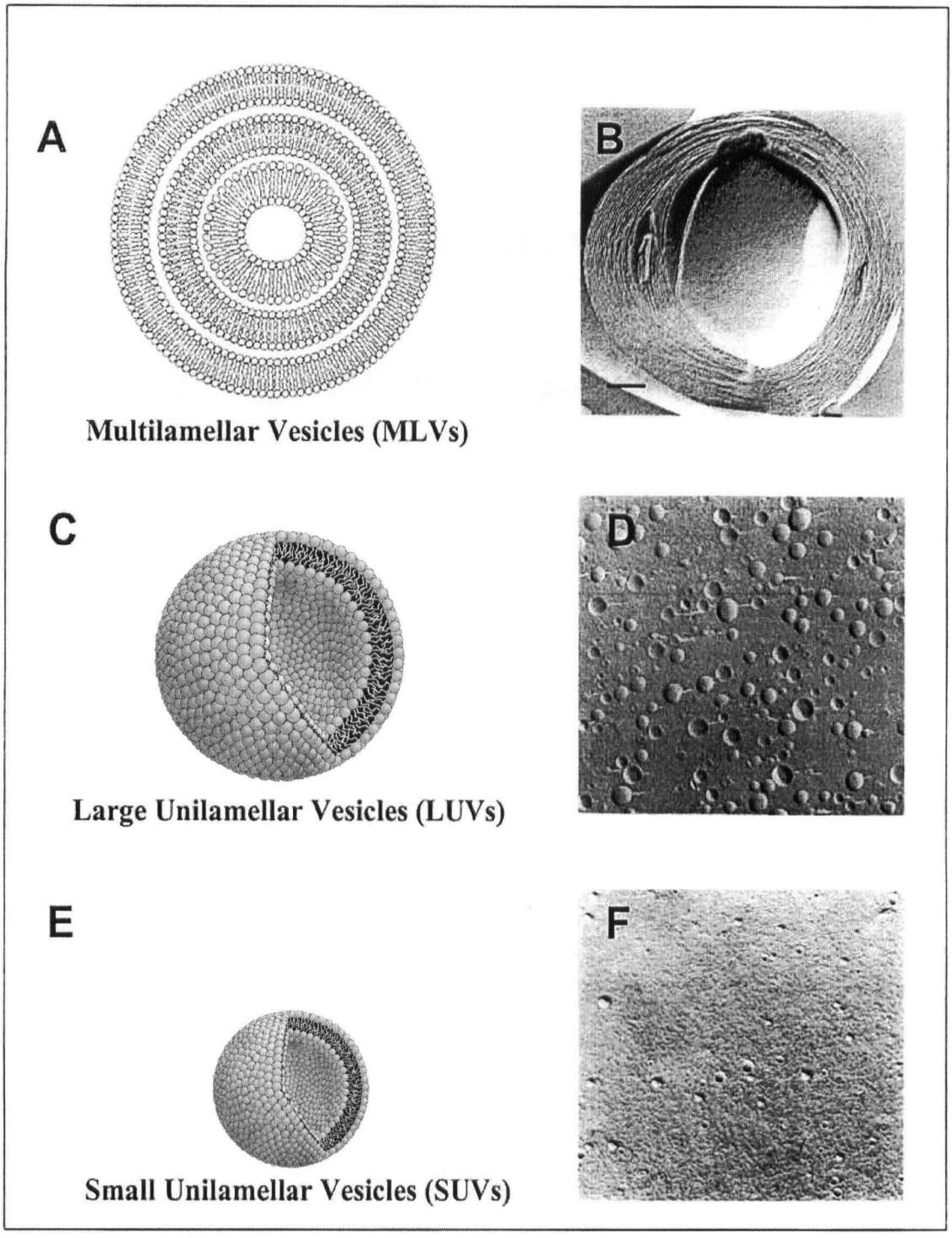

Figure 7: (A, C, E) Schematic representation and (B, D, F) freeze-fracture images of multilamellar vesicles (MLVs), large unilamellar vesicles (LUVs), and small unilamellar vesicles (SUVs) (modified from [21]).

1.3. Phase behavior of phospholipid membranes

The primary principle underlying drug release from thermosensitive liposomes is the transition from one phase to another at a phospholipid-specific temperature.

Lipid bilayers can exist in two different phases, in a gel ($L_{\beta'}$) phase or in a liquid-crystalline (L_{α}) phase. The transition between these two phases is driven by the gain in configurational entropy of the acyl chains and can be monitored by various techniques such as fluorescence spectroscopy [53], fluorescence microscopy [54], infrared spectroscopy [55], nuclear magnetic resonance (NMR) [56], or differential scanning calorimetry (DSC) [57]. DSC is commonly used to measure endothermic and exothermic events within a material that undergoes structural changes in response to changes in temperature and perhaps the most direct technique to study phase transitions and is used. Using DSC, four characteristic parameters of the phase transition can be obtained (Figure 8): first, the onset and maximum of the pre-transition; second, the onset and maximum of the main transition, which is usually referred to as the phase transition temperature abbreviated T_C (also T_M); third, the area under the curve (AUC) of the main transition, which is proportional to the transition enthalpy (ΔH) and reflects the energy required to melt the acyl chains; and fourth, the peak width (W), which corresponds to the "cooperativity" of the transition and describes the number of molecules that undergo a transition simultaneously [58].

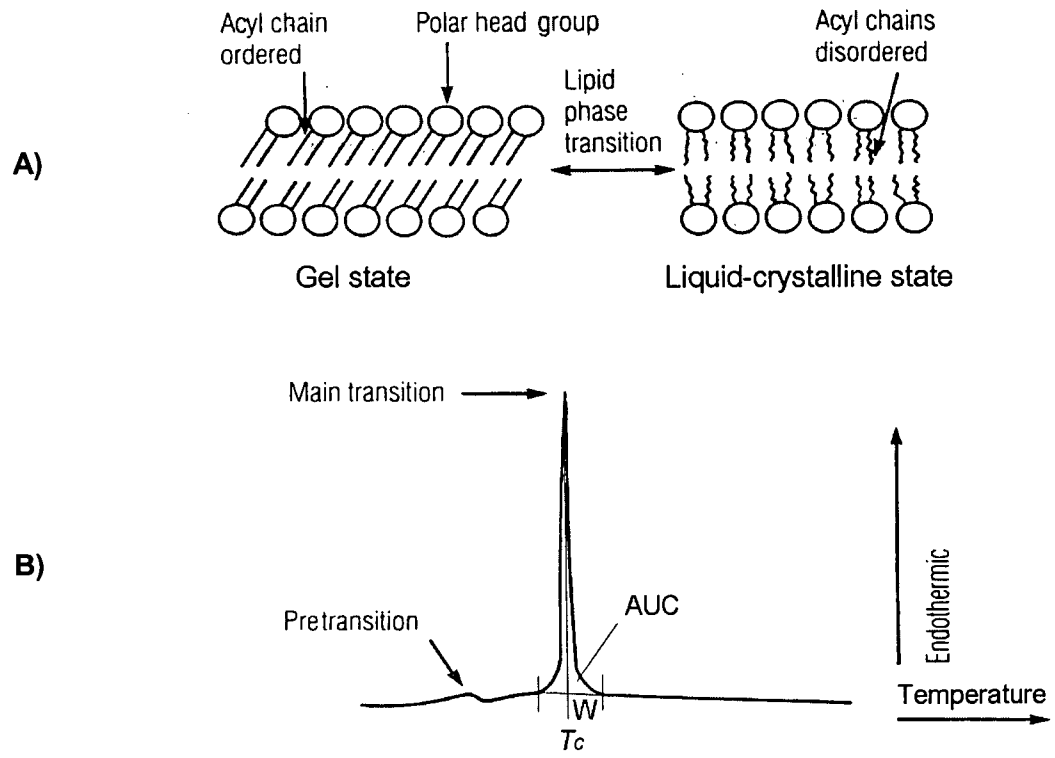

Figure 8: (A) Schematic representation of the gel to liquid-crystalline phase transition of phospholipid bilayers and (B) a corresponding DSC diagram. AUC = area under the curve; T_C = phase transition temperature; W = width (modified from [30]).

1.3.1. Pre-transition

The transition between the gel and the liquid-crystalline phase consists of two separate events, the pre-transition and the main transition. The endotherm of the pre-transition as measured by DSC is small and often undetected in contrast to the main transition. At temperatures below the pre-transition temperature (T_C'), the phospholipid membrane is in the L_{β}' phase, at which the electrostatic interactions between the head groups are maximized. At this temperature, the acyl chains are maximally packed but

exhibit a lower degree of order in comparison to the head group organization. The greater disorder and therefore increased volume in the centre of the lipid bilayer can be accommodated by a bend of the acyl chains with the upper part of the chain tilted by approximately 30° with respect to the bilayer plane [59, 60]. X-ray diffraction data have confirmed the existence of this tilt in dipalmitoyl phosphatidylcholine (DPPC) membranes [61].

As the temperature increases towards T_C', some intermolecular hydrophobic interactions and van-der-Waals bonds between acyl chains are overcome by their gain in kinetic energy and the phospholipids straighten into a perpendicular orientation and form the P_{β}' phase. In addition, conformational changes of the head groups contribute to the pretransition enthalpy [62]. In the P_{β}' phase, the phospholipid membrane exhibits periodic ripples to accommodate the increased molecular volume of phospholipids. Therefore, the P_{β}' phase is often referred to as the ripple phase (Figure 9). However, the illustration of phospholipid membrane phases depicted in Figure 9 is clearly an oversimplification and other models exist predicting tilt angles in some but not all phospholipid species, such as phosphatidyl ethanolamine [37, 63]. Furthermore, this classical view of the pre-transition event has been challenged and a new model has been developed explaining pre-transition by acyl chain melting processes only without the need for the presence of a phospholipid tilt below the pre-transition temperature [64].

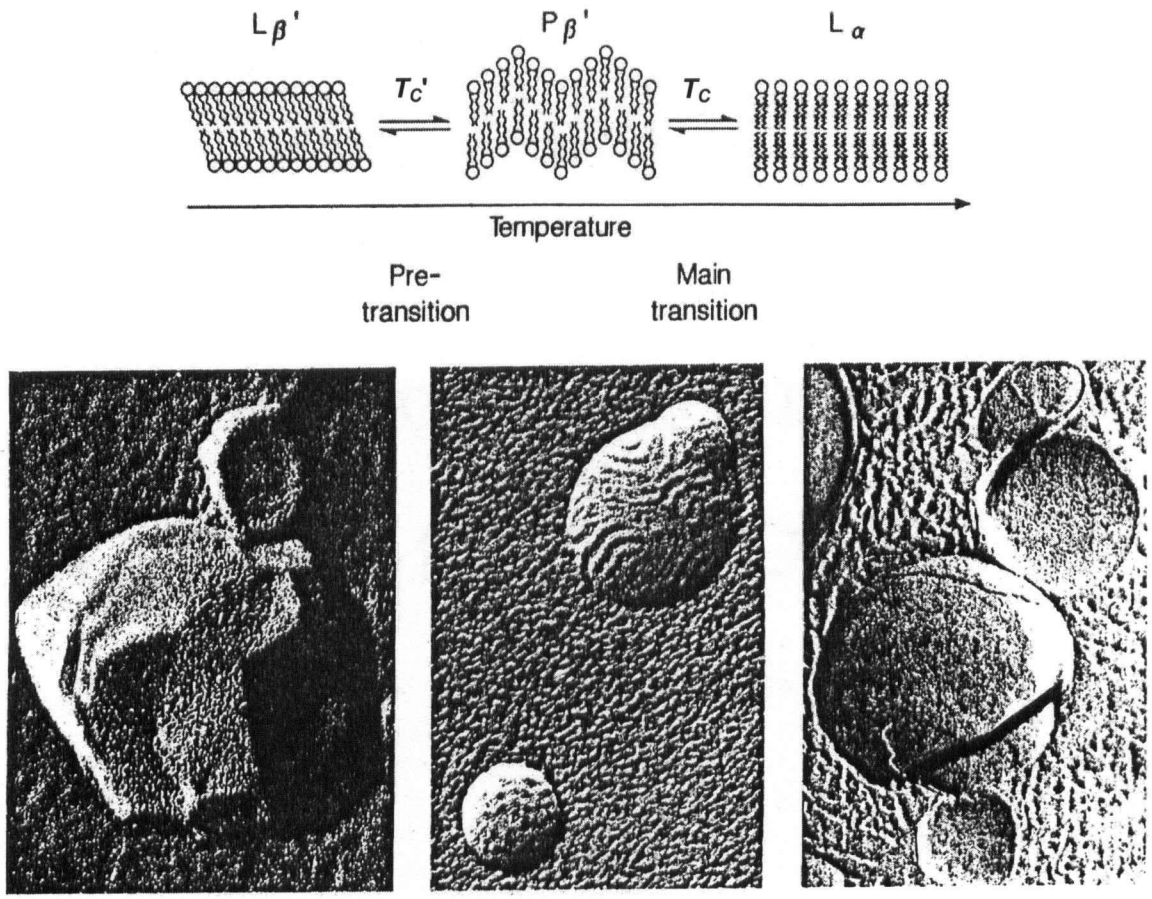

Figure 9: Schematic diagram of the L_{β}' to P_{β}' to L_{α} phase transition of phospholipid bilayers and corresponding freeze fracture electron microscopy images (modified from [8]).

1.3.2. Main transition

The major event of the phase transition process is the main transition. In contrast to the pre-transition, which is thought to be predominantly based on conformational changes of the head group or their connection to the tail group, the main transition is based on conformational changes of the acyl chains in the tail group of phospholipid molecules. In the gel phase, all phospholipid acyl chains straighten in *all-trans* position, allowing maximal hydrophobic and van-der-Waals interactions within the molecule and

between neighboring molecules. As the temperature and thus the in kinetic energy of the molecule increases, carbon-carbon (C-C) bonds rotate and *trans-gauche* isomeric conformations are introduced. This conformational change leads to 120° acyl chain kinks and the molar volume of the membrane increases. Above the T_C of the phospholipid molecules, acyl chains undergo frequent *trans-gauche* isomerizations resulting in a liquid-crystalline membrane with less intermolecular interactions. The energy of a phospholipid molecule in *gauche* conformation is 0.5 kcal/mol higher than that in *trans* conformation and the energy barrier between them is 3.6. kcal/mol [65]. It is assumed that two neighboring C-C bonds per acyl chain are in *gauche* position at any one time to minimize steric interactions with neighboring acyl chains. This conformational change results in a decrease in chain length by one CH_2 unit length (1.27 Å) and an increase in volume of the phospholipid molecule by approximately 25-50 $Å^3$ (Figure 10). Consequently, the volume of the phospholipid membrane bound vesicle increases during phase transition by about 2.5% [66]. The difference in density between the gel phase and the liquid-crystalline phase is approximately 1.4% [62].

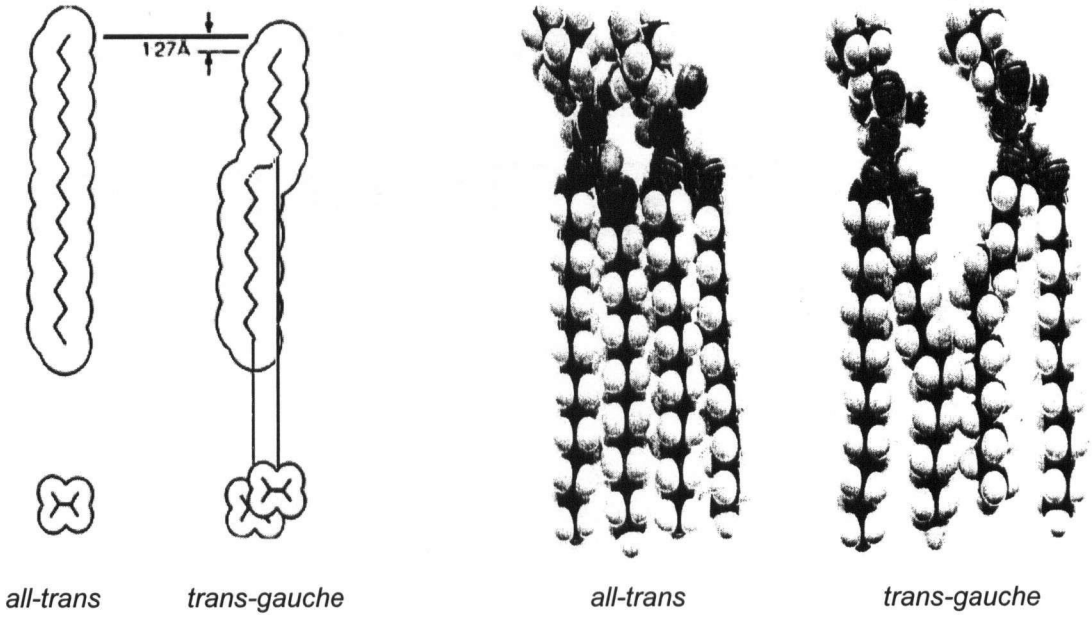

Figure 10: Effect of *trans-gauche* isomerization on the conformation of dipalmitoyl phosphatidylcholine (modified from [66]).

1.3.3. Transition temperatures of phospholipids

The T_C and the enthalpy of gel to liquid-crystalline phase transitions of phospholipid bilayers depend on whether one or two acyl chains are bound to the glycerol backbone, the length and saturation of both acyl chains, the position of the double bond in the acyl chain, and on the head group species (Table 2). The T_C of e.g. phosphatidylcholine increases by approximately 20°C for each additional two-carbon atoms. Accordingly, the enthalpy of the transition increases by 2-3 kcal/mol [30]. The presence of a cis double bond between e.g. the 9th and the 10th carbon atom (C_9) reduces the T_C remarkably by approximately 75°C whereas the enthalpy is not significantly affected [67]. The head group of a phospholipid species affects the T_C of phospholipid

bilayers but has only little effect on the enthalpy of the transition [62] (Table 2).

The presence of a double bond in the acyl chains of phospholipid molecules decreases their molecular interactions and increases the molar volume of the phospholipid molecule. Different double bond positions have different effects on the molar volume of the phospholipid and therefore different effects on the T_C. A minimum in the T_C and ΔH has been observed for 1,2, diatadec-cis-enoyl-phosphatidylcholine and 1-octadecanoyl-2-octadec-cis-enoyl-phosphatidylcholine when the cis double bond is either between C_9 and C_{10} or between C_{10} and C_{11}. The T_C and ΔH minimum can likely be attributed to the maximum molar volume of the phospholipid gained by the double bond position at C_9 or C_{10}, approximately midway in the acyl chain [67]. Lysophospholipids with only one acyl chain attached to the glycerol backbone do not form bilayers in the liquid-crystalline phase but aggregate in micelles. Upon heating, lysolipids transition from the gel phase to a liquid micellar phase, marked T_C^* in Table 2.

Table 2: Transition temperatures (T_C), pretransition temperatures (T_C'), and enthalpies (ΔH) of the gel to liquid-crystalline phase transition and gel to liquid-crystalline micellar transition temperatures (T_C^*) of phospholipids. = Double bond; – single bond (adapted from [30, 62, 37, and 68].

# of C-atoms in acyl chain 1 / 2	*Bond-type at C_9 in acyl chain 1 / 2*	*Head group species*	*T_C, T_C', T_C^* (°C)*	*ΔH (kcal/mol)*
14 / 14 (dimyristoyl)	– / –	choline	T_C 23 (30) T_C 23.7 (62) T_C' 14 (37)	6 (30) 6.26 (62)
16 / 16 (dipalmitoyl)	– / –	choline	T_C 41 (30) T_C 41.7 (62) T_C' 35 (37)	8 (30) 9.69 (62)
18 / 18 (distearoyl)	– / –	choline	T_C 54 (30) T_C 58.2 (62) T_C' 49 (37)	10 (30) 10.84 (62)
16 / 16 (dipalmitoleoyl)	= / =	choline	T_C -36 (30)	9 (30)
18 / 18 (dioleoyl)	= / =	choline	T_C -20 (30) T_C -22 (62, 37)	9 (30) 7.6 (62)
14 / 14 (dimyristoyl)	– / –	ethanolamine	T_C 51 (62, 37)	6.6 (30)
16 / 16 (dipalmitoyl)	– / –	ethanolamine	T_C 63 (30, 62, 37)	9 (30)
18 / 18 (distearoyl)	– / –	ethanolamine	T_C 82 (37)	-
14 / 14 (dimyristoyl)	– / –	glycerol	T_C 23 (37)	-
16 / 16 (dipalmitoyl)	– / –	glycerol	T_C 41 (30, 37)	9 (30)
18 / 18 (distearoyl)	– / –	glycerol	T_C 54 (37)	-
16 / - (monopalmitoyl)	– /	choline	T_C^* 3 (68)	4 (68)
18 / - (monostearoyl)	– /	choline	T_C^* 26 (68)	7 (68)

1.3.4. Influence of cholesterol on the phase transition

Cholesterol is a hydrophobic steroid molecule present in serum that can integrate into the phospholipid membrane. Cholesterol reduces the enthalpy of the phase transition or even eliminates it at a concentration greater than approximately 25 mol% (Figure 11). Cholesterol fluidizes the membrane in the gel phase by inhibiting adaptation of the all-trans configuration of acyl chains. Cholesterol also decreases the motional freedom and the probability of trans-gauche isomerizations of the acyl chains and increases the packing density of phospholipids in the liquid-crystalline phase while separating phospholipid head-groups [37, 62] (Figure 12). As a consequence, membrane permeability is altered depending on the cholesterol membrane concentration. In DPPC bilayers containing less than 33 mol% cholesterol, X-ray data indicate the presence of two phases, pure DPPC and a mixed phase of cholesterol and DPPC at a molar ratio of 1:2. The presence of these two phases increases the membrane permeability. A molar ratio of 1:2 is the preferred ratio of cholesterol in a phospholipid membrane, since at least seven phospholipid molecules are needed to surround one cholesterol molecule, leading to a 1:1.9 molar cholesterol/lipid ratio. Thus, the membrane is homogeneous at this 1:2 molar ratio and membrane permeability is decreased because of an increased phospholipid packing density [66].

Phospholipid membranes containing more than approximately 25 mol% cholesterol are not considered thermosensitive in the sense that the permeability of the membrane does not increase dramatically at its T_C. The permeability increase is rather gradual during phase transition because the cooperativity of phospholipid molecules is decreased due to preferential interaction with cholesterol molecules.

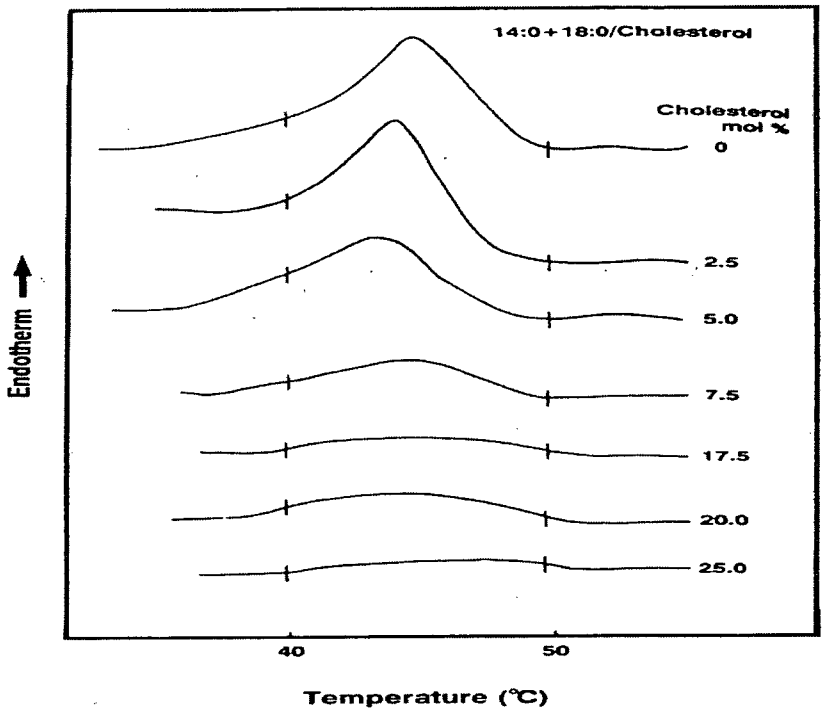

Figure 11: Influence of cholesterol on the gel to liquid-crystalline phase transition of DMPC/DSPC bilayers (molar ratio: 1:1) (adapted from [69]).

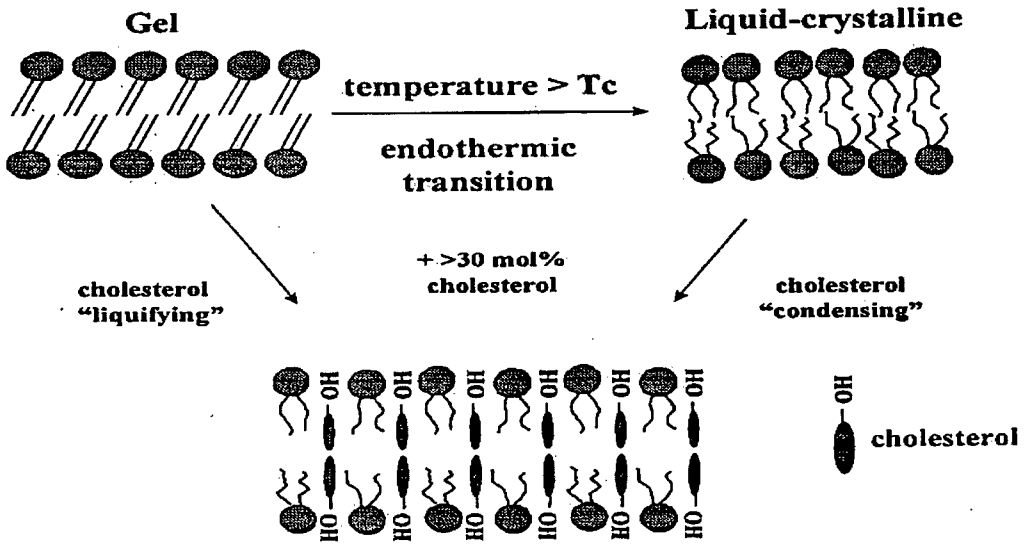

Figure 12: Schematic representation of the influence of cholesterol on the gel to liquid-crystalline phase transition of phospholipid bilayers (adapted from [30]).

1.3.5. Influence of pH, ions, and pressure on the phase transition

Considerations about the influence of pH, ions, and pressure on the phase transition are of relatively minor importance given that these factors are relatively constant during drug encapsulation and release processes.

However, the T_C of phospholipid membranes depends on their ionization- and hydration-state and can be altered by protonation and cationic binding. The charge of the phospholipid head group depends on its pK_a and the pH of its environment. At physiological pH, head groups of most phospholipids are neutral but biological membrane surfaces are usually negatively charged due to the presence of negatively charged phospholipids and proteins associated with the membrane [30]. Thus, anions usually do not interact with phospholipid membranes but protons and cations can bind electrostatically to the membrane surface, which increases the membrane's T_C (Table 3). The effect has mainly been attributed to a competition between phospholipid headgroups and bound ions for water molecules at the membrane surface leading to partial phospholipid dehydration [70].

Table 3: Effect of pH on the T_C of phospholipid bilayers. DM = dimyristoyl; DP = dipalmitoyl; DH = dihexadecyl; PC = phosphatidylcholine; PE = phosphatidylethanolamine (after [70]).

Phospholipid species	*T_C (°C)*		
	pH 1	*pH 8*	*pH 13*
DMPE	54	49.5	24
DMPC	36	23	23
DPPE	67	63.5	42
DPPC	50	42	42
DHPE	71.5	68.5	44
DHPC	54	43.5	43.5

Since the liposome volume increases during phase transition as discussed in section 1.3.2., the T_C of a phospholipid bilayer increases with an increase in pressure (ΔP) according to the Clausius-Clapeyron equation:

$$\Delta P = \frac{\Delta H \Delta T}{T_C (V_l - V_g)} \qquad \textit{(Equation 3)}$$

where ΔH and ΔT are the increase in enthalpy and temperature, respectively, which are assumed to be small and V_l and V_g is the molar volume of the lipid in the liquid-crystalline phase, and the gel phase, respectively. At a pressure of 136 atm, the T_C of DPPC was shown to increase by 3°C, which is consistent with the known values for ΔH and ΔV [71].

1.3.6. Thermodynamics of the gel to liquid-crystalline phase transition

The change in enthalpy (ΔH) during gel to liquid-crystalline phase transition, reflects the energy required to induce trans-gauche isomerization of (i.e. to melt) phospholipid acyl chains in the membrane. It has to be assumed for a first-order transition that the two phases are separate and distinct. In other words, at temperatures below T_C only the gel phase is stable because of its lower free energy, at T_C both phases are stable, and at temperatures above T_C only the liquid-crystalline phase is stable. The thermodynamic driving force that determines the phase behavior, i.e the change in Gibbs free energy (ΔG), is given by:

$$\Delta G = \Delta H - T_C \Delta S \qquad \textit{(Equation 4)}$$

with ΔH = enthalpy change, T_C = phase transition temperature, and ΔS = entropy change.

At equilibrium during phase transition $\Delta G = 0$ and ΔH is given by:

$$\Delta H = T_C \Delta S \qquad \textit{(Equation 5)}$$

Accordingly, the entropy (ΔS), which reflects the degree of disorder within a system, is given by: $\Delta S = \Delta H / T_C$ *(Equation 6)*

and, the phase transition temperature (T_C) can be described as:

$$T_C = \Delta H / \Delta S \qquad \textit{(Equation 7)}$$

In a lipid bilayer, however, the two phases are not fully separate and distinct. They do not occupy different spaces but rather occupy spaces or regions within the same membrane and interactions at these borders or grain boundaries are significant. The area occupied per mole lipid in the gel phase is smaller than in the liquid-crystalline phase. Therefore, lipids in a liquid-crystalline domain formed in the bulk gel phase are under compression and lipids in a gel domain formed in the bulk liquid-crystalline phase are under tension [62]. The free energy of a liquid-crystalline domain in a gel membrane under compression is different from the free energy of a gel domain in a liquid-crystalline membrane under tension and thus, the phase transition occurs over a relatively broad temperature range. The Gibbs free energy for the gel-to-liquid-crystalline phase transition is defined as: $G_g\text{-}G_l = (H_g\text{-}H_l) - T_C\,(S_g\text{-}S_l)$ *(Equation 8)*

where G_g, H_g, and S_g refer to free energy, enthalpy, and entropy of the gel phase and G_l, H_l, and S_l refer to free energy, enthalpy, and entropy of the liquid-crystalline phase, respectively. Because of the greater order of the system in the gel phase the value of S_g is smaller than S_l and the value of H_g is smaller than H_l. Transition from the gel phase into the liquid-crystalline phase becomes thermodynamically possible, when the temperature rises above T_C, at which $T_C\,(S_g\text{-}S_l)$ becomes positive enough for $G_g\text{-}G_l$ to be negative [62]. The transition results in an increase in free energy and the membrane transforms from the gel into the liquid-crystalline phase.

1.4. Drug encapsulation into liposomes

Two methods are commonly used to encapsulate drugs into liposomes, passive encapsulation and active encapsulation. Passive encapsulation has the disadvantage that the majority of the drug is lost during the process and therefore active encapsulation is employed whenever possible. Whether the active encapsulation method is possible depends mainly on the chemical structure of the drug.

1.4.1. Passive drug encapsulation

Hydrophobic drugs are preferentially encapsulated passively into MLVs where they partition primarily in the phospholipid membrane since MLVs possess a large membrane surface area and hydrophobic drugs possess a high membrane partition coefficient. The amount of hydrophobic drug that can be incorporated into the membrane depends on the drug's membrane partition coefficient and on the ability of the membrane to maintain its integrity with embedded drug. Hydrophilic drugs are encapsulated primarily into LUVs or SUVs, where they are entrapped in the aqueous interior of the vesicle [72, 73].

1.4.1.1. Drug encapsulation into MLVs

Hydrophobic drugs such as amphotericin B can be incorporated into the liposome membrane by mixing the drug with lipids in organic solvents before liposome preparation [74]. A disadvantage of using MLV drug formulations is that hydrophobic drugs partitioned in the liposome membrane are often not well retained and exhibit a relative high exchange or leakage rate *in vivo* [75, 76]. Hydrophilic drugs can be encapsulated in MLVs, especially if their trapped volume is enhanced by the freeze thaw

technique [44]. However, the liposome species of choice for hydrophilic drugs are SUVs and even more so LUVs.

1.4.1.2. Drug encapsulation into SUVs and LUVs

To passively encapsulate hydrophilic drugs into SUVs and LUVs, the drug is dissolved in the lipid hydration buffer. The amount of drug that can be encapsulated depends primarily on the trapped volume of the liposome and the drug's solubility. Trapped volumes of SUV are in the order of 0.2 μl/μmol, whereas trapped volumes of LUVs are in the order of 1.5 μl/μmol. Trapping efficiencies can be as low as 1% [50], or as high as 90% [77] depending on the drug and lipid concentrations and on the specific technique used to generate liposomes.

1.4.2. Active drug encapsulation

Amphipathic drugs with suitable pK_a values can be encapsulated actively into SUVs and LUVs. When drug molecules possess protonation sites and can exist in an equilibrium between protonated and unprotonated states between pH values of approximately pH 4 and pH 9, drugs can be encapsulated actively into liposomes by establishing a transmembrane pH or other ion gradient across the liposome bilayer [78]. Transmembrane pH gradients can be established by hydrating the lipid film in acidic buffer and exchanging the buffer outside the liposomes with buffer of physiological pH using column chromatography or by increasing the pH outside liposomes by dialysis or titration. Drugs that can be actively encapsulated into liposomes are typically amphiphilic amine drugs such as anticancer drugs of the anthracycline family, vincristine, and mitoxanthrone [78]. The structure of these drugs is heterocyclic, which adds

sufficient hydrophobicity to the molecule to permeate the phospholipid membrane when the molecule is uncharged. The most commonly used biocompatible buffers for establishing pH gradients are citrate and ammonium sulfate buffer on the inside and N-[2-hydroxyethyl]Piperazine-N'-[2-ethanesulfonic acid] (HEPES) buffered saline (HBS) on the outside of the liposome membrane [78, 79].

The principles of active and passive drug encapsulation into liposomes are illustrated in Figure 13. In brief, neutral unprotonated drug molecules at physiological pH cross the liposome membrane freely, become protonated inside the liposomes at a low pH and are trapped inside. The concentration of the protonated drug inside ($[BH^+]_{in}$) and outside the liposome ($[BH^+]_{out}$) depends on the liposomal inner and outer volumes (V_{in}, V_{out}), the dissociation constant of the drug (k), and on the concentration of the hydrogen ions inside ($[H^+]_{in}$) and outside the liposome ($[H^+]_{out}$). Since V_{in} / V_{out} in equation 10 is small, and k is a constant, the formula reduces to:

$$\frac{[BH^+]_{in}}{[BH^+]_{out}} = \frac{[H^+]_{in}}{[H^+]_{out}} \qquad \textit{(Equation 9)}$$

Since pH is defined as -log $[H^+]$, a difference of e.g. 3 pH units across the liposome membrane results in a 1000-fold difference in drug concentration from the inside of liposomes to the outside. Trapping efficiencies are usually close to 100% and drug leakage can be reduced especially if the drug precipitates out of solution inside the liposome because the concentration of the membrane permeable unprotonated form of the drug is then further reduced [80]. In this case, the ratio between drug concentrations inside and outside the liposomes can exceed the predicted value according to the formula given in Figure 13 [81].

Passive drug loading

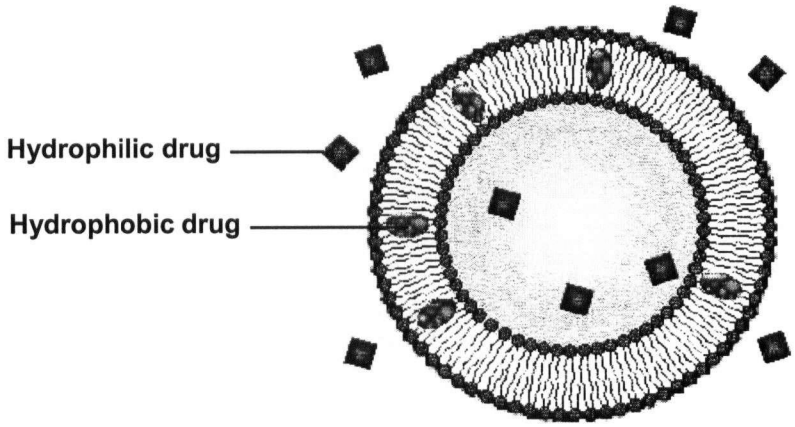

Active drug loading

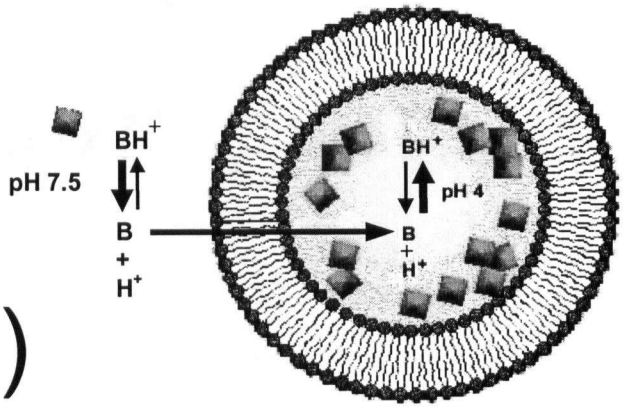

$$\frac{[BH^+]_{in}}{[BH^+]_{out}} = \frac{V_{in}}{V_{out}} \left(\frac{k + [H^+]_{in}}{k + [H^+]_{out}} \right)$$

(Equation 10)

Figure 13: Schematic representation of passive and active drug loading into liposomes. B = drug base; H^+ = hydrogen ions; BH^+ = protonated base; $[BH^+]_{in}$, $[BH^+]_{out}$ concentrations of protonated drug inside and outside the liposome; $[H^+]_{in}$, $[H^+]_{out}$ = concentration of hydrogen ions inside and outside the liposome; V_{in}, V_{out} = volumes inside and outside liposomes; k = dissociation constant of the drug.

1.5. Factors influencing drug retention in liposomes

For some liposome formulations, drug retention properties can differ dramatically between results obtained *in vivo* and those obtained *in vitro*. For example, mitoxanthrone-loaded DMPC/cholesterol liposomes released less than 2% of the drug after 72 h *in vitro* but 73% of the drug was released within 48 h *in vivo*. No such difference was found in mitoxanthrone-loaded DSPC/cholesterol liposomes [82].

1.5.1. Drug retention *in vitro*

Drug release from liposomes *in vitro* depends on several factors including the liposome membrane composition, temperature, the drug's membrane partition coefficient, and the liposome stability.

In both, cholesterol-containing liposomes and cholesterol-free liposomes, but especially in the latter, drug retention is dependent on the T_C of the membrane and therefore on temperature. The membrane permeability of liposomes increases with increasing temperature and is significantly higher at or above the T_C of the membrane. Therefore, the most commonly used liposome formulations are lipid mixtures derived from natural sources such as egg or soy or composed of one or two synthetic lipid species with T_C values above room temperature or physiological temperatures, i.e. dimyristoyl-, dipalmitoyl-, and distearoyl-phosphatidylcholines or phosphatidylethanolamines and mixtures of those. Their respective T_C values are 23°C, 41°C, and 56°C for phosphatidylcholines or 51°C, 63°C, and 74°C for phosphatidylethanolamines.

Since cholesterol condenses the liposome membrane at temperatures above its T_C (see section 1.3.4), the presence of cholesterol in the liposome membrane increases drug

retention for liposomal formulations with low T_C values [69, 83].

Drug retention in LUVs increases with decreasing membrane partition coefficients and thus with the polarity of the drug. The presence of PEG-lipids in the membrane also has a significant impact on the stability of the liposomal drug formulation not only *in vivo*, as discussed in section 1.6.2., but also *in vitro*. Incorporation of PEG-lipids in the liposome membrane prevents vesicle aggregation [84] but has either no effect or decreases drug retention [85, 86], depending on the encapsulated drug, the PEG-lipid species and amount of PEG-lipid present in the membrane.

1.5.2. Drug retention *in vivo*

In addition to factors influencing drug retention *in vitro*, surface charge and liposome size also influence drug retention *in vivo* [87]. After *in vivo* exposure, membrane components can exchange into the serum and from there into cell membranes or high-density lipoproteins (HDL) and thus destabilize the liposome membrane [88, 89]. The presence of cholesterol in the membrane reduces this effect [90, 91]. Cholesterol, serum proteins, and the apoA-1 lipoprotein of HDL can also adsorb and integrate into the liposome membrane, especially if the membrane surface is negatively charged [94], and cause membrane destabilization [92, 93]. For example, MLVs containing 30 mol% of negatively charged phosphatidylserine, phosphatidylglycerol, or phosphatidylinositol were cleared 25-, 18-, or 15-times faster in comparison to liposomes containing phosphatidylcholine, which is zwitterionic and neutral at physiological pH [95].

1.5.2.1. Reticuloendothelial system (RES)

Adsorption of opsonins, a class of serum proteins including antibodies and complement proteins [96, 97] is believed to trigger recognition of liposomes by the RES, also named the mononuclear-phagocyte system (MPS). Liposomes are then eliminated from systemic circulation by phagocytic cells. It has been shown that the circulation half-life of liposomes is negatively correlated with the serum protein binding ability of negatively charged liposomes [96].

The RES is a broad system of cells including endothelial cells, fibroblasts, histiocytes (stationary macrophages) and monocytes (white blood cells). The latter two phagocytic cell types make up the majority of the RES. Cells of the RES, particularly liver macrophages (Kupffer cells), which line the endothelial surface of liver sinusoids, and stationary spleen macrophages play a major role in the clearance of potentially harmful particles from the blood stream such as micro-organisms, immune-complexes, cell fragments, red blood cells, and platelets.

Liposomes in systemic circulation enter the spleen through the splenic artery. In the intricate capillary meshwork of the spleen, liposomes smaller than 100 nm in size are taken up preferentially by spleen macrophages [98]. From the spleen, blood continues to the liver where particles extravasate into liver sinusoids through the discontinuous hepatic vasculature and are readily taken up by Kupffer cells, especially if greater than approximately 200-300 nm in diameter [99, 100]. It has been further shown that liposomes larger than 200 nm in size are more rapidly cleared from the circulation as compared to liposomes smaller than 200 nm. SUVs and LUVs thus accumulate in the liver and spleen after intravenous (*i.v.*) injection [101]. However, these liposome size

cut-off values differ between studies and the mechanisms involved are not well understood but generally, it appears that liposomes of approximately 100 nm in size exhibit the longest systemic circulation life-times. *In vivo* clearance of liposomes is also dependent on the administered liposome dose since the uptake processes can be saturated and certain opsonins can be depleted from systemic circulation, especially after chronic liposome administration [102, 103].

1.5.2.2. Sterically stabilized liposomes

Liposomal drug formulations that do not retain drugs for at least 24 h to ensure high tumor accumulation have little benefit in the treatment of solid tumors in comparison to free drug administration [104-106]. In early successful approaches to increase the longevity of liposomes, the phospholipid ganglioside GM1 was incorporated into the liposome membrane [107]. More recently, PEG-lipids were incorporated into the liposome membrane leading to long-circulating liposomes, which are often referred to as sterically stabilized or Stealth™ liposomes. PEG-lipids have the advantage that the PEG-polymer can be attached to a variety of different phospholipid molecules and that the length of the PEG moiety can be varied resulting in a great variety of PEG-lipids, providing the approach a great degree of versatility.

By incorporating PEG-lipids into the liposome membrane a protective polymer coat is formed around the outer liposomal surface extending maximally 3.5 nm, 6.5 nm, or 11.5 nm above the liposome surface for PEG_{350}, PEG_{2000}, or PEG_{5000}, respectively [108, 109] (Figure 14). The amount of PEG-phospholipids in the liposome bilayer needed to cover the surface of the liposome depends mainly on the length of the PEG moiety [108].

The polymer coat is believed to prevent opsonins from integration into the liposome membrane, which allows liposomes to escape RES clearance [87, 96, 110]. Addition of 4-5 mol% DSPE-PEG_{2000} has been shown to provide a maximum 4-fold increase in circulation longevity [111] and a 2-fold reduction in liver accumulation [112]. Furthermore, liposomes containing PEG-lipids have been shown to exhibit enhanced efficacy in comparison to liposomes not containing PEG-lipids [113] and this increase in therapeutic activity was attributed to their increased circulation life-time [106]. However this traditional view of the role of PEG-lipids has recently been challenged and it appears that the primarily role of PEG-lipids in the liposome membrane may be the prevention of liposome aggregation and fusion with biological membranes [114, 115].

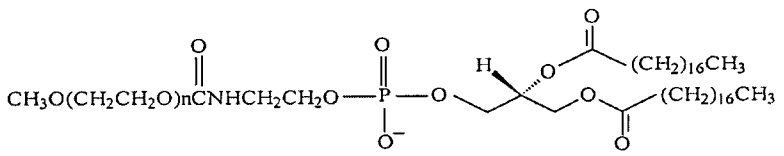

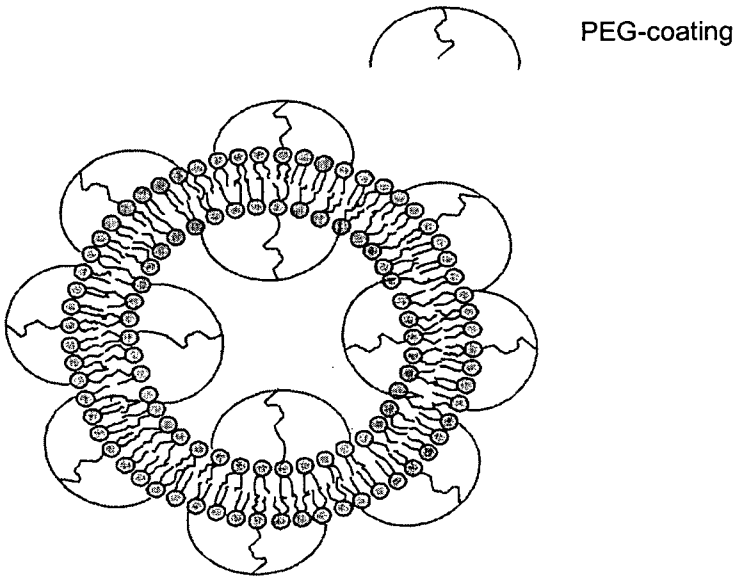

Figure 14: Molecular structure of DSPE-PEG (n = 45 for PEG_{2000}) and an illustration of a liposome with PEG-coating.

1.6. Membrane dynamics in cholesterol-free liposomes

Membrane dynamics described in this section of the present thesis occur only in thermosensitive liposomes, i.e. liposomes that do not contain cholesterol. Processes described in the following sections do not have to be taken into consideration in the presence of cholesterol in the liposome membrane since cholesterol decreases the motional freedom and cooperativity of phospholipid molecules due to preferential interaction of phospholipids with cholesterol molecules [37, 62].

1.6.1. Domain formation during phase transition

When the temperature of a lipid membrane reaches T_C, initially small regions or nuclei of liquid-crystalline lipid will be formed in the gel phase membrane. These nuclei grow in size as the temperature increases until eventually all of the lipid will be in the liquid-crystalline phase. The formation and growth of these liquid-crystalline regions introduces stress on the membrane because the volume of phospholipids in the liquid-crystalline phase is greater than that in the gel phase [66]. Therefore, liquid-crystalline domains in a gel membrane are under compression. As these regions grow and fuse, the membrane becomes liquid-crystalline with inserted gel domains, which now are under tension [62] (Figure 15).

Similarly, when a phospholipid bilayer is cooled down from temperatures above its T_C to temperatures below it, relatively ordered gel-phase domains are formed within the liquid-crystalline membrane. The packing of lipids in these domains are not as regular as in the gel phase and continuous domain growth will lead to an altered gel phase with many vacancies and defects [116]. This altered gel phase is metastable and will

change into the more ordered gel phase with time to maximize intermolecular interactions. In each domain of the gel-phase membrane, phospholipids are oriented in a certain crystal lattice and each lattice has a different orientation. Therefore, boundary regions exist in the gel phase membrane where domains meet and the degree of disorder within the membrane is highest at domain-separating boundaries. Depending on the tilt angle (α) between lattices of neighboring domains, boundaries are regarded as (low-angle) tilt boundaries or (large-angle) grain boundaries [117] (Figure 16). As modeled by Mouritsen and Zuckermann [118-120], the T_C at grain boundary areas is slightly lower than that of membrane domains and thus, phospholipids at grain boundaries melt at temperatures a few degrees below the T_C of the bulk lipid.

Interestingly, the permeability of a phospholipid membrane is highest at the T_C, even higher than its permeability above the T_C. A permeability maximum for Na^+ ions has been observed at the mid-point of the phase transition [121] where equal amounts of gel domains and liquid-crystalline domains are separated by so-called interfacial lipid with the highest degree of defects and free energy [122].

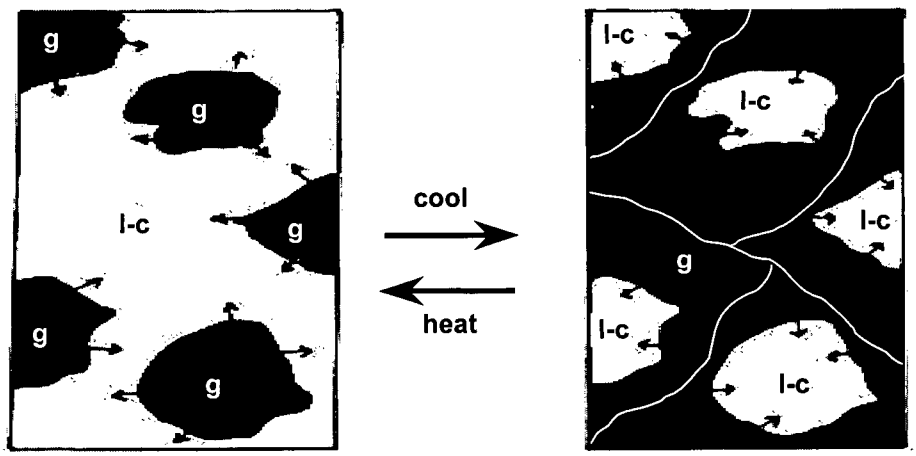

Figure 15: Domain and grain boundary formation during phase transition. g = gel phase; l-c = liquid-crystalline phase (modified from [62]).

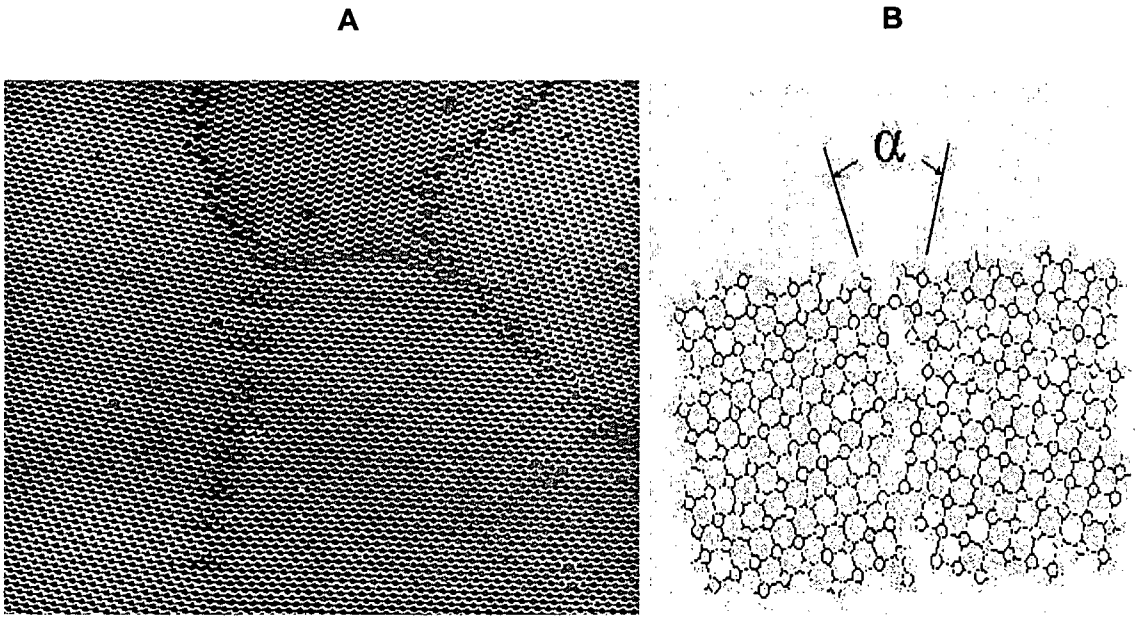

Figure 16: (A) Grain boundaries illustrated by rafts of soap bubbles and (B) a schematic representation of the phospholipid crystal lattice structure. α = tilt angle (adapted from [123]).

1.6.2. Hydrolysis of phospholipids

When liposomes are extruded at temperatures above their T_C and loaded with drug at elevated temperatures at low pH, phospholipid molecules are subjected to acid-catalyzed hydrolysis. The degree of hydrolysis is a major factor determining the shelf-life of liposomal drug formulations and depends mainly on storage time, temperature, and pH. Hydrolysis rates are usually low and can be largely ignored, especially if the liposome membrane contains cholesterol. However, in the absence of cholesterol accumulation of hydrolysis products can dramatically influence the membrane structure and local membrane composition, especially upon phase transition.

Ester bonds between acyl chains of the phospholipid molecule and the glycerol backbone are susceptible to acid- and base-catalyzed hydrolysis following pseudo first

order kinetics. A hydrolysis minimum has been observed at pH 6.5 [124]. For example, when 1,2-diacyl-sn-glycerol-3-phosphoylcholine is hydrolyzed, initially both acyl chains are cleaved by the same rate but the more stable isomer 1-acyl-sn-glycerol-3-phosphoylcholine is predominantly formed because of acyl chain migration (Figure 17). The hydrolysis rate is dependent on the temperature and can be described by the Arrhenius equation:

$$k = A\, e^{-Ea/RT} \qquad \textit{(Equation 11)}$$

where k = rate constant, A = frequency factor, E_a = activation energy, R = universal gas constant (8.314 J K^{-1} mol^{-1}), T = temperature in degrees Kelvin [124].

The hydrolysis rate is independent of the ionic strength of the buffer or the presence of oxygen in the sample. At pH 4 and a temperature of 5°C the observed hydrolysis rate for phosphatidylcholine is reported at approximately 2 mol% per month [125].

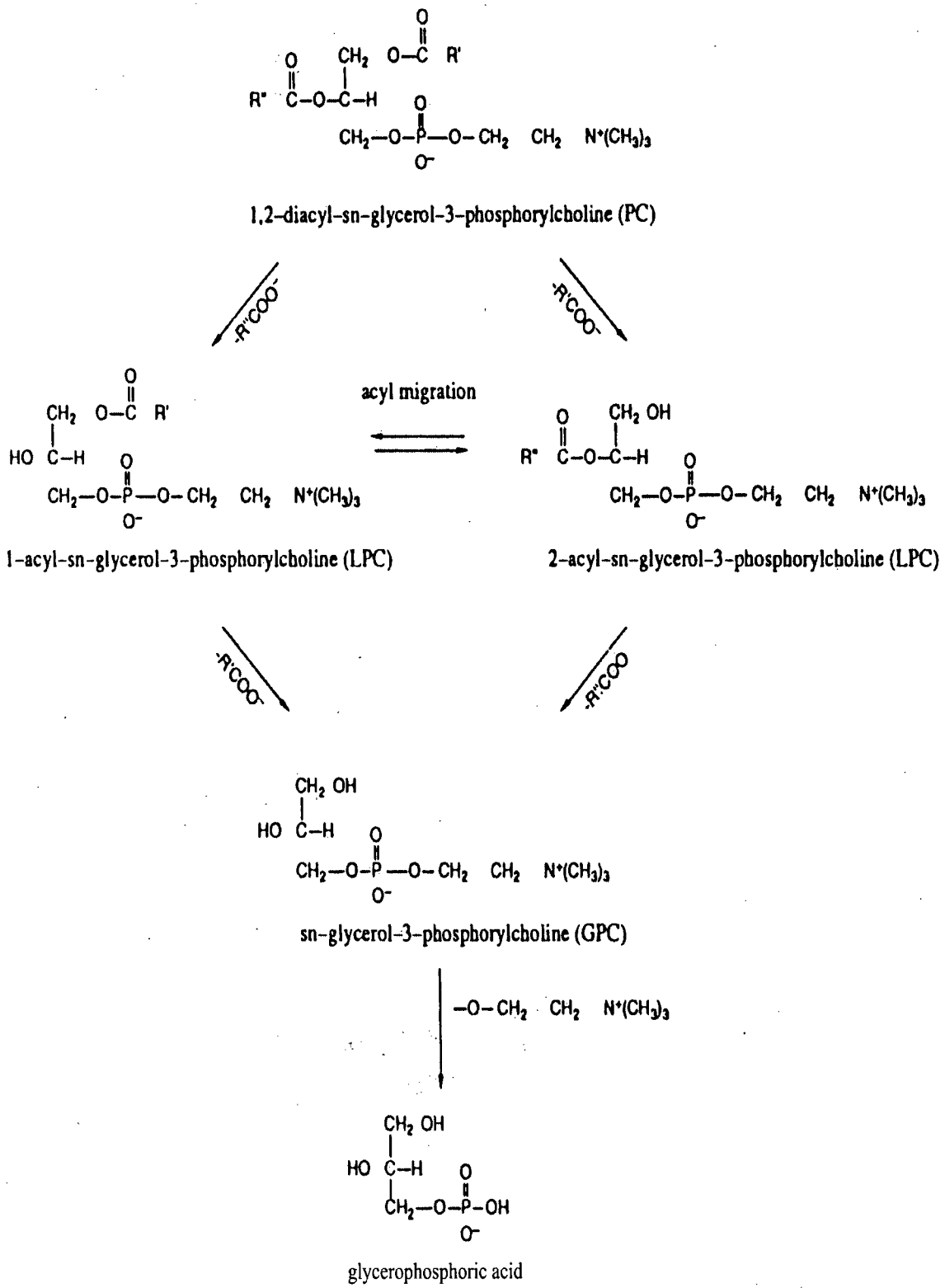

Figure 17: Chemical reactions during phospholipid hydrolysis (modified from [126]).

1.6.3. Lateral phase separation

When a membrane is composed of several phospholipid species or when lysolipids accumulate in liposome membranes as a result of hydrolysis it is generally assumed that the membrane constituents are homogeneously distributed throughout the membrane. Phospholipids are considered miscible if their T_C difference is less than 20°C, especially if they possess the same head group species [127]. The transition temperature of the membrane then falls in between the T_C values of all its constituents depending on the relative amount of the phospholipid species in the membrane. However, when the temperature of the membrane is decreased from temperatures above, to temperatures below the T_C of one of its constituents, lateral phase separation can occur within membrane domains, especially if the T_C difference of membrane components is more than 20°C. When a mixed membrane composed of two phospholipids is cooled from temperatures above, to temperatures below its T_C lipids with the higher T_C concentrate in gel phase domains within the liquid crystalline membrane composed of a lipid mixture richer in the phospholipid with the lower T_C [62, 127]. The effects of temperature in a mixed membrane may be best described in a phase diagram (Figure 18). A two component mixture of completely miscible phospholipids with the composition x exists in both liquid-crystalline and gel phase at temperatures between t_1 and t_3 (Figure 18A). At an intermediate temperature t_2, the liquid-crystalline phase has the composition x_1 and thus is richer in the phospholipid with the lower T_C, whereas the gel phase has a composition x_2 and is richer in the phospholipid with the higher T_C.

Phospholipids that are immiscible in the gel phase will not co-crystallize upon cooling. Different phospholipid molecules will separate into gel domains composed

almost solely of the component with the higher T_C and in liquid-crystalline domains composed almost solely of the component with the lower T_C, which are co-located with grain boundaries (Figure 18B).

In liposomes consisting of a 1:1 mixture of dimyristoylphosphatidylcholine (DMPC, T_C = 23.5°C) and dimyristoylphosphatidylethanolamine (DMPE, T_C = 51°C) lateral phase separation has been observed with 80% DMPC in the liquid crystalline phase and 80% DMPE in the gel phase at a temperature of 37°C [128, 63]. This effect can be reversed by addition of cholesterol as observed in giant liposomes [129] but cholesterol itself tends to accumulate in phase boundary regions [130]. For a thermodynamic discussion on phase separation see [128]. Lateral phase separation has also been observed in the gel phase of DMPC/DMPE mixtures [131], in mixtures of dipalmitoylphosphatidylethanolamine (DPPE) and dipalmitoylphosphatidylcholine (DPPC) [132], and in mixtures of DPPC and diarachidoylphosphatidylcholine (DAPC) [133]. In DMPC / DSPC bilayers, DSPC gel phase domains were exactly superimposed upon each other across the bilayer [134]. Furthermore, after nucleation of lateral phase separation by transition of mixed membranes from the liquid crystalline phase to the gel phase, membrane components are reported to diffuse into locally enriched areas against their concentration gradient (uphill diffusion) [128, 135].

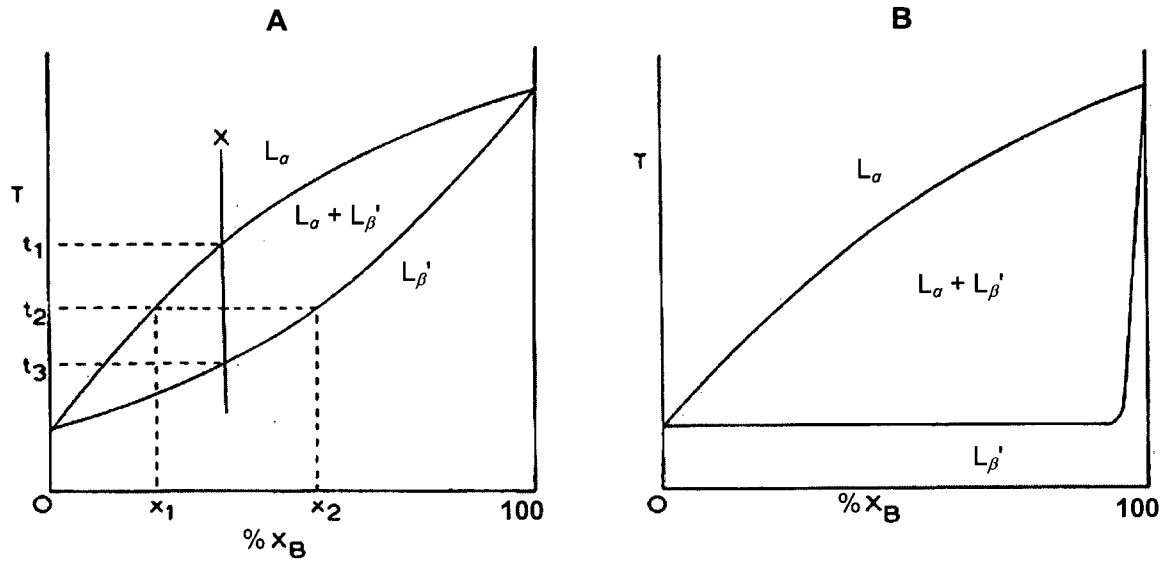

Figure 18: Phase diagram of a mixed phospholipid membrane exhibiting (A) miscibility and (B) immiscibility in the gel phase. T = temperature; L_α = liquid-crystalline phase; L_β' = gel phase; t_1 = minimum temperature above T_C; t_2 = temperature within T_C; t_3 = maximum temperature below T_C; $\%X_B$ = percentage of component B in the respective phase (modified from [66].

1.6.4. Influence of lysolipids on membrane properties

Membrane components of the investigated liposome formulation that are proposed in this thesis to segregate into grain boundaries are the lysolipids MPPC and MSPC and the PEG-lipid DSPE-PEG_{2000}. Lysolipids play a significant role in signalling pathways of biological membranes leading to e.g. cell proliferation, differentiation, aggregation, fusion, smooth muscle contraction, and chemotaxis [136]. Some of these responses might be a result of lysolipid-induced changes in membrane properties. When injected into rats, cholesterol-free liposomes containing increasing amounts of lysolipids decreased the ability of the RES to clear carbon particles from the blood stream in a lysolipid-concentration dependent manner. This RES depression effect was not observed

in cholesterol-containing liposomes up to a concentration of 10 mol% lysolipid in the liposome membrane [137]. These results indicate that lysolipids are cytotoxic at higher concentrations and that they appear to be more bioavailable in cholesterol-free liposomes.

Lysolipids can exchange in and out of membranes. When the lysolipid MPPC is added to the buffer outside lysolipid-free giant liposomes at buffer concentrations below the CMC of MPPC, membrane saturation is reached at MPPC membrane concentrations of approximately 3 mol%. At concentrations above the CMC of MPPC, membrane saturation is reached at MPPC concentrations greater than 30 mol% [138-140].

In cholesterol-free liposomes, the presence of lysolipids in the membrane increases the membrane permeability especially at temperatures below T_C as measured by europium (III) ion efflux. At temperatures above T_C the membrane permeability increased with increasing temperature and lysolipid concentration ranging from 7-27 mol% lysolipid [141]. However, the membrane permeability of partially hydrolyzed liposomes, measured by the leak-in rate of calcein, decreased up to a lysolipid concentration of approximately 10 mol% and increased at higher concentrations [142]. These results are consistent with the hypothesis that lysolipids accumulate at grain boundaries and decrease the membrane permeability by occupying membrane defects as discussed in the previous sections. This interpretation is supported by the observation that membrane impurities accumulate at grain boundaries as modeled by Laradji *et al.* [143] and revealed by resonance energy transfer experiments [144].

Analysis of liposomes by nuclear magnetic resonance (NMR) suggested almost complete phase separation of lysolipids in the gel phase membrane at temperatures below the T_C of the bulk phospholipid and it was speculated that locally concentrated lysolipids

form small ion channels with at least four lysolipid molecules per channel, two on each leaflet of the bilayer [141]. In cholesterol-containing liposomes, lysolipids also increase membrane permeability but increasing amounts of cholesterol in the membrane counteracts this effect [145, 146]. These findings may explain the cytotoxic effects of lysolipid-containing liposomes on cells of the RES by inducing ion channels in the cell membrane.

1.7. Triggered drug release from liposomes

An effective way of triggering drug release from liposomes is probably one of the most sought after innovations in the field of liposome research since it offers the ability to control the delivery of drugs to tumors much more effectively than by currently used liposomal drug formulations. For example, encapsulating cisplatin in sterically stabilized liposomes enhanced tumor drug delivery in comparison to free cisplatin administration but this increased tumor drug accumulation did not translate into increased efficacy in a variety of tumor models [2]. Also, a DMPC/cholesterol liposomal mitoxanthrone formulation possessing poor drug retention properties exhibited increased efficacy in comparison to a liposomal DSPC/cholesterol mitoxanthrone formulation in which the drug was well retained [82, 147].

Drugs in a liposomal formulation are not available to tumor cells if not released from their carrier. Thus, in some cases leakier drug formulations can have advantages over less leaky formulations but finding a liposomal drug formulation with the right balance between drug release and drug retention properties is challenging. Ideally, drug retention should be maximal before and minimal after tumor accumulation and much of

the current liposome research is dedicated to the development of a release mechanism controlling this change in liposome drug retention properties [148].

Several triggered drug release mechanisms have been proposed and investigated for liposomal delivery of anticancer drugs [11]. Previously, internal triggers such as the low pH environment of hypoxic tumors [149] and tumor-associated cell surface antigens [150] have been used to differentiate between tumors and healthy tissue and to trigger drug release from liposomes. However, the pH difference between hypoxic tumors and normal tissue is usually in the order of less than one pH unit and a cell surface antigen that is expressed at high levels in a variety of tumor cells but not in normal cells has yet to be found. Thus, potential targets for a triggered drug release mechanism based on the low pH environment of hypoxic tumors or tumor-associated cell surface antigens are difficult to identify. An externally activated trigger may therefore be more practical for targeted liposomal drug delivery. One such method of triggering drug release externally is applying heat locally to the target site at which thermosensitive liposomes have accumulated. This approach in comparison to internally triggered drug release from liposomes has the disadvantage that the tumor has to be located before the trigger can be activated. However, triggering drug release externally is less dependent on variable internal factors of the tumor and its environment and thus bears the potential that drug release can be better controlled.

1.7.1. Tumor hyperthermia

Local tumor hyperthermia alone has been explored for the use as an anticancer treatment since the early 1900s [151, 152]. The treatment is confined to tumors of

detectable size where localized hyperthermia can be applied since malignant cells are not more sensitive to hyperthermia than normal cells. However, cells are more sensitive to hyperthermia in an acidic environment, which is present in poorly perfused, hypoxic, and malnourished sections of large tumors [153].

Poorly perfused hypoxic tumor sections can also be heated to higher temperatures than well-perfused areas, since the cooling effect from blood perfusion is lacking and tumor regression can be achieved in animals and humans without damaging the surrounding healthy tissue [153]. Hyperthermia can also destroy capillaries and collapse microcirculation [154, 155]. When hyperthermia is used alone, approximately 50% of treated tumors in animals and humans regress but hyperthermia is not sufficient to eradicate tumors [156].

Significant cytotoxicity occurs at temperatures greater than 41°C and cell survival after hyperthermia decreases exponentially with increasing temperature and heating time. At temperatures between 40°C and 42.5°C an increase in temperature of 1°C is equivalent to an increase in heating time by a factor of 4-6. Above a temperature of 42.5°C, an increase in temperature of 1°C is equivalent to an increase in heating time by a factor of 2. However, large differences in cellular response to hyperthermia exist between tissues and animal species [153]. Cells are most susceptible to hyperthermia in S-phase and mitosis and disintegrate during G_1-interphase, a few hours after the treatment probably because of membrane damage. In normal and tumor cells, thermo-tolerance develops immediately after hyperthermia, protecting cells against a second dose of hyperthermia probably by heat-induced induction of repair protein and heat-shock protein expression. The effect peaks at 12-48 h and decays at 3-5 days after exposure [157, 158].

The combination of hyperthermia with radiation has been investigated extensively as a strategy to circumvent the insensitivity of cells to radiation when hypoxic or in S-phase. The combination of the two treatments seems intuitive since cells are most susceptible to hyperthermia when hypoxic or in S-phase [151]. The combination of hyperthermia with chemotherapy has also been investigated since it bears the potential that the combined efficacies are more than additive. Chemotherapeutics reach the well-perfused areas of a tumor in higher concentrations than poorly perfused hypoxic areas, whereas hyperthermia has the greater damaging effect in those poorly perfused hypoxic areas [151]. Mild local hyperthermia also leads to vasodilation, a 1.5 to 2-fold increase in blood flow (5 to 10-fold in normal tissue) [153], and an increase in vascular permeability at the tumor site, which increases the delivery of cytotoxic agent to the tumor. In addition, synergistic cytotoxic effects of chemotherapy with various drugs in combination with hyperthermia have been observed [159]. For example, the sensitivity of cells to alkylating agents and cisplatin increases linearly with temperature but for bleomycin and anthracyclines a threshold sensitivity has been observed at a temperature of 42-43°C. In contrast, an increase in temperature affects the cytotoxicity antimetabolites and vinca alkaloids only marginally [152, 153].

The main problem with local hyperthermia, however, is that a uniform regional rise in temperature within tight limits (41-42°C) seems to be impossible to achieve, especially in tumors that are surrounded by other tissue and blood vessels. The most common techniques to induce hyperthermia include infusion of hot saline into body cavities, regional perfusion with heated blood [160], radiofrequency radiation [161], microwave radiation [162-165], and ultrasound radiation [166, 167]. Each technique has

its advantages and disadvantages and all techniques are confronted with the problem that the temperature distribution within the tumor is uneven and almost impossible to determine precisely. Differences in tumor temperatures as great as 5°C have been documented by using radiofrequency as the heat source [161].

1.7.2. Thermosensitive liposomes

When used in combination with liposomal drug formulations, local hyperthermia leads to a 10 to 50-fold increase in liposome extravasation when applied for 1 h at 41-42°C [12, 151, 168]. When evaluated in preclinical tumor models, most thermosensitive liposomal drug formulations in combination with hyperthermia improve tumor drug uptake or tumor growth delay in mice approximately 2 to 9-fold (maximally 17-fold) when compared to either no hyperthermia or free drug [12]. Interestingly, tumor uptake and tumor growth delay do often not correlate, which may be explained by the fact that drug release from traditional thermosensitive liposomes is slow and often incomplete and current methods of determining tumor uptake do not differentiate between free drug released from the liposomes and encapsulated drug.

The usefulness of thermosensitive liposomes in anticancer therapy in a clinical setting depends on utilizing lipid compositions that have a T_C above body temperature to prevent drug leakage when in blood circulation. After drug-loaded thermosensitive liposomes accumulate passively at the tumor site through permeable blood vessels with discontinuous endothelial lining, drugs can be released by heating the tumor to temperatures above the T_C of the phospholipid membrane [168, 169]. Thus, higher drug concentrations can be reached within the tumor in comparison to the surrounding tissue

and decreased side effects of the liposomal drug formulation can be achieved. This feature becomes important especially for anti-cancer drugs with low therapeutic indices because the success of the therapy is often limited by the relatively low drug concentration that can be reached at the target site as a result of the drug's side effects to other tissues.

In general, thermosensitive liposomes are liposomes that do not contain cholesterol since cholesterol decreases the motional freedom and the probability of trans-gauche isomerizations of the acyl chains [37, 62] (see section 1.3.4.). This, in turn, eliminates the dramatic changes in membrane permeability associated with gel to liquid crystalline phase transition.

The composition of previously investigated thermosensitive liposomes was based on dipalmitoylphosphatidylcholine (DPPC) with a phase transition temperature of 41°C. Distearoylphosphatidylethanolamine (DSPE) and DSPE-PEG was added to the formulation to increase its T_C and circulation half-life, respectively. These thermosensitive liposome formulations include: DPPC (100%) [170], DPPC/DSPC (molar ratio: 7:3) [171], DPPC/DSPC (molar ratio: 9:1) [169, 172], and DPPC/DSPC/DSPE-$PEG_{1000\ or\ 5000}$ (molar ratio: 9:1:0.3) [169]. The main disadvantage of these thermosensitive liposome formulations is the relatively broad temperature range of their phase transition resulting in a relatively slow and incomplete release of their contents (Figure 19).

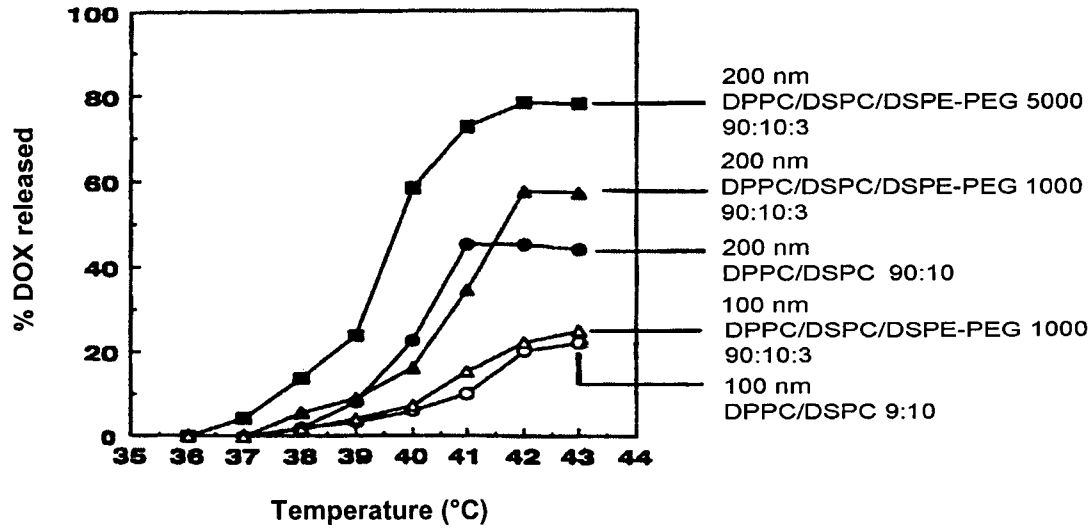

Figure 19: Effect of liposome size and DSPE-PEG content on DOX release from DPPC/DSPC liposomes (adapted from [169]).

A novel approach for temperature triggered drug release of liposomes was achieved by incorporation of 10 mol% of the lysolipid monopalmitoyl phosphatidylcholine (MPPC) in the liposomal DPPC membrane. The presence of lysolipid in the liposome membrane enhanced the release rate of encapsulated carboxyfluorescein, decreased the onset temperature, and narrowed the temperature range at which drug is released [13]. Interestingly, the temperature at which DOX is released is approximately one degree lower than the T_C of DPPC/MPPC/DSPE-PEG liposomes (Figure 20) in contrast to pure DPPC liposomes, which release DOX at phase transition (Figure 21).

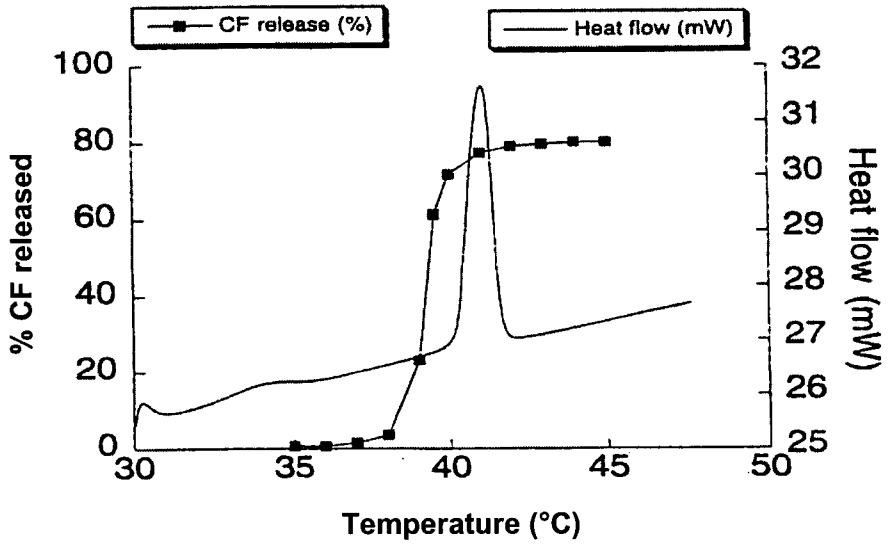

Figure 20: DSC thermogram and release of carboxyfluorescein (CF) from DPPC/MPPC liposomes (molar ratio: 9:1) (adapted from [13]).

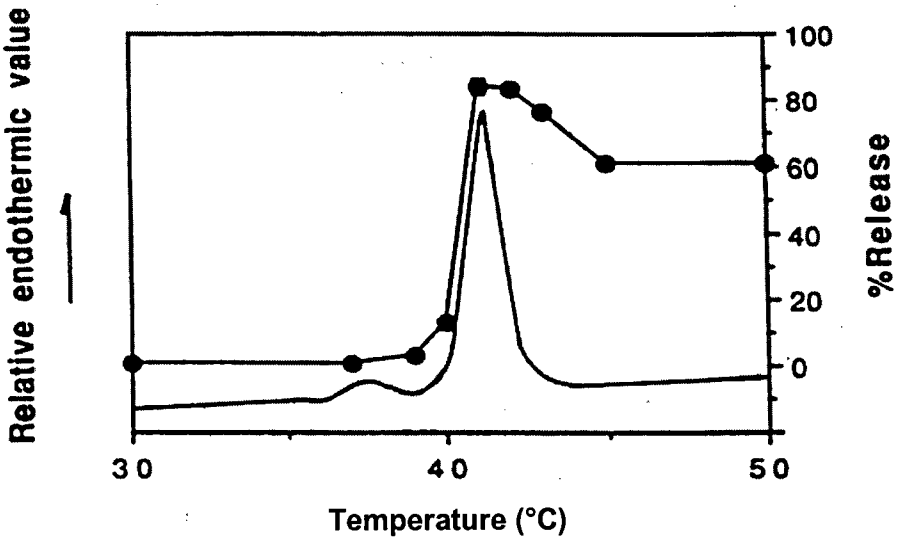

Figure 21: DSC thermogram and release of DOX from DPPC liposomes (adapted from [170]).

Prior to this study, the mechanism by which these lysolipid-containing thermosensitive liposomes (LTSL) release their contents so rapidly upon heating was not understood. The hypothesis by Needham and co-workers was that above T_C lysolipids dissociated from the DPPC membrane and create membrane defects, which increase the membrane permeability. In addition, the formation of boundary regions in mixed membranes was thought to contribute to the increased membrane permeability but the concept was not further investigated [13, 14].

MPPC-containing DOX-loaded thermosensitive liposomes in combination with mild hyperthermia reduced the growth of human squamous FaDu tumors implanted in mice and resulted in complete regressions of 11 out of 11 tumor lasting up to 60 days post-treatment [1]. This exciting finding is a very promising indication of the improved therapeutic effect that may be achievable by controlled drug release using thermosensitive liposomal formulations of DOX.

1.8. Doxorubicin (DOX)

The only two liposomal anticancer drug formulations currently approved by the Federal Drug Administration of the USA (FDA) and used clinically are Caelyx® (= Doxil® in the USA), a liposomal formulation of DOX, and DaunoXome® a liposomal daunorubicin formulation. Initial work on drug encapsulation into LTSL was conducted with DOX as the model drug and this liposomal DOX formulation showed promising efficacy results [1]. For these reasons, and because DOX can easily and efficiently encapsulated into liposomes, is easy to quantitate because of its fluorescence characteristics, and because it is inexpensive and widely available, DOX was chosen as

the model compound for drug loading, drug release and efficacy experiments in this thesis.

DOX (10-((3-amino-2,3,6-trideoxy-alpha-L-lyso-hexopyranosyl) oxy)-7,8,9,10-tetrahydro-6,8,11-trihydroxy-8-(hydroxyacetyl)-1-methoxy-5,12-naphthacene-dione), also known among other names as adriamycin, adriablastine, adriacin, or rubex, is an antibiotic and antineoplastic agent of the anthracycline family (Figure 22). Since the early 1970s, anthracyclines (DOX, daunorubicin, idarubicin, etc.) and alkylating agents (cyclophosphamide, melphalan, etc.) are the most versatile and most frequently used chemotherapeutic agents in the clinic [5]. DOX was originally isolated from the aquatic bacterium *Streptomyces peucetius var. coesius* found in the Adriatic Sea. Approximately 500 other active *Streptomyces* products known as rhodomycins because of their colorful red appearance have so far been isolated or derivatized [6, 173].

Anthracyclines are amphipathic molecules consisting of a hydrophobic aglycone heterocycle with a quinone and a hydrochinone functional group and a hydrophilic aminosugar (daunosamine) moiety [174]. Anthracyclines have three protonation sites, one at the amino group of the aminosugar moiety (pKa_1: 8.15) and two at the hydrochinone functional group of the aglycone moiety, one at C_{11} (pKa_2: 10.16) and one at C_6 (pKa_3: 13.2). Protonation at these three sites shifts the color of the molecules from orange to red to blue [175].

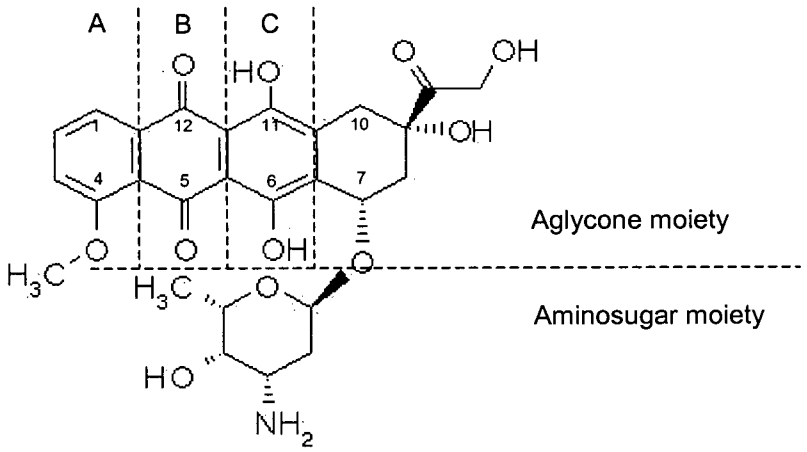

doxorubicin

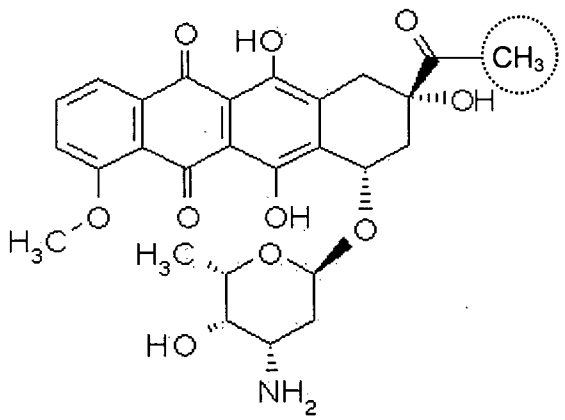

daunorubicin

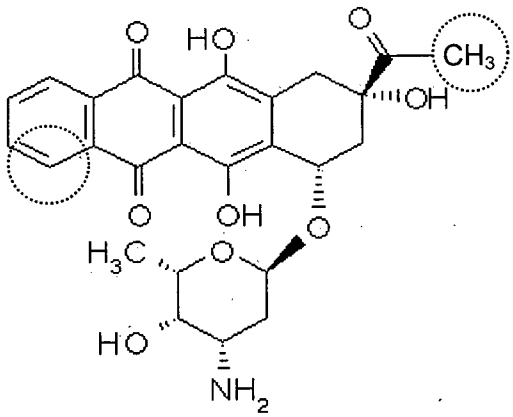

idarubicin

Figure 22: Chemical structures of the anthracyclines DOX, daunorubicin, and idarubicin. (A) methylphenyl ether functional group; (B) quinone functional group, (C) hydrochinone functional group. A + B + C = dihydroxy anthraquinone chromophore. Encircled are structural differences of daunorubicin and idarubicin to DOX.

1.8.1. Physical properties of DOX:

Molecular formula:	$C_{27}H_{29}NO_{11}$
Molecular weight:	543.53 (HCl salt: 579.99)
Melting point:	229-231°C (HCl salt: 204-205°C)
Appearance:	orange-red hygroscopic crystalline needles
Water solubility:	92.8 mg/L at 25°C (0.16 mM)
Partition coefficient:	log P = 1.27 (in n-octanol/water)
pKa_1:	8.15 (amino group in aminosugar moiety) [175]
pKa_2:	10.16 (C_{11}) [175]
pKa_3	13.2 (C_6) [175]
pH in water:	4.0 - 5.5 (at 5 mg/ml)
Dimerization:	> 10^{-5} M [176]
Fluorescence:	λ_{ex} = 470 nm; λ_{em} = 500-600 nm

1.8.2. Liposomal DOX

In the presence of citrate or sulfate, DOX aggregates inside liposomes at concentrations greater than approximately 26 mM, a concentration approximately 100-fold higher than its aqueous solubility limit [81, 177]. Inside the liposomes, 99% of DOX aggregates in the form of crystalline fibrous-bundles, as revealed by cryo-TEM imaging [81]. The planar heterocycles of the aglycone moiety of the DOX molecule stack on top of each other bridged by citrate molecules and form fibers. Fibers align in a hexagonal arrangement with a separation of approximately 3 - 3.5 nm between fibers and form bundles of approximately 12-60 fibres per bundle. Bundles are flexible and twisted every

50 nm by 60° (Figure 23). If DOX molecules are bridged by the smaller sulfate ions, fibers are more rigid with a separation of approximately 2.7 nm between fibers. If DOX molecules are complexed with monovalent lactobionic acid, fibers are not formed at a concentration of 20 mM. At a concentration of 200 mM, individual fibers form but fibers do not aggregate into bundles [81].

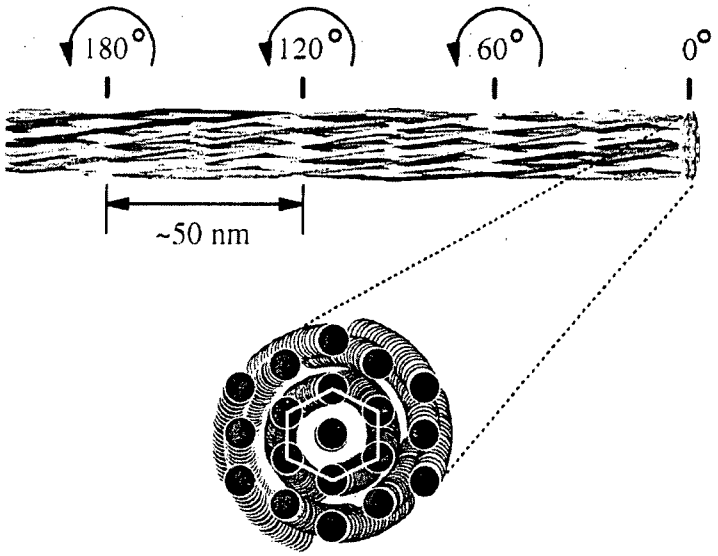

Figure 23: Schematic representation of DOX fibrous bundles (adapted from [81].

1.8.3. Clinical use of DOX and mechanism of action

DOX is used extensively in the treatment of bone and soft tissue sarcomas and carcinomas of the lung, breast, thyroid, bladder, ovary, testis, head, and neck [5, 178]. DOX is also used against leukemias and lymphomas but daunorubicin is the primarily treatment against acute leukemias. The overall response rates for DOX is 45% for thyroid cancer, 41% for lymphomas, 33% for bladder carcinomas, 26% for sarcomas, 25% for ovarian carcinomas, 24% for leukemias [179].

In the body, DOX distributes widely throughout tissues and organs and is cleared from plasma with an elimination half-life of approximately 30 h [6, 179]. In humans, DOX is metabolized in the liver by P450 enzymes including CYP3A4 to doxorubicinol, 7-deoxy-doxorubicinone, and 7-deoxy-doxorubicinolone as the major metabolites. Parent drug and metabolites are excreted in bile and urine [5, 6, 180].

DOX has multiple mechanisms of action but the main antitumor activity of DOX and other anthracyclines stems from their ability to intercalate with DNA resulting in blockade of DNA-, RNA- and protein-synthesis. Anthracyclines are also topoisomerase II inhibitors and can cause DNA single-strand breaks, impair DNA repair, and thus are mutagenic, cancerogenic, and teratogenic [5, 179]. Because of their quinone-hydroquinone functional group, anthracyclines are thought to be involved in free radical formation in the nuclear membrane leading to the formation of oxygen free radical species leading to DNA damage [174]. Thus, DOX is not only active in the S-phase but also in the interphases of the cell cycle. Anthracyclines can interact with cell membranes and have been shown to bind specifically to spectrin, a protein involved in maintenance of membrane structure and to cardiolipin, a phospholipid found in high concentrations in cardiac mitochondria and membranes of malignant cells. This binding preference to cardiolipin may explain cardiotoxic side effects of DOX [5].

Anthracyclines have narrow therapeutic indices. The acute dose-limiting toxicity of DOX is bone-marrow suppression, leukopenia, and stomatitis (inflammation of the mucosa in the mouth) occurring in 80% of treated patients. Other side effects include alopecia (hair loss) (100%), nausea and vomiting (20-55%), cardiac toxicity, i.e. supraventricular arrhythmias, heart block, ventricular tachycardia and even congestive

heart failure in 1-10% of patients. Local reactions include severe pain, erythemas (flushing of the skin) and deep ulceration. The LD_{50} of DOX in mice is 570 mg/kg *p.o.* and 9 mg/kg *i.v.* [5, 179].

Triggered release liposome technology attempts to minimize these severe dose-limiting and effect-limiting side effects of anticancer drugs by localizing the release of chemotherapeutic agents at the tumor site.

1.9. Multidrug resistance (MDR)

A variety of cancers such as ovarian cancer, small cell lung cancer, and advanced breast cancer respond well to chemotherapy but frequently relapse after an initial response [181]. One of the reasons and one of the greatest challenges in the treatment of cancer is the development of MDR [182]. In a few instances, tumors are inherently resistant to chemotherapy, but in most instances tumors develop resistance after a response to the initial treatment. Even more detrimental to the outcome of anticancer therapy is the development of resistance to a large number of drugs that tumor cells were never exposed to and which are structurally and functionally not related to the initial drug. This phenomenon is named MDR, which occurs approximately in one third of all newly diagnosed cases of cancer in North America, and its occurrence usually increases the speed of the disease's progression and limits intervention [183].

The rational behind the development of a thermosensitive liposomal DOX formulation is to expose tumor cells to higher drug concentrations than those that can be achieved by administration of the free drug or non-thermosensitive liposomes. This becomes especially useful in the treatment of MDR tumors overexpressing P-

glycoprotein (PGP), a membrane-bound efflux pump for xenobiotics. The underlying assumption here is that these higher drug concentrations may overcome the increased PGP-mediated drug efflux from MDR tumor cells.

1.9.1. Mechanisms of MDR

Several mechanisms can lead to the development of MDR but one major contributor to the phenomenon is the ability for cells to increase their efflux of xenobiotics such as drug molecules by overexpressing PGP [184]. Other mechanisms are based on increased drug metabolism and mutations of drug binding sites. Associated with these mechanisms of resistance particularly relevant to DOX are overexpression of glutathione-S-transferase and a mutation in the topoisomerase II gene [182, 183, 185], which are discussed briefly in this section. Other mechanisms based on regulation of apoptosis and alteration of signal transduction have been described in the literature but are not discussed in this section.

1.9.1.1. P-glycoprotein (PGP)

PGP is a 170 kDa homoduplex membrane-spanning transport protein encoded in the *mdr*1 gene. The protein structure is well preserved across mammalian species, binds to a variety of structurally unrelated drugs including anthracyclines, vinca alkaloids, epipodophyllotoxins, and taxanes, and acts as an ATP-dependent efflux pump [182]. Highest concentrations of PGP are found in the adrenal cortex and kidneys, and intermediate levels are found in lung, liver, stomach, duodenum, lower jejunum, and colon [183, 186]. PGP is also found in low levels in the placenta and specialised endothelial cells of the brain, testis, and dermis [184]. Since the protein is found mainly

at blood-tissue barrier sites and works against concentration gradients between tissue compartments it is assumed to play a key role in the maintenance of the blood-brain barrier and might be involved in secretory processes [182].

The predominant genetic alteration related to PGP-mediated MDR is overexpression due to gene amplification, but overexpression of PGP has also been described on the level of RNA and protein only [182, 187]. The diagnosis of PGP overexpression is predictive for early disease relapse and poor survival in children with embryonal sarcomas and chemosensitivity is typically inversely correlated with *mdr*1 expression, although exceptions exist. These are named atypical MDR, in which MDR that is not based on PGP overexpression [181].

1.9.1.2. Glutathione-S-transferase

MDR can be caused by overexpression of glutathione-S-transferase, a Phase II metabolic enzyme found mainly in liver and kidney. The enzyme conjugates reduced glutathione to polar xenobiotics including DOX, mitoxantrone, and cisplatin, often after previous Phase I metabolism, and increases xenobiotic excretion through specific active transporters [183]. One such transport protein, named multidrug resistance associated protein can also be overexpressed and contribute to MDR [188]. Since the supply of the conjugation substrate glutathione is limited and can be depleted if not constantly supplied with nutrients, glutathione-S-transferase mediated MDR can cease in contrast to PGP-mediated MDR. Overexpression of glutathione-S-transferase has been considered responsible for MDR especially in tumors of the bladder, ovaries, and stomach [184].

1.9.1.3. Topoisomerase II

During gene transcription and DNA replication and recombination the DNA double helix has to unpack and thus gyrate around its axis. Two enzymes are required for this process, topoisomerase I, which causes transient single strand breaks and topoisomerase II, which causes transient double strand breaks. Strand breaks are resealed by a complex of topoisomerase II and ligases [185]. Several anticancer drugs such as DOX, mitoxantrone, and etoposide bind to topoisomerase II, stabilise DNA-enzyme complexes, prevent DNA religation, and trigger apoptosis [184]. Topoisomerase II-mediated MDR can be caused by mutations of the topoisomerase II drug binding site and downregulation of topoisomerase II protein levels, due to a decreased half-life of the mutant protein, and possibly associated upregulation of topoisomerase I. Topoisomerase II-mediated MDR can be distinguished from other MDR forms by the remaining sensitivity of MDR cells to vinca alkaloids, which do not affect topoisomerase II [185].

1.10. Techniques to study liposomes and phospholipid membranes

1.10.1. Quasi-elastic light scattering (QELS)

QELS (= photon correlation spectroscopy) uses particle-induced interference of a laser beam to derive the particle's size by their Brownian mobility in a solvent. A He/Ne laser beam is focused into a glass tube containing a dilute suspension of particles at constant temperature and viscosity. The light is scattered form particles in all directions. The intensity of the scattered light depends on the molecular weight, the volume, and the shape of the particles as well as on the difference of the refractive indices of particles and the surrounding solvent. The incident light wave with the intensity I_0 represents a rapidly

oscillating electrical field (amplitude E_0, frequency approximately 10^{15} Hz) causing the polarizable (free) electrons of the particles to oscillate at the same frequency. These oscillating electrons give rise to a new oscillating electric field, which radiates in all directions and forms the scattered light wave. Its intensity (I_S) is given by the square of its amplitude (E_S^2). When particles are much smaller than the laser light wavelength, they fall in the so-called Rayleigh region (here approximately 100 nm). All polarizable electrons then oscillate in phase and E_S is proportional to the number of polarizable electrons and thus to the molecular weight (MW) or volume (V) multiplied by the incident wave amplitude E_0. The intensity (I_S) of the scattered light wave is further dependent on the refraction of the particles (n_p) and the solvent (n_s). Thus, I_S is given by:

$$I_S = f(n_p, n_s)\,(MW)^2 \text{ or } V^2\, I_0 \qquad \textit{(Equation 12)}$$

Scattered light waves from many particles interfere at the pinhole aperture of a photomultiplier detector, located usually at a 90° angle to the laser (Figure 24). Thus, the net scattering light intensity fluctuates randomly in time due to Brownian motion of the particles. The key principle QELS uses to determine particle size is the dependence of the time scale of the interference pattern on the particle size. Smaller particles produce rapid fluctuating interference patterns whereas bigger particles produce slow fluctuating interference patterns. Thus, QELS determines the diffusion coefficient (D) and the particle radius (R) from the fluctuating light scattering signal using the Stokes-Einstein relation:

$$D = KT / 6\,\pi\,\eta\,R \qquad \textit{(Equation 13)}$$

where K = Boltzmann's constant, T = temperature, and η = shear viscosity of the solvent.

From this equation it becomes apparent why the solvent's temperature and viscosity have to be kept constant (Nicomp 370, Submicron particle sizer manual).

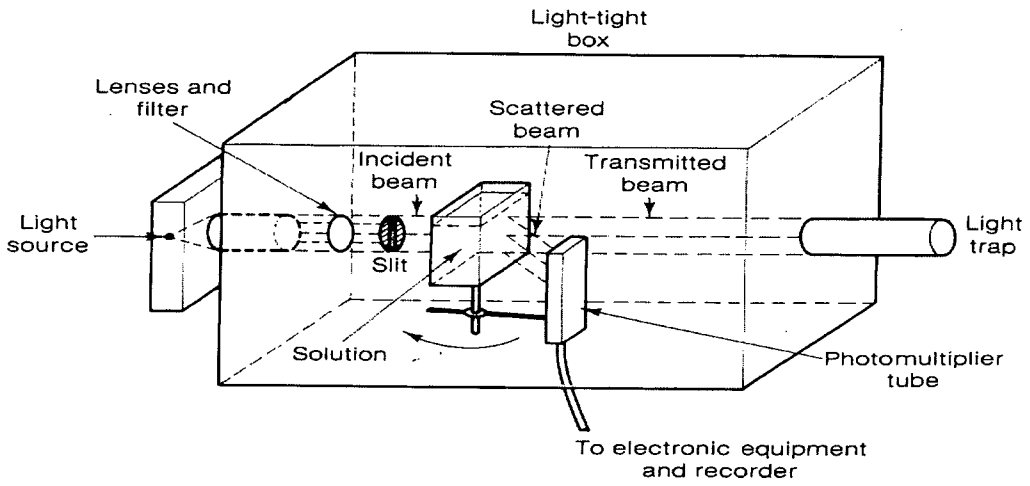

Figure 24: Schematic representation of the QELS apparatus (adapted from [189]).

1.10.2. Fluorescence quenching and fluorescence excimer formation

Fluorescence occurs generally in polyaromatic hydrocarbons or heterocycles (fluorophores). These molecules can absorb photons of the energy $h\nu_{EX}$ (h = Planck's constant, ν = frequency) and become excited into the singlet excited state (S_1'). This process distinguishes fluorescence from chemoluminescence in which the excited state is caused by a chemical reaction. The singlet excited state exists for a finite time (typically 1–10 nsec) during which the fluorophore undergoes conformational changes and interacts with its environment. The energy of the singlet excited state (S_1') is thus partially dissipated, yielding a relaxed singlet excited state (S_1) from which fluorescence emission originates. A photon with the energy $h\nu_{EM}$ is emitted and the fluorophore returns to its ground state (S_0). Due to energy dissipation during the excited-state lifetime, the energy of the emitted photon is lower, and therefore of longer wavelength, than the excitation photon with the energy $h\nu_{EX}$. The difference in energy or wavelength ($h\nu_{EX}$ - $h\nu_{EM}$) is called the Stokes shift [190] (Figure 25).

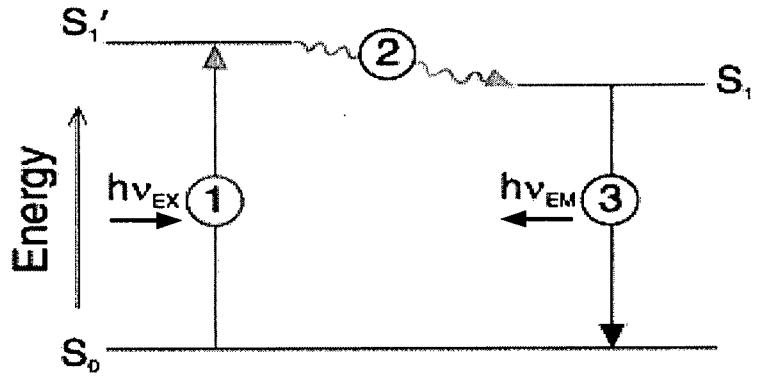

Figure 25: Jablonski diagram illustrating fluorescence. ① Excitation of the fluorophore from the ground state (S_0) to the singlet excited state (S_1'); ② Partial energy dissipation to the relaxed singlet excited state (S_1); ③ Fluorescence emission and return to the ground state (modified from [190]).

The fluorescence intensity is defined by the Beer–Lambert law as the product of the molar extinction coefficient, optical path length, and solute concentration, as well as on the fluorescence quantum yield of the fluorophore, the excitation source intensity, and the fluorescence collection efficiency of the instrument. In dilute solutions or suspensions, the fluorescence intensity is linearly proportional to the concentration of the solute. When the sample's absorbance intensity exceeds a value of approximately 0.05 at a path length of 1 cm, the relationship becomes non-linear because too much light is absorbed in the solution (inner filter effect) and due to self-absorption of the fluorescence emission (self-quenching). During fluorescence quenching, the fluorescence quantum yield decreases but the fluorescence emission spectrum is not affected. Some excited fluorophores such as pyrenehexadecanoic acid (PHDA) interact with each other and form excited-state dimers (excimers). In contrast, to self-quenching, this process alters the fluorescence emission spectrum (Figures 26 and 27).

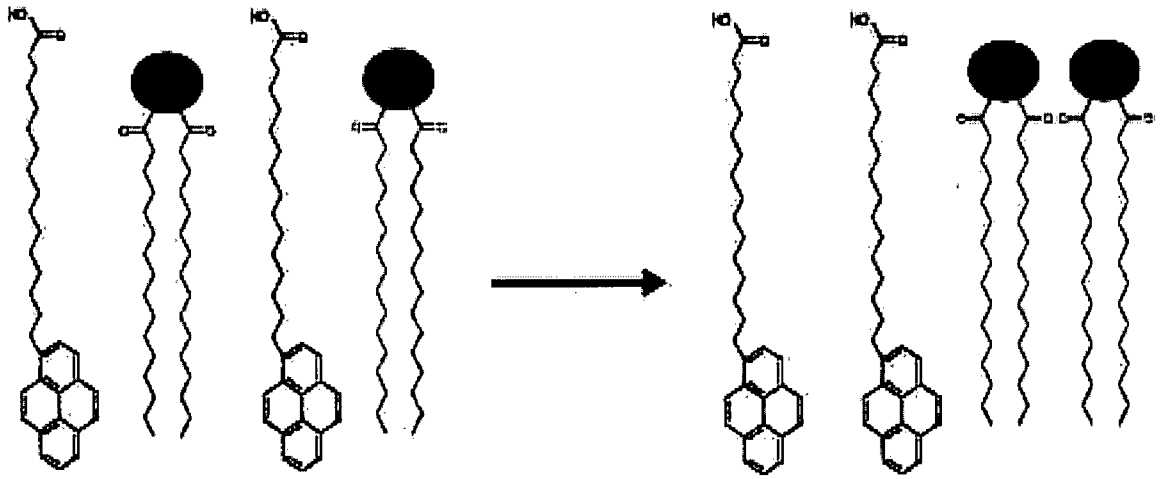

Pyrene monomer fluorescence: λ_{em} = 378 nm Pyrene excimer fluorescence: λ_{em} = 470 nm

Figure 26: Schematic representation of excimer formation by pyrenehexadecanoic acid (PHDA) in a phospholipid membrane. Locally concentrated PHDA emits red-shifted fluorescence due to excimer (excited state dimer) formation when excited at λ_{ex} = 320 nm.

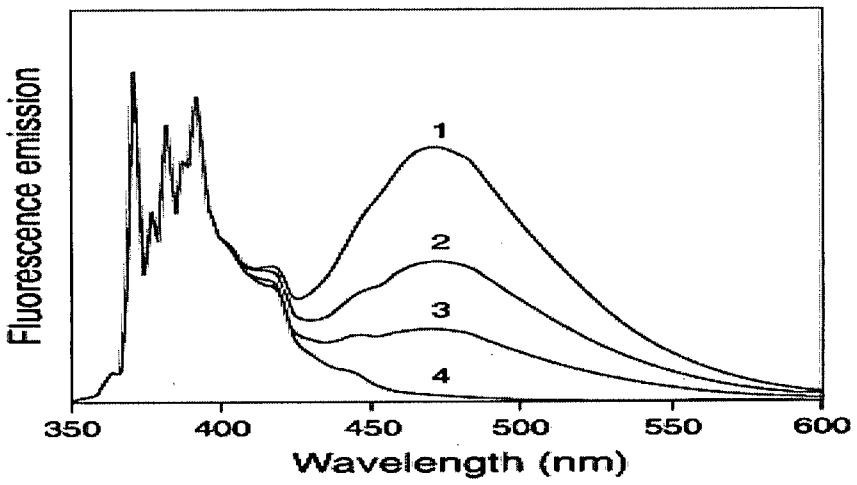

Figure 27: Effect of pyrene excimer formation on the fluorescence emission spectrum. (1) 2 mM pyrene, purged with argon to remove oxygen; (2) 2 mM pyrene, air-equilibrated; (3) 0.5 mM pyrene (argon-purged), and (4) 2 μM pyrene (argon-purged).

1.10.3. Differential scanning calorimetry (DSC)

In most DSC instruments, two metal pans, one empty reference pan and one identical pan containing the sample, sit on a pair of platforms connected to a heater and a platinum resistance thermometer (or thermocouple). Both pans are heated at the same rate, usually at approximately 2-10°C per minute. The temperatures of the two platforms are compared and the electrical power supplied to each heater and adjusted so that the temperatures of both the sample and the reference remain equal to the programmed temperature (Figure 28). The amount of energy that has to be supplied to or withdrawn from the sample to keep the temperatures the same between the sample and the reference is displayed as the ordinate of a DSC thermogram. The rate of energy absorption by the sample is proportional to the specific heat of the sample since the specific heat at any temperature determines the amount of thermal energy necessary to change the sample's temperature. Exothermic or endothermic enthalpy changes associated with absorption or generation of heat are computed into peaks of DSC thermograms, whose areas under the curve are proportional to the total enthalpy change. The measuring principle in DSC is the comparison of the heat flow rate between the sample and the reference pan, which are heated or cooled at the same rate. Analysis of a DSC thermogram enables the determination of the transition temperature (T_C) onset, peak, and maximum (T_{max}) and the enthalpy of the transition (ΔH). The onset temperature (T_C) is extrapolated and the enthalpy value is calculated from the area under the transition peak. The sharpness of the transition peak ($\Delta T_{½}$) can be measured as the width at half-peak height and is an index of the cooperative nature of the transition [57].

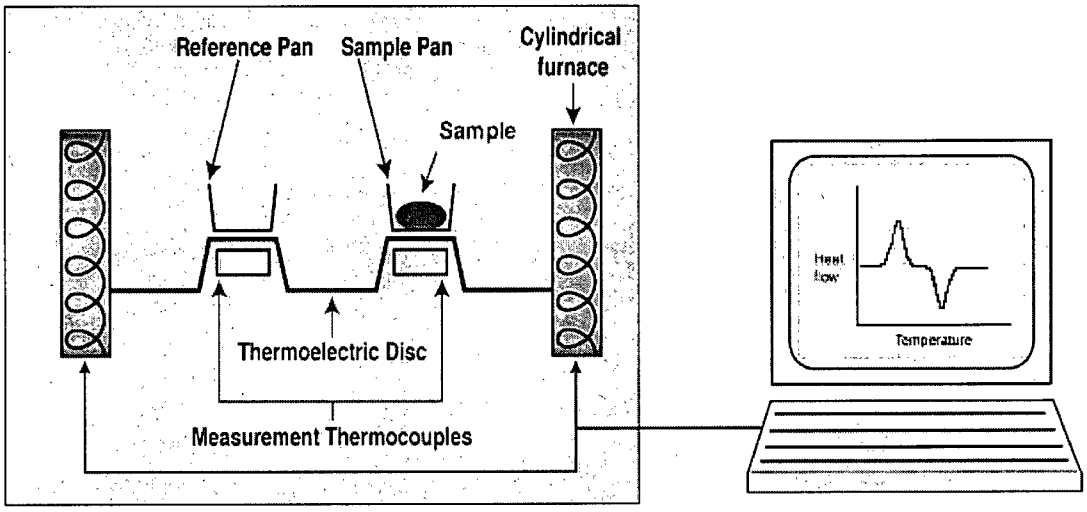

Figure 28: Schematic representation of the DSC apparatus.

1.10.4. Cryogenic transmission electron microscopy (cryo-TEM)

Liposome samples for cryo-TEM analysis are prepared in vitrified water. Vitrified water is solid amorphous water that forms when water is cooled so rapidly that water molecules are prevented from arranging in a crystal lattice structure. The formation of cubic ice crystals that may destroy fragile structures in the sample is therefore prevented and water and sample molecules are solidified in a similar structure as they were in the liquid state [191, 192]. Spherical objects such as liposomes appear in the two-dimensional cryo-TEM image as circles with a dark rim, where the material density is highest. Disc-shaped objects in a face-on position appear as circles or ovals, depending on their position in the sample, without a dark rim. Disc-shaped objects in an edge-on position appear as dark lines (Figures 29-30).

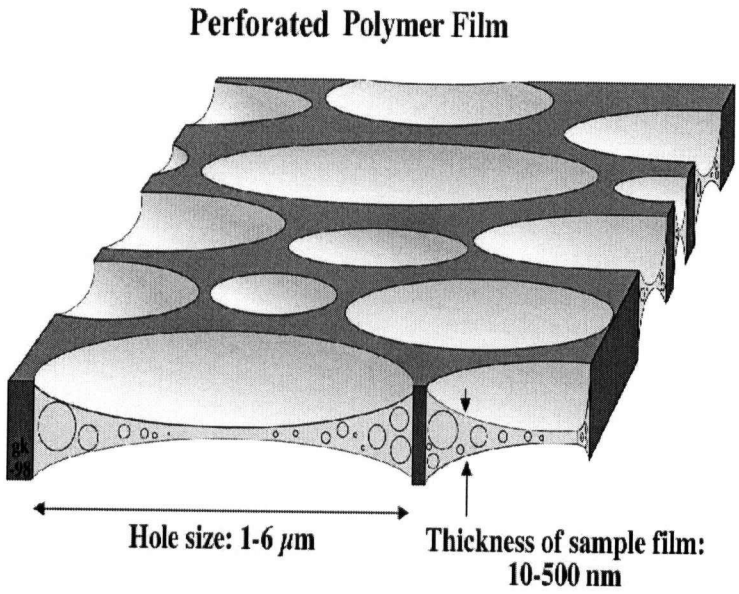

Figure 29: Schematic representation of vitrified liposomes in a perforated polymer film (adapted from[193]).

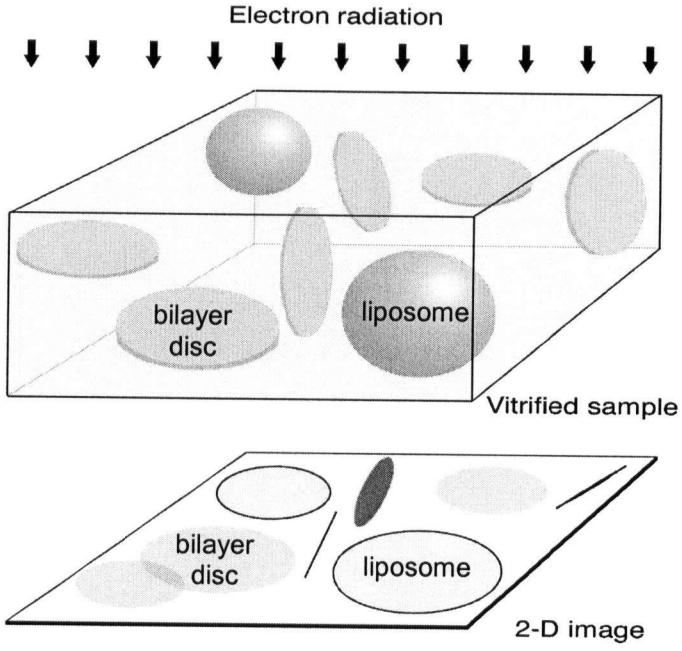

Figure 30: Resemblance of liposomes and bilayer discs on a 2-dimensional cryo-TEM image (modified from [193]).

2. HYPOTHESES AND OBJECTIVES

2.1. Hypotheses

A) Lysolipids accumulate in grain boundaries of the LTSL membrane as a result of lateral phase separation upon cooling liposomes through their T_C.

B) Drug release is triggered at a temperature close to the T_C of the formulation as a result of lysolipids leaving the membrane and creating membrane defects or by physical alterations of the liposome membrane structure.

C) The extremely rapid drug release properties of LTSL will be beneficial in the use of LTSL as drug delivery vehicles in the treatment of solid tumors overexpressing PGP.

2.2. Objectives

A) To characterize the effect of lysolipid incorporation into the membrane of cholesterol-free liposomes on drug encapsulation with the DOX as the model drug.

B) To characterize the impact of lysolipids on DOX release from LTSL *in vitro* and *in vivo*.

C) To characterize altered membrane properties associated with the presence of lysolipids in the liposome membrane.

D) To determine the plasma and tissue distribution time-profile as well as the efficacy of LTSL-DOX in mice bearing a human breast cancer MDR tumor xenograft.

3. EXPERIMENTAL

3.1. Chemicals

1,2-Distearoyl-*sn*-glycero-3-phosphatidylcholine (DSPC), 1,2-dipalmitoyl-*sn*-glycero-3-phosphatidylcholine (DPPC), 1,2-dimytyroyl-*sn*-glycero-3-phosphatidyl-choline (DMPC), 1-palmitoyl-2-hydroxy-*sn*-glycero-3-phosphatidylcholine (MPPC), 1-stearoyl-2-hydroxy-*sn*-glycero-3-phosphatidylcholine (MSPC), and 1,2-distearoyl-*sn*-glycero-3-phosphatidylethanol-amine-N-[methoxy(polyethylene glycol)-2000] (DSPE-PEG_{2000}) were purchased from Avanti Polar Lipids Inc. (Alabaster, AL). Palmitic acid was purchased from Nu-Chek Prep Inc. (Elysian, MN). ^{3}H-Cholesterol hexadecyl ether was obtained from Amersham Pharmacia Biotech (Piscataway, NJ) or from Perkin Elmer Life Sciences, Inc. (Boston, MA). ^{14}C-Methylamine hydrochloride was obtained from Amersham Pharmacia Biotech (Piscataway, NJ). ^{14}C-1-Palmitoyl-2-hydroxy-*sn*-glycero-3-phosphatidylcholine (^{14}C-MPPC) was obtained from Perkin Elmer Life Sciences, Inc. (Boston, MA). 1-Pyrenehexadecanoic acid was purchased from Molecular Probes, Inc. (Eugene, OR). Doxorubicin-HCl (DOX) vials containing 10 mg of DOX and 52.6 mg of lactose were purchased from Pharmacia & Upjohn Co. (Kalamazoo, MI) or from Faulding (Vaudreuil, QC, Canada). N-[2-hydroxyethyl]piperazine-N'-[2-ethanesulfonic acid] (HEPES), cholesterol, n-octyl β-D-glucopyranoside (OGP), sodium dodecyl sulfate (SDS), and Sephadex G-50 were purchased from Sigma Chemical Company (St. Louis, MO). Triton® X-100 was obtained from Bio-Rad Laboratories (Richmond, CA). Ketalean® (ketamine HCl containing 0.01% benzethonium chloride as a preservative) and Xylamax® (xylazine HCl containing 0.9% methylparaben and 0.1% propylparaben as preservatives) were purchased from Bimeda-MTC Cambridge, ON, Canada). Atravet® (acepromazine maleate) were purchased from Ayerst Laboratories, Montreal, MO,

Canada). Dulbecco's Modified Eagle's Medium (DMEM) and Hank's Balanced Salt Solution (with and without Ca^{2+} and Mg^{2+}) (HBSS) was purchased from StemCell Technologies Inc. (Vancouver, BC, Canada). Other chemicals were purchased from common sources. All chemicals were of reagent grade and used without further purification.

3.2. Buffers

Citrate buffer:

Citrate buffer (300 mM), pH 4, was prepared by dissolving 18.9 g of sodium citrate dihydrate and 18.0 g of citric acid monohydrate in 500 ml of distilled water. Citrate buffers at other pH were prepared by dissolving 31.515 g of citric acid in 500 ml of distilled water. Buffers were titrated to the desired pH with concentrated sodium hydroxide solution. To prevent bacterial growth, citrate buffers were filtered through 0.22 μm cellulose acetate filters (Easy flow™ Filter, Becton Dickinson and Company, Frankin Lakes, NJ) and stored at a temperature of 4°C.

HEPES buffered saline (HBS) stock solution:

HBS was prepared by dissolving 9.532 g of HEPES and 17.532 g of sodium chloride in 500 ml of distilled water. The buffer was titrated to pH 7.5 with concentrated sodium hydroxide solution. Before use, the stock solution was diluted 1:4 (vol/vol) resulting in HBS at a concentration of 20 mM HEPES and 150 mM NaCl.

Sodium carbonate buffer:

Sodium carbonate buffer (0.5 M) was prepared by dissolving 5.299 g of Na_2CO_3 in 500 ml of distilled water.

3.3. Preparation of liposomes

TSL were composed of DPPC/DSPE-PEG_{2000} (molar ratio: 90:4). LTSL were composed of DPPC/MPPC/DSPE-PEG_{2000} or DPPC/MSPC/DSPE-PEG_{2000} (molar ratio: 90:10:4). NTSL were composed of DSPC/Cholesterol/DSPE-PEG_{2000} (molar ratio: 55:45:5). Liposomes were prepared by the lipid film hydration method [51]. Briefly, lipids and cholesterol were dissolved in chloroform and combined with trace amounts of [^{3}H]-cholesterol hexadecyl ether as a liposome marker [194]. For special liposome preparations, trace amounts of [^{14}C]-MPPC, or PHDA were added. MPPC and MSPC were dissolved in chloroform/methanol (2.5:1 vol/vol). For liposomes containing PHDA, all lipids were dissolved in chloroform/methanol (2.5:1 vol/vol).

The solvent of the lipid mixture was evaporated under a gentle stream of nitrogen gas until the solution became viscous. Lipid films were flash-dried under high vacuum (29.5" Hg = 13.33 mbar = 98.7% vacuum) for 1 h to increase the lipid film surface area and stored under low vacuum (22" Hg = 267 mbar = 74% vacuum) overnight to remove traces of solvents. Dried lipid films were either used immediately or stored at a temperature of -20°C under a nitrogen atmosphere.

Lipid films were hydrated with 300 mM citrate buffer, pH 4 for at least 45 min at a concentration of 100 mg/ml and a temperature of 55°C for LTSL and TSL or 60°C for NTSL, a temperature approximately 10 degrees higher than the T_C of the bulk lipid. Only NTSL were frozen in liquid nitrogen and thawed at 60°C five times before extrusion. Liposomes were extruded ten times through two stacked polycarbonate track-etch membranes with a pore size of 100 nm (Whatman Inc. Nuclepore, Newton, MA) at a temperature of 55°C for LTSL and TSL or 60°C for NTSL using a thermobarrel extruder

(Lipex Biomembranes Inc., Vancouver, B.C., Canada) attached to a Julabo VC5/3 circulating water bath (Julabo Labortechnik GmbH, Seelbach, Germany).

3.4. Particle size determination by QELS

For size determination of liposomes by QELS, liposomes were diluted with 0.9% sodium chloride solution to a concentration of approximately 2 mg/ml in disposable borosilicate glass tubes (Kimble glass Inc., Vineland, N.J., USA) and analyzed on a fixed-angle Nicomp 270 Submicron Particle Sizer (Pacific Scientific, Santa Barbara, CA). Measurements were taken at a temperature of 23°C, a wavelength of 633 nm, and a count rate of approximately 350 kHz. The channel width was automatically set at approximately 11-13 μsec, the viscosity was set at 0.945 cp, and the refraction index at 1.334. For size determinations of liposomes, the volume-weighted Gaussian analysis for vesicles was used and each sample was analyzed for at least 7 min. The accuracy of size determinations was evaluated by measuring the size distribution of a 90 nm Nanosphere™ particle standard (Duke Scientific Corporation, Palo Alto, CA) consisting of polymer microspheres in water with an average size of 92 nm ± 3.7 nm.

3.5. Turbidity measurements

As a second method of assessing changes in particle size, the absorbance of light (turbidity) in the liposome sample was determined on a Beckman DU-64 UV-visible spectrophotometer (Beckman Instruments Inc., Fullerton, CA) at a wavelength of 350 nm, the absorbance maximum for LTSL. Liposomes were diluted in HEPES buffered saline (pH 7.5) at a concentration of 20 mg/ml. The absorbance of samples was

measured after equilibrating the sample to room temperature before and after heating the samples repetitively to a temperature of 45°C for 10 min.

3.6. Determination of transmembrane pH gradients

Transmembrane pH gradients were measured according to the procedure by Harrigan *et al.* [195, 196] using methylamine as a proton marker. Trace amounts of ^{14}C-methylamine at approximately 0.2 μCi were incubated at a temperature of 37°C for 10 min with ^{3}H-cholesterol hexadecyl ether (^{3}H-CHE)-labelled LTSL containing MPPC and NTSL bearing a pH gradient across the membrane. Unencapsulated ^{14}C-methylamine was removed on a Sephadex G-50 mini-column in a centrifugal field of 680 g for 2 min. Methylamine concentrations before and after separation of unencapsulated methylamine were determined based on scintillation counts of the ^{14}C- and ^{3}H-labels. pH Gradients across the liposome membrane were calculated by determining methylamine concentrations outside and inside liposomes (see section 1.4.2.). To calculate the methylamine concentration inside the liposomes, trapped volumes of LTSL were determined by hydrating ^{3}H-CHE-labelled lipid films with 300 mM citrate buffer, pH 4, containing trace amounts of ^{14}C-labelled lactose (2 μCi/ml). Liposomes were extruded as described in section 3.3. and unencapsulated lactose was removed from the sample on a Sephadex G-50 mini-column in a centrifugal field of 680 g for 2 min. The trapped volume was calculated based on scintillation counts for ^{3}H and ^{14}C before and after removing unencapsulated lactose. The mean trapped volume of LTSL was determined at 1.35 μl/μmol lipid. The mean trapped volume of NTSL was determined previously at 1.2 μl/μmol lipid [51].

pH Gradients and trapped volumes were calculated as follows since the ratio of entrapped to unentrapped methylamine is directly related to the pH gradient across the membrane:

$$CH_3NH_3^+ \rightleftharpoons CH_3NH_2 + H^+$$

$$K_d = \frac{[CH_3NH_2][H^+]}{[CH_3NH_3^+]} \qquad \textit{(Equation 14)}$$

Assuming the dissociation constant outside the liposomes $(K_d)_{out}$ is equal to the dissociation constant inside the liposomes $(K_d)_{in}$:

$$\frac{[CH_3NH_2]_{out}[H^+]_{out}}{[CH_3NH_3^+]_{out}} = \frac{[CH_3NH_2]_{in}[H^+]_{in}}{[CH_3NH_3^+]_{in}} \qquad \textit{(Equation 15)}$$

At equilibrium $[CH_3NH_2]_{out} = [CH_3NH_2]_{in}$ as the neutral molecule is membrane permeable, thus:

$$\frac{[CH_3NH_3^+]_{in}}{[CH_3NH_3^+]_{out}} = \frac{[H^+]_{in}}{[H^+]_{out}} \qquad \textit{(Equation 16)}$$

The trapped volume (A) of 100 nm liposomes in μl/μmol was calculated by dividing the volume trapped inside the vesicles (M) in μl by the amount of lipid in μmol eluted from the column (L) (A = M / L).

$$M = \frac{[^{14}C]\text{-counts in 10 } \mu\text{l eluted from the column in dpm}}{[^{14}C]\text{-counts in 10 } \mu\text{l of the initial liposome suspension before separation on the column in dpm}} \qquad \textit{(Equation 17)}$$

$$L = \frac{[^{3}H]\text{-counts in 10 } \mu\text{l eluted from the column in dpm}}{\text{specific activity of the lipid stock solution in dpm/}\mu\text{mol}} \qquad \textit{(Equation 18)}$$

The methylamine concentration inside the liposomes (Y) in dpm/µl was calculated by:

$$Y = \frac{[^{14}C]\text{-counts in 10 } \mu l \text{ eluted from the column in dpm}}{M} \qquad \textit{(Equation 19)}$$

To calculate the methylamine concentration outside the liposomes, the total trap-volume in 100 µl of the initial liposome suspension (T) was calculated by:

$$T = \frac{[^{14}C]\text{-counts in 10 } \mu l \text{ of the initial liposome suspension before separation on the column in dpm} \quad M}{\text{specific activity of the lipid stock solution in dpm/}\mu\text{mol}} \qquad \textit{(Equation 20)}$$

The concentration of unentrapped methylamine outside the liposomes (V) in dpm/µl was calculated by:

$$V = \frac{[^{14}C]\text{-counts in 10 } \mu l \text{ of the initial liposome suspension before separation on the column in dpm} \quad - T\ Y}{10} \qquad \textit{(Equation 21)}$$

The pH gradient across the liposome membrane can thus be calculated by:

$$-\Delta pH = \log\frac{Y}{V} \qquad \textit{(Equation 22)}$$

Since the pH gradient is given by

$$-\Delta pH = \log\frac{[CH_3NH_3^+]_{in}}{[CH_3NH_3^+]_{out}} \qquad \textit{(Equation 23)}$$

3.7. pH Gradient-dependent drug loading of liposomes

DOX was encapsulated into liposomes using the pH-gradient driven loading protocol by Mayer *et al.*, also referred to as "remote drug loading" [78, 80, 197]. The pH gradient across the liposome membrane was generated using two different methods. In one method (buffer exchange method), the extravesicular 300 mM citrate buffer (pH 4) was exchanged with 20 mM HEPES, 150 mM NaCl buffer (pH 7.5) on a Sephadex G-50 column. In a second method (titration method), the extravesicular citrate buffer was titrated to pH 7.5 by adding 0.5 M sodium carbonate solution (pH 11.2) to liposomes at a volume ratio of 0.63. To encapsulate DOX into pH-adjusted liposomes, both DOX solution at a concentration of 5.88 mg/ml in 0.9% saline or at 10 mg/ml in distilled water and liposomes at a concentration of 100 mg/ml were preheated for 10 min to a temperature of 36°C ± 1°C for TSL and LTSL or to 60°C ± 1°C for NTSL. DOX solution was added at a drug-to-lipid ratio of 0.05 mg/mg for TSL and LTSL or 0.2 mg/mg for NTSL. The mixture was incubated for 40 min in a Julabo VC5/3 circulating water bath (Julabo Labortechnik GmbH, Seelbach, Germany) with intermittent vortex mixing every 10 min at a temperature of 36°C ± 1°C for TSL and LTSL or for 10 min at 60°C ± 1°C for NTSL if not stated otherwise. The sample was cooled down to room temperature and unencapsulated drug was removed on a Sephadex G-50 mini-column in a centrifugal field of 680 g for 2 min, if encapsulation was not complete.

3.7.1. Determination of the degree of DOX loading

The amount of encapsulated DOX was calculated by determining the drug-to-lipid weight ratio before and after free DOX separation. The amount of lipid in the sample was determined by counting 2 x 10 µl of sample before and after free DOX separation on

a Sephadex G-50 mini-column in 5 mL of Pico-Fluor™ 15 scintillation cocktail (Packard, Meriden, CT) on a Packard 1900 scintillation counter (Packard, Meriden, CT). Lipid concentrations were calculated based on the initial ^{3}H-cholesterol hexadecyl ether labelling efficiency of the liposome preparation. The amount of DOX in the sample was determined fluorometrically. Aliquots of 50 μl sample were separated on a Sephadex G-50 mini-column in a centrifugal field of 680 g for 2 min to remove free DOX. For *in vitro* assays, 5 μl of the sample and the spin column eluent were diluted in 100 μl HEPES and 900 μl of 1% Triton X-100. The mixture was boiled, cooled down to room temperature and analyzed on a Perkin Elmer Luminescence Spectrometer LS50 B (Perkin Elmer, Wellesley, MA) with an excitation wavelength (λ_{ex}) of 470 nm and an emission wavelength (λ_{em}) of 550 nm. The amount of DOX in the sample was derived from a standard curve.

3.8. DOX extraction from blood and tissues

Plasma samples were used directly without further dilution. Tissues and organs were homogenized using a Polytron PT-MR 3100 tissue homogenizer (Kinematica AG, Littau, Switzerland) and diluted with distilled water (10% weight per volume for liver tissue, 50% weight per volume for other tissues). DOX standards were prepared in glass test tubes containing control tissues or HBS with 0, 20, 80, 160, 320, 640, 800, 1600, 3200, 6400, 8000, or 12800 ng DOX per tube.

Either 200 μl of tissue homogenate or a defined volume of plasma was adjusted to 200 μl with distilled water and placed into a test tube. To the diluted sample, 600 μl of distilled water was added followed by 100 μl of 10% sodium dodecyl sulfate (SDS) and

100 µl of 10 mM sulfuric acid. After brief mixing on a vortex mixer, 2 ml of isopropanol/chloroform (1:1 vol/vol) was added and each test tube was mixed on a vortex mixer for 1 min. Samples were frozen at a temperature of -20°C overnight or at -80°C for at least 2 h in order to promote protein aggregation. Samples were thawed at room temperature, mixed again on a vortex mixer for 1 min, and the organic (bottom) phase was separated from the aqueous (top) phase and proteins (interphase) on an Eppendorf centrifuge 5810 R (Eppendorf-Netheier-Hinz GmbH, Hamburg, Germany) at 1500 g for 20 min. The bottom layer was carefully transferred into a clean glass tube with a Pasteur pipette and the test tube was sealed to prevent solvent evaporation. Samples were analyzed by fluorescence spectroscopy (λ_{ex} 470 nm, λ_{em} 550 nm) on a Perkin Elmer Luminescence Spectrometer LS50 B (Perkin Elmer, Wellesley, MA). The amount of doxorubicin in the sample was derived from a standard curve.

3.9. Determination of the lysolipid content of liposomes

Liposome aliquots were dissolved in 950 µl of methanol/chloroform (9:1 vol/vol). To determine MPPC concentrations, 100 µl of sample were injected into the injection port of the HPLC apparatus without further dilution. To determine DPPC concentrations, 1 ml of methanol/chloroform (90:1 vol/vol) containing DMPC as an internal standard at a concentration of 1.5 mg/ml was added to 200 µl of dissolved sample and 20 µl of that dilution were injected into the injection port of the HPLC apparatus. Lipids were separated at a temperature of 30°C on a Waters 2690 separation module equipped with a Symmetry C8 (4.6 x 250 mm i.d.) reverse phase column (Waters Co., Milford, MS). The column was eluted with 100% methanol as the mobile phase at flow rate of 1.0 ml/min. Phospholipids were detected on a SEDEX Model 75 evaporative light scattering detector

(S.E.D.E.R.E., Alfortville Cedex, France) at a temperature of 50°C and a nitrogen pressure of 3.5 bar in the evaporation chamber. Chromatography peaks were identified by comparison of their retention times with those of authentic standards. MPPC could be separated from MSPC. Amounts of MPPC present in the sample were determined by dividing the area under the curves by the slope of calibration curves of authentic standards. Amounts of DPPC present in the sample were determined by dividing the ratios of areas under the phospholipid curves and those of the internal standard by the slope of calibration curves from ratios of the authentic standard and the internal standard.

3.10. DOX dequenching assay

Since DOX is a fluorescent compound, the principle of fluorescence self-quenching was used to determine release rates for DOX from TSL and LTSL. DOX molecules form dimers and thus self-quench above a concentration of approximately 10^{-2} mM (= 0.01 μmol/ml) [176]. In liposomes loaded at a drug-to-lipid ratio of 0.05 mg/mg the DOX concentration is approximately at 6.5 mM. Thus, the fluorescence signal of DOX molecules is self-quenched inside liposomes.

LTSL-DOX at a volume of 10 μl and a DOX concentration of 2 mg/ml were diluted with 2.99 ml of HBS buffered saline in a 3 ml quartz cuvette (Hellma GmbH & Co KG, Müllheim, Germany). The cuvette was equilibrated to a temperature of 37°C, 38°C, 39°C, 40°C, 41°C, or 42°C. The fluorescence intensity was measured at a fixed time interval every 1-10 sec for 10 min and every 5-10 min thereafter on a Perkin Elmer Luminescence Spectrometer LS50 B (Perkin Elmer, Wellesley, MA). After 2.5 h or 4 h, 300 μl of the detergent n-octyl β-D-gluco-pyranoside (OGP) at a concentration of 250 mM was added to release all encapsulated DOX. The relative amount of released DOX

was derived from a standard curve and calculated based on the 100% value after addition of OGP.

3.11. Determination of permeability coefficients

Permeability coefficients for LTSL and TSL were calculated from drug release curves generated by the DOX dequenching assay. The permeability coefficient (P) is defined as: $P = J / (A\ \Delta C)$ *(Equation 24)*

where J = drug flux (μmol/sec), A = total liposome membrane surface area (cm^2), and ΔC = drug concentration gradient across the liposome membrane ($\mu mol/cm^3$) [198]. Drug flux (J) across the liposome membrane is equivalent to the drug release constant and can be derived from the initial linear slope of the drug release graph. The total membrane surface area (A) was calculated from the relationship:

A = total moles of lipid N_A average lipid molecular area *(Equation 25)*

where N_A = Avogadro's number = 6.022×10^{23}. The value of 0.6 nm^2 was used as the average lipid molecular area [199], and the total amount of moles of lipid was calculated at approximately 0.5 μmol.

Since the concentration of lipids in the DOX dequenching assay was at 0.13 mg/ml and the average molecular weight of lipids in LTSL is 789.95, the lipid concentration was at 0.169 μmol/ml, which calculates to approximately 0.5 μmol of lipid in the 3 ml cuvette. However, only 0.25 μmol of lipid was used for calculating the total membrane surface area since the membrane consists of a double layer. Thus, the total membrane surface area (A) was calculated at 914.3 cm^2. The trapped volume of LTSL was determined at 1.35 μl/μmol lipid, which calculated to a total trapped volume of 0.6 μl for 0.5 μmol lipid. At a drug-to-lipid ratio of 0.05 mg/mg and a molecular weight of

DOX-HCl at 579.99, the total amount of DOX in liposomes was calculated to 0.0345 μmol in 0.6 μl, which calculates to a concentration of 0.0568 μmol/μl. Since there was no DOX outside of liposomes initially, ΔC was calculated at 56.8 μmol/cm^3.

3.12. Pyrene hexadecanoic acid (PHDA) accumulation assay

To determine rearrangements of lysolipids in the liposome membrane, the fluorescent label PHDA was used as a marker to monitor the local distribution of lysolipids in the liposome membrane [200]. PHDA was added to the membrane of LTSL, TSL, and NTSL at a concentration of 5 mol%. The absorption maximum of PHDA in water is at a wavelength of 322 nm. When excited at this wavelength, the emission maximum of the monomer is at 378 nm and shifts to 470 nm when PHDA dimers (excimers) are formed. Thus, accumulation of PHDA in the liposome membrane can be monitored by the PHDA monomer/excimer ratio (E/M ratio).

PHDA was dissolved in chloroform/methanol (2.5:1 vol/vol) at a concentration of 8 mg/ml. The PHDA solution was stored at RT because the compound crystallized when stored in the fridge. TSL containing PHDA at a concentration of 0.2, 2, 5, and 10 mol% and LTSL and NTSL containing 5 mol% PHDA were prepared at a lipid concentration of 100 mg/ml in 300 mM citrate buffer, pH 4, (see also section 4.3.7.) by dissolving appropriate amounts of lipid and PHDA in chloroform/methanol (2.5:1 vol/vol). When liposomes were prepared from lipids dissolved in 100% chloroform, extrusion was slow indicating deposition of lipid, presumably PHDA, on the filter membrane. PHDA-containing liposomes were diluted to a lipid concentration of 1 mg/ml and 30-50 μl of this dilution was mixed with 1.45-1.47 ml citrate buffer (300 mM) in a quartz cuvette (Hellma GmbH & Co KG, Müllheim, Germany). The final lipid concentration was 20-30

μg/ml. Samples were analyzed on a Luminescence Spectrometer LS50 B (Perkin Elmer, Wellesley, MA). The peak excitation was at 322.8 nm. When excited at 322 nm, the peak emission of the monomer was at 378.0 nm, the peak emission of the excimer was at 450-500 nm with a maximum at approximately 470 nm. There was no interfering peak of liposomes without PHDA in citrate buffer. The excited state lifetime has been reported by the PHDA manufacturer to be dependent on the presence of oxygen in the buffer. Thus, oxygen was removed from samples by purging nitrogen through the cuvette for 30 min and subsequently sealing cuvette was with parafilm. However, there was no difference observed between emission spectra in the presence or absence of oxygen. For the PHDA accumulation assay, liposome samples were kept at a temperature of 38-40°C in the fluorometer by heating the cuvette holder with a Julabo VC5/3 circulating water bath (Julabo Labortechnik GmbH, Seelbach, Germany).

3.13. Lysolipid membrane retention assay

LTSL were labeled with trace amounts of ^{14}C-MPPC and ^{3}H-CHE at a ratio of 0.7 by adding appropriate amounts of dissolved labels to lipids dissolved in chloroform. Liposomes were prepared by the method of lipid film hydration in 300 mM citrate buffer, pH 4. The sample was split in half and one half was kept at a temperature of 22°C, the other half was heated to a temperature of 50°C. The outside buffer of both samples was exchanged with HBS, pH 7.5, on a Sephadex G-50 column. The lysolipid/lipid ratio determined by the ^{14}C-MPPC / ^{3}H-CHE ratio of liposomes in HBS was calculated by counting 10 μl aliquots of sample before and after buffer exchange on Packard 1900 scintillation counter (Packard, Meriden, CT).

3.14. Differential scanning calorimetry (DSC)

DSC was used to determine the T_C of thermosensitive liposomes. Liposome samples were transferred into sample pans (Perkin Elmer, Norwalk, CT) at a volume of 30 μl and a concentration of 100 mg/ml. Samples were analyzed on a Pyris I DSC (Perkin Elmer, Norwalk, CT) at scan rates of 2°C/min or 10°C/min at a temperature range between 36°C and 50°C. The DSC instrument was calibrated with indium (m.p. 156,61 °C) (Perkin Elmer, Norwalk, CT) and p-nitrotoluene (1-methyl-4-nitrobenzene, m.p. 52-54°C), (Aldrich Chem Co. Milwaukee, WI) as standards. Calibrations were accepted if onset melting temperatures of both standards fell within 1% of literature values. T_C values were determined as the onset of the heat flow peak.

3.15. Cryo-transmission electron microscopy (cryo-TEM)

Cryo-TEM images of liposomes were taken in Dr. Katarina Edwards' lab at the Department of Physical Chemistry at the University of Uppsala, Uppsala, Sweden, to elucidate structural changes of liposomes after phase transition.

Diluted liposome samples were transferred onto a copper grid coated with a perforated polymer film in a custom-build environmental chamber at controlled temperature and humidity conditions to minimize water evaporation. Excess sample was removed by aspiration onto a filter paper. Sample films were then vitrified by submersion in liquid ethane at -173°C and transferred into a Zeiss EM 902-A transmission electron microscope at a temperature of -165°C. Cryo-TEM images were taken in zero-loss bright-field mode and an acceleration voltage of 80 kV. The procedure is described in detail elsewhere [201]. On average, eight cryo-TEM images were

generated per sample and the sections of the images presented in this thesis were carefully chosen to represent the typical impression of all images.

3.16. Animals and treatment

In vivo properties of the LTSL-DOX formulation were determined in adult female Bragg albino (Balb/c) mice and the efficacy of the formulation was tested in adult female immunodeficient Rag2-M mice bearing MDR human breast cancer tumors. Mice were originally purchased from Charles River Laboratories, Inc. (Wilmington, MA) and bred at the animal facility of the BC Cancer Research Centre. Mice were used when approximately at 20 g of weight and were anaesthetized with a combination of ketamine and xylazine or tranquilized with acepromazine to regulate their body temperature in a custom-built mouse incubator.

3.16.1. Anesthetics

Ketamine (2-[o-chlorophenyl]-2-[methylamino] cyclohexanone hydrochloride, Ketalar®, Ketaset®, Ketalean®), an arylcycloalkylamine, is a rapid-acting injectable general anesthetic with an elimination half-life in cats of approximately one hour and a wide therapeutic index. Ketamine possesses sedative, analgesic, amnesic, and dissociative properties and causes overstimulation of the CNS by blocking GABA and possibly serotonin, norepinephrine, and dopamine. Ketamine administration may cause increased cardiac output, increased blood pressure, increased heart rate, catalepsy (abnormal maintenance of postures), and hypothermia and is thus often given in combination with xylazine [6] [202].

Xylazine (N-(2,6-dimethylphenyl)-5,6-dihydro-4H-1,3-thiazin-2-amine hydro-

chloride, Rompun®, AnaSed®, Xylamax®), an alpha-2-adrenergic agonist, is a rapid-acting injectable sedative and weak analgesic with muscle relaxing properties. Xylazine causes CNS depression, and decreases norepinephrine release. Its elimination half-life in dogs is approximately 30 min. Xylazine may induce emesis, hyper- or hypothermia, increased initial blood pressure followed by a decrease in blood pressure, increased cardiac output, and cardiac arrhythmias and should not be used in stressed animals [202].

Acepromazine (acetyl-2 (dimethylamino-3 propyl)-10 phenothiazine maleate, Atravet®, Plegicil®, Notensil®) a phenothiazine, is one of the most commonly used neuroleptic tranquillizers in veterinary medicine. Its mechanism of action is only partially understood but it involves blockage of post-synaptic dopamine and alpha-1 receptors in the CNS. Acepromazine causes, tranquillization, muscle relaxation, vasodilation, and has anti-emetic effects. Acepromazine has no analgesic properties and may cause hypothermia. Its elimination half-life in horses is approximately 3 h [202].

3.16.2. Body temperature regulation of mice

The body temperature of mice can increase up to 39°C as a response to stress induced by handling and treatment [203, 204]. Therefore, mice that were treated with thermosensitive liposomes were anaesthetised or tranquillised and their body temperature was regulated in a mouse incubator, designed and developed by L. Ickenstein and custom-built at the BC Cancer Agency workshop. The body temperature of mice had to be monitored and regulated because in anaesthetised or tranquillised mice the body temperature can drop to life-threatening temperatures [205].

The mouse incubator consists of two joint Plexiglas chambers insulated by Styrofoam and connected by air vents (Figure 31). Air is drawn into a Nikon NP-2 heater

(Nikon Instruments Inc., Melville, NY) (A) through the air intake chamber (B). The air intake chamber contains a water-filled dish to moisten the air. Heated air is expelled into the air chamber (C) from which it reaches the animal chamber (D) through air vents. The animal chamber is divided into 15 separate compartments separated by removable Plexiglas walls. The front of each compartment has a slid opening through which the tail of the animal can be accessed for treatment. The animal chamber can be opened by three lids covering five chambers each. One compartment holds a thermostat connected to the heat source.

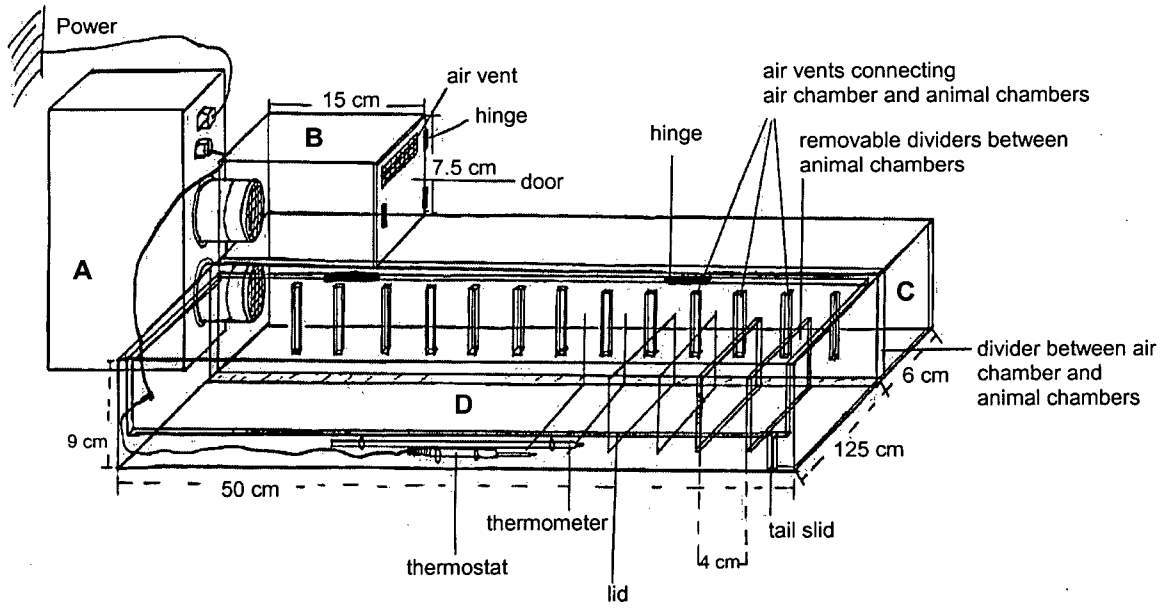

Figure 31: Technical drawing of the mouse incubator. (A) Nikon NP-2 heater; (B) air intake chamber; (C) air chamber; (D) animal chambers. Final dimensions: 59 cm / 9 cm / 21 cm (length / height / depth).

To regulate the body temperature of anaesthetised or tranquillised mice, animals were placed in the mouse incubator. Several compartment temperatures were monitored

simultaneously on a Model 46 TUC Tele-Thermometer using YSI 400-thermistor probes (Yellow Springs Inc., Yellow Springs, OH). Mean compartment temperatures were at 37°C ± 0.5°C in the central compartments 4-12 (Table 4). Thus, only compartments 4-12 were used for hyperthermia experiments and only three mice were treated simultaneously at any given time. The rectal temperature of anaesthetised or tranquillised mice was monitored in regular time intervals on a multichannel Model 46 TUC Tele-Thermometer (Yellow Springs Inc., Yellow Springs, OH) using YSI 400 probes (Yellow Springs Inc., Yellow Springs, OH). The body temperatures of mice were maintained at 37°C or 40°C by adjusting the temperature of the animal chambers accordingly.

Table 4: Mean temperatures and standard deviations (STD) of individual chambers of the mouse incubator (n = 3).

Mean chamber temperature (°C)														
STD														
1	2	3	4	5	6	7	8	9	10	11	12	13	14	15
33.4	35.4	36.2	36.8	37.4	37.5	37.3	37.3	37.1	36.8	36.6	36.5	36.1	35.5	33.6
0.35	0.20	0.15	0.20	0.20	0.10	0.23	0.23	0.12	0.25	0.21	0.10	0.12	0.46	0.23

3.16.3. Determination of drug retention of LTSL-DOX *in vivo*

Drug retention properties of liposomes were investigated in adult female Balb/c or Rag2-M mice. Mice were either not anaesthetized or anaesthetized by intraperitoneal (*i.p.*) injection with ketamine/xylazine at a dosage of 80/20 mg/kg or tranquilized by intramuscular (*i.m.*) injection with acepromazine at a dosage of 6 mg/kg if not stated

otherwise. Sedated mice were placed in the mouse incubator (Figure 31) to maintain their body temperature. DOX-loaded liposomes were administered by a single *i.v.* bolus injection via the tail vein at a dosage of 5-20 mg/kg DOX (10-400 mg/kg lipid) as indicated for each experiment in the result section. The injection volume was 0.2 ml. Mice were sacrificed at selected time intervals by carbon monoxide suffocation and approximately 1 ml of blood was collected into EDTA-coated microtainers (Becton Dickinson, Oakville, ON, Canada) by cardiac puncture. Blood samples were placed on ice and plasma was separated immediately from blood cells at a temperature of 4°C in a centrifugal field of 350 g for 15 min. Mice were cared for in accordance with the principles and guidelines of the Canadian Council on Animal Care.

3.16.4. Determination of liposome thermosensitivity after *in vivo* exposure

To determine the liposome thermosensitivity after *in vivo* exposure, LTSL-DOX or TSL-DOX was injected into the tail vein of Rag2-M mice at a dosage of 20 mg/kg. Mice were sacrificed at 10 min, 20 min, 30 min, or 60 min after injection by carbon monoxide suffocation and approximately 1 ml of blood was collected into EDTA-coated microtainers (Becton Dickinson, Oakville, ON, Canada) by cardiac puncture. Blood from three mice was pooled, placed on ice, and plasma was separated immediately from blood cells at a temperature of 4°C in a centrifugal field of 350 g for 15 min. Plasma samples were split in half. One half was heated for 30 min to a temperature of 37°C the other half was heated for 10 min to 45°C in a circulating water bath. Liposomes not injected into mice served as a control. Doxorubicin released from liposomes was removed from plasma on a Sephadex G-50 spin column in a centrifugal field of 680 g for

2 min. Lipid and DOX plasma levels were determined by scintillation counts and fluorescence spectroscopy, respectively (see sections 3.7.1. and 3.8).

3.16.5. Determination of lysolipid retention in LTSL after *i.v.* injection into mice

LTSL containing MSPC were labeled with ^{14}C-MPPC and ^{3}H-CHE at an activity ratio of 0.9 dpm/dpm) by adding appropriate amounts of labels to lipids dissolved in chloroform. The solvent was evaporated under a gentle stream of nitrogen and the remaining lipid film was dried under vacuum over night. Liposomes were prepared by the method of lipid film hydration in 300 mM citrate buffer, pH4. The outside buffer was exchanged with HEPES buffered saline, pH 7.5, on a Sephadex G-50 column and liposomes were loaded with DOX at a drug-to lipid ratio of 0.05 mg/mg at a temperature of 37°C for 40 min. Adult female Balb/c mice were tranquilized by *i.m.* injection with acepromazine at a dosage of 6 mg/kg and placed in the mouse incubator. The body temperature was monitored with a rectal temperature probe. The body temperature of one group of 18 mice was maintained at 37°C, the body temperature of another group of 18 mice was maintained at 40°C by adjusting the temperature of the incubation chamber accordingly. DOX-loaded liposomes were administered by single *i.v.* bolus injection via the tail vein at a dosage of 10 mg/kg DOX (200 mg/kg lipid). Three mice maintained at a temperature of 37°C were killed at 10 min, 30 min, 1 h, 2 h, 4 h, or 8 h after injection, respectively. Three mice maintained at a temperature of 40°C were killed at 5 min, 10 min, 15 min, 30 min, 45 min, or 1 h after injection, respectively. Approximately 1 ml of blood was collected into EDTA-coated microtainers (Becton Dickinson, Oakville, ON, Canada) by cardiac puncture. Blood samples were placed on ice and plasma was separated immediately from blood cells at a temperature of 4°C in a centrifugal field of

and 350 g for 15 min. Aliquots of plasma and blood cells were counted on a scintillation counter. Prior to counting, whole blood samples were solubilized by adding 0.5 ml of Solvable™ (Packard Bioscience B.V., Gronningen, The Netherlands) to 10 μl of sample. After samples were incubated at a temperature of 50°C overnight and cooled down to room temperature, 50 μl of 200 mM EDTA, 200 μl of 30% hydrogen peroxide solution, and 25 μl of 10 N HCl was added. Samples were mixed on a vortex mixer and incubated for 1 h at room temperature before 5 ml of Pico-Fluor™ 15 scintillation cocktail (Packard, Meriden, CT) was added. Samples were counted on a Packard 1900 scintillation counter (Packard, Meriden, CT) repetitively over the course of three days ensured the absence of quenching effects.

3.16.6. Determination of lysolipid and DOX retention in LTSL after incubation with whole blood, plasma, or buffer

LTSL containing MSPC were labeled with ^{14}C-MPPC and ^{3}H-CHE at an activity ratio of 0.6 dpm/dpm and loaded with DOX at a drug-to-lipid ratio of 0.05 mg/mg by the buffer exchange method. Blood from adult female Balb/c mice was collected into EDTA-coated microtainers by cardiac puncture and stored on ice. Plasma was separated from half of the total blood volume at a temperature of 4°C in a centrifugal field of 350 g for 15 min. To 1 ml of blood, plasma, or HBS, 4 mg of LTSL-DOX was added to match concentrations after LTSL-DOX injection into mice and the mixture was incubated at a temperature of 37°C. Aliquots of blood (150 μl) were withdrawn at 5 min, 10 min, 30 min, 1 h, 2 h, and 4 h after injection and plasma was separated from blood cells at a temperature of 4°C in a centrifugal field of 350 g for 15 min. Aliquots of 50 μl of whole

blood, plasma from whole blood, plasma, or HBS were separated on a Sephadex G-50 spin column to remove free DOX and free lysolipid. Aliquots of 10 μl of the spin column eluent were counted on a scintillation counter for ^{14}C and ^{3}H. To 100 μl of the spin column eluents, 700 μl of dest. H_2O, 100 μl of 10% SDS, and 100 μl of 10mM H_2SO_4 was added and mixed. Subsequently, 2 ml of isopropanol/chloroform 1:1 (vol/vol) was added and mixed on a vortex mixer for 1 min to extract encapsulated DOX. The mixture was stored over night at -20°C. Samples were brought to room temperature, mixed again on a vortex mixer for 1 min and the organic layer was separated from the aqueous layer in a centrifugal field of 680 g for 10 min. The organic layer was transferred into a fresh test-tube and analyzed by fluorescence spectroscopy. The amount of DOX in the sample was derived from a standard curve.

3.16.7. Human tumor xenografts

MDA435/LCC6^{MDR1} estrogen receptor negative human breast cancer cells were used for human tumor xenografts. Cells originated from the laboratory of Dr. Robert Clarke (George Washington University, Washington, DC) and were stored at a temperature of -196°C in liquid nitrogen. To generate the MDA435/LCC6^{MDR1} cell line, the *mdr*1 gene responsible for overexpressing PGP was stablely transfected into a MDA435/LCC6 cell line resulting in an approximately 30-fold PGP overexpression of. Clinically, PGP overexpression has been observed to be typically 2-3 fold [206].

MDA435/LCC6^{MDR1} cells were thawed and cultured in Dulbecco's Modified Eagle's Medium (DMEM) for 2 to 3 passages before injecting approximately 5 x 10^6 cells in 0.5 ml of Hank's Balanced Salt Solution (HBSS) intraperitoneally (*i.p.*) into immunodeficient Rag2-M mice originally purchased from Taconic (Germantown, NY).

Rag2 mice are deficient in the recombinase activating 2 gene. Homozygous Rag2-M mice are unable to generate mature T- or B-lymphocytes, and thus lack a functional immune system. Otherwise, Rag2-M mice have normal hematopoiesis. Two to three weeks after inoculation, ascites cells were harvested by aspiration of the peritoneal fluid and placed in 5 ml HBSS. Cells were counted using a hemocytometer and diluted to a concentration of approximately 20 x 10^6 cells/ml. To culture the cells further, 0.5 ml of the cell suspension was re-injected into two Rag2-M mice. The procedure can be repeated for a maximum of 20 mouse-to-mouse passages. For human tumor xenografts, cells were separated from medium in a centrifugal field of 1000 g for 5 min and the supernatant was discarded. Using a 27 gauge needle 10^6 cells/50 μl were injected subcutaneously (*s.c.*) in the back or the thigh fat pad of mice. Tumor growth was monitored daily by measuring tumor volume with calipers. Mice were terminated when tumors started to ulcerate, when mice were showing signs of distress, or when tumors exceeded a volume of 1 cm^3 in diameter. For simplicity reasons the tumor mass (M) in g or volume (V) in cm^3 was estimated assuming a tumor tissue density of 1 g per cm^3 by:

$$\text{M or V} = \frac{\text{width}^2 \times \text{length}}{2} \qquad \textit{(Equation 26)}$$

3.16.8. Tumor temperature regulation in mice

In an initial attempt, mice were tranquilized with acepromazine at a dosage of 6 mg/kg by *s.c.* injection. Mice were placed in the mouse incubator and their body temperatures were measured with a rectal YSI 400 probe (Yellow Springs Inc., Yellow Springs, OH) attached to a multichannel Model 46 TUC Tele-Thermometer (Yellow

Springs Inc., Yellow Springs, OH). A second probe was attached to their thigh, thighs were wrapped in gauze, and Vaseline™ was applied to their thighs to increase heat conduction. Thighs were heated with a tube coil attached to a Julabo VC5/3 circulating water bath (Julabo Labortechnik GmbH, Seelbach, Germany) to a temperature of 41°C (Figures 32 and 33). Body temperatures were maintained at approximately 37°C. Since mice were not anesthetized, their body movements did not allow for uniform heating of their thighs. Thus, an anesthesia protocol was developed to anesthetize mice for at least 1.5 h.

In this second approach, mice were anesthetized with a combination of ketamine and xylazine or with a combination of ketamine and acepromazine at varying combinations and DOX was administered at a dosage of 5 mg/kg after mice were anesthetized. Mice were monitored during and 24 h after the treatment for any signs of toxicity induced by the combined administration of DOX and anesthetics. When mice were anesthetized with a combination of ketamine/xylazine at dosages of 80/20 mg/kg, 80/8, or 100/10 mg/kg by *i.p.* injection, administration of a second maintenance dose of ketamine/xylazine at 40/10 mg/kg was necessary at 30-45 min after the initial dose to maintain the anesthesia for at least 1.5 h. After recovery from anesthesia, mice appeared distressed according to the appearance of their fur and behavior.

A dosage of ketamine/acepromazine at 100/2.5 mg/kg administered by *i.m.* injection resulted in anesthesia lasting for at least 1.5 h and mice showed no signs of toxicity at 24 h after the treatment. However, maintaining a uniform thigh temperature of 41°C was difficult to achieve even when mice were fully anesthetized since the response of the thigh temperature was delayed by several minutes after the temperature of the

water bath was adjusted. In addition, the measured thigh temperature was found variable depending on the placement of the probe on the leg and the tightness of the wrapping. The hyperthermia procedure using a heat coil was furthermore found impractical for treatment of more than one mouse at a time and was therefore abandoned.

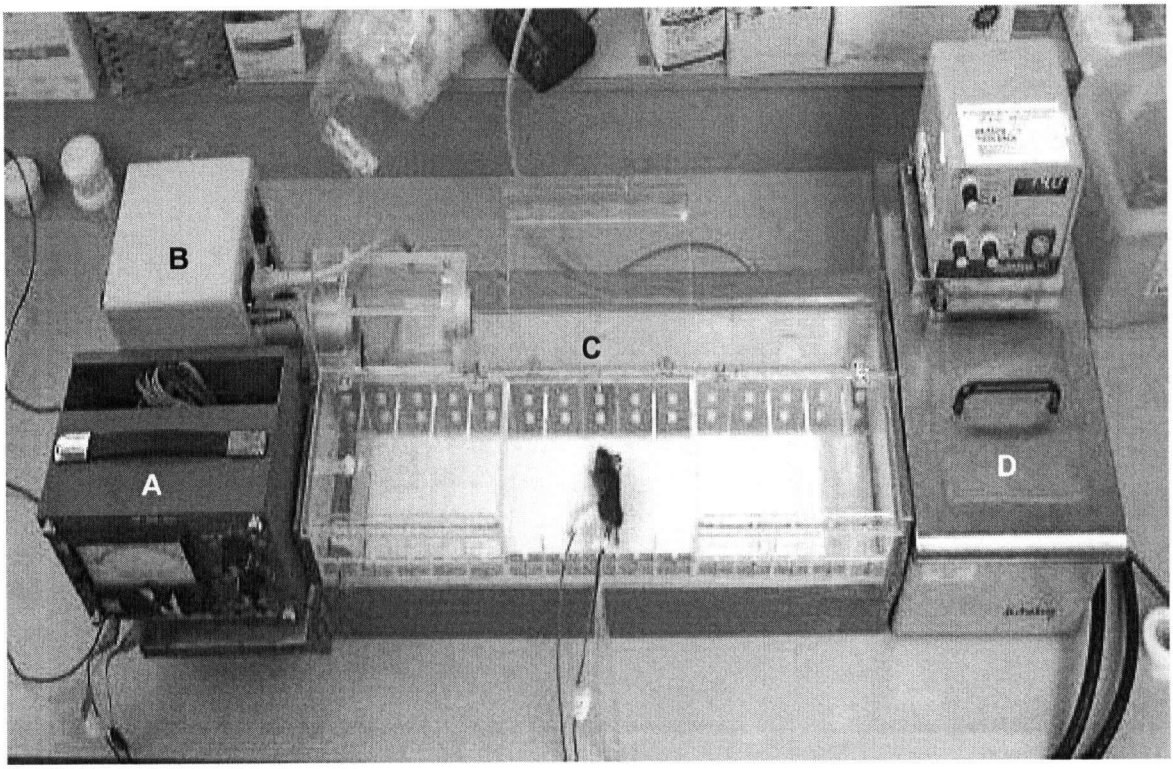

Figure 32: Initial experimental set-up for tumor hyperthermia experiments. Tumors were inoculated in the mice's thighs and tumors were heated with a tube coil attached to a water bath. (A) Model 46 TUC Tele-Thermometer; (B) Nikon NP-2 heater; (C) custom-made mouse incubator; (D) circulating water bath.

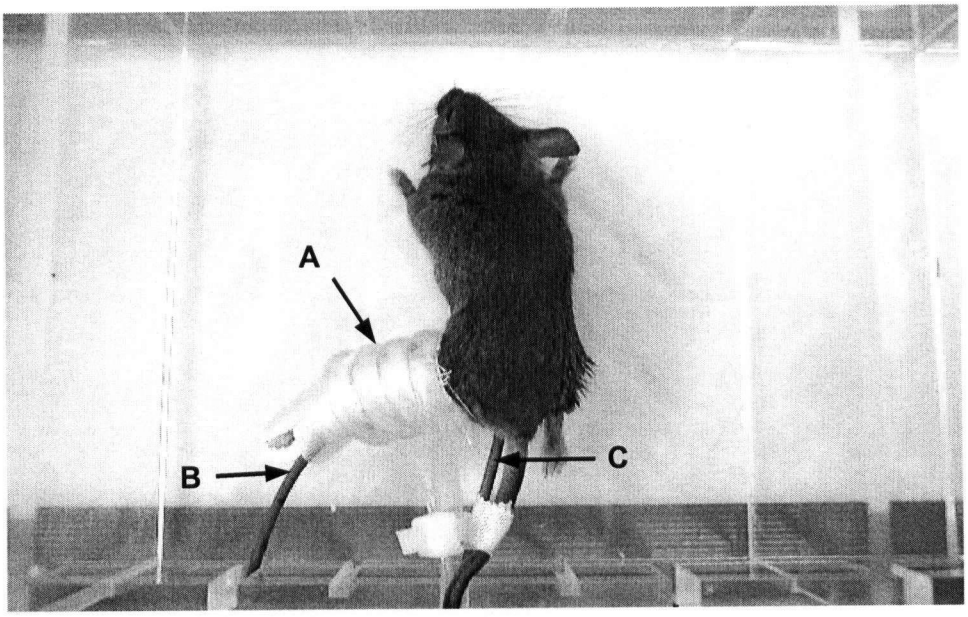

Figure 33: Detail of initial experimental set-up for tumor hyperthermia experiments. (A) Custom-made heat coil; (B) YSI 400-thermistor tumor probe; (C) YSI 400-thermistor rectal probe.

In a third and final approach, Rag2-M mice were inoculated with subcutaneous MDA435/LCC6^{MDR1} human breast cancer tumors on their backs and anesthetized with ketamine/acepromazine at a dosage of 100/2.5 mg/kg by *i.m.* injection. Mice were placed in the mouse incubator and their body temperatures were measured with a rectal YSI 400 probe (Yellow Springs Inc., Yellow Springs, OH). Tumors were heated using a fiberoptic light source (High Intensity Illuminator NI-150, Nikon Instruments Inc., Melville, NY) with the light beam focused on the tumor area (Figures 34 and 35). Tumor temperatures were measured with a hypodermic 33 gage RTD needle probe (Omega Technologies, Stamford, CT) inserted into the center of the tumor and recorded with a multichannel OM-3000 data-logger (Omega Technologies, Stamford, CT). Tumor temperatures were maintained at 41°C since heating tumors to a temperature of 42°C

resulted in some instances in burned areas of the tumor surface. Tumor temperatures were adjusted by adjusting the intensity of the light source.

Body temperatures of mice could easily maintained in the range of 30-40°C. Tumor temperatures could be adjusted quickly and precisely without any time delay when changing between temperatures and tumor temperatures could be maintained precisely at 40- 43°C. After treatment, mice were placed back into their cages and cages maintained at a temperature of 30-36°C in an incubator until mice recovered from anesthesia. Mice were anesthetized for approximately 2 h and no signs of toxicity were detected at 24 h after treatment.

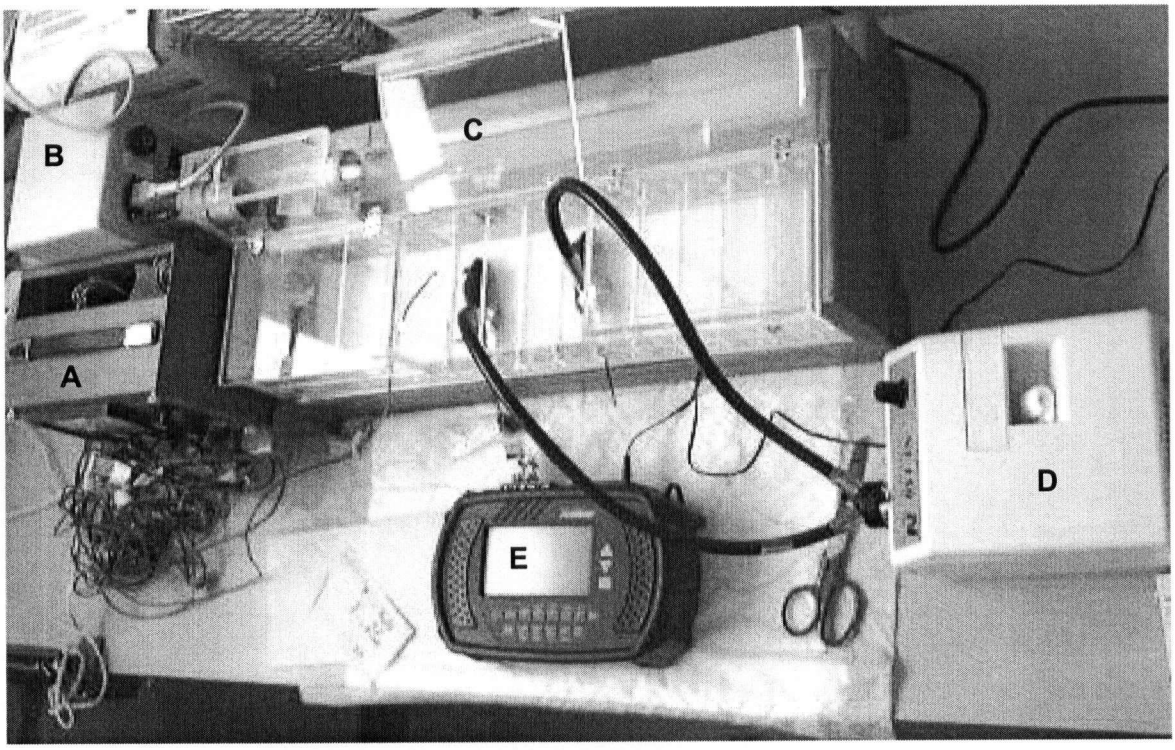

Figure 34: Final experimental set-up for tumor hyperthermia experiments. Tumors were inoculated in the mice's backs and tumors were heated with a fiberoptic light. (A) Model 46 TUC Tele-Thermometer; (B) Nikon NP-2 heater; (C) custom-made mouse incubator; (D) fiberoptic light source; (E) OM-3000 data-logger.

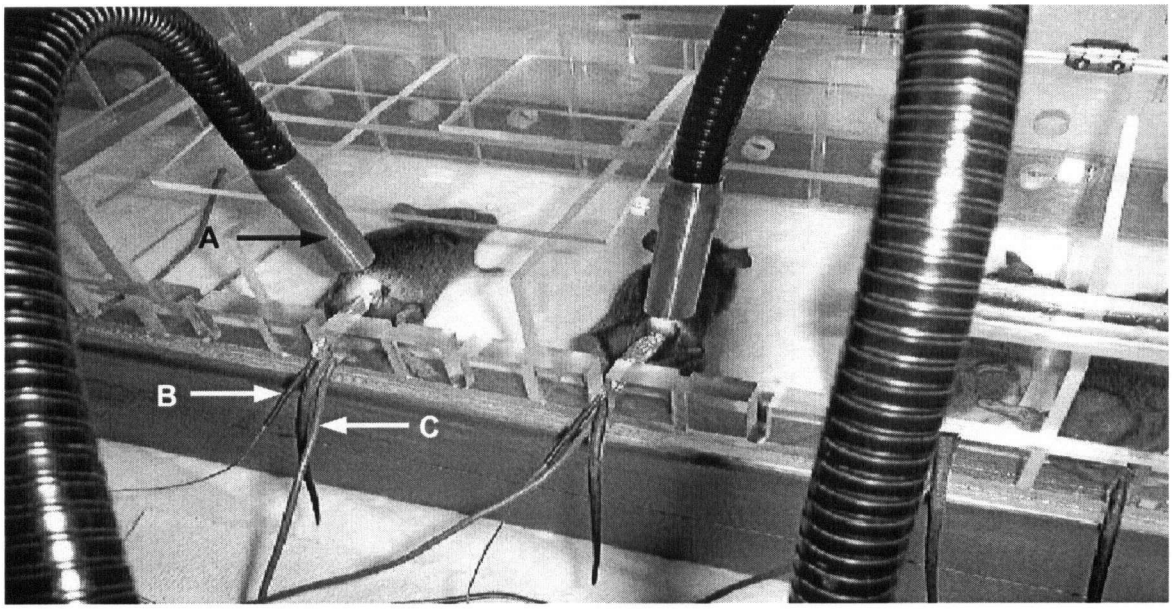

Figure 35: Detail of final experimental set-up for tumor hyperthermia experiments. (A) Fiberoptics; (B) hypodermic 33 gage RTD needle probe; (C) YSI 400-thermistor rectal probe.

3.16.9 Efficacy of LTSL-DOX in MDR tumor bearing mice

Rag2-M mice bearing MDA435/LCC6^{MDR1} tumors on their backs were anesthetized with ketamine/acepromazine at a dosage of 100/2.5 mg/kg by *i.m.* injection. Body temperatures of mice were adjusted in the mouse incubator by regulating the chamber temperature and measured with a rectal probe. The initial approximated mass of tumors before treatment ranged between 20 mg and 31 mg (0.02-0.031 cm^3). Tumors were heated to a temperature of 41°C using a fiberoptic light source. Tumor temperatures were measured with a hypodermic needle probe inserted into the centre of the tumor.

After tumor temperatures reached 41°C, six tumor-bearing mice per treatment group were injected *i.v.* via the tail vein with saline, free DOX at a dosage of 5 mg/kg, or

LTSL-DOX at a dosage of 5 mg DOX/kg. The dosage was the same as that reported earlier resulting in 11 out of 11 total cures after treatment with LTSL-DOX in combination with hyperthermia [1]. The injection volume was 0.2 ml. Tumors were maintained at a temperature of 41°C for 1 h after injection in one half of the mice in each treatment group. Tumors of the other half of mice were not treated with hyperthermia. After treatment, mice were placed back into their cages and cages were maintained at a temperature of 30-36°C in an incubator until mice recovered from anesthesia. Tumor volumes were measured every day or every other day. Mice were cared for in accordance with the principles and guidelines of the Canadian Council on Animal Care.

3.17. Pharmacokinetic analysis

Pharmacokinetic parameters such as area under the curve (AUC_{0h-4h}), area under the moment curve ($AUMC_{0h-4h}$), mean residence time (MRT_{0h-4h}), elimination rate constant (k), half-life ($t_{½}$), total body clearance (Cl), and volume of distribution at steady state (V_{ss}), were determined by non-compartmental analysis using WinNonlin software, version 1.5. (Pharsight Corp., Mountain View, CA). Drug elimination from plasma was assumed to follow first order kinetics and four to five time points were included in the estimation of the terminal elimination phase. AUC_{0h-4h} and $AUMC_{0h-4h}$ were calculated using the linear trapezoidal rule. MRT was estimated as the ratio of $AUMC_{0h-4h}$ and AUC_{0h-4h}. Cl was calculated as the ratio of the $Dose_{i.v}$ and the AUC_{0h-4h}. V_{ss} was calculated as $Dose_{i.v}$ / [$AUMC_{0h-4h}$ / AUC_{0h-4h}^2]. k was calculated from the slope of the line of best fit for the values associated with the terminal portion of the plasma concentration time curve. $t_{½}$ was calculated as 0.693/k.

3.18. Statistical analysis

Mean values of the control group and the treatment groups were analyzed by one way analysis of variance (ANOVA). Differences between pairs of mean values were tested by the Student Newman-Keuls test. Mean differences with a p value (Type I error) of less than 0.05 were considered significantly different.

4. RESULTS

The results chapter of the present thesis is divided into two parts and each part is discussed separately in the discussion chapter. In part I, physicochemical properties of LTSL were investigated *in vitro* and compared to those of TSL and NTSL. In part II, the behavior of LTSL after *in vivo* exposure in mice was investigated and compared to that of TSL and NTSL. Initially, the lysolipid MPPC was used in the LTSL formulation but was later exchanged for MSPC, which has two carbon atoms more in both acyl chains than MPPC. This modification of the LTSL formulation increased the onset temperature of drug release from LTSL slightly and thus increased the safety margin for hyperthermia as a result of slightly elevated body temperatures in *in vivo* applications. The composition of LTSL used in experiments described in sections 4.1.1.-4.1.5. was DPPC/MPPC/DSPE-PEG (molar ratio: 90/10/4). In all other experiments, the composition of LTSL was DPPC/MSPC/DSPE-PEG (molar ratio: 90/10/4) if not indicated otherwise. The compositions of TSL and NTSL formulations remained the same in all experiments and were DPPC/DSPE-PEG (molar ratio: 90/4) and DSPC/Cholesterol/DSPE-PEG (molar ratio: 55/45/4), respectively.

Part I: Physicochemical characterization of LTSL

4.1. Characterization of DOX encapsulation into LTSL

One goal in the development of a liposomal drug formulation is to maximize the amount of drug that can be encapsulated in a given amount of liposomes. Thus, the dependence of DOX encapsulation into LTSL on temperature, time, and the lysolipid content of the LTSL membrane was investigated.

4.1.1. T_C values of LTSL and TSL

T_C values of LTSL with the composition DPPC/MPPC/DSPE-PEG (molar ratio: 90/10/4), LTSL with the composition DPPC/MSPC/DSPE-PEG (molar ratio: 90/10/4), and TSL with the composition DPPC/DSPE-PEG (molar ratio: 90/4) were determined for freshly prepared liposomes in citrate buffer, pH 4, on the inside and outside of the liposome membrane by DSC analysis. T_C values of TSL with the composition DPPC/DSPE-PEG (molar ratio: 90/4), were also determined for liposomes prepared in citrate buffer, pH 2 and pH 6.5. The DSC instrument was calibrated with indium (m.p. 156,61°C) and p-nitrotoluene (m.p. 52-54°C) as standards (Figures 36 and 37).

At pH 4, the mean T_C value of LTSL containing MPPC was at a temperature of 40.1°C. The mean T_C value of LTSL containing MSPC was at 42°C and the mean T_C value of TSL was at 42.5°C. LTSL containing MPPC had significantly lower T_C than both, LTSL containing MSPC and TSL ($p < 0.001$), but the mean T_C value of LTSL containing MSPC was not significantly different from that of TSL. At pH 2, the T_C of TSL was at 46.7°C, a temperature 4 degrees higher than the T_C of TSL prepared at pH 4 ($p < 0.001$). At pH 6.5, the T_C of TSL was at 43.3°C, but the difference to the T_C of TSL prepared at pH 4 (42.5°C) was not significant (Table 5). A representative DSC thermogram of TSL in 300 mM citrate buffer, pH 4, is shown in Figure 38.

Table 5: T_C values of LTSL containing MPPC (DPPC/MPPC/DSPE-PEG, molar ratio: 90/10/4), LTSL containing MSPC (DPPC/MSPC/DSPE-PEG, molar ratio: 90/10/4), and TSL (DPPC/DSPE-PEG, molar ratio: 90/4) in 300 mM citrate buffer pH 2, 4, or 6.5. Liposomes were at a concentration of 100 mg/ml; the heating rate was at 10°C/min. Values in parentheses indicate the standard error of mean values (SEM). [a] = $p < 0.001$ versus LTSL containing MPPC; [b] = $p < 0.001$ versus TSL, pH 4; n.d. = not determined.

	T_C onset values (°C) (SEM)		
	pH 2	*pH 4*	*pH 6.5*
LTSL containing MPPC	n.d.	40.09 (0.21) n = 5	n.d.
LTSL containing MSPC	n.d.	42.0 [a] (0.15) n = 4	n.d.
TSL	46.66 [a,b] (0.12) n = 3	42.53 [a] (0.31) n = 4	43.31 [a] (0.1) n = 3

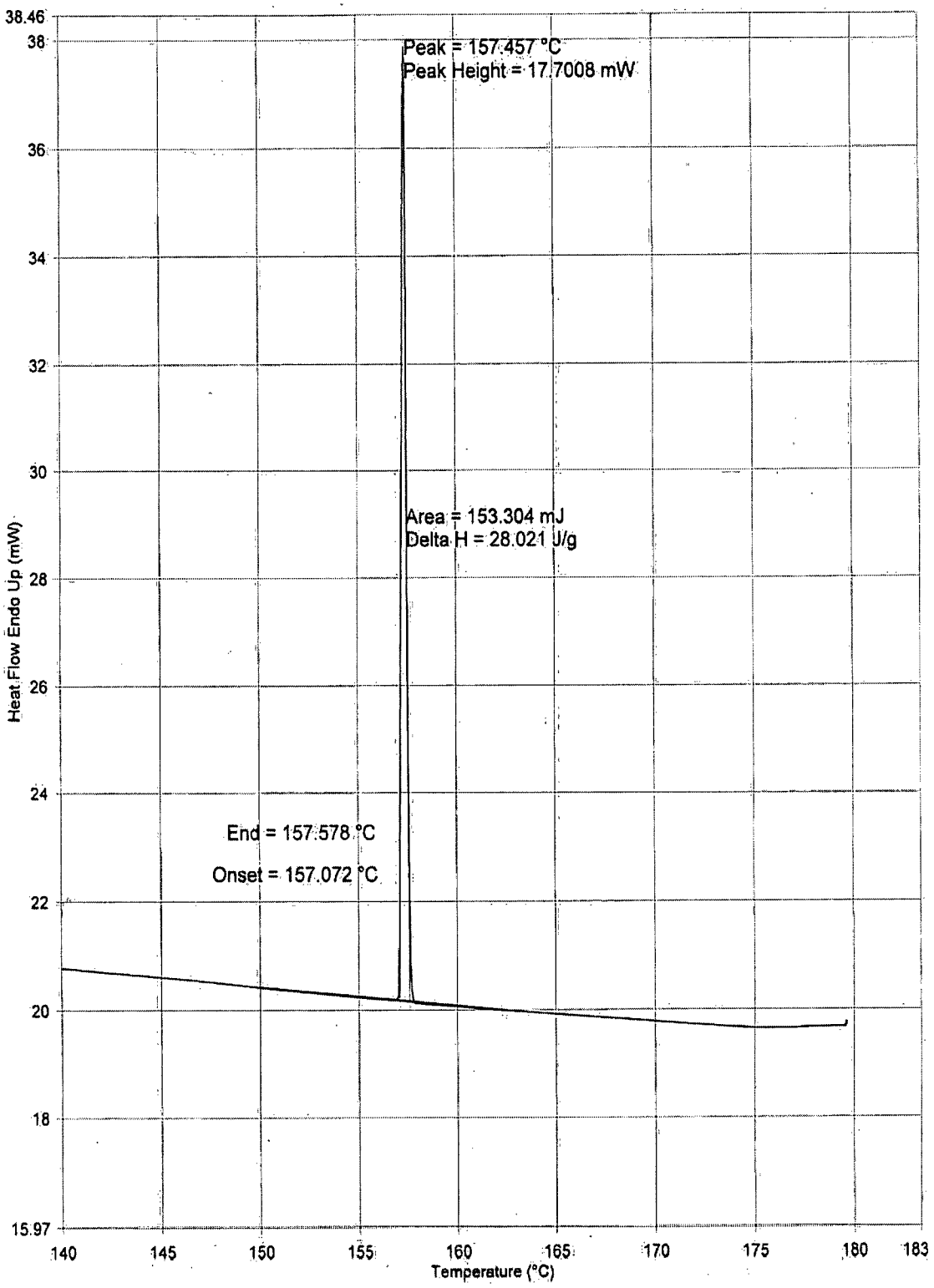

Figure 36: Representative DSC thermogram of the indium standard. The heating rate was at 2°C/min.

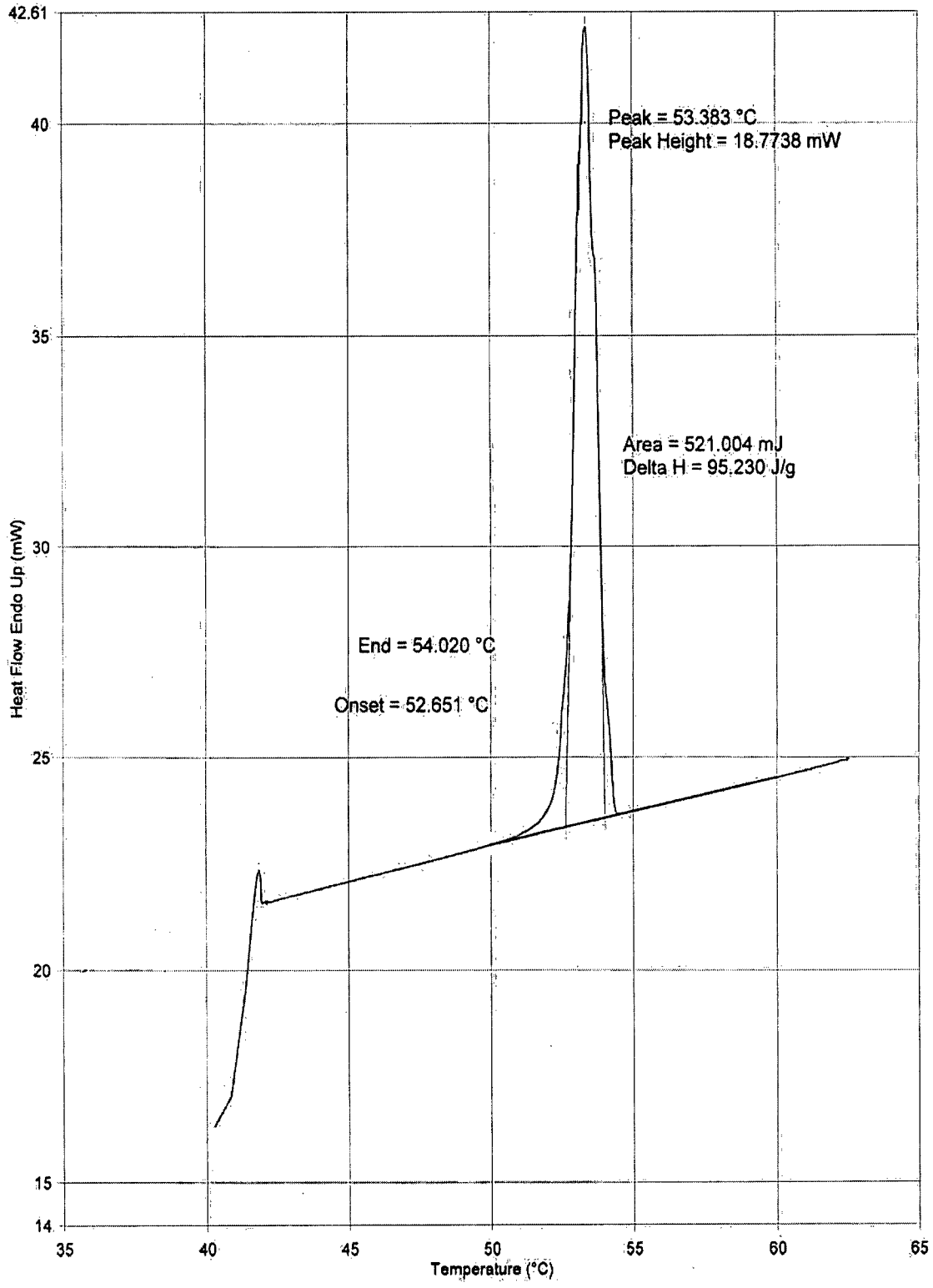

Figure 37: Representative DSC thermogram of the p-nitrotoluene standard. The heating rate was at 2°C/min.

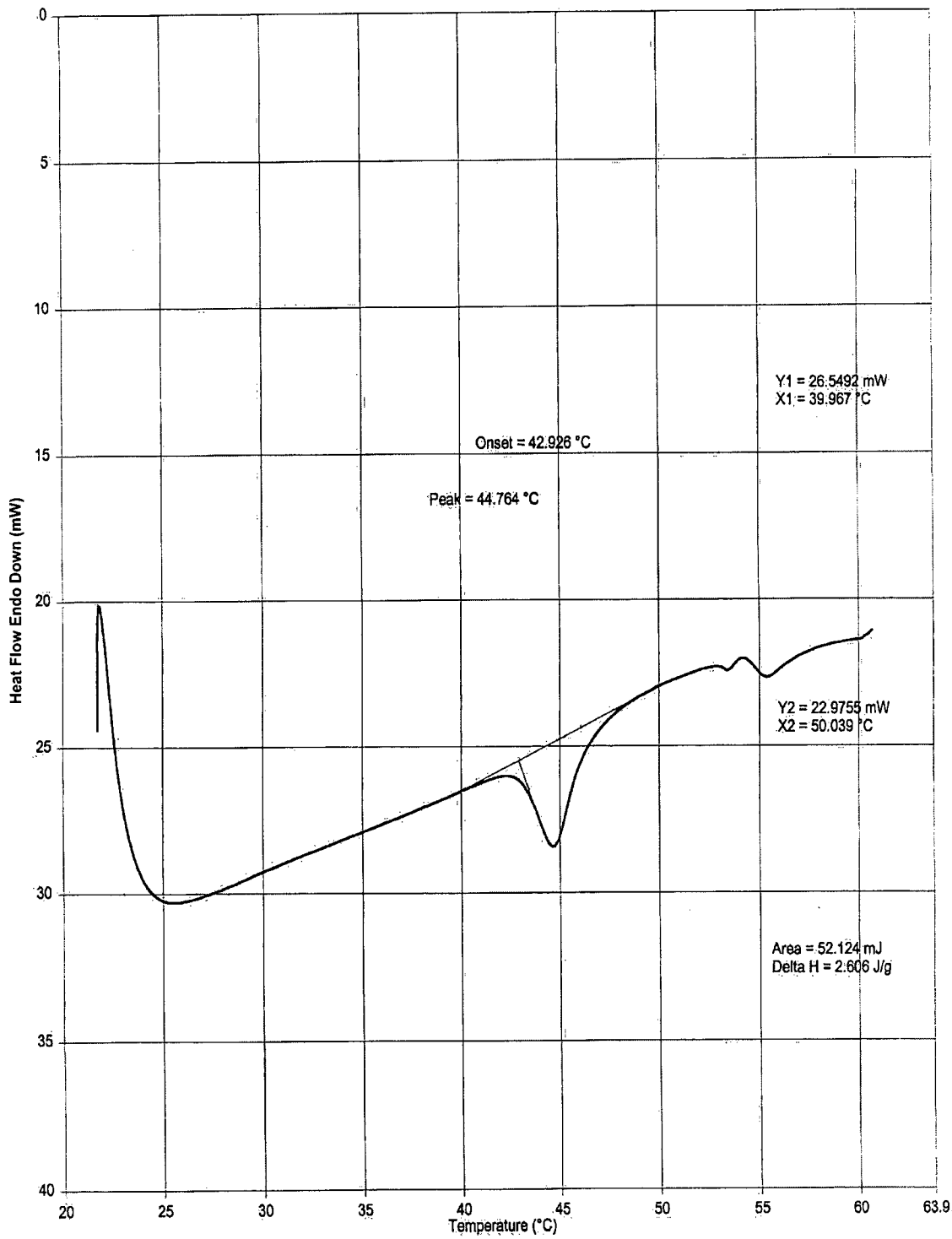

Figure 38: Representative DSC-thermogram of freshly prepared TSL (DPPC/DSPE-PEG, molar ratio: 90/4) in 300 mM citrate buffer, pH 4, at a concentration of 100 mg/ml. The heating rate was at 10°C/min.

4.1.2. Temperature dependence of DOX encapsulation into LTSL

LTSL exhibiting a transmembrane pH gradient (pH 4 inside, pH 7.5 outside) were incubated with DOX at a drug-to-lipid ratio of 0.05 mg/mg and incubated for 20 min without freeze thawing. The transmembrane pH gradient was generated by titrating the extravesicular citrate buffer with sodium carbonate to pH 7.5. Incubation temperatures ranged from 32°C to 60°C with one-degree increments between 32°C and 42°C and a ten-degree increment between 50°C and 60°C. LTSL without a transmembrane pH gradient prepared at pH 4 and pH 7.5 served as a control and were incubated with DOX at temperatures of 32°C, 37°C, and 60°C under the same conditions as LTSL with a transmembrane pH gradient.

Mean encapsulation efficiencies for DOX increased with increasing temperatures between 32°C to 37°C and were greater than 90% at temperatures between 34°C and 37°C (Figure 39). At temperatures greater than 37°C, encapsulation efficiencies decreased greatly. At 39°C or higher temperatures, mean loading efficiencies remained relatively constant at 17.4%. These baseline loading efficiencies did not differ significantly from those achieved using LTSL without a transmembrane pH gradient in citrate buffer pH 7.5 (19.4%, Figure 39) or pH 4 (17.0%, data not shown) indicating DOX membrane association. Based on these results, an incubation temperature of 37°C was chosen for all following encapsulation experiments to maximize drug loading and minimize the incubation time.

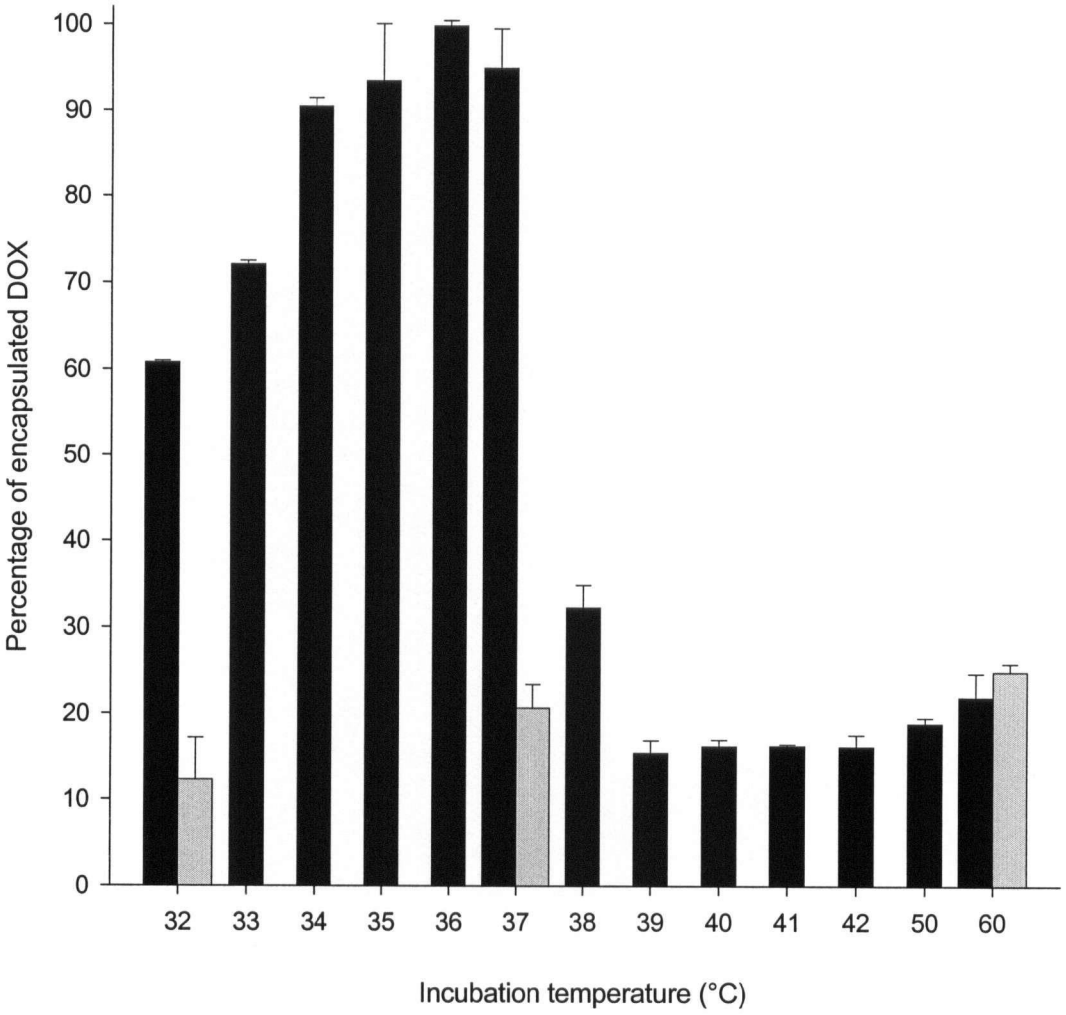

Figure 39: Temperature dependence of DOX encapsulation into LTSL. The pH gradient across the liposome membrane was created by titrating the extravesicular citrate buffer with sodium carbonate (■). LTSL without a pH gradient at pH 7.5 served as a control (■). DOX was loaded at a drug-to-lipid ratio of 0.05 mg/mg for 20 min. Error bars indicate the standard error of mean values (n = 3).

4.1.3. Dependence of DOX encapsulation into LTSL on time, different drug-to-lipid weight ratios, and the extravesicular buffer

To determine optimal incubation conditions for maximal drug loading, LTSL with a transmembrane pH gradient were incubated with DOX at drug-to-lipid ratios of 0.05 mg/mg, 0.1 mg/mg, or 0.2 mg/mg for 10 min, 20 min, 30 min, 40 min, or 50 min at a temperature of 37°C. The transmembrane pH gradient was generated either by titrating the extravesicular citrate buffer to pH 7.5 with sodium carbonate or by exchanging the extravesicular buffer with HEPES buffered saline (HBS), pH 7.5, using gel filtration chromatography. NTSL served as a control and were incubated with DOX at a drug-to-lipid weight ratio of 0.2 for 10 min at a temperature 60°C.

Quantitative DOX encapsulation was achieved for a drug-to-lipid ratio of 0.05 mg/mg and an incubation time of at least 20 min for LTSL in sodium carbonate-titrated citrate buffer or in HBS (Figure 40). DOX encapsulation was incomplete at higher drug-to-lipid weight ratios and reached a maximum at an incubation time of approximately 30 min. These encapsulation parameters were contrasted by those of NTSL, in which DOX could be encapsulated quantitatively at a drug-to-lipid ratio of 0.2 mg/mg after incubation at a temperature of 60°C for 10 min. For LTSL in sodium carbonate-titrated citrate buffer, maximum encapsulating efficiencies were 100%, 49%, and 25% when loaded at drug-to-lipid ratios of 0.05 mg/mg, 0.1 mg/mg, or 0.2 mg/mg, respectively. Accordingly, the maximal amounts of DOX per mg lipid that could be encapsulated under these incubation conditions were 0.05 mg, 0.049 mg, and 0.05 mg, respectively (Figure 41). Thus, the mean upper DOX loading limit for this LTSL formulation in sodium carbonate-titrated citrate buffer was 0.05 mg DOX/mg lipid.

For LTSL exchanged into HBS using gel filtration chromatography, maximum encapsulating efficiencies were 97%, 83%, and 38% when loaded at drug-to-lipid ratios of 0.05 mg/mg, 0.1 mg/mg or 0.2 mg/mg, respectively (Figure 40). Accordingly, the maximal amount of encapsulated DOX per mg lipid that could be encapsulated under these incubation conditions was 0.049 mg at a drug-to-lipid ratio of 0.05 mg/mg, and increased significantly ($p < 0.001$) to 0.083 mg or 0.076 mg at drug-to-lipid ratios of 0.1 mg/mg or 0.02 mg/mg, respectively (Figure 41). Thus, the mean upper DOX loading limit for this LTSL formulation in HBS was 0.08 mg DOX/mg lipid.

Overall, these results indicate that DOX can be encapsulated into LTSL in sodium carbonate-titrated citrate buffer with efficiency values close to 100% when loaded at temperatures ranging from 34°C to 37°C for at least 20 min at a drug-to-lipid of 0.05 mg/mg. At this and lower drug-to-lipid ratios, it is not necessary to remove remaining free DOX from encapsulated DOX after loading. When liposomes were loaded in HBS the amount of encapsulated DOX per mg lipid could be increased to a maximum of 0.08 mg.

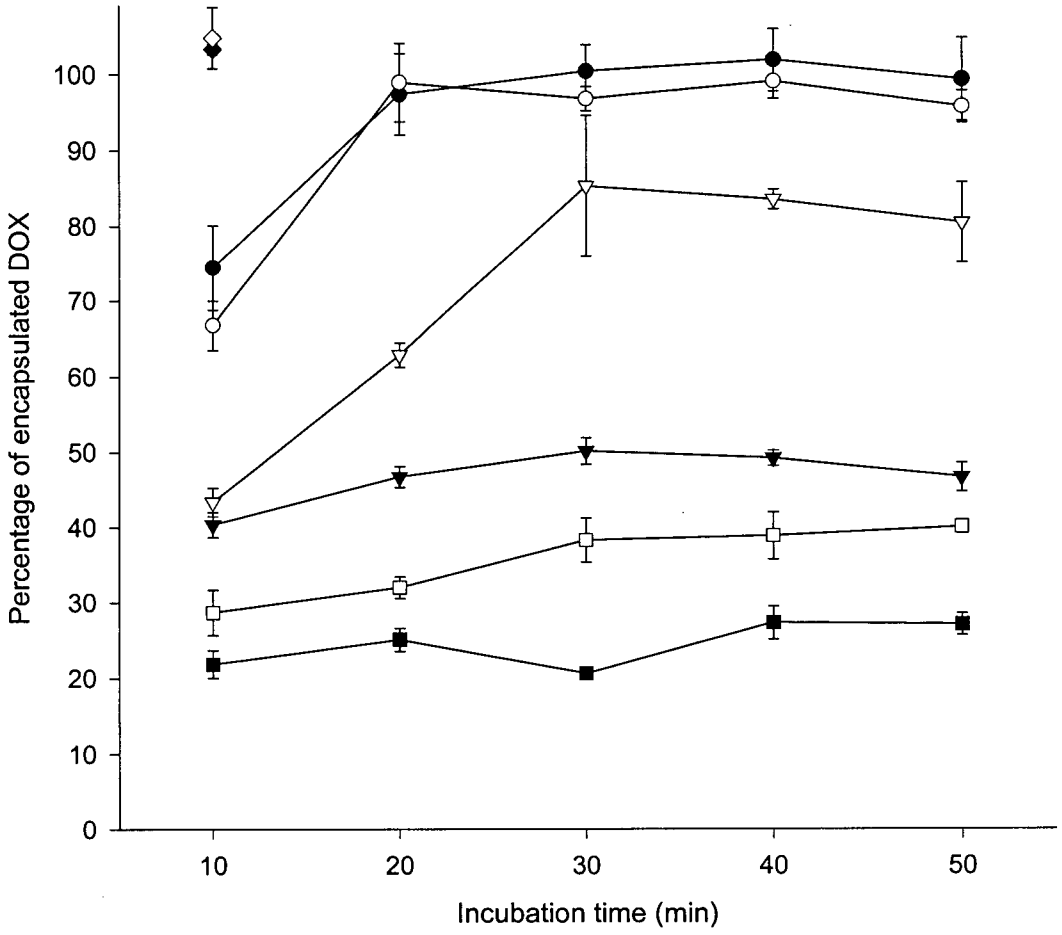

Figure 40: Time dependence of DOX encapsulation into LTSL at different drug-to-lipid weight ratios. The pH gradient across the liposome membrane was created either by titrating the extravesicular citrate buffer with sodium carbonate (closed symbols) or by exchanging the extravesicular citrate buffer with HBS (pH 7.5) (open symbols). DOX was loaded at 37°C for 10, 20, 30, 40, or 50 min at a drug-to-lipid ratio of 0.05 mg/mg (●○), 0.1 mg/mg (▼▽), or 0.2 mg/mg (□■). NTSL were incubated with DOX for 10 min at 60°C at a drug-to-lipid ratio of 0.2 mg/mg (◆◇). Error bars indicate the standard error of mean values (n = 3).

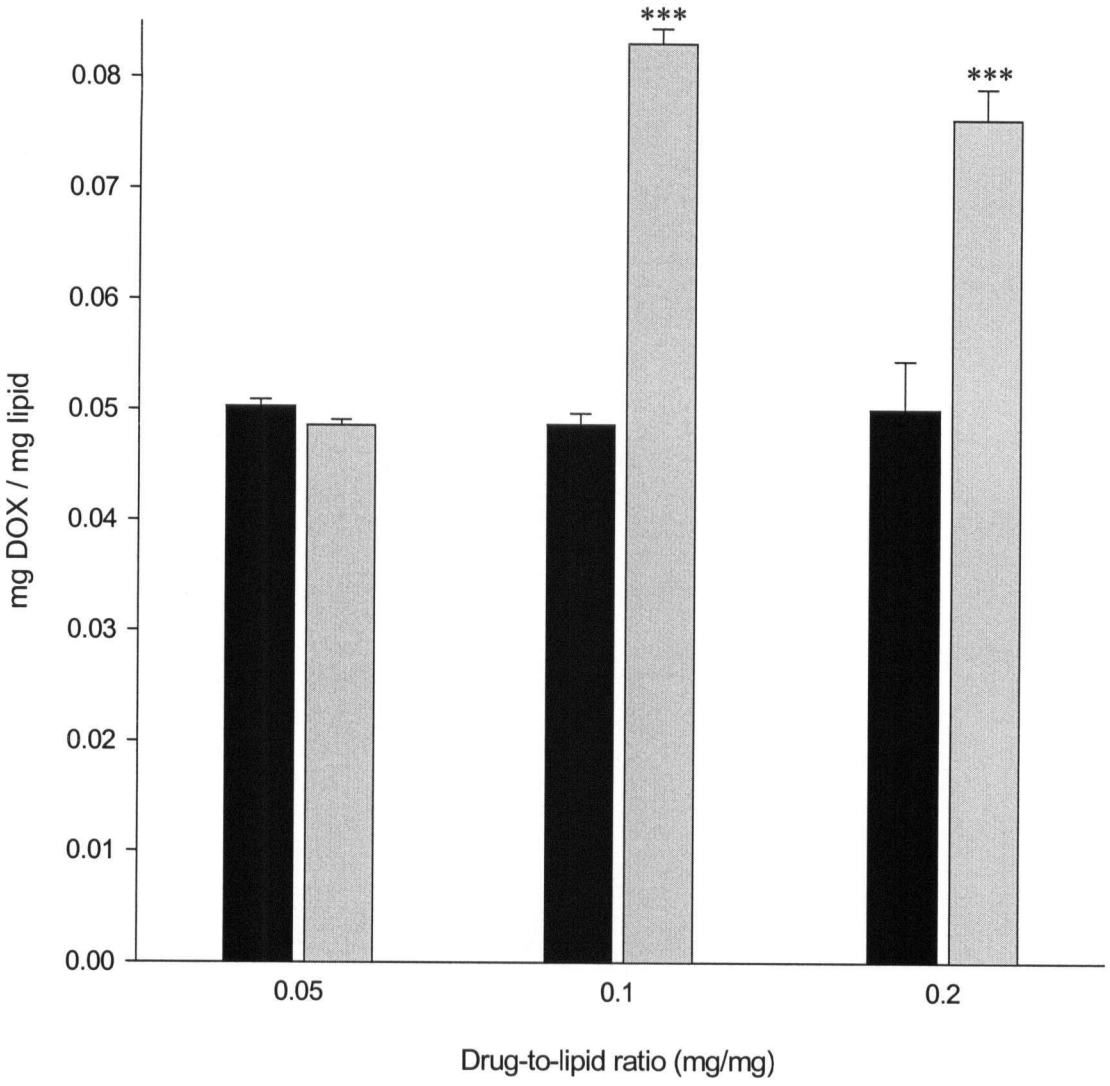

Figure 41: Dependence of DOX encapsulation into LTSL on the extravesicular buffer. pH Gradients were created for active DOX encapsulation by titrating the extravesicular 300 mM citrate buffer, pH 4, to pH 7.5 with appropriate amounts of sodium carbonate (■) or by exchanging the extravesicular 300 mM citrate buffer, pH 4, with HBS, pH 7.5 on a Sephadex G-50 column (■). Mean drug-to-lipid ratios from Figure 40 were averaged for encapsulation times between 30 min and 50 min. *** $p < 0.001$ versus loading efficiency at a drug-to-lipid ratio of 0.05 mg/mg. Error bars indicate the standard error of mean values (n = 3).

4.1.4. Transmembrane pH gradients after DOX encapsulation

In order to investigate if differences in the DOX loading limits between LTSL and NTSL could be explained by changes in the pH gradient across the liposome membrane, pH gradients were determined after exchanging the extravesicular citrate buffer with HEPES buffered saline before and after encapsulating DOX at drug-to-lipid ratios of 0.05 mg/mg, 0.1 mg/mg, or 0.2 mg/mg. As a control, the pH gradients of NTSL before and after DOX encapsulation at a drug-to-lipid ratio of 0.2 mg/mg were determined.

The mean pH gradient in LTSL before DOX encapsulation was at 2.63 units across the membrane and decreased significantly ($p < 0.05$) by approximately 0.5 units to 2.2, 2.1, and 2.08 units after loading with DOX at drug-to-lipid ratios of 0.05 mg/mg, 0.1 mg/mg, or 0.2 mg/mg, respectively. However, the remaining pH gradient in LTSL after DOX encapsulation at drug-to-lipid ratios of 0.05 mg/mg, 0.1 mg/mg, or 0.2 mg/mg was still greater than 2 units across the membrane. When heated for one minute to a temperature of 60°C, the mean pH gradient in LTSL dissipated almost completely to approximately 0.3 units. pH Gradients after heating samples to a temperature of 60°C were not determined in NTSL because NTSL were loaded with DOX at this temperature.

Changes of pH gradients in LTSL after DOX loading were similar to those in NTSL after loading with DOX at a drug-to-lipid ratio of 0.2 mg/mg. In NTSL, the mean pH gradient in LTSL before DOX encapsulation was at 2.65 units across the membrane and decreased to approximately 2 units after loading with DOX at a drug-to-lipid ratio of 0.2 mg/mg. However, the difference between pH gradients before and after DOX loading was not significantly different. (Table 6).

Table 6: Transmembrane pH gradients in liposomes before and after DOX encapsulation at various drug-to-lipid weight ratios. pH Gradients were created by titrating the outside citrate buffer of lysolipid-containing thermosensitive liposomes (LTSL) and non-thermosensitive liposomes (NTSL) with appropriate amounts of a 0.5 M sodium carbonate solution. pH Gradients were determined by [^{14}C] methylamine encapsulation before DOX loading at the indicated drug-to-lipid weight ratios. Values in parentheses indicate the standard error of mean values (SEM). * = $p < 0.05$; *** = $p < 0.001$ versus pH gradient before DOX encapsulation; n.d. = not determined.

	pH gradient (SEM)				
	before DOX loading	*after DOX loading at the indicated drug-to-lipid ratios (mg/mg)*			*after heating to 60°C*
		0.05	*0.1*	*0.2*	
LTSL	2.63 (0.13) n = 5	2.20 * (0.16) n = 5	2.10 * (0.14) n = 5	2.08 * (0.14) n = 5	0.27 *** (0.04) n = 3
NTSL	2.65 (0.41) n = 3	n.d.	n.d.	1.97 (0.16) n = 3	n.d.

4.1.5. Dependence of DOX encapsulation on the lysolipid content of the LTSL membrane

In order to evaluate the dependence of DOX encapsulating efficiency on the percentage of MPPC in the liposomal membrane, LTSL containing 12.5 mol%, 15 mol%, or 20 mol% MPPC were loaded with DOX at drug-to-lipid ratios of 0.05 mg/mg, 0.1 mg/mg, or 0.2 mg/mg at 37°C for 20 min. These MPPC membrane concentrations were chosen because hyperthermia-triggered drug release reached a maximum at a MPPC concentration of 10 mol% [13], but in an acidic environment, additional MPPC (and palmitic acid) is generated by DPPC hydrolysis during storage [124, 126].

At a drug-to-lipid ratio of 0.05 mg/mg, quantitative DOX encapsulation could be achieved at MPPC concentrations in the LTSL membrane of 12.5 mol% and 15 mol%. When the MPPC concentration was increased to 20 mol% the mean percentage of DOX encapsulation decreased to 36%. At a drug-to-lipid ratio of 0.1 mg/mg, the mean percentage of DOX encapsulation was 73%, 56% and 24% at MPPC concentrations of 12.5 mol%, 15 mol%, and 20 mol%, respectively. At a drug-to-lipid ratio of 0.2 mg/mg, the mean percentage of DOX encapsulation was 45%, 30%, and 11% at MPPC concentrations of 12.5 mol%, 15 mol%, and 20 mol%, respectively (Figure 42). Results indicate that encapsulation efficiencies in LTSL are dependent on MPPC membrane concentrations with an upper limit of 15 mol% for quantitative DOX encapsulation at a drug-to-lipid ratio of 0.05 mg/mg.

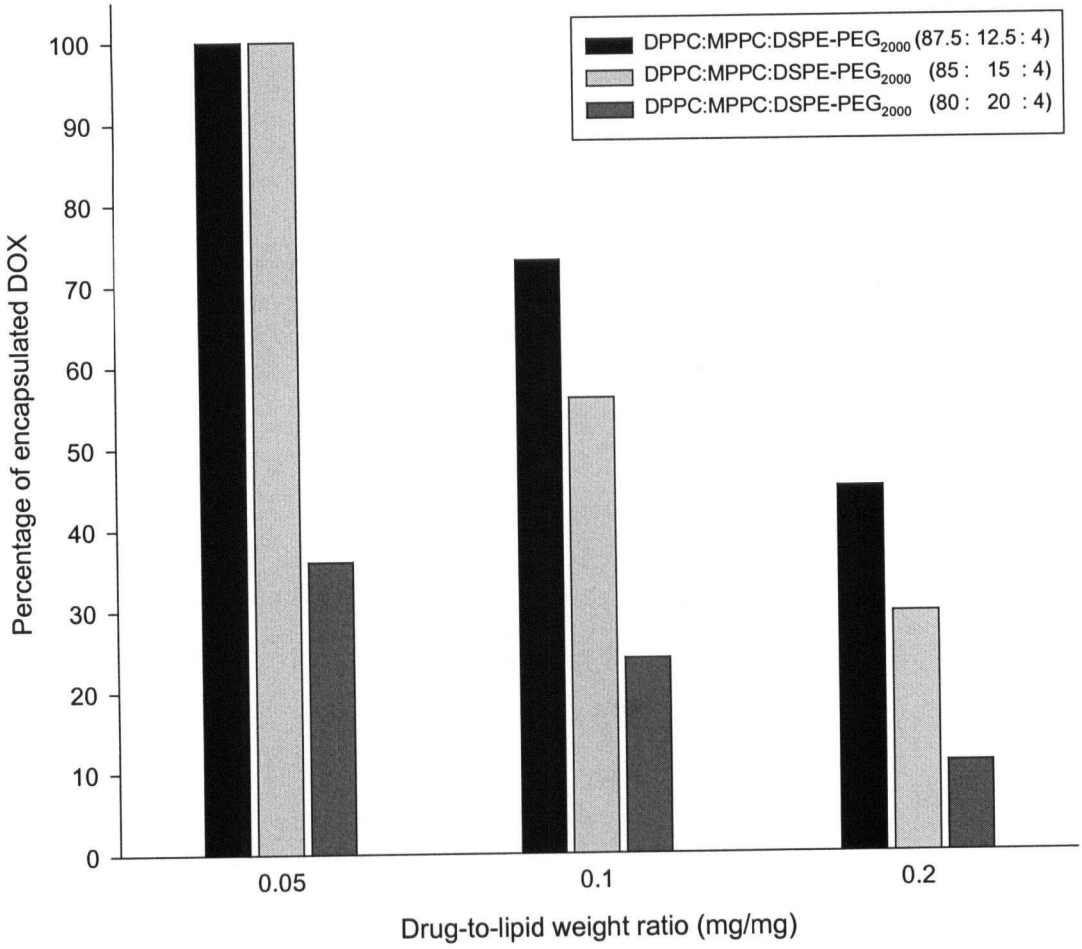

Figure 42: Dependence of DOX encapsulation on the drug-to-lipid weight ratio and the MPPC content of the LTSL membrane. Liposomes contained MPPC at a concentration of 12.5 (■), 15 (■), or 20 (■) mol%. The pH gradient across the liposome membrane (inside pH 4, outside pH 7.5) was created by exchanging the extravesicular 300 mM citrate buffer, pH 4, with HBS, pH 7.5, on a Sephadex G-50 column. DOX was loaded at drug-to-lipid ratios of 0.05 mg/mg, 0.1 mg/mg, or 0.2 mg/mg at a temperature of 37°C for 20 min. Encapsulation efficiencies were determined in duplicate.

4.2. Characterization of DOX release from LTSL

To investigate proposed conformational changes in the liposome membrane during phase transition the effect of cycling, LTSL, TSL, and NTSL through their T_C was investigated by cryo-TEM imaging (see section 3.15.).

Cryo-TEM images of LTSL-DOX vitrified at temperatures above and below its T_C revealed that at a temperature below the T_C of the formulation (22°C) the morphology of LTSL is polyhedral, especially when smaller in size. DOX is in a crystalline state inside LTSL in form of fibrous bundles as reported earlier by Li and coworkers [81, 177] (Figure 43A). At a temperature above the T_C of the formulation (45°C) the morphology of LTSL is spherical, liposome discs are present in the sample, and DOX is released from liposomes as revealed by the presence of DOX aggregate structures outside liposomes (Figure 43B and 43C).

In contrast, the morphology of NTSL is spherical at temperatures of 22°C or 50°C (Figure 44). In NTSL, the formation of DOX fibrous bundles appears to extend beyond the physical boundaries of unloaded liposomes and stretches the membrane in the direction of bundle growth. This effect could not be observed in LTSL, which possess a more rigid membrane at temperatures below its T_C. DOX was not released from NTSL at a temperature of 50°C, the maximum temperature that could be achieved by the experimental conditions (Figure 44B).

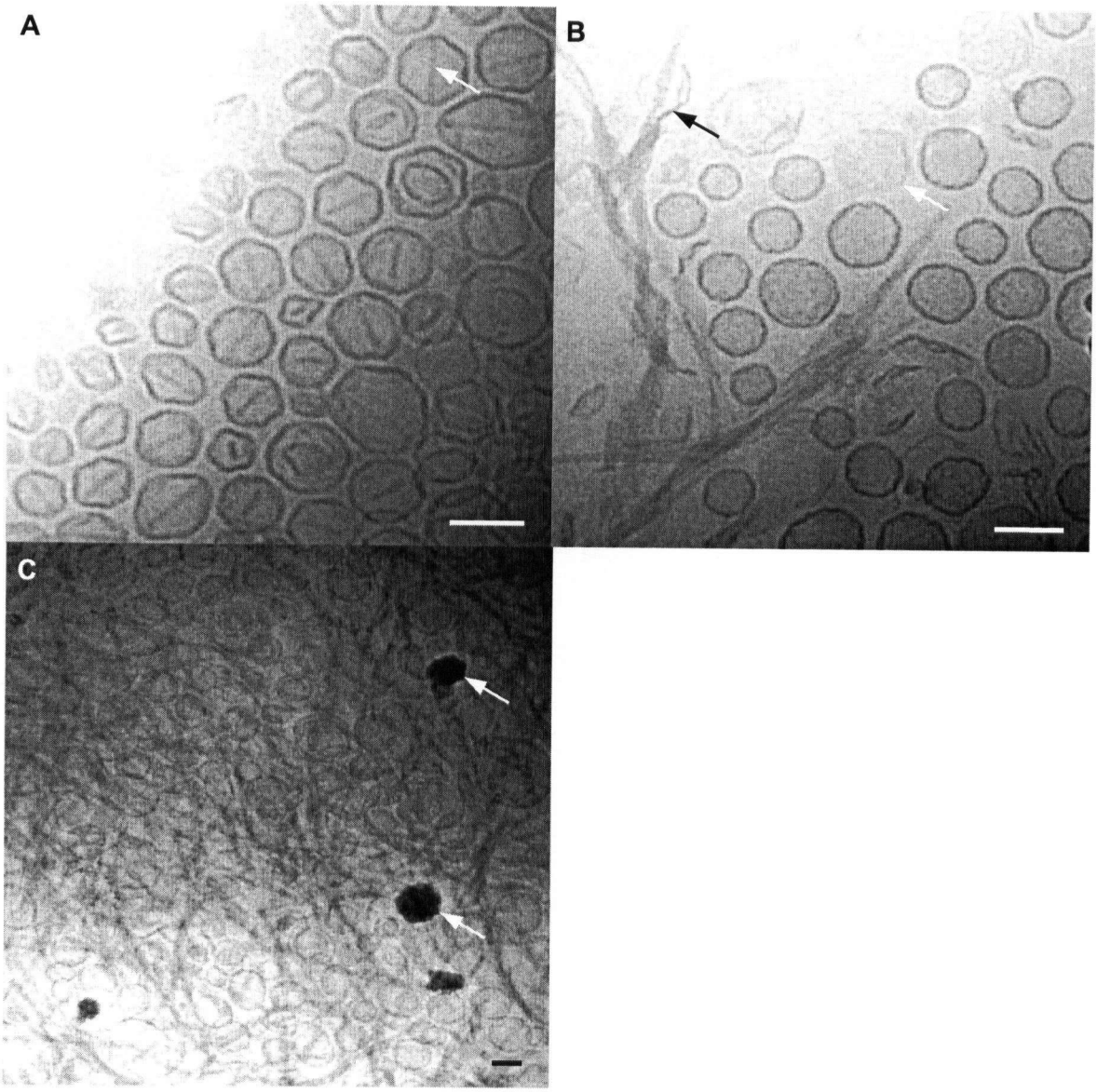

Figure 43: Cryo-TEM images of LTSL-DOX at temperatures of (A) 22°C and (B, C) 45°C. The arrow in (A) indicates DOX fibrous bundles inside liposomes. The black arrow in (B) indicates DOX fibrous bundles outside liposomes. The white arrow in (B) indicates a bilayer disc. White arrows in (C) indicate ice crystals. Scale bars indicate a size of 100 nm.

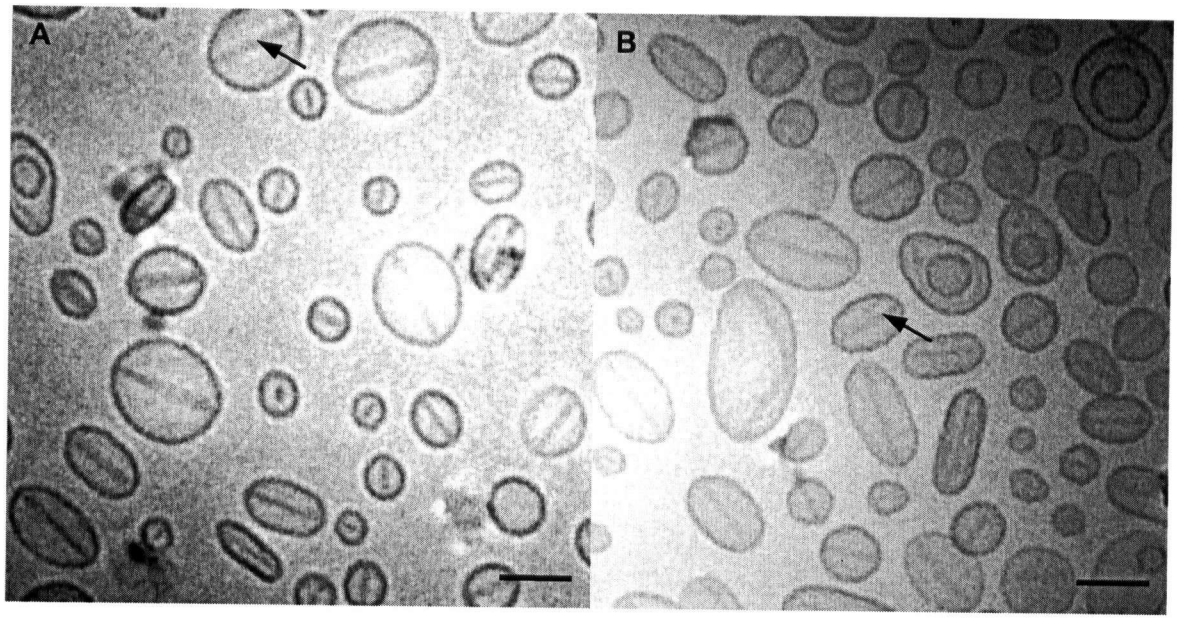

Figure 44: Cryo-TEM images of NTSL-DOX at temperatures of (A) 22°C and (B) 50°C. Arrows indicate DOX fibrous bundles inside liposomes. Scale bars indicate a size of 100 nm.

4.2.1. Temperature dependence of the release rate of DOX from LTSL

Drug release rates from LTSL were determined at temperatures ranging from 37°C to 42°C by the method of fluorescence dequenching (see section 3.10.). The percentage of DOX released from liposomes was derived from a standard curve (Figure 45).

At temperatures of 37°C and 38°C DOX was not released from LTSL over the course of 4 h. The small increase in fluorescence intensity within the first half hour was consistent between individual experiments and remains unexplained (Figures 46 and 47).

At a temperature of 39°C, approximately 10% of encapsulated DOX was released at 10 min, 33% was released at 1 h, 67% at 2 h, and 82% was released at 3 h. The percentage of DOX released from liposomes increased linearly until approximately 2.5 h

when approximately 78% of encapsulated DOX was released (R^2 = 0.99) and reached a plateau at 3 h when approximately 83% of encapsulated DOX was released. From then on until the end of the study, the percentage of DOX released continued to increase slightly to approximately 90% at 6 h (Figures 46 and 47).

At a temperature of 40°C, DOX released from LTSL increased dramatically. Approximately 47% of encapsulated DOX was released at 5 min, 74% was released at 10 min, 83% at 20 min, and 90% was released at 1 h. The percentage of DOX released from liposomes increased linearly until approximately 10 min when approximately 74% of encapsulated DOX was released (R^2 = 0.97) and reached a plateau at 1 h when approximately 90% of encapsulated DOX was released. From then on until the end of the study, the percentage of DOX released continued to increase slightly to approximately 97% at 4 h (Figures 46 and 47).

At a temperature of 41°C, DOX released from LTSL increased even further. Approximately 50% of encapsulated DOX was released at 5 sec, 79% was released at 20 sec, and 82% was released at 5 min. The percentage of DOX released from liposomes increased linearly until approximately 3 sec when approximately 42% of encapsulated DOX was released (R^2 = 0.99) and reached a plateau at 20 sec when approximately 79% of encapsulated DOX was released. From then on until the end of the study, the percentage of DOX released continued to increase slightly to approximately 97% at 4 h (Figures 46 and 47).

At a temperature of 42°C, approximately 50% of encapsulated DOX was released at 0.4 sec, 78% was released at 2.5 sec, and 85% was released at 25 sec. The percentage of DOX released from liposomes increased linearly until approximately 0.6 sec when

approximately 57% of encapsulated DOX was released ($R^2 = 0.93$) and reached a plateau at 25 sec when approximately 85% of encapsulated DOX was released. From then on until the end of the study, the percentage of DOX released continued to increase slightly to approximately 99% at 4 h (Figures 46 and 47).

In comparison, at a temperature of 42°C DOX release from TSL was much slower. Approximately 55% of encapsulated DOX was released at 10 min, 79% was released at 20 min, and 88% was released at 30 min. The percentage of DOX released from liposomes increased linearly until approximately 10 min when approximately 55% of encapsulated DOX was released ($R^2 = 0.93$) and reached a plateau at 35 min when approximately 92% of encapsulated DOX was released. From then on until the end of the study, the percentage of DOX released continued to increase slightly to approximately 98% at 1 h (Figures 46 and 47).

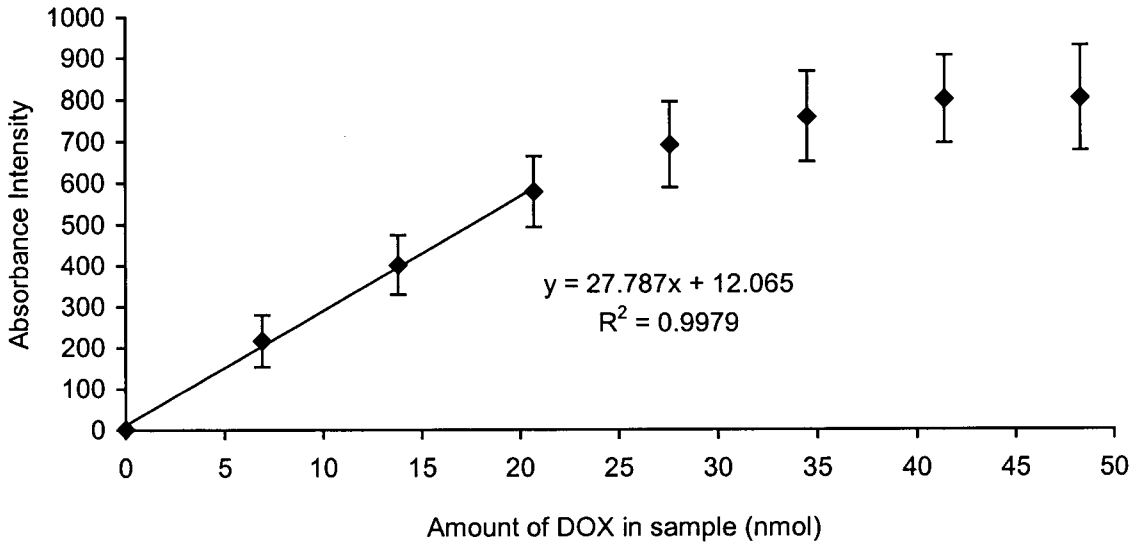

Figure 45: Standard curve of the DOX dequenching assay. Error bars indicate the standard deviation (n = 5).

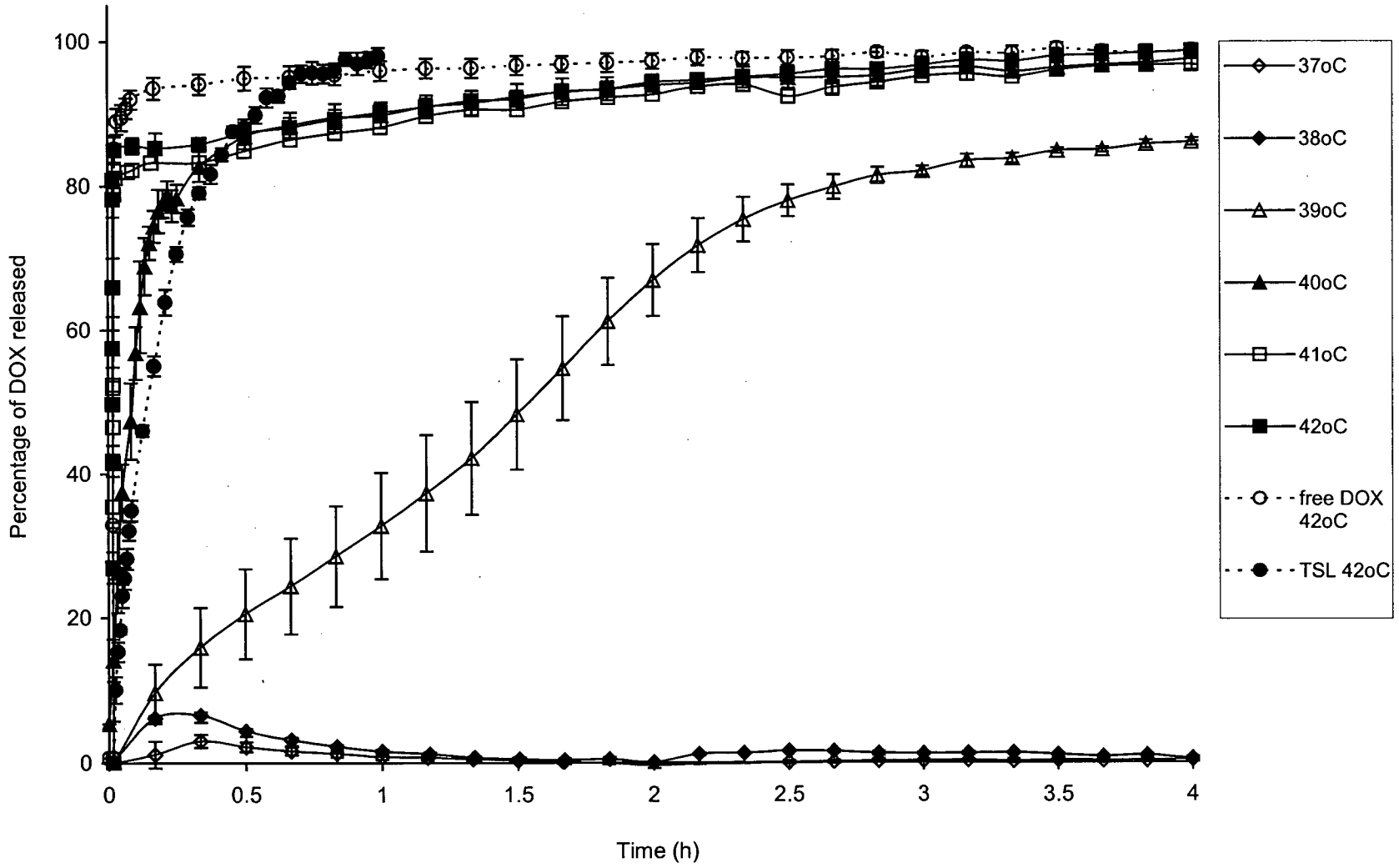

Figure 46: Temperature dependence of DOX released from LTSL. Error bars indicate the standard error of mean values (n = 3).

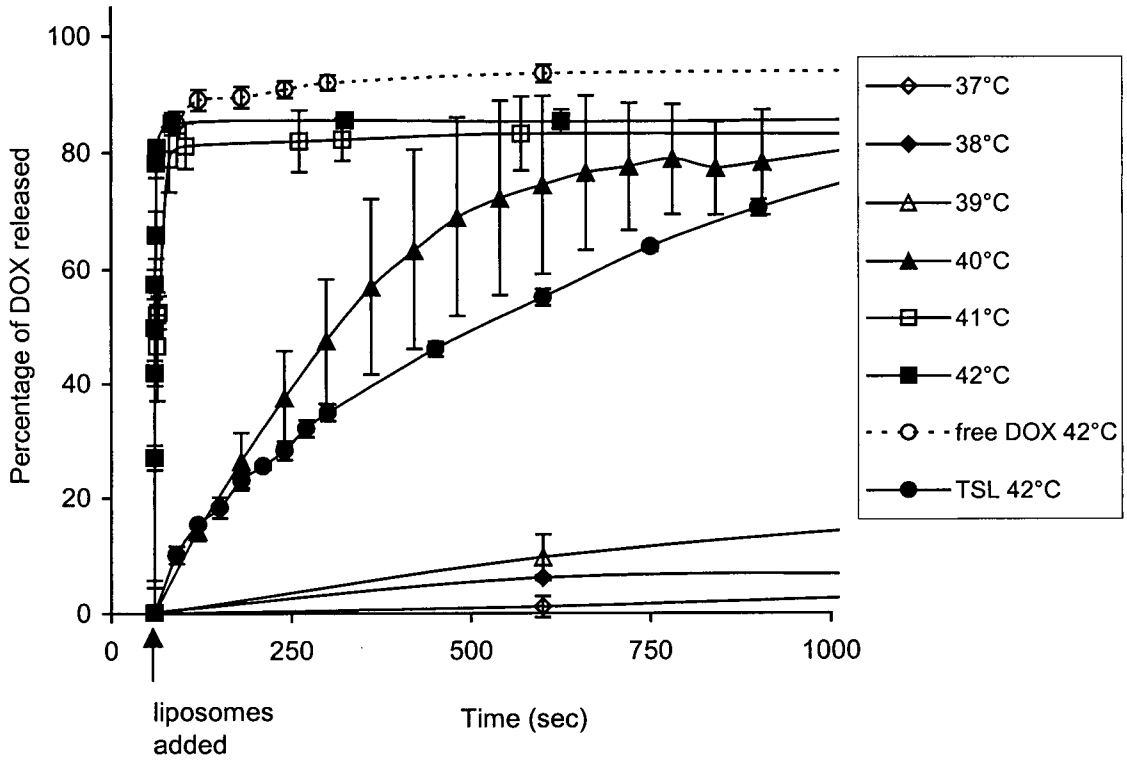

Figure 47: Temperature dependence of DOX released from LTSL (detail of Figure 46). Error bars indicate the standard error of mean values (n = 3).

4.2.2. Temperature dependence of the permeability coefficients of LTSL for DOX

Permeability coefficients were calculated from drug release curves as a measure of comparison between drug release rates from LTSL at different temperatures and between drug release rates from LTSL and TSL (see section 3.11.).

At temperatures of 37°C and 38°C, DOX was not released from LTSL and thus drug flux and permeability coefficients could not be determined at these temperatures. At higher temperatures between 39°C and 41°C drug flux across the membrane and membrane permeability coefficients increase linearly (R^2 = 0.99) with increasing temperature. At temperatures of 41°C and 42°C permeability coefficients of LTSL were calculated at 6.31 x 10^{-9} and 3.33 x 10^{-8}, respectively (Table 7, Figure 48). In comparison, the permeability coefficient of TSL at 42°C was at 2.84 10^{-10}, a value approximately 100 times lower than that in LTSL, which compares well to literature values [207] and is indicative of a different drug release mechanism in LTSL and TSL.

Table 7: Temperature dependence of DOX flux across the LTSL membrane and permeability coefficients of LTSL (n = 3).

Temperature (°C)	*DOX flux (µmol/sec)*	*Permeability coefficient (cm/sec)*
37	-	-
38	-	-
39	1.40 E-6	2.73 E-11
40	2.31 E-5	4.50 E-10
41	3.24 E-4	6.31 E-9
42	1.71 E-3	3.33 E-8
42 TSL	1.46 E-05	2.84 E-10

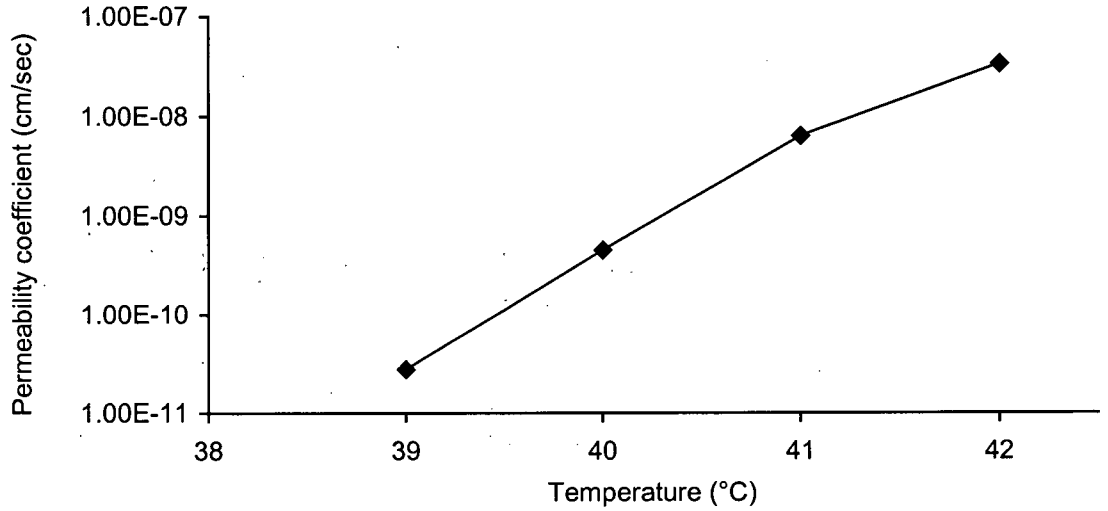

Figure 48: Temperature dependence of the permeability coefficients of LTSL for DOX.

4.3. Novel mechanisms of drug release from LTSL

In this section of the thesis, morphological features of LTSL and TSL were examined using cryo-TEM before and after cycling liposomes through their T_C in order to gain insight into structural changes of the LTSL membrane during phase transition. To cycle liposomes through their T_C, samples were heated for 10 min to a temperature of 45°C (for liposomes prepared at pH 4 and 6.5) or 50°C (for liposomes prepared at pH 2) in a circulating water bath and cooled to room temperature (22°C). This cycle was carried out one time or five times before QELS size analysis.

4.3.1. Effect of cycling liposomes through their T_C on the formation of membrane discs (cryo-TEM studies)

When LTSL and TSL were prepared freshly and never cooled to temperatures below the T_C of the formulation (Figure 49A and 49C) or when LTSL were cooled once to a temperature below the T_C of the formulation (Figure 50A) membrane discs were initially not present in the sample. When liposomes were then heated again to temperatures above their T_C, a small number of bilayer discs appeared in the sample (Figures 49 B, 49D, and 50B). After five T_C cycles, the amount of open liposomes and bilayers discs increased (Figure 50C). At temperatures below the T_C of LTSL, liposomes exhibited polyhedral shapes with faceted surfaces and this appearance was more pronounced in liposomes with smaller diameters (Figure 50). Bilayer discs were smaller than the liposomes from which they derived with an average size of approximately 50 nm. The dark circles within liposomes in Figure 50B represent an artifact of invaginated liposomes, which occurs in a hyperosmotic environment when the buffer outside liposomes concentrates due to water evaporation.

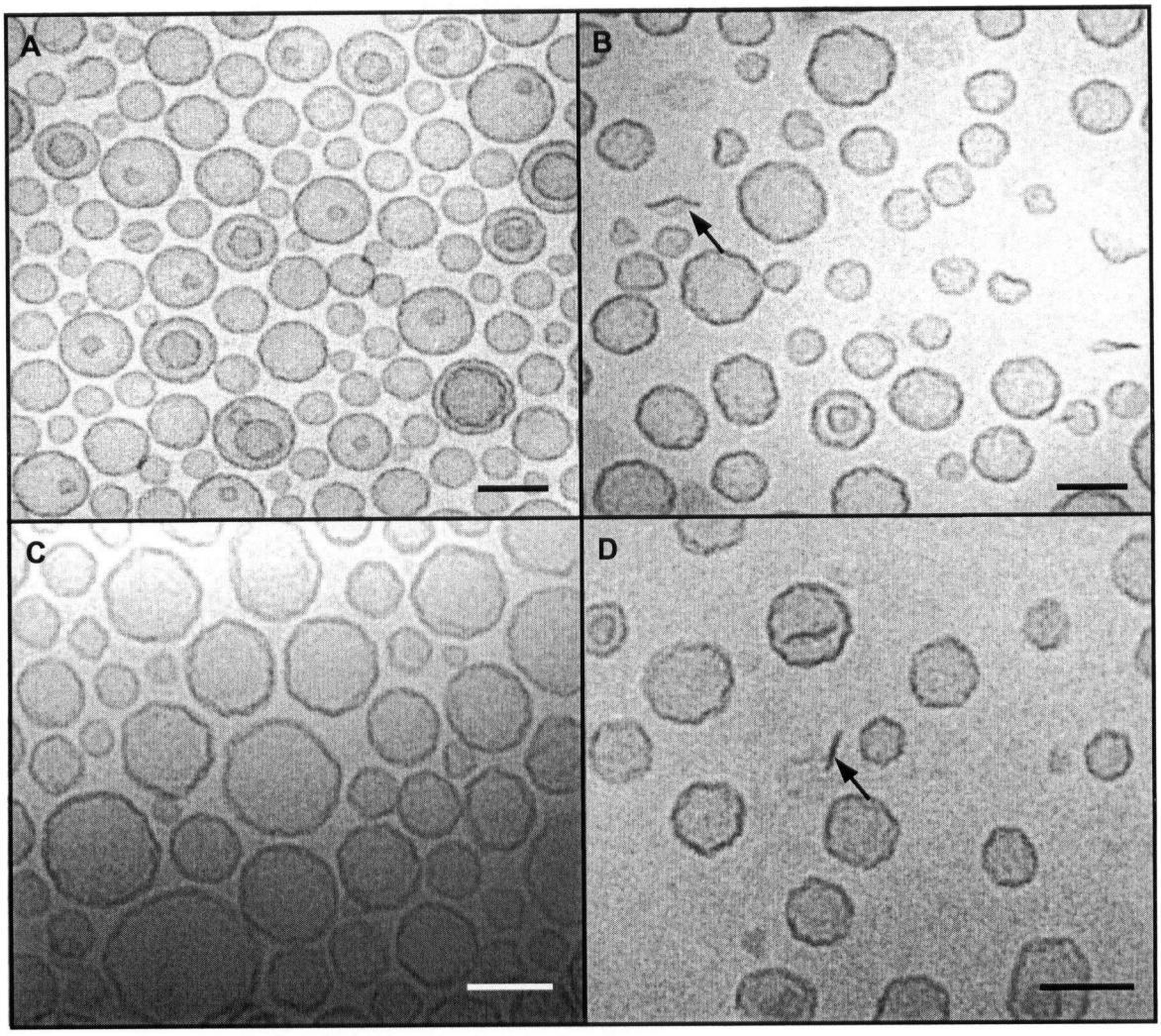

Figure 49: Cryo-TEM images of (A, B) LTSL and (C, D) TSL at a temperature of 50°C. Liposomes were either not cycled trough their T_C (A, C) or cycled trough their T_C one time (B, D). Arrows indicate bilayer discs. Scale bars indicate a size of 100 nm.

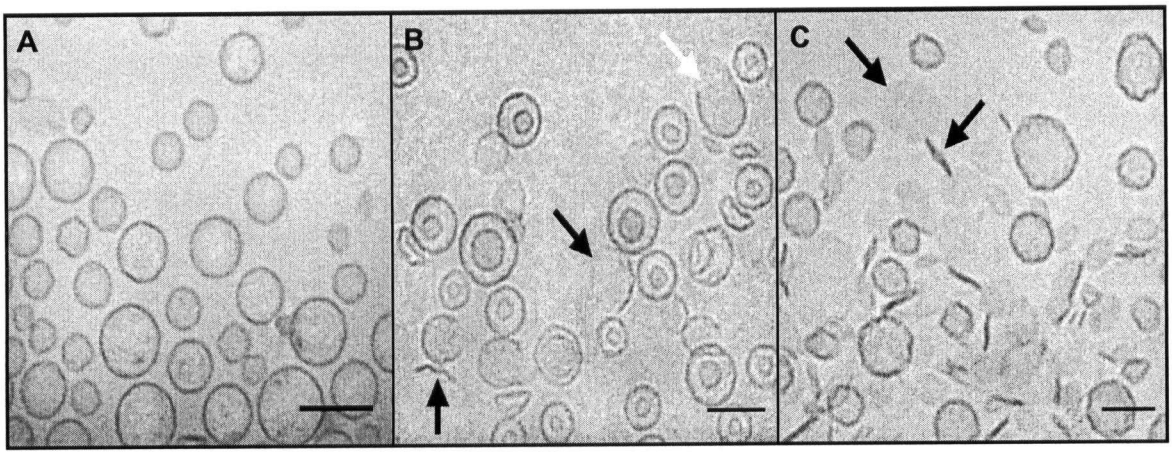

Figure 50: Cryo-TEM images of LTSL before and after cycling liposomes through their T_C. LTSL were vitrified from a temperature of (A) 22°C, (B) 50°C, or (C) after cycling liposomes five times through their T_C. The white arrow indicates an open liposome, black arrows indicate bilayer discs. Scale bars indicate a size of 100 nm.

4.3.2. Membrane composition dependency of disc formation

Based on the hypothesis that micelle-forming membrane components are responsible for disc formation during phase transition, the contribution of the two LTSL membrane components capable of forming micellar aggregates, namely DSPE-PEG_{2000} and MSPC, were investigated.

In the LTSL sample without PEG-lipid, bilayer discs could not be detected before (Figure 51A) or after (Figure 51B) cycling liposomes five times through their T_C. In the LTSL sample without MSPC (= TSL) containing 4 mol% PEG-lipid, bilayer discs were not present initially (Figure 51C) but appeared after cycling the sample five times through T_C (Figure 51D). The amount of bilayer discs after T_C cycling was less than in liposomes containing both PEG-lipid and MSPC together (compare to Figure 50C). When TSL were prepared containing 8 mol% PEG-lipid in the membrane, bilayer discs were already present in the sample before cycling liposomes through their T_C and the

number of discs increased after T_C cycling in comparison to TSL containing 4 mol% PEG-lipid (Figures 51E and 51F).

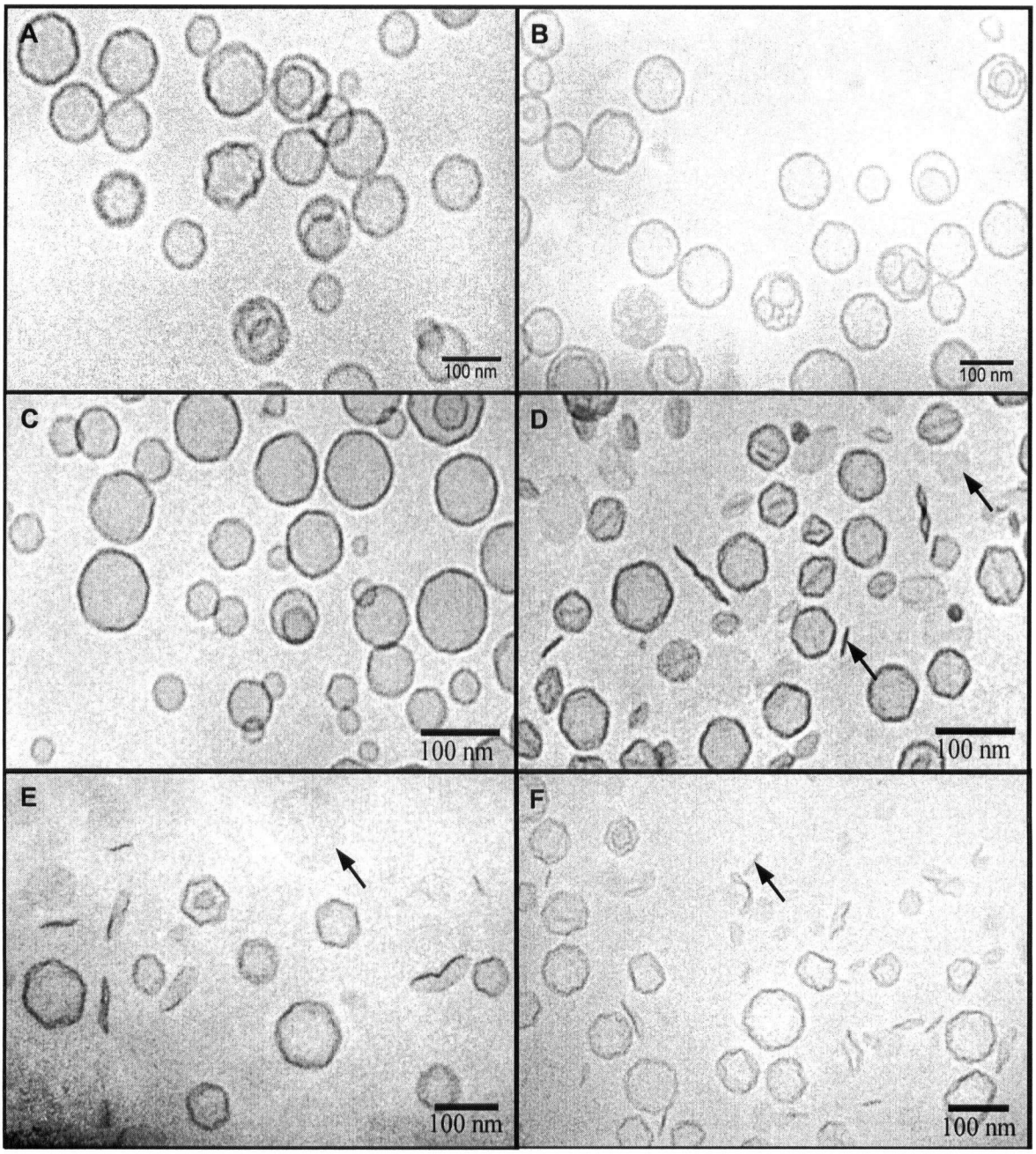

Figure 51: Cryo-TEM images of (A, B) LTSL without DSPE-PEG_{2000} (DPPC/MPPC, molar ratio: 90:10), (C, D) TSL containing 4 mol% DSPE-PEG, and (E, F) TSL containing 8 mol% DSPE-PEG before (A, C, E) and after (B, D, F) cycling liposomes five times through their T_C. Samples were vitrified from a temperature of 45°C (LTSL) or 22°C (TSL). Arrows indicate bilayer discs.

4.3.3. Effect of cycling liposomes through their T_C on the size distribution and the relative absorbance intensity (turbidity)

Cryo-TEM images revealed the formation of membrane discs after cycling liposomes through their T_C but the extent of disc formation cannot be assessed by analyzing cryo-TEM images because the amount of discs varies from image to image. Therefore, the quantitative impression of disc formation can easily be biased. In this section of the thesis the extent of disc formation was assessed by determining particle size and the turbidity of the sample since turbidity depends on the amount of light scattering from particles in the sample, which depends on the particle size and the wavelength of the scattered light. Differences in the average particle size were not analyzed statistically since size determinations were performed from a singe sample on a single day. The intent for these experiments was not to detect statistically significant differences in particle size but a decrease in particle size was used as a relative indication of disc formation as a function of time, temperature, and pH.

When NTSL were stored for 16 months in 300 mM citrate buffer, pH 4, at a temperature of 4°C, T_C cycling had no effect on the average particle size, which was at 115.6 nm (STD 37.5 nm) before and at 114.3 nm (STD 37.6 nm) and 112.8 (STD 35.3 nm) after T_C cycling one time or five times, respectively (Figure 52). When LTSL were stored under the same conditions for one day or one month, the average particle size (97.9 nm, STD 24.2) did also essentially not change after cycling liposomes through their T_C one time (101.3 nm, STD 32 nm) or five times (102.1, STD 28.1) (Figures 52 and 53).

When LTSL were stored under the same conditions for two or three months the average particle size decreased after one T_C cycle from 115.9 nm (STD 40.5 nm) and 88.4

nm (STD 15.3 nm), respectively, to 30.4 nm (STD 14.9 nm) and 34 nm (STD 8.5 nm), respectively (Figure 52 and 53). When TSL were stored under the same conditions for three months the average particle size decreased after one T_C cycle from 94.6 nm (STD 24.6 nm) to 36.4 nm (STD 3.9 nm) (Figure 52).

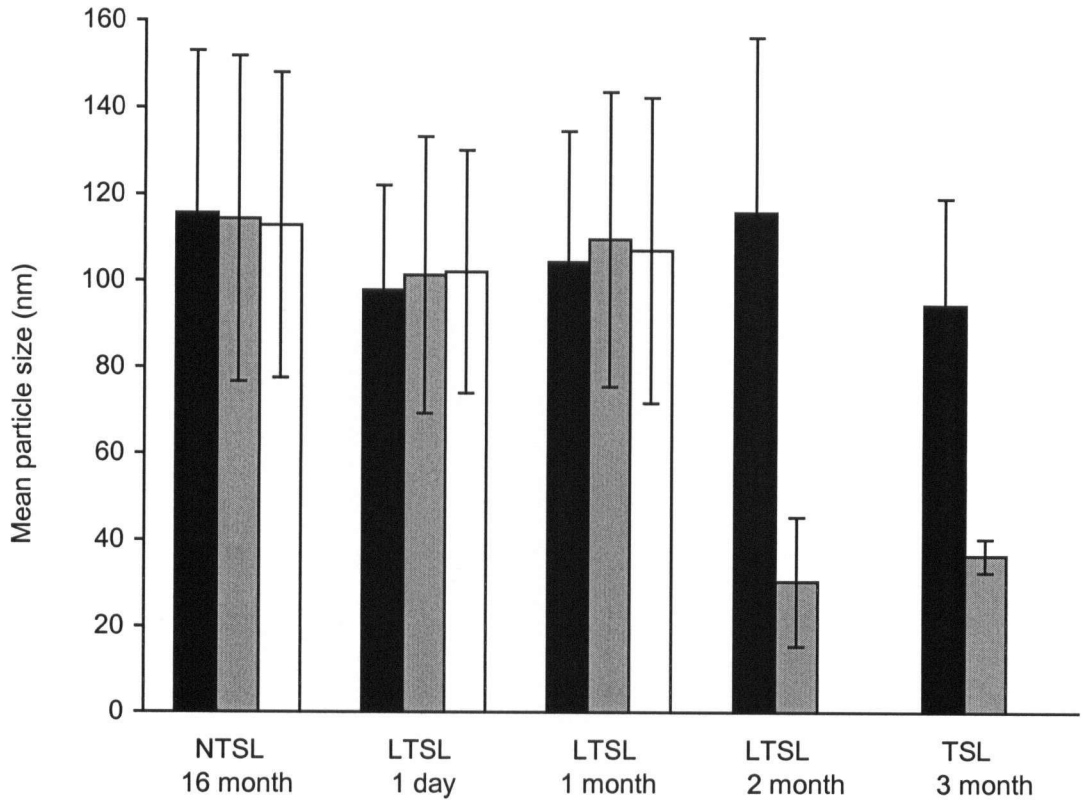

Figure 52: Mean particle size of liposomes stored in 300 mM citrate buffer, pH 4, at a temperature of 4°C before (■) and after cycling liposomes one time (■) or five times (□) through their T_C. Error bars indicate the standard deviation.

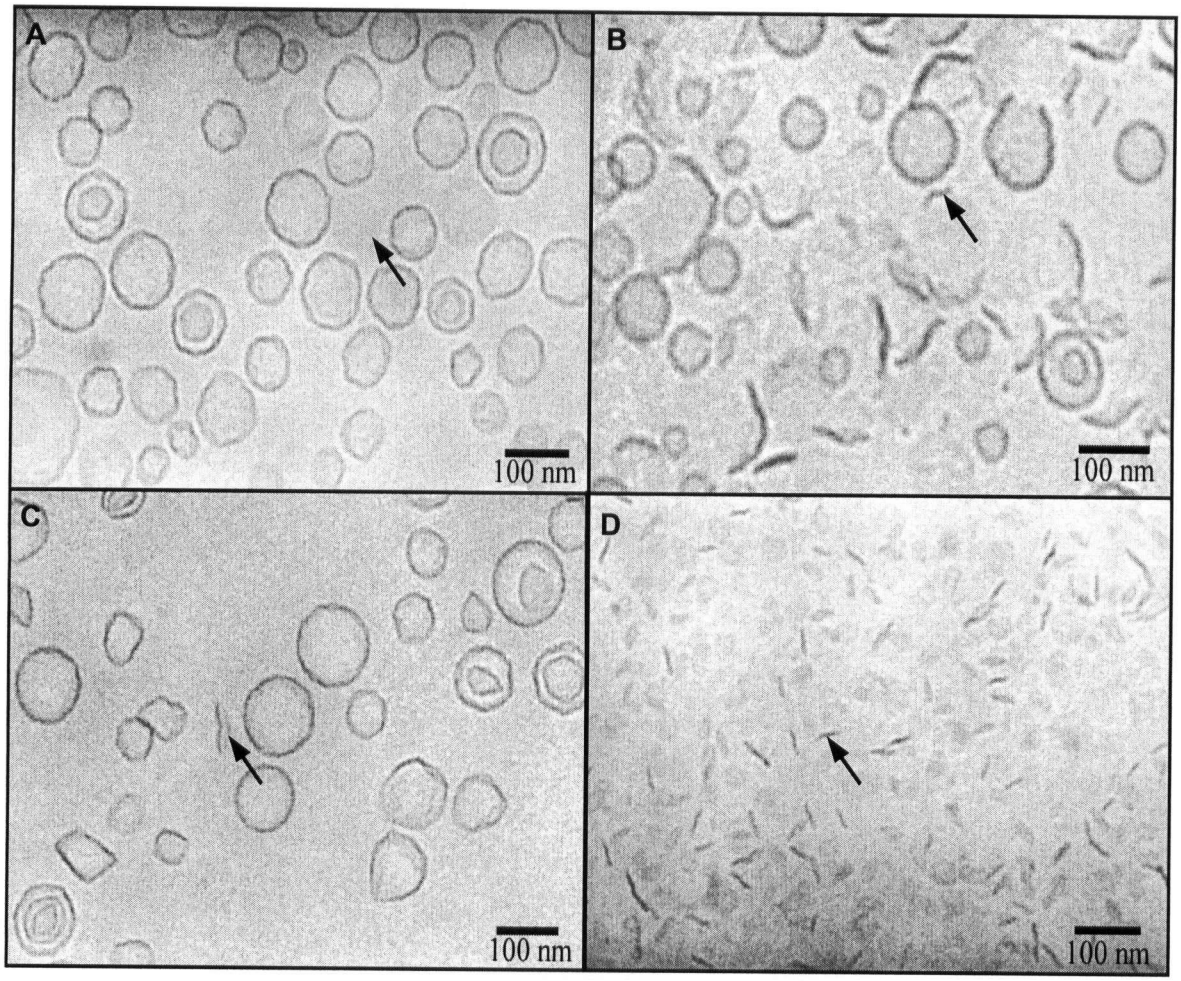

Figure 53: Cryo-TEM images of (A, B) freshly prepared and (C, D) 3 month old LTSL before (A, C) and after (B, D) cycling five times (fresh liposomes) or one time (3 month old liposomes) through their T_C. Arrows indicate bilayer discs.

When LTSL were stored for three weeks in 300 mM citrate buffer, pH 4, at a temperature of 4°C the average particle size decreased with each T_C cycle from initially 116.2 nm (STD 25.6 nm) to 102.6 nm (STD 41.1 nm) after one cycle to 87.5 nm (STD 40.5 nm) after two cycles to 72.6 nm (STD 30.4 nm) after tree cycles to 68.9 nm (STD 31.6 nm) after four cycles to 63.8 nm (STD 32.4 nm) after five cycles (Figure 54).

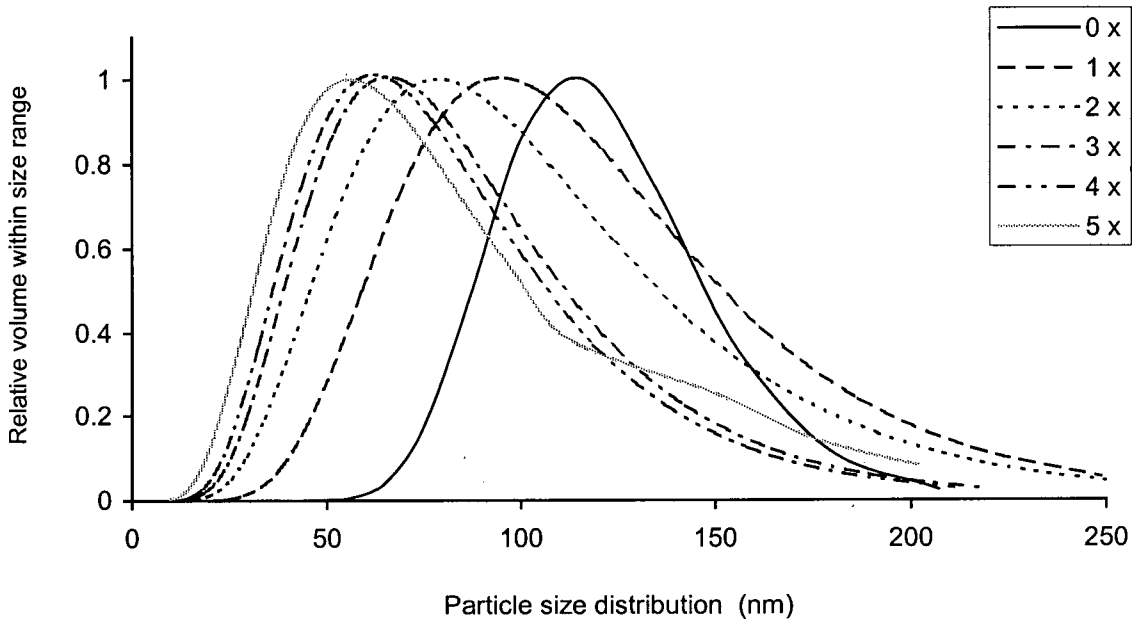

Figure 54: Particle size distribution of LTSL stored for 3 weeks at pH 4 at a temperature of 4°C before (0 x) and after cycling liposomes one to five times through their T_C.

It was speculated that the time-dependency of disc formation was a result of acid-catalyzed hydrolysis and the generation and accumulation of hydrolysis products in the liposome membrane over time. Therefore, LTSL were prepared containing 10 mol%, 15 mol%, or 20 mol% MSPC (DPPC/MSPC/DSPE-PEG_{2000}, molar ratio 80 / 10, 15, or 20 / 4), LTSL containing 10 mol% MSPC and 10 mol% MPPC (DPPC/MSPC/MPPC/DSPE-PEG_{2000}, molar ratio 80/10/10/4), and LTSL containing10 mol% MSPC, 5 mol% MPPC, and 5 mol% of and palmitic acid (PA) (DPPC/MSPC/MPPC/PA/ DSPE-PEG_{2000}, molar ratio 80/10/5/5/4). The outside citrate buffer (pH 4) of the LTSL preparation containing 10 mol% MSPC was exchanged with 150 mM HBS (pH 7.5) and all liposomes were stored at a temperature of 4°C. Liposomes were cycled through their T_C one time or five times and the particle size before and after T_C cycling was determined by QELS.

When LTSL containing 10 mol%, 15 mol% or 20 mol% MSPC or containing 10 mol% MSPC, 5 mol% MPPC, and 5 mol% PA were stored for one day in citrate buffer at a temperature of 4°C the average particle size did essentially not change after cycling liposomes through their T_C one time or five times (Figure 55). However, cryo-TEM images of LTSL containing 10 mol% MSPC, 5 mol% MPPC, and 5 mol% PA revealed that membrane discs were present in the sample before T_C cycling and the number of discs increased after cycling liposomes through their T_C five times (Figure 56). After repetitive T_C cycling, some liposomes still remained intact, small (30-40 nm) discs appeared, but also larger membrane structures, approximately 150 nm in size were present in the sample (Figure 56). The comparison between results obtained from size determinations and cryo-TEM images highlights the fact that measuring the average particle size by QELS can lead to a false interpretation of the data when the particle population is polymorphic and heterogeneous in size.

LTSL containing 20 mol% MSPC or 10 mol% MSPC and 10 mol% MPPC aggregated after preparation, which was apparent in the gel-like consistency of the preparation. The average particle size of aggregated liposomes containing 10 mol% MSPC and 10 mol% MSPC was variable and dependent upon dilution.

When LTSL were stored at a temperature of 4°C after exchanging the outside 300 mM citrate buffer, pH 4, with 150 mM HBS, pH 7.5, for two months the average particle size essentially did not change after one or five T_C cycles (Figure 55). When LTSL were stored under the same conditions for nine months the average particle size decreased slightly after one T_C cycle and even further after five T_C cycles (Figure 55).

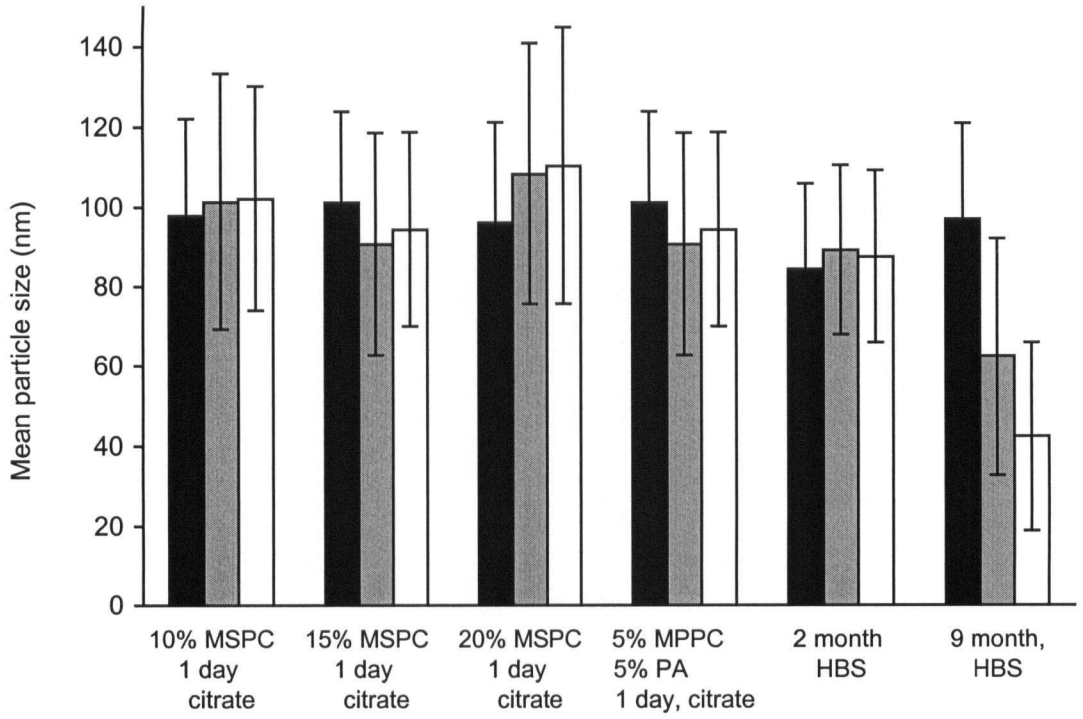

Figure 55: Mean particle size of LTSL containing various amounts of lysolipid and palmitic acid (PA) stored at a temperature of 4°C in citrate or after exchanging the outside citrate buffer with HBS before (■) and after cycling liposomes one time (■) or five times (□) through their T_C. Error bars indicate the standard deviation.

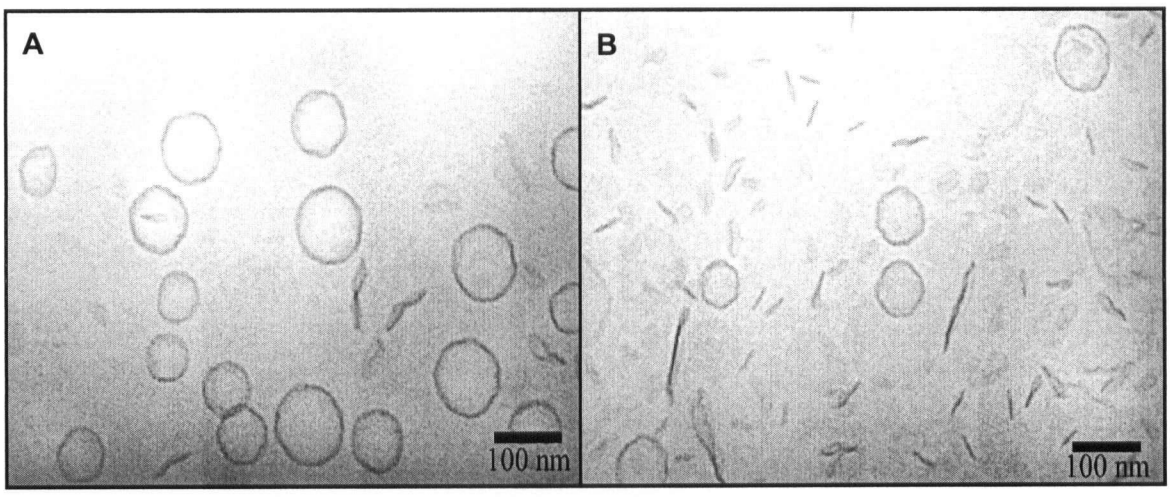

Figure 56: Cryo-TEM images of freshly prepared LTSL containing 10 mol% MSPC and 5 mol% of the DPPC-hydrolysis products MPPC and palmitic acid (A) before and (B) after cycling five times through their T_C.

The change in the sample's turbidity was used as a second measure of a change in particle size since the amount of light scattered from particles depends on their size at a fixed wavelength of light source. The mean relative absorbance of LTSL decreased with each T_C cycle by approximately 1% per cycle. The decrease was significant with every cycle or every other cycle in comparison to the absorbance intensity of the previous cycle ($p < 0.05$). In TSL, the decrease was initially greater than in LTSL at approximately 3% after the first cycle but the mean relative absorbance did not decrease significantly any further in subsequent cycles. The mean relative absorbance in NTSL did not change significantly when cycled up to six times between temperatures of 45°C and 22°C for 10 min each in accordance to results obtained by cryo-TEM image analysis (Figure 57).

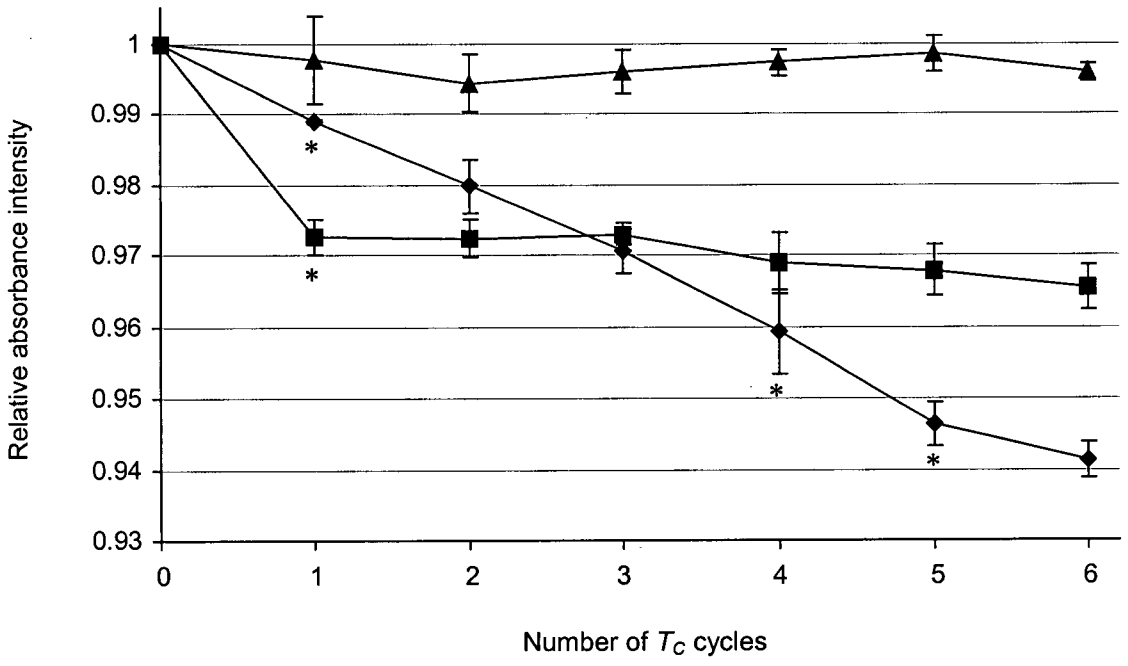

Figure 57: Relative absorbance intensity of NTSL (▲), TSL (■), and LTSL (◆) before and after cycling liposomes one to six times through their T_C. * = $p < 0.05$ in comparison to the absorbance intensity of the previous cycle. Error bars indicate the standard error of mean values (n = 3).

4.3.4. Effect of storage time, pH, and temperature on the formation of membrane discs

Results of the proceeding sections suggested that the time-effect of disc formation after cycling liposomes through their T_C was dependent on the pH of the storage buffer. Therefore, it was hypothesized that the time effect on disc formation after T_C cycling may be a consequence of phospholipid hydrolysis leading to accumulation of lysolipid in the membrane. To test this hypothesis, TSL were prepared at pH 2, pH 4, or pH 6.5 and stored at a temperature of 4°C or 22°C for up to 22 weeks. The stability of the pH of the samples was confirmed once a month. For size determination by QELS, aliquots of liposomes samples were diluted with 0.9% sodium chloride solution to a concentration of approximately 2 mg/ml. The average particle size was determined before and after heating the sample to a temperature of 45°C for liposomes stored at pH 4 and 6.5 or to 50°C for samples stored at pH 2 since the T_C of TSL at pH 2 is slightly elevated at 46.7°C (see Table 5). Samples were equilibrated to room temperature prior to size analysis. However, no difference was found in the average particle size when liposomes were stored at pH 2 and heated to a temperature of 45°C or 50°C. Cryo-TEM images were generated before and after cycling liposomes through their T_C from liposomes stored for selected time intervals or when size analysis indicated a change in the average particle size.

The average particle size of TSL stored at pH 2 and a temperature of 4°C decreased after cycling liposomes one time through their T_C from 87 nm to approximately 40 nm between 1 day and 5 weeks (35 days) of storage (Figure 58). Cryo-TEM images revealed that even on the same day of preparation (Figure 59) or 5 days after preparation

(Figure 60) open liposomes were present in the sample before T_C cycling and essentially all liposomes disintegrated into discs after T_C cycling. Between 5 weeks and 22 weeks (154 days) of storage at pH 2 the average particle size after T_C cycling increased continuously from 40 nm at 5 weeks to an average size of 111.7 nm at 22 weeks of storage (Figure 58).

When TSL were stored at pH 4 and a temperature of 4°C the average particle size of 88 nm did essentially not change after T_C cycling for up to 9 weeks (63 days) of storage (Figure 58). Cryo-TEM images revealed however, that after storage for 10 days a small number of membrane discs was present in the sample after T_C cycling (Figure 61). Between 9 weeks and 20 weeks (140 days) of storage at pH 4, the average particle size after T_C cycling decreased gradually to approximately 32 nm. At 22 weeks (154 days) of storage the average particle size increased slightly to 41 nm (Figures 58).

When TSL were stored at pH 6.5 and a temperature of 4°C the average particle size of 93 nm did essentially not change after T_C cycling for the investigated time period of 22 weeks (154 days) (Figure 58). Cryo-TEM images revealed that membrane discs were not present in the sample when liposomes were stored for 3 weeks at pH 6.5 before or after liposomes were cycled through their T_C (Figure 62).

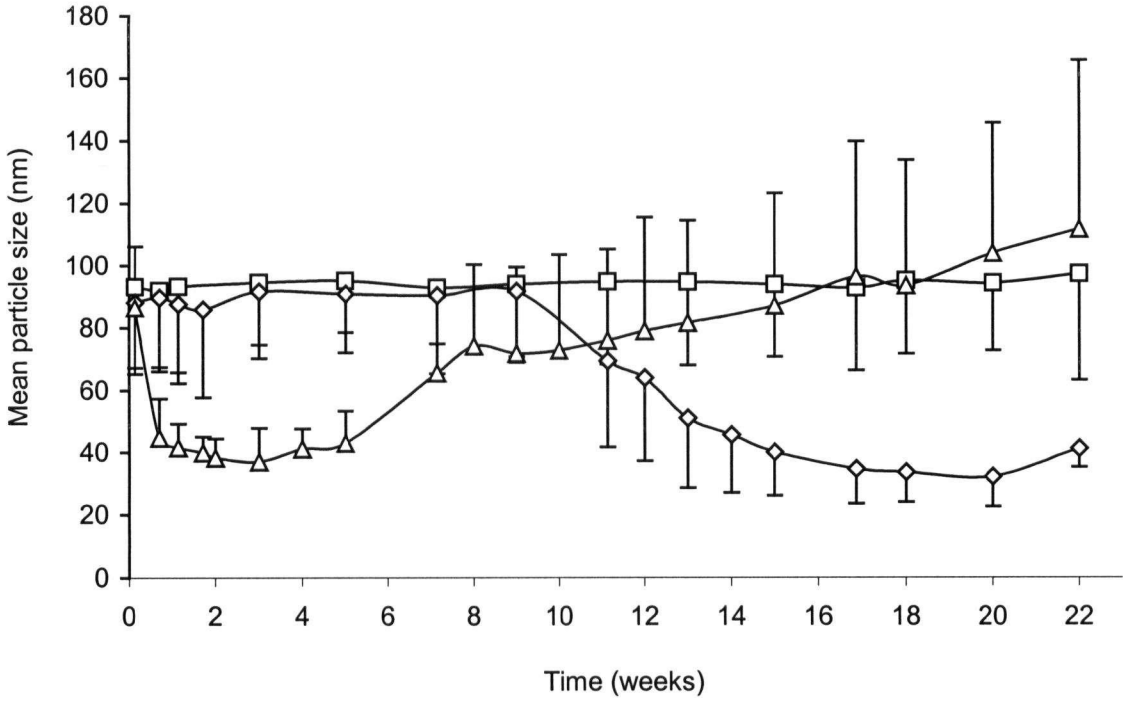

Figure 58: Mean particle size of TSL stored at a temperature of 4°C in citrate buffer at pH 2 (△), pH 4 (◇), or pH 6.5 (□) after cycling liposomes one time through their T_C. Error bars indicate the standard deviation.

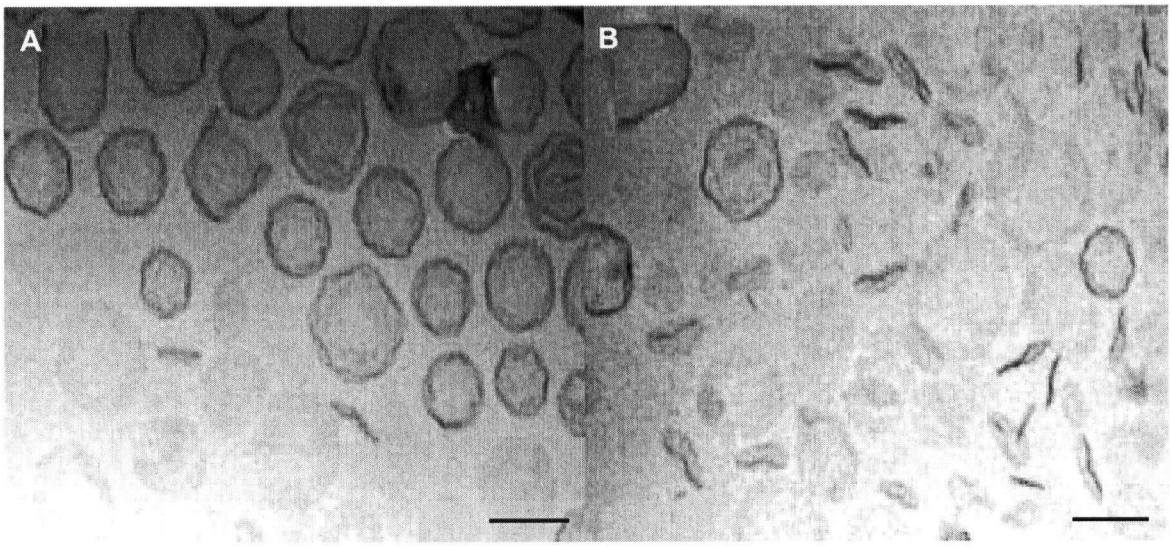

Figure 59: Cryo-TEM images of freshly prepared TSL in citrate buffer, pH 2, (A) before and (B) after cycling liposomes one time through their T_C. Scale bars indicate a size of 100 nm.

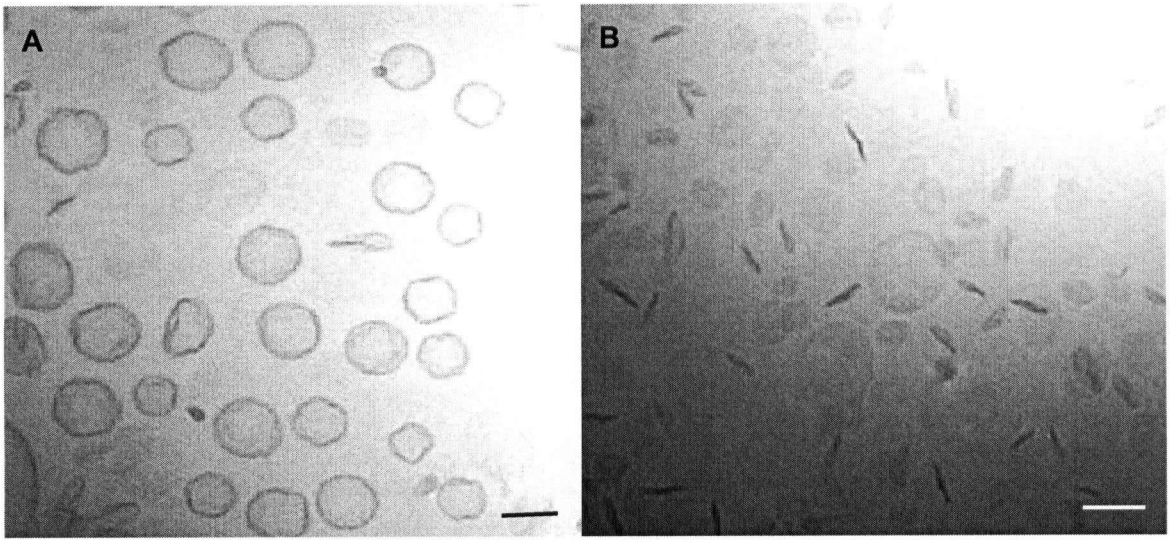

Figure 60: Cryo-TEM images of TSL stored for 5 days at a temperature of 4°C in citrate buffer, pH 2, (A) before and (B) after cycling liposomes one time through their T_C. Scale bars indicate a size of 100 nm.

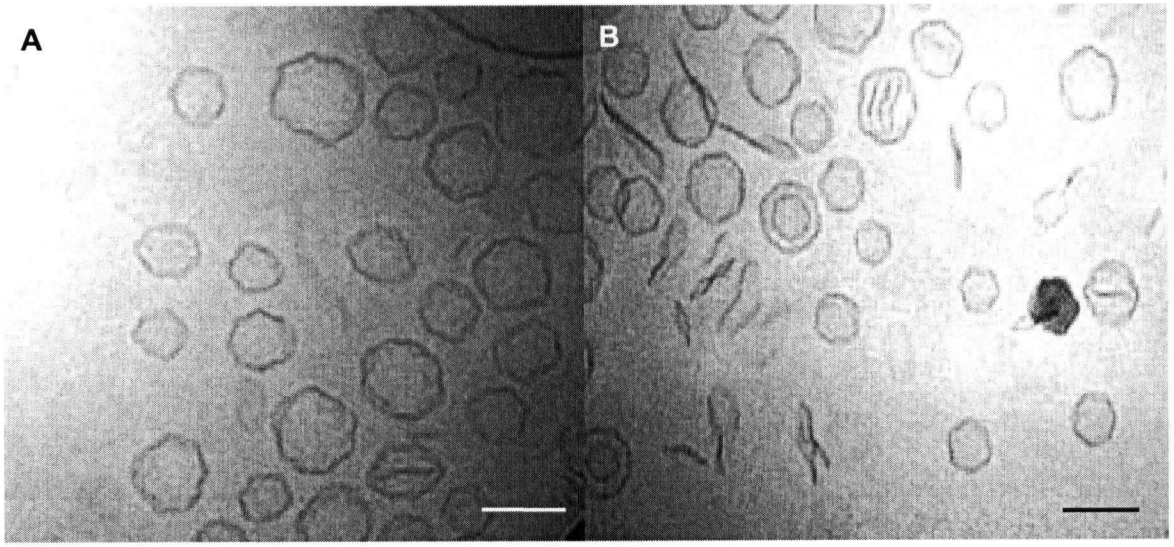

Figure 61: Cryo-TEM images of TSL stored for 10 days at a temperature of 4°C in citrate buffer, pH 4, (A) before and (B) after cycling liposomes one time through their T_C. Scale bars indicate a size of 100 nm.

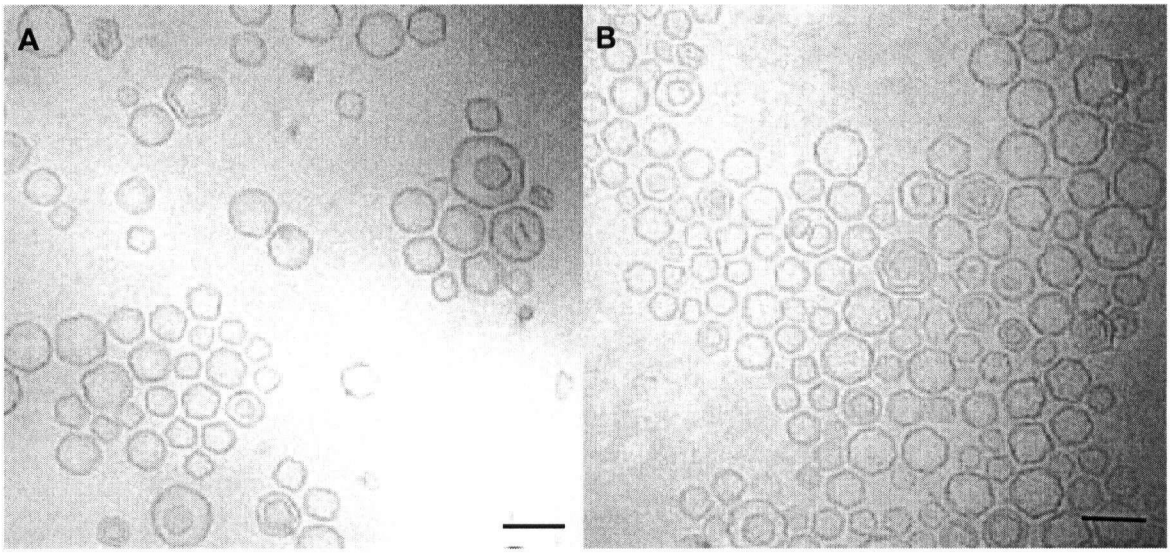

Figure 62: Cryo-TEM images of TSL stored for 3 weeks at a temperature of 4°C in citrate buffer, pH 6.5, (A) before and (B) after cycling liposomes one time through their T_C. Scale bars indicate a size of 100 nm.

When liposomes were stored at higher temperatures, the process of disc formation after T_C cycling occurred earlier in time. The average particle size of TSL stored at pH 2 and a temperature of 22°C decreased after cycling liposomes one time through their T_C from 86 nm to approximately 40 nm after one day of storage (Figure 63). Cryo-TEM images revealed that on the same day of preparation open liposomes were present in the sample before T_C cycling and essentially all liposomes disintegrated into discs after T_C cycling with a very homogeneous size distribution (39.2 nm, STD 5.9) (Figure 64). Between 1 day and 4 weeks (28 days) of storage the average particle size increased continuously from 40 nm at 1 day to an average size of 134 nm at 4 weeks (Figure 63). After 21 and 28 days of storage, the size distribution increased considerably and the viscosity of the sample increased indicating liposome aggregation and membrane fusion. Cryo-TEM images of liposomes after 11 days (Figure 65) and 3 weeks (21 days) of

storage (Figure 66) at pH 2 confirmed that liposomes were no longer present in the sample after T_C cycling but instead membrane discs and sheets appeared and the size of discs increased with increasing storage time.

When TSL were stored at pH 4 and a temperature of 22°C the average particle size of 94 nm decreased gradually for up to two weeks to approximately 32 nm. From then on, the average particle size increased until the end of the investigated time period at 22 weeks (154 days) to approximately 82 nm (Figure 63). Cryo-TEM images generated after 7 days and 10 days of storage at pH 4 revealed that with increasing storage time an increasing number of liposomes disintegrated into discs when liposomes were cycled through their T_C (Figure 67).

When TSL were stored at pH 6.5 and a temperature of 22°C the average particle size of 95 nm did essentially not change after T_C cycling for the investigated time period of 22 weeks (154 days) (Figure 63). Cryo-TEM images revealed that membrane discs were not present in the sample when liposomes were stored for 4 weeks at pH 6.5 before or after liposomes were cycled through their T_C (Figure 68).

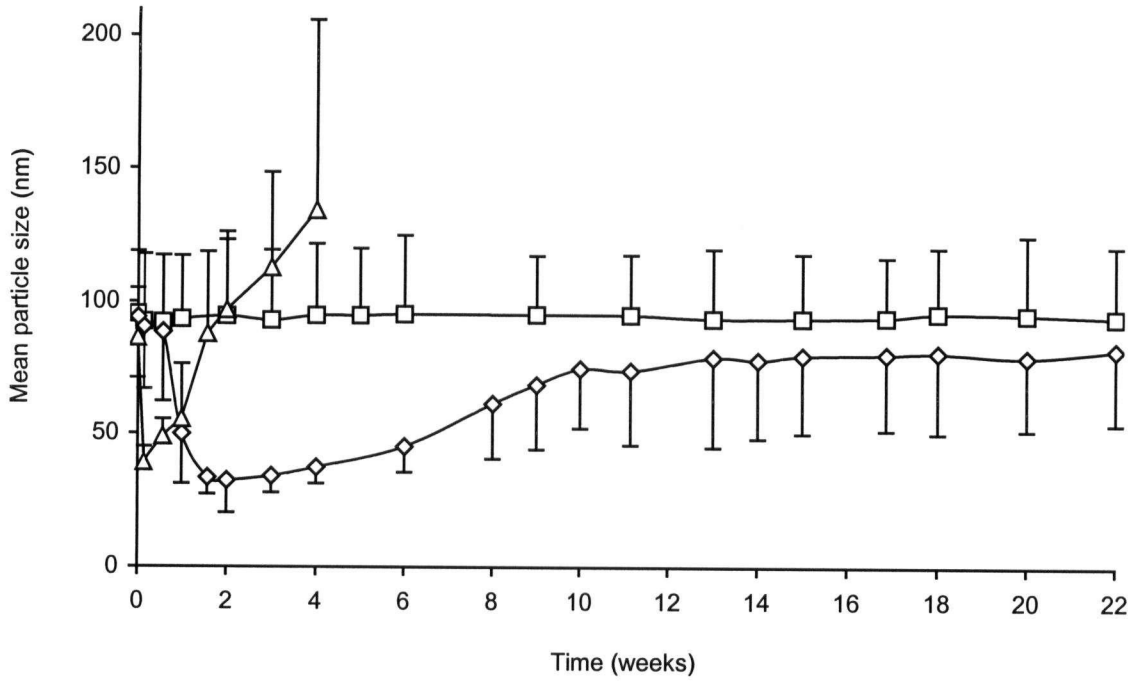

Figure 63: Mean particle size of TSL stored at a temperature of 22°C in citrate buffer at pH 2 (△), pH 4 (◇), or pH 6.5 (□) after cycling liposomes one time through their T_C. Error bars indicate the standard deviation.

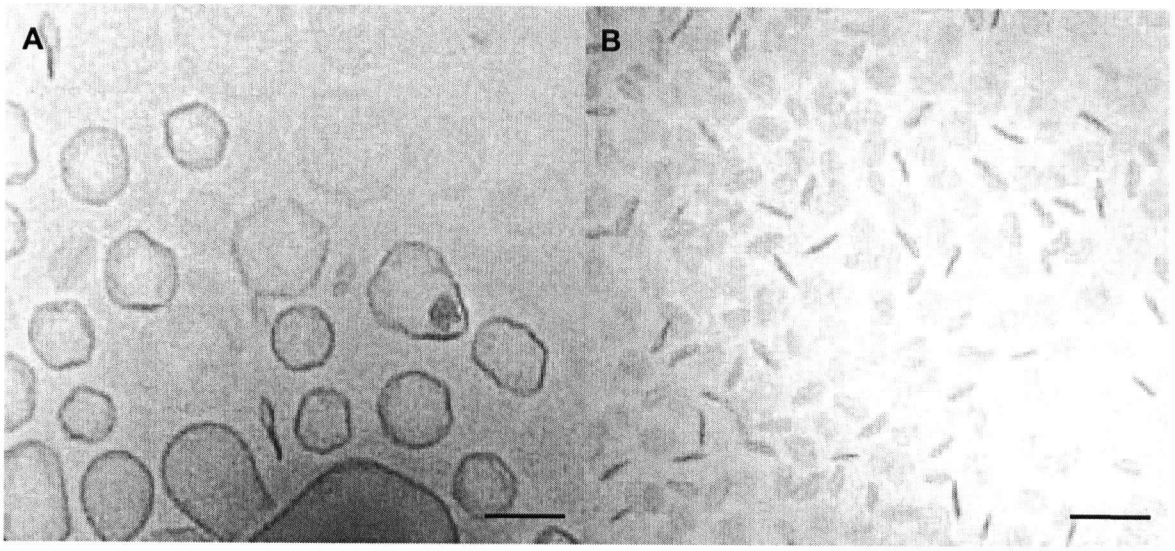

Figure 64: Cryo-TEM images of TSL stored for 1 day at a temperature of 22°C in citrate buffer, pH 2, (A) before and (B) after cycling liposomes one time through their T_C. Scale bars indicate a size of 100 nm.

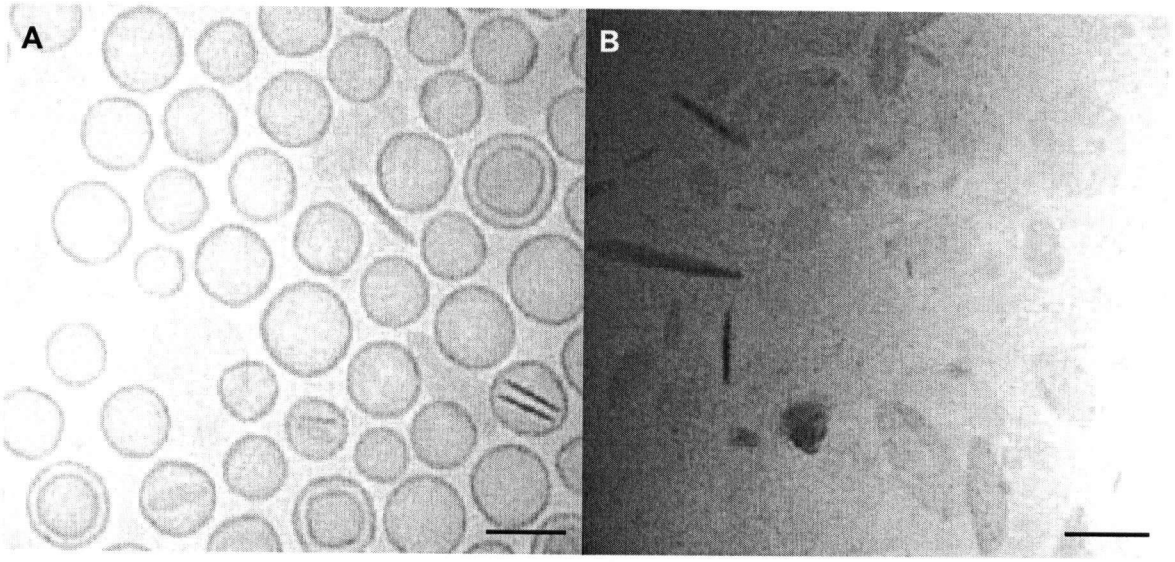

Figure 65: Cryo-TEM images of TSL stored for 11 days at a temperature of 22°C in citrate buffer, pH 2, (A) before and (B) after cycling liposomes one time through their T_C. Scale bars indicate a size of 100 nm.

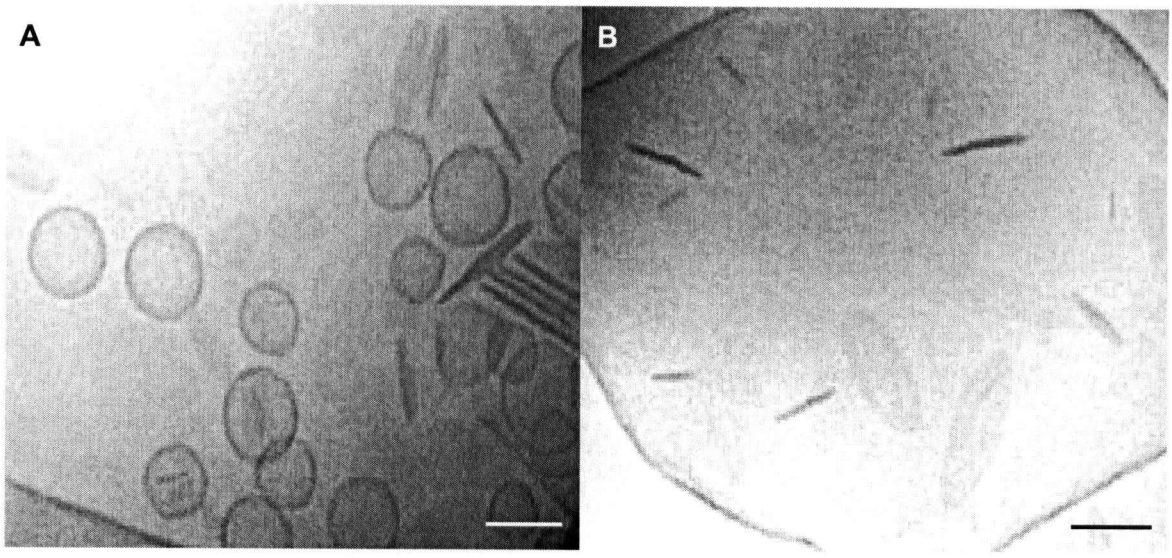

Figure 66: Cryo-TEM images of TSL stored for 3 weeks at a temperature of 22°C in citrate buffer, pH 2, (A) before and (B) after cycling liposomes one time through their T_C. Scale bars indicate a size of 100 nm.

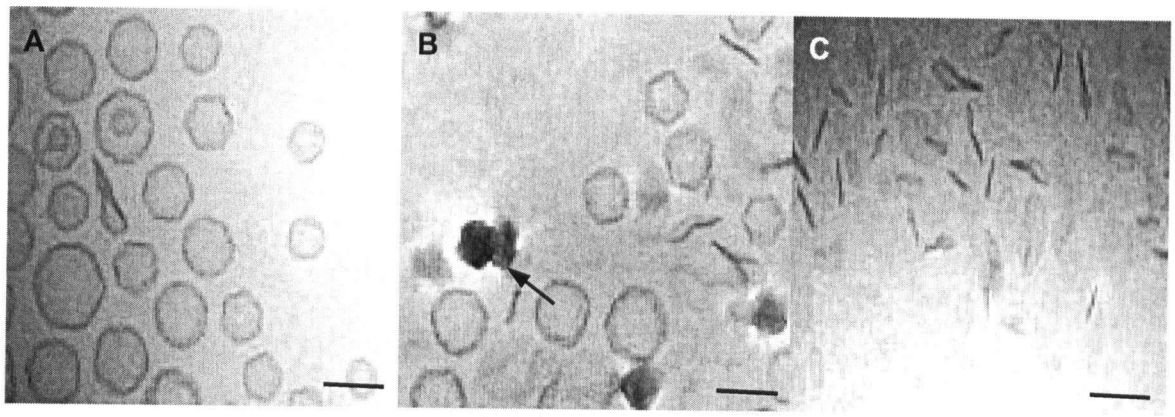

Figure 67: Cryo-TEM images of TSL stored for (A, B) 7 days or (C) 10 days at a temperature of 22°C in citrate buffer, pH 4, (A) before and (B, C) after cycling liposomes one time through their T_C. The arrow indicates ice crystals. Scale bars indicate a size of 100 nm.

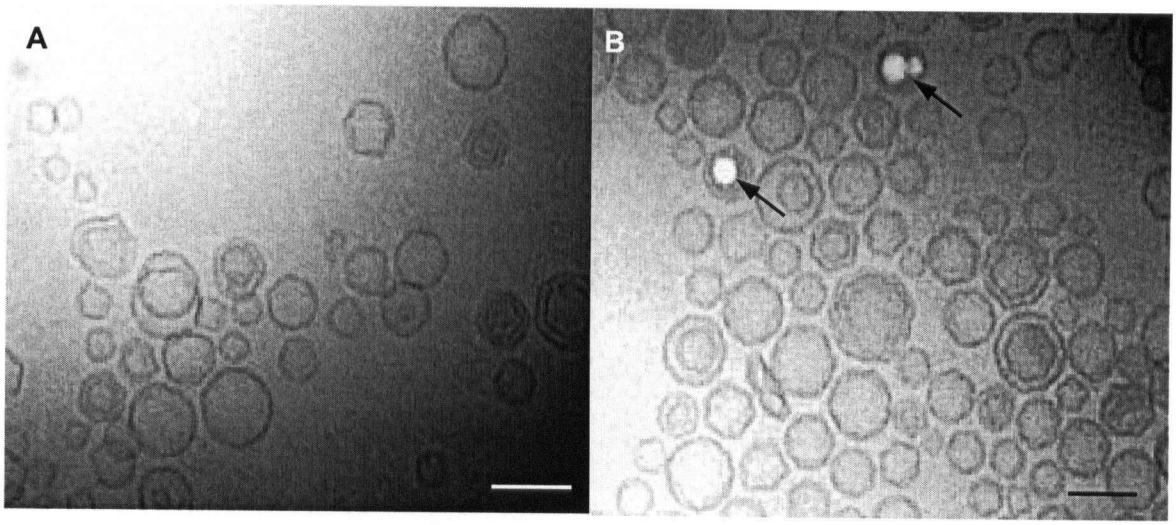

Figure 68: Cryo-TEM images of TSL stored for 4 weeks at a temperature of 22°C in citrate buffer, pH 6.5, (A) before and (B) after cycling liposomes one time through their T_C. Arrows indicate radiation damage by the electron beam. Scale bars indicate a size of 100 nm.

4.3.5. DSC thermograms of disc formation

Results of the previous experiments revealed that disc formation after cycling liposomes through their T_C is only a minor event in freshly prepared LTSL and TSL but a major event in aged and thus partially hydrolyzed TSL. The exact time when disc formation becomes a major event depends on the storage temperature and the pH of the storage buffer. In this section of the thesis it was examined whether a major restructuring event such as the formation of membrane discs would be detectable by DSC.

TSL freshly prepared in citrate buffer, pH 2, and TSL stored for 23 days in citrate buffer, pH 4, at a temperature of 22°C were analyzed by DSC. After the temperature of the sample was equilibrated back to room temperature the same sample was analyzed again under the same experimental conditions. DSC thermograms of freshly prepared TSL at pH 2, and of TSL stored for 23 days at pH 4 revealed that two thermal events occurred in both samples (Figures 69 and 71). The thermal events that occurred at the higher temperatures at 46.5°C and 44.5°C in TSL stored at pH 2 or pH 4, respectively, was approximately at the T_C of the original sample and was thus attributed to the main melting phase transition. The thermal events that occurred at the lower temperatures at 41.8°C and 41.7°C in TSL stored at pH 2 or pH4, respectively, was attributed to disc formation since drug release from LTSL has been shown previously to occur at temperatures a few degrees lower than their T_C. This observation explains the lack of difference in the average particle size when liposomes stored at pH 2 were heated to temperatures of 45°C or 50°C despite the fact that the T_C of TSL stored at pH 2 was determined at a temperature of 46.7°C. The reason is likely that disc formation occurs at temperatures approximately 2-3 degrees below the T_C of the liposome membrane. When

the same samples were analyzed once again DSC peaks that occurred at the lower temperatures were no longer present in the thermograms (Figures 70 and 72) indicating that disc formation occurred only or primarily during the first cycle through the T_C of the formulation.

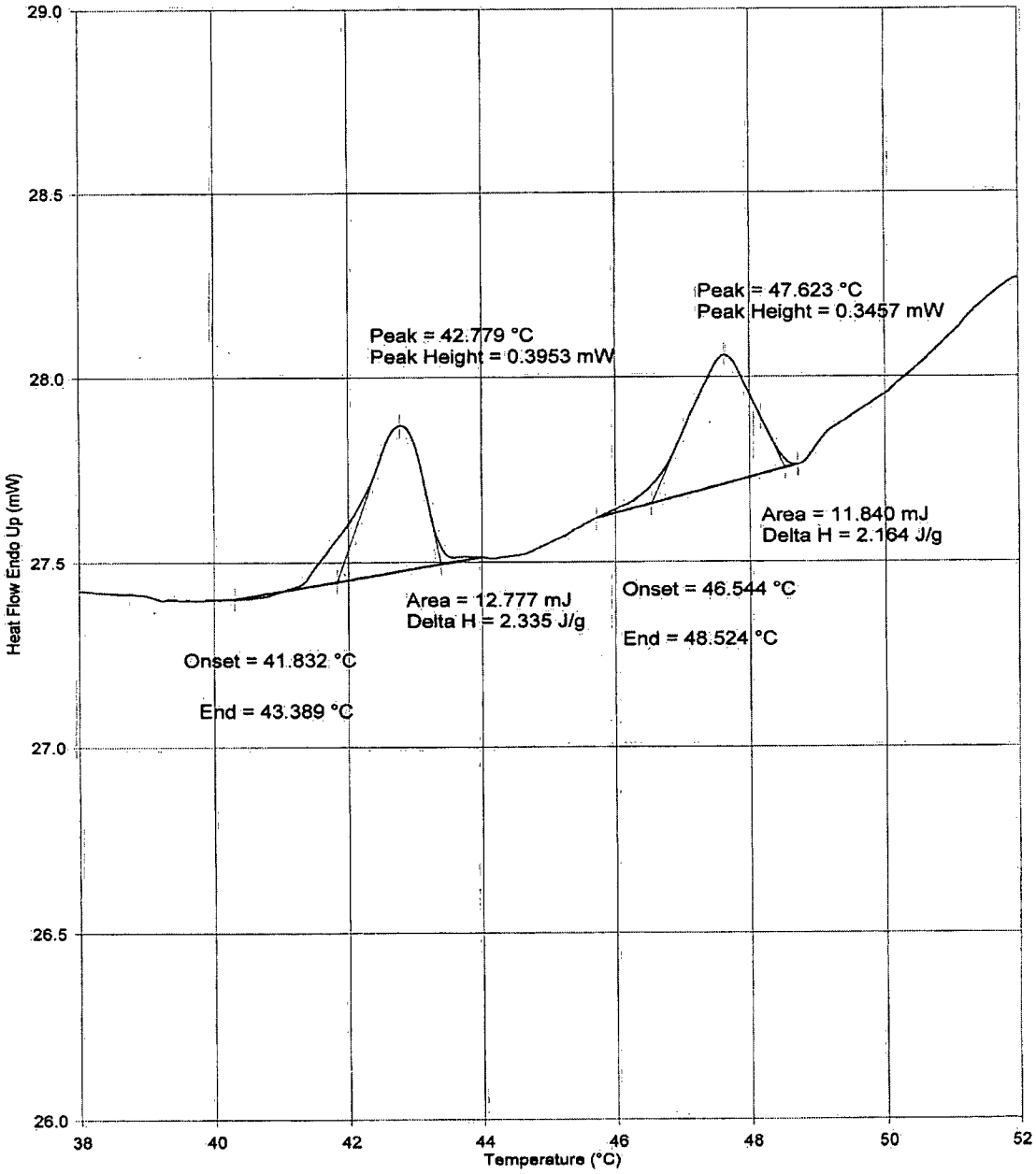

Figure 69: DSC thermogram of freshly prepared TSL in 300 mM citrate buffer, pH 2, at a lipid concentration of 100 mg/ml. The heating rate was at 10°C/min.

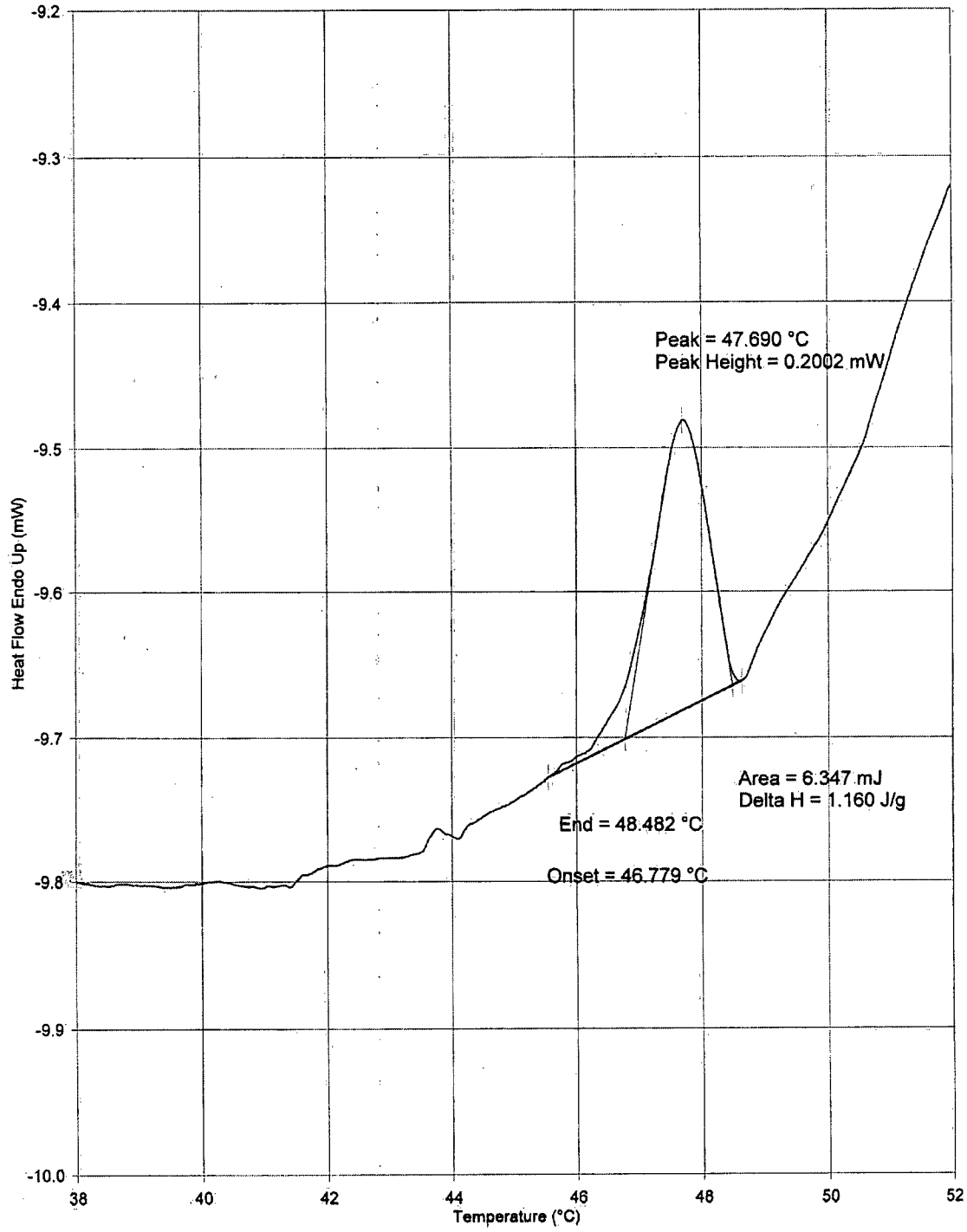

Figure 70: DSC thermogram of freshly prepared TSL in 300 mM citrate buffer, pH 2, at a lipid concentration of 100 mg/ml. The thermogram is recorded from the second run of the same sample used in Figure 69. The heating rate was at 10°C/min.

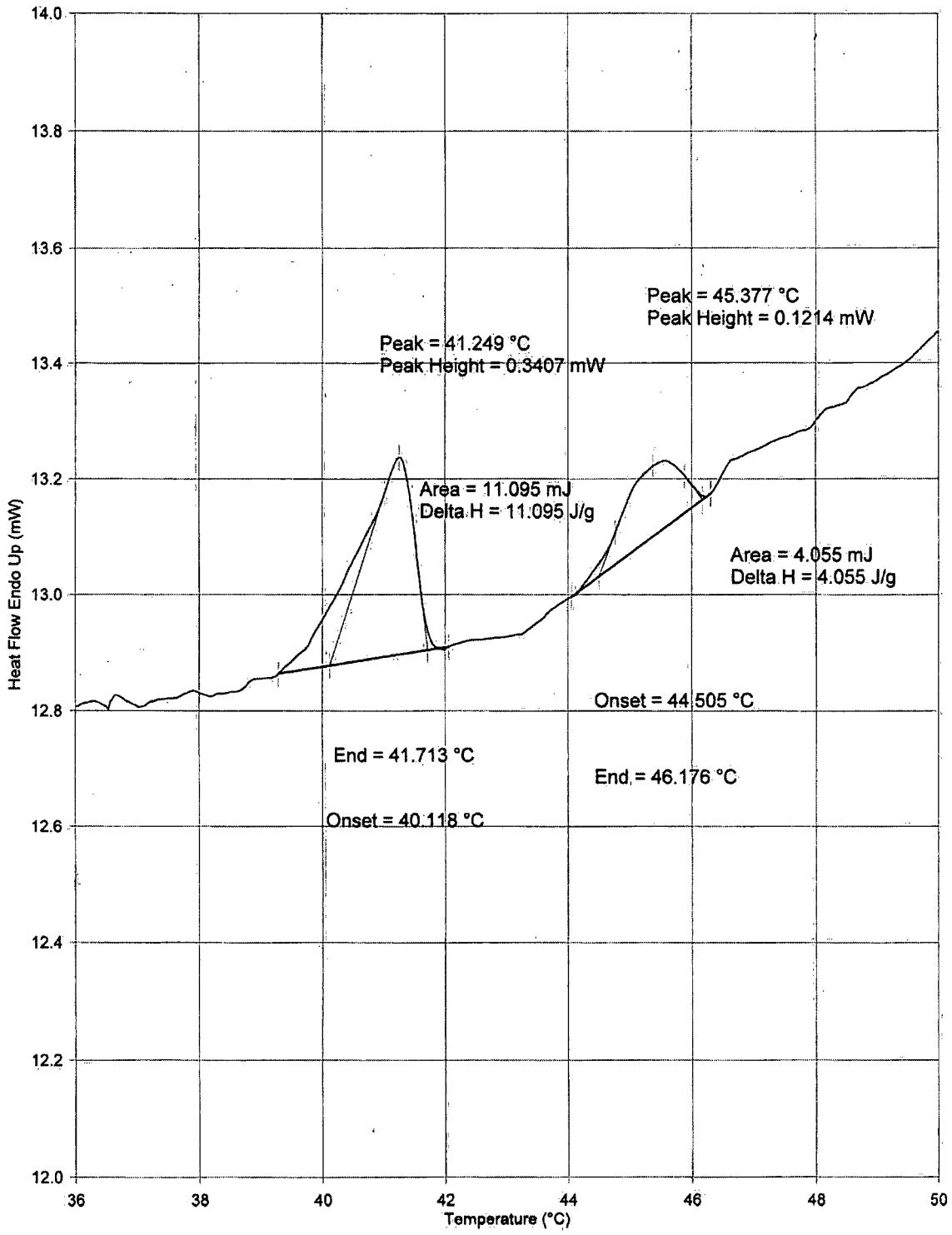

Figure 71: DSC thermogram of TSL stored for 23 days at a temperature of 22°C in 300 mM citrate buffer, pH 4, at a lipid concentration of 100 mg/ml. The heating rate was at 10°C/min.

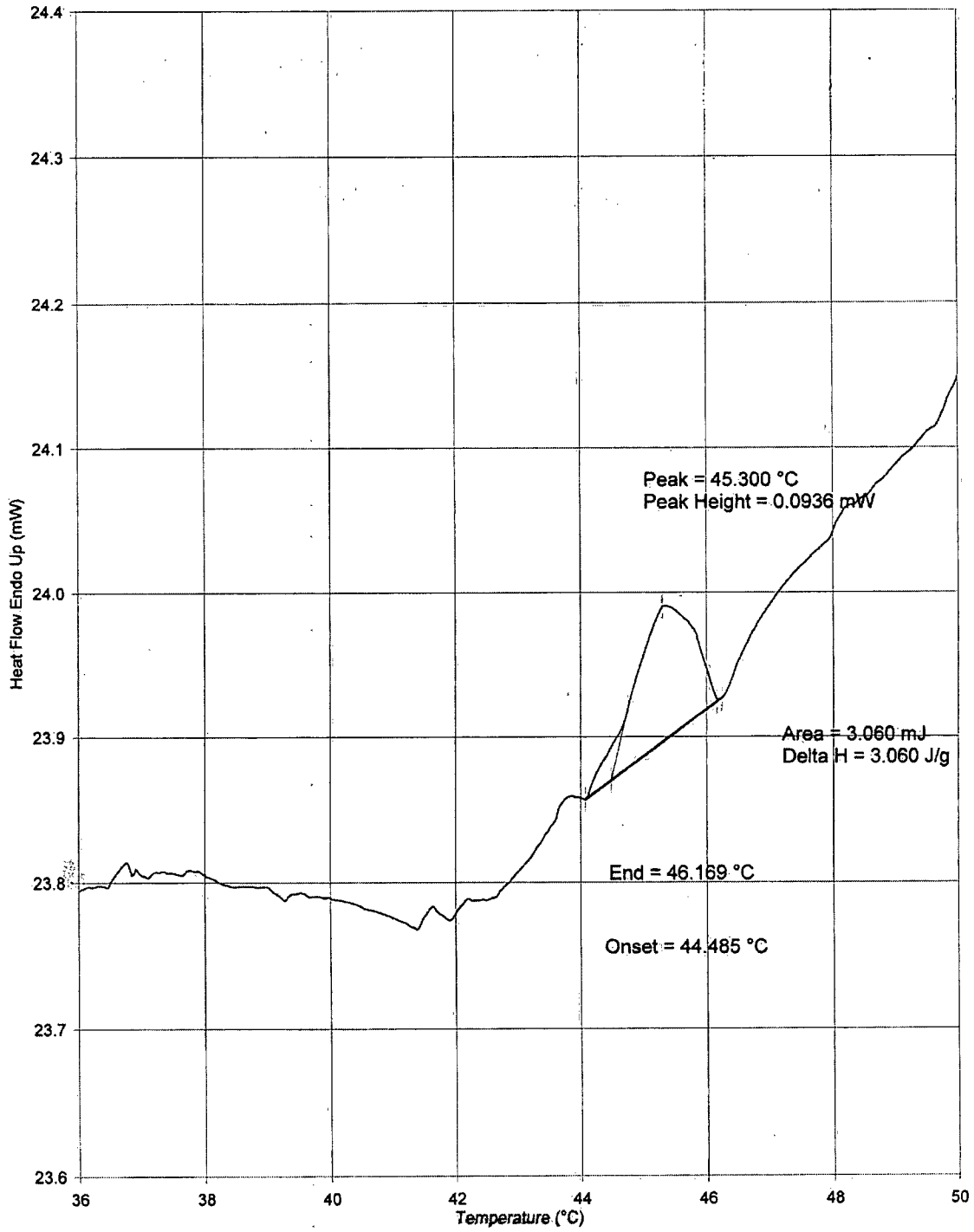

Figure 72: DSC thermogram of TSL stored for 23 days at a temperature of 22°C in 300 mM citrate buffer, pH 4, at a lipid concentration of 100 mg/ml. The thermogram is recorded from the second run of the same sample used in Figure 71. The heating rate was at 10°C/min.

4.3.6. Effect of storage time, pH, and temperature on phospholipid hydrolysis

From the previous experiments it became evident that the process of disc formation after cycling liposomes through their T_C occurs only to a small extend in freshly prepared LTSL in citrate buffer, pH 4, in the combined presence of both, PEG-lipid and lysolipid together. Thus, a concentration of 10 mol% of lysolipid in the LTSL membrane is not sufficient to trigger disc formation after T_C cycling. Discs form readily when additional lysolipid is added to the membrane or when liposomes are partially hydrolyzed by acid-catalyzed hydrolysis. To determine the exact percentage of lysolipid in the membrane necessary to trigger disc formation after T_C cycling, TSL membrane components were quantitated from samples stored in citrate buffer at pH 2, 4, or 6.5 at a temperature of 4°C or 22°C for up to 22 weeks. From the generated lysolipid content-time profiles hydrolysis rates in the individual samples were calculated.

TSL at a concentration of 100 mg/ml were stored at in 300 mM citrate buffer at pH 2, 4, or 6.5 at a temperature of 22°C or 4°C and 50 µl aliquots were frozen at -20°C every 7 or 14 days. Liposome samples were analyzed by HPLC to determine the amounts of DPPC and the hydrolysis product MPPC in the sample. Representative HPLC chromatograms of standards and sample are shown in Figure 73.

The molar percentage of MPPC in the TSL sample stored at a temperature of 22°C in citrate buffer, pH 2, increased linearly ($R^2 = 0.97$) for 9 days from initially 7% to approximately 47% of membrane components. From then on until 36 days after preparation, the molar percentage of MPPC stayed relatively constant and decreased to approximately 24% at 105 days. The molar percentage of DPPC decreased linearly on a logarithmic scale ($R^2 = 0.95$) for 36 days from initially 90% to approximately 21% and

further to approximately 10% at 105 days (Figure 74A).

The molar percentage of MPPC in the TSL sample stored at a temperature of 22°C in citrate buffer, pH 4, increased linearly ($R^2 = 0.98$) for 42 days from initially 1% to approximately 29% of all membrane components. From then on until 112 days after preparation, the molar percentage of MPPC increased further to approximately 40% and stayed from then on relatively constant until 176 days. The molar percentage of DPPC decreased linearly on a logarithmic scale ($R^2 = 0.97$) during the investigated time period of 176 days from approximately 94% to approximately 40% (Figure 74B).

The molar percentage of MPPC in the TSL sample stored at a temperature of 22°C in citrate buffer, pH 6.5, increased linearly ($R^2 = 0.86$) during the investigated time period of 197 days from initially 0% to approximately 5% of all membrane components. The molar percentage of DPPC did essentially not change during the investigated time period of 197 days and stayed at approximately 98% (Figure 74C).

The molar percentage of MPPC in the TSL sample stored at a temperature of 4°C in citrate buffer, pH 2, increased linearly ($R^2 = 0.95$) for 42 days from initially 7% to approximately 33% of all membrane components. From then on until 84 days after preparation, the molar percentage of MPPC increased further to approximately 43% and stayed relatively constant until the end of the study at 176 days. The molar percentage of DPPC decreased linearly on a logarithmic scale ($R^2 = 0.96$) during the investigated time period of 176 days from approximately 90% to approximately 26% (Figure 75A).

The molar percentage of MPPC in the TSL sample stored at a temperature of 4°C in citrate buffer, pH 4, increased linearly ($R^2 = 0.98$) during the investigated time period of 197 days from approximately 1.4% to approximately 15%. The molar percentage of

DPPC decreased linearly on a logarithmic scale ($R^2 = 0.92$) during the investigated time period of 197 days from approximately 94% to approximately 70% (Figure 75B).

The molar percentage of MPPC in the TSL sample stored at a temperature of 4°C in citrate buffer, pH 6.5, increased linearly ($R^2 = 0.7$) during the investigated time period of 197 days from initially 0% to approximately 4% of all membrane components. The molar percentage of DPPC did essentially not change during the investigated time period of 197 days and stayed at approximately 99% (Figure 75C).

Hydrolysis rates of TSL stored at a temperature of 22°C in citrate buffer at pH 2, 4, or 6.5 decreased with increasing pH of the storage buffer and were at 130.7, 18.2, or 0.7 mol%/month, respectively (Table 8). Hydrolysis rates of TSL stored at a temperature of 4°C in citrate buffer at pH 2, 4, or 6.5 were approximately 10-fold lower at 19.3, 2, or 0 mol%/month, respectively (Table 8).

Table 8: Hydrolysis rates in TSL after storage at temperatures of 22°C or 4°C in 300 mM citrate buffer at pH 2, pH 4, or pH 6.5.

	Hydrolysis rate (mol%/month)		
Storage temperature	*pH of storage buffer* 2	4	6.5
22°C	130.7	18.2	0.7
4°C	19.3	2	-

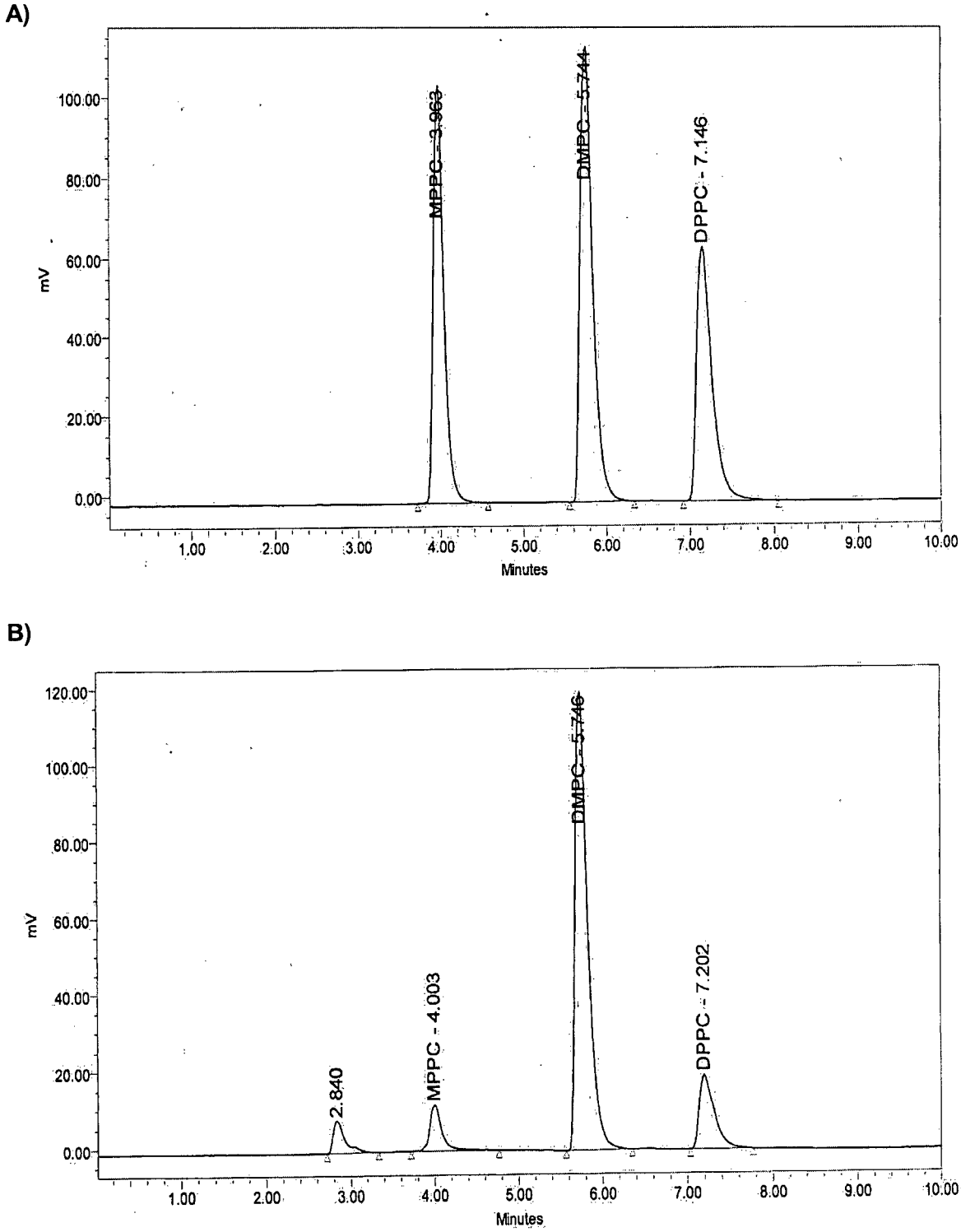

Figure 73: Representative HPLC chromatograms of (A) phospholipid standards (DMPC = internal standard) and (B) TSL stored for 16 weeks in 300 mM citrate buffer, pH 4, at a temperature of 22°C and a lipid concentration of 100 mg/ml.

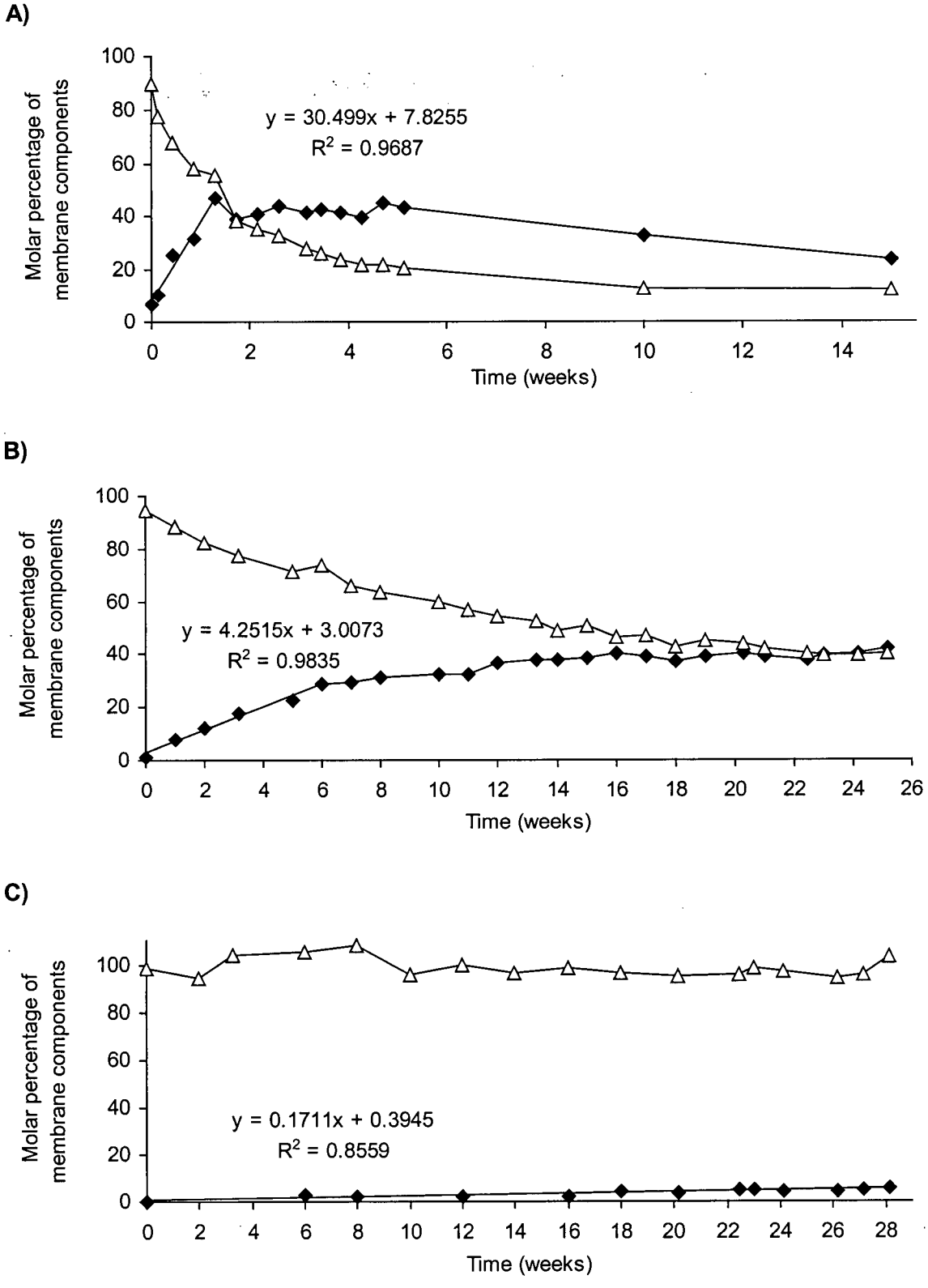

Figure 74: Molar percentage of MPPC (◆) and DPPC (△) in TSL stored at a temperature of 22°C in 300 mM citrate buffer at (A) pH 2, (B) pH 4, or (C) pH 6.5.

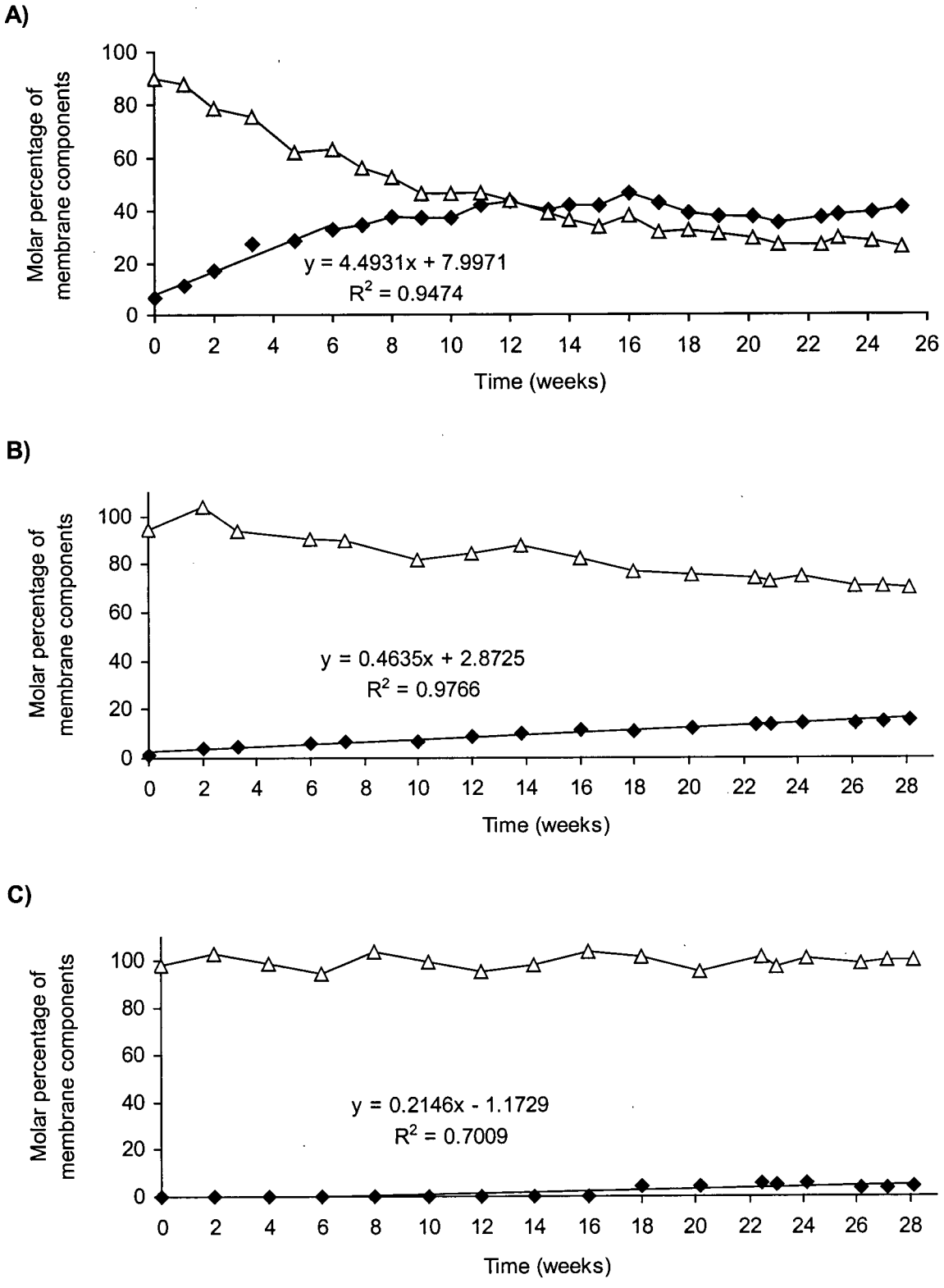

Figure 75: Molar percentage of MPPC (◆) and DPPC (△) in TSL stored at a temperature of 4°C in 300 mM citrate buffer at (A) pH 2, (B) pH 4, or (C) pH 6.5.

4.3.7. Redistribution of PHDA in the LTSL membrane

Pyrene hexadecanoic acid (PHDA), a pyrene derivative, was used as a fluorescent probe to simulate the distribution of lysolipids in the LTSL membrane. Above a certain concentration PHDA forms dimers (excimers) causing the emission wavelength to shift from 378 nm to 470 nm. Thus, accumulation of PHDA in the liposome membrane can be monitored as the PHDA monomer/excimer ratio (E/M ratio).

TSL were prepared containing 0.2, 2, 5, or 10 mol% PHDA. The peak excitation was at a wavelength of 316-333 nm with a maximum at 322.8 nm. When excited at 322 nm, the peak emission of the monomer was at 378.0 nm with a secondary peak at 398.8 nm. At PHDA concentrations up to 2 mol% in the TSL membrane, the excimer peak of PHDA at 470 nm could not be observed. At PHDA concentration of 5 mol% and 10 mol%, an excimer peak appeared in the emission spectrum at a wavelength of 450-500 nm with a maximum at approximately 470 nm (Figure 76). Since at a PHDA concentration of 10 mol% the excimer peak was already close to its maximum height PHDA was added to the TSL, LTSL, and NTSL membrane at a concentration of 5 mol% for subsequent PHDA accumulation experiments. The excited state lifetime und thus the excimer emission intensity has been reported by the manufacturer to be dependent on the presence of oxygen in the buffer. However, there was no difference observed between emission spectra before or after removal of oxygen by purging nitrogen through the cuvette containing liposomes for 30 min (Figure 77). The T_C of this formulation was at 42.3°C as determined by DSC analysis and thus unaffected by incorporation of 5 mol% PHDA (Figure 78).

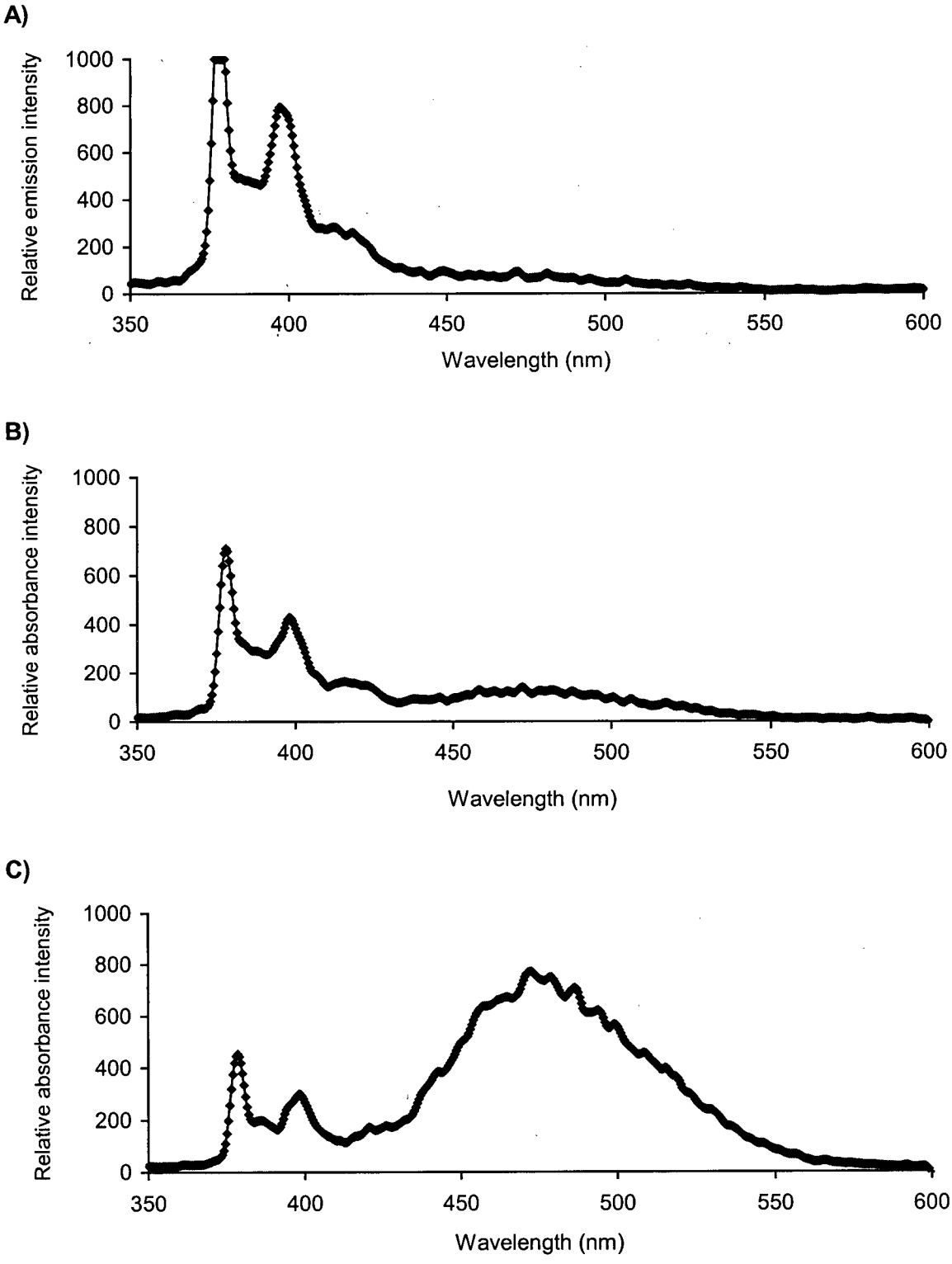

Figure 76: Fluorescence emission spectra of PHDA-labelled TSL in 300 mM citrate buffer, pH 4, at a temperature of 22°C and a lipid concentration of 20-30 μg/ml containing (A) 2 mol%, (B) 5 mol%, or (C) 10 mol% PHDA.

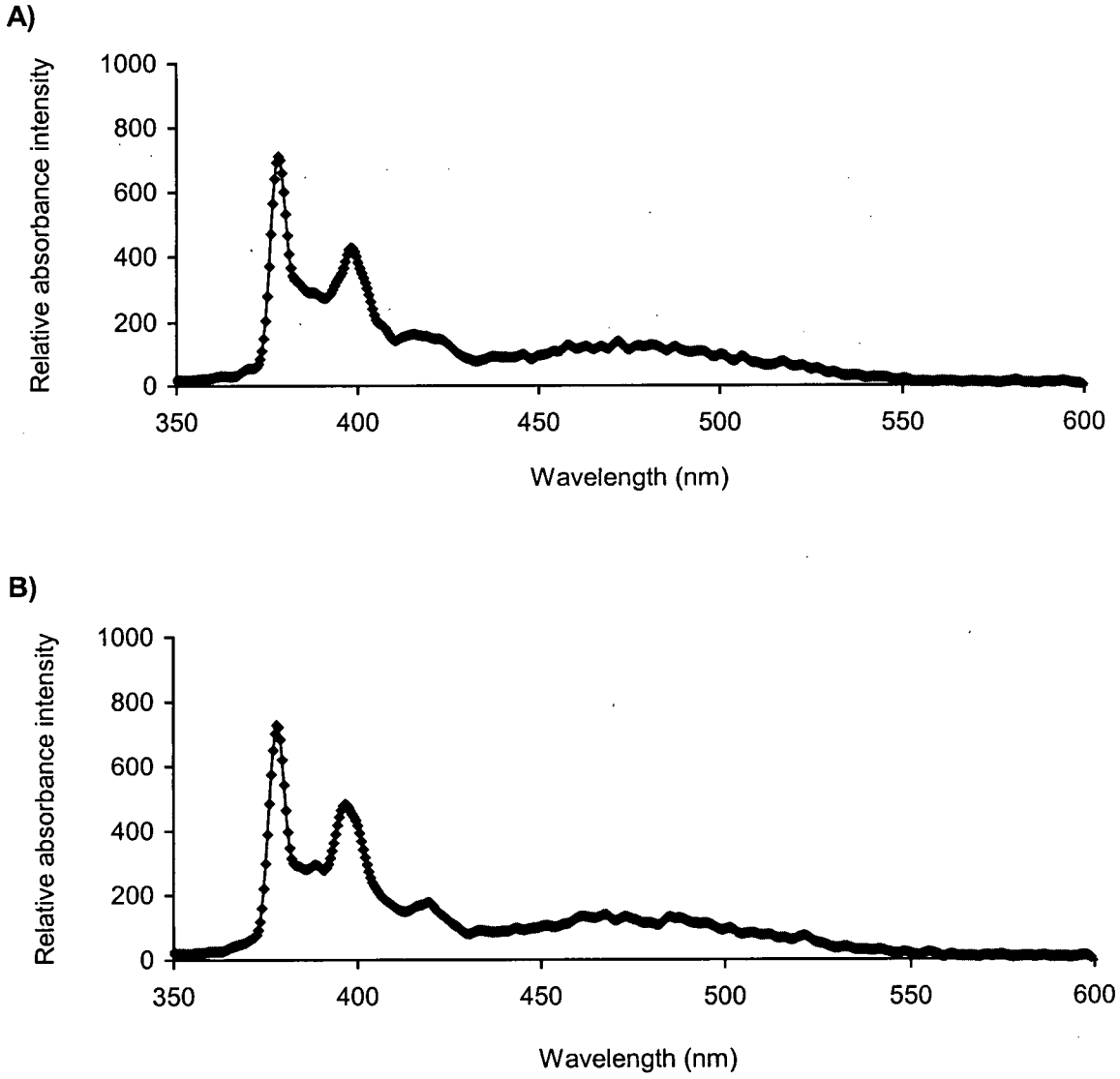

Figure 77: Fluorescence emission spectra of PHDA-labeled TSL in 300 mM citrate buffer, pH 4, at a temperature of 22°C and a lipid concentration of 20-30 μg/ml containing 5 mol% PHDA in (A) the presence of oxygen or (B) after removal of oxygen by nitrogen purging for 30 min.

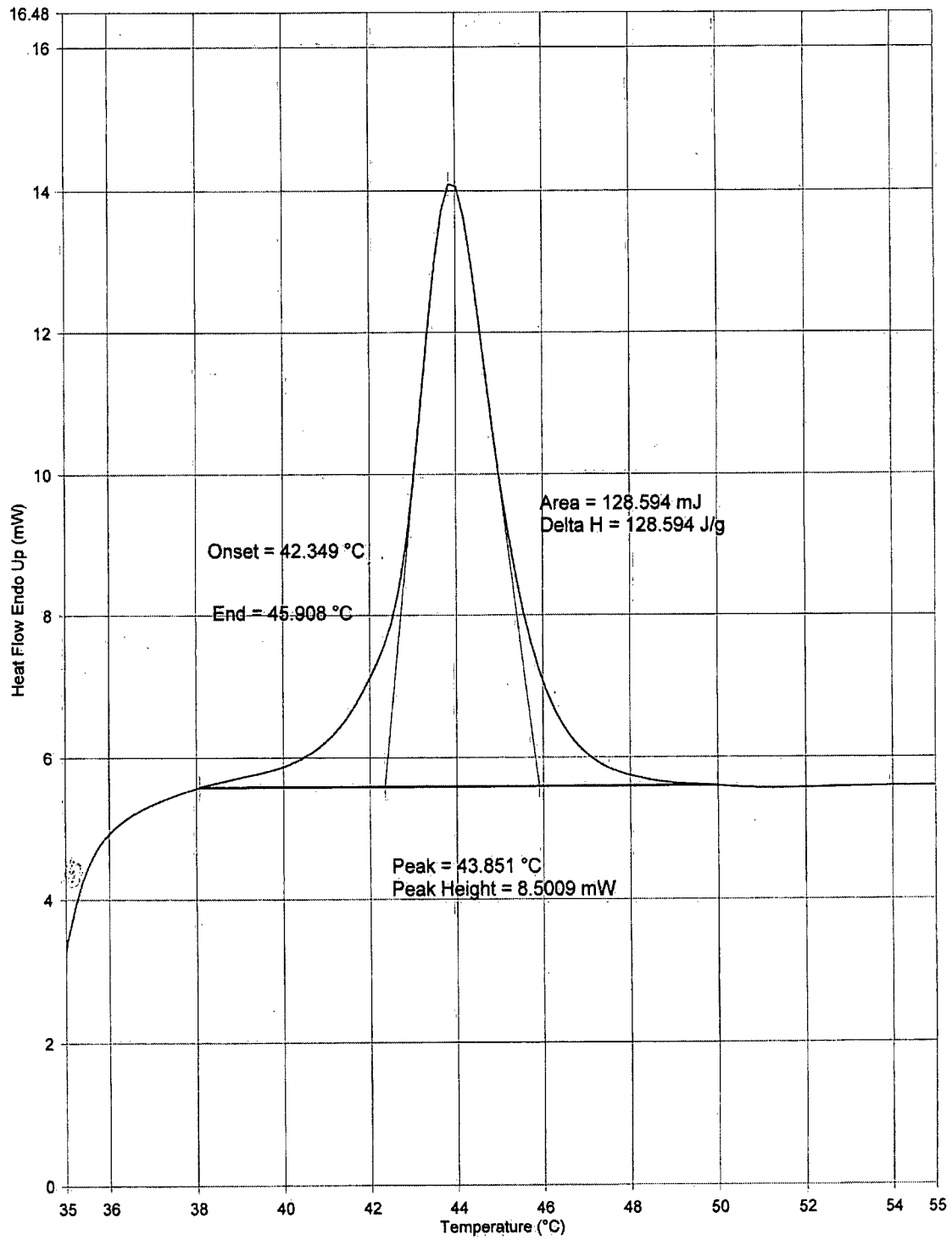

Figure 78: DSC thermogram of freshly prepared PHDA-labeled TSL MLVs containing 5 mol% PHDA in 300 mM citrate buffer, pH 4, at a lipid concentration of 100 mg/ml. The heating rate was at 10°C/min.

When liposomes were always maintained at a temperature of 55°C after extrusion and cooled down to 25°C at a rate of approximately 1°C/min, the excimer to monomer (E/M) ratio was higher in LTSL than those in TSL and both were higher than those in NTSL at all temperatures. E/M ratios decreased linearly with decreasing temperatures in all formulations but stayed constant or increased slightly below the T_C in LTSL and TSL (Figure 79).

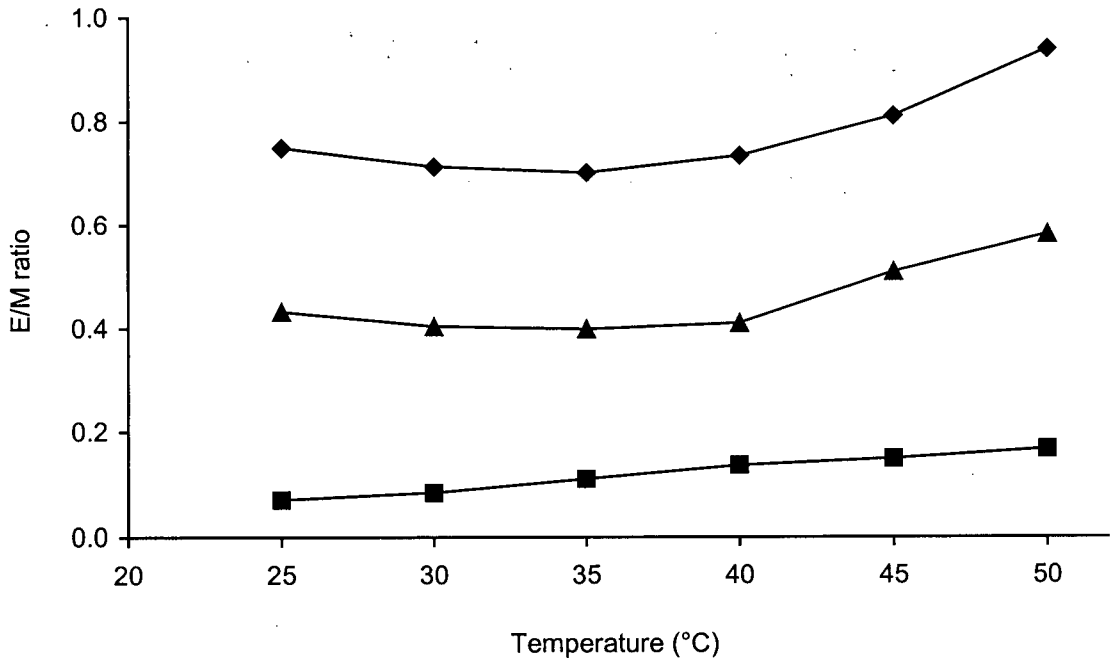

Figure 79: Temperature dependence of excimer formation in PHDA-labeled TSL (▲), LTSL (◆), and NTSL (■) containing 5 mol% PHDA in 300 mM citrate buffer, pH 4, at a lipid concentration of 20-30 μg/ml. Liposomes were maintained at a temperature of 55°C after extrusion and cooled down at a rate of approximately 1°C/min.

When liposomes were maintained at temperatures between 38°C and 40°C, the PHDA E/M ratio of TSL increased significantly ($p < 0.05$) over the course of four days versus the day of preparation (day 0) by approximately 60%. Starting at three days at a temperature of 38°C, the E/M ratio did not increase significantly any further versus the previous day. In LTSL, the PHDA E/M ratio increased significantly ($p < 0.01$) over the course of five days versus the day of preparation (day 0) by approximately 15%. Starting at five days at 38°C, the E/M ratio did not increase significantly any further versus the previous day. In NTSL, the E/M ratio did not increase significantly over the investigated time period (Figures 80 and 81).

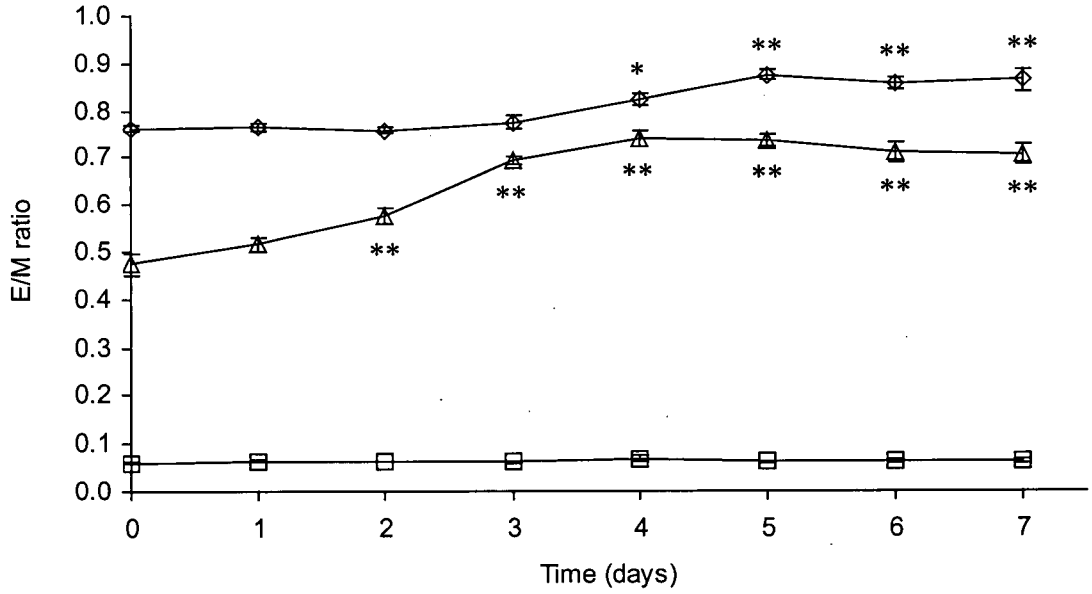

Figure 80: Time dependence of excimer formation in PHDA-labelled TSL (△), LTSL (◇), and NTSL (□) containing 5 mol% PHDA at a temperature of 38-40°C in 300 mM citrate buffer, pH 4, at a lipid concentration of 20-30 μg/ml. E/M ratio = excimer/monomer ratio. * = $p < 0.05$; ** = $p < 0.01$ versus day 0. Error bars indicate the standard error of mean values (n = 4 for TSL; n = 3 for LTSL and NTSL).

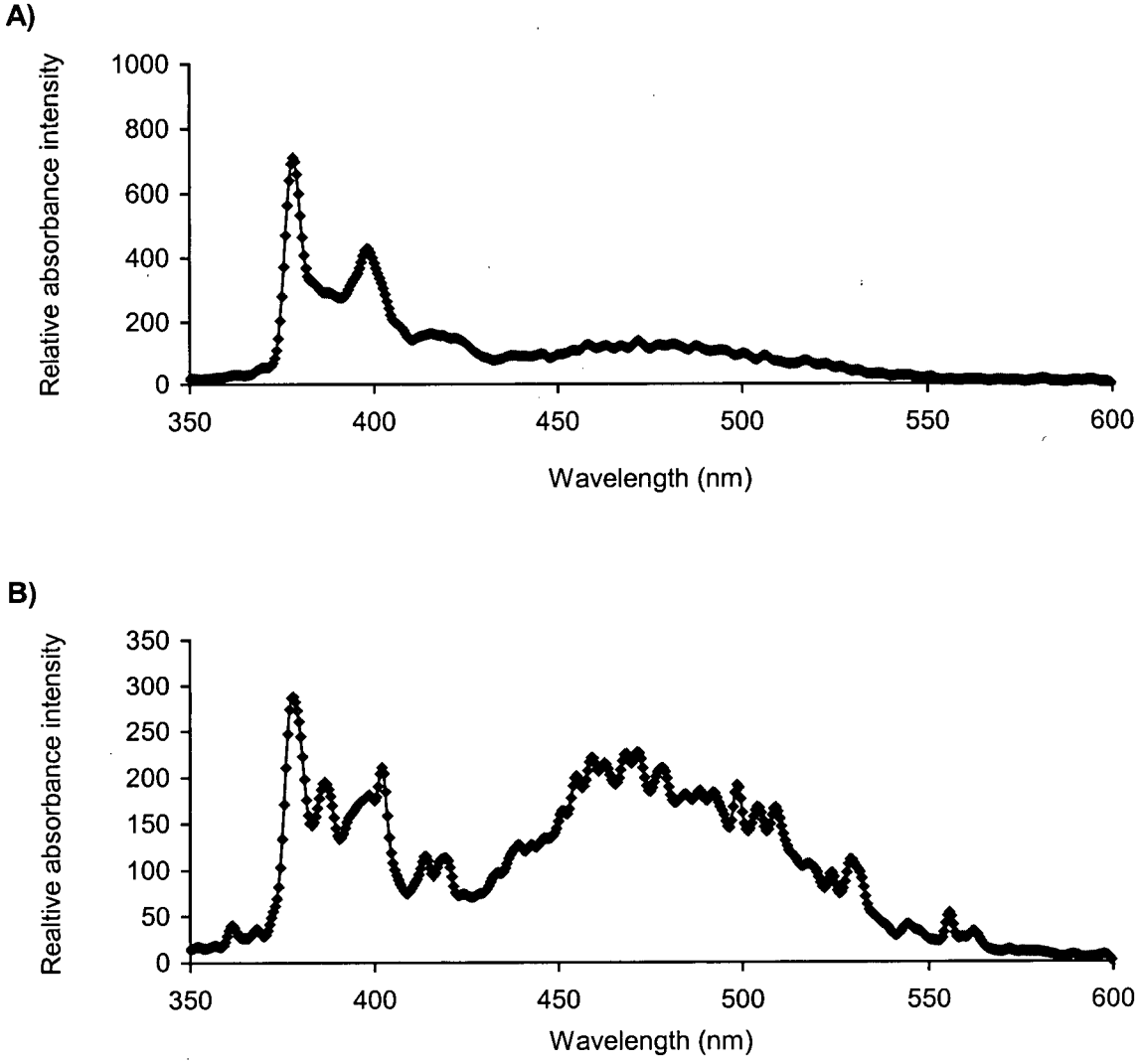

Figure 81: Fluorescence emission spectra of PHDA-labeled TSL in 300 mM citrate buffer, pH 4, at a lipid concentration of 20-30 μg/ml containing 5 mol% PHDA at (A) the day of preparation or (B) after storage for 7 days at a temperature of 38-40°C.

When PHDA-labeled TSL were stored for 4 weeks at a temperature of 22°C and cycled once through their T_C (10 min at 50°C and cooling to 22°C) the particle size decreased from 110.6 nm (STD 24.4 nm) to 69.2 nm (STD 25.3 nm). In PHDA-labeled LTSL, the particle size decreased from 110.4 nm (STD 22.0 nm) before T_C cycling to 85.4 nm (STD 38.3 nm) after T_C cycling. There was no change in particle size in PHDA-labeled NTSL (100.6 nm; STD 29 nm before T_C cycling and 99.2 nm; STD 30.1 nm after T_C cycling) under the same experimental conditions (Figure 82). Accordingly, the PHDA E/M ratio increased by 80% or 40% nm in PHDA-labeled TSL or LTSL, respectively, after cycling through their T_C but not in NTSL (Figure 83). Results indicate a separation of grain boundaries with incorporated PHDA. There was no change in particle size or E/M ratios after T_C cycling when PHDA-labeled TSL, NTSL, or NTSL were stored for 28 days at 4°C (data not shown).

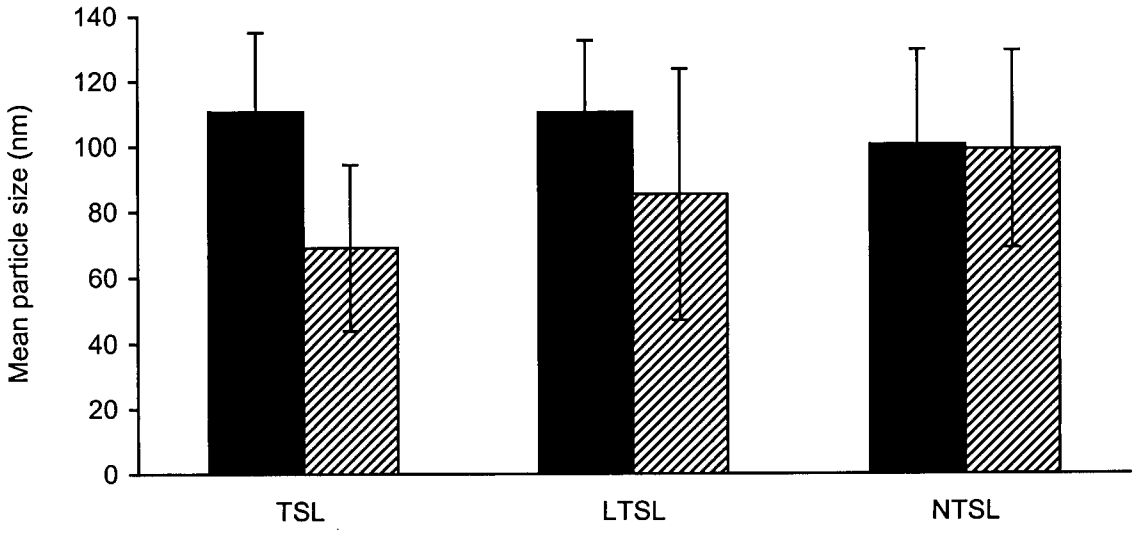

Figure 82: Mean particle size of PHDA-labelled TSL, LTSL, and NTSL stored for 28 days at a temperature of 22°C in 300 mM citrate buffer, pH 4, before (■) and after (▨) cycling liposomes one time through their T_C. Error bars indicate the standard deviation (n = 3).

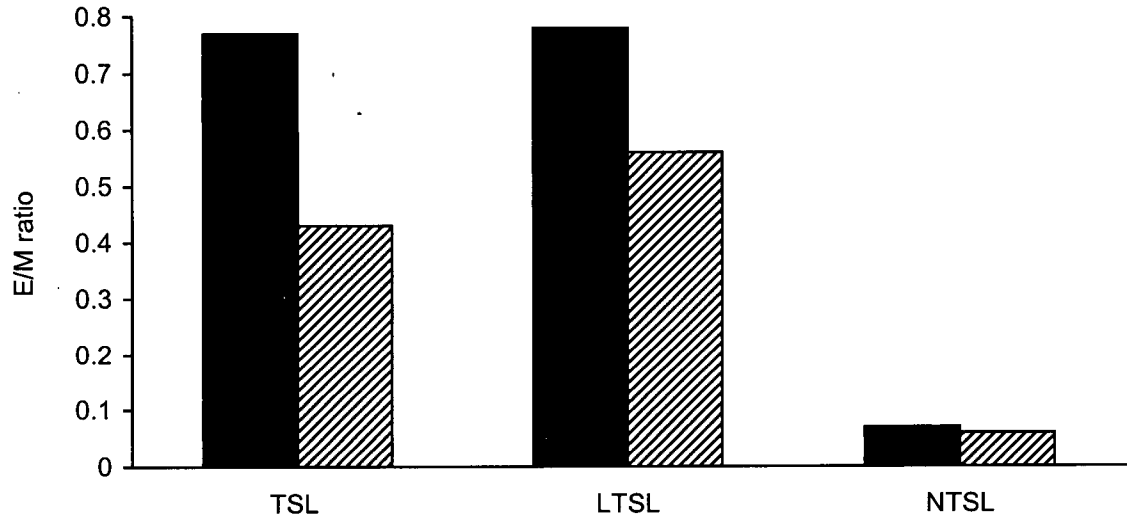

Figure 83: Mean excimer/monomer (E/M) ratio of PHDA-labelled TSL, LTSL, and NTSL stored for 28 days at a temperatures of 22°C in 300 mM citrate buffer, pH 4, before (■) and after (▨) cycling liposomes one time through their T_C. E/M ratios were measured in duplicate.

4.3.8. Lysolipid membrane retention after T_C cycling

To test the alternative hypothesis that the drug release mechanism in LTSL is based on lysolipids leaving the liposome membrane after cycling liposomes through their T_C, a LTSL sample containing trace amounts of ^{14}C-MPPC and ^{3}H-CHE as labels for the lysolipid and the liposome, respectively, was prepared and split in half. One half was kept at a temperature of 22°C the other half was heated to 50°C and cooled back to 22°C. The outside buffer of both samples was exchanged with HBS, pH 7.5, on a Sephadex G-50 column to separate potentially released lysolipids. When free ^{14}C-MPPC was added to a Sephadex G-50 spin column, the amount of radioactivity after separation was at 0.25% of the initial radioactivity, indicating that the radiolabel is retained by the Sephadex G-50 column.

The lysolipid/lipid ratio determined by the ^{14}C-MPPC / ^{3}H-CHE ratio of liposomes in HBS after cycling liposomes through their T_C, was not significantly different from the initial lysolipid/lipid ratio before T_C cycling or from the ^{14}C-MPPC / ^{3}H-CHE ratio before exchanging the outside buffer (Figure 84).

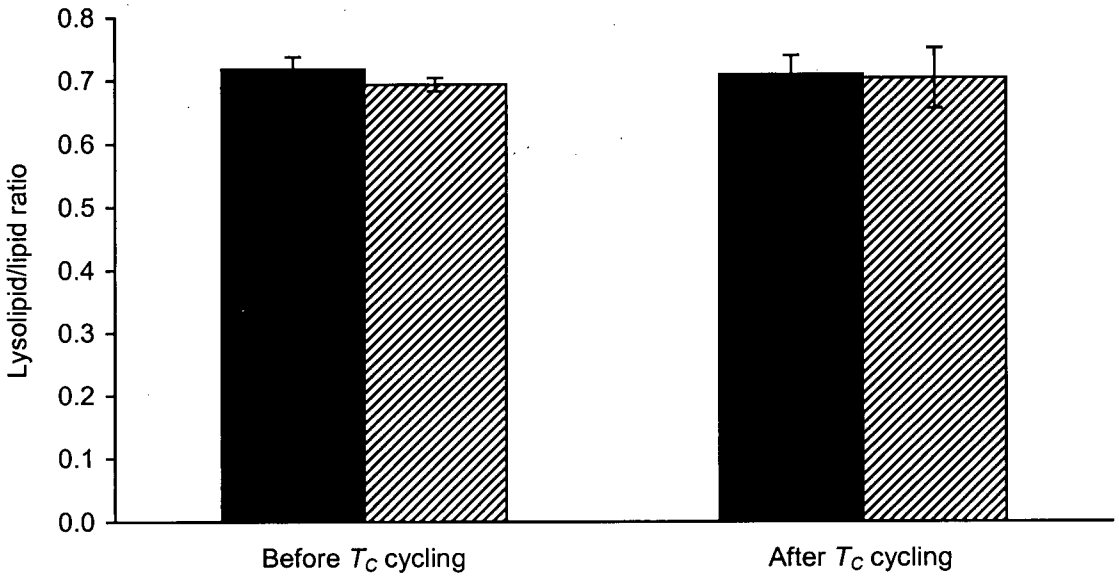

Figure 84: Lysolipid/lipid ratios in LTSL before and after cycling liposomes one time through their (T_C) before (■) and after (▨) exchanging the 300 mM citrate buffer, pH4, outside liposomes with HBS, pH 7.5. Error bars indicate the standard error of mean values (n = 3).

Part II: Properties of LTSL *in vivo*

4.4. DOX retention of LTSL *in vivo*

As described in section 1.5., the properties of liposomes can change considerably after *i.v.* injection. Membrane components can exchange out into the serum and destabilize the liposome membrane [88, 89]. Cholesterol, serum proteins, and the apoA-1 lipoprotein of high density lipoproteins (HDL) can also adsorb and integrate into the liposome membrane and cause membrane destabilization [92] [93], especially if the membrane surface is negatively charged [94]. Therefore, the performance of LTSL was characterized *in vivo* and compared to that of TSL and NTSL.

4.4.1. Tissue distribution of lipid and DOX after *i.v.* injection of LTSL-DOX into mice

NTSL were loaded with DOX at a drug-to-lipid ratio of 0.2 mg/mg by the titration method (see section 3.7.) and injected into adult female Rag2-M mice at a dosage of 20 mg DOX/kg. Three mice were sacrificed at 10 min, 1 h, or 8 h after injection, respectively, blood was collected into EDTA-coated microtainers by cardiac puncture, and their major organs were harvested and frozen at a temperature of -20°C until later analysis. Plasma lipid and DOX concentrations were determined by scintillation counting and fluorescence spectroscopy, respectively.

Mean plasma lipid concentrations increased initially from 2 mg/ml at 10 min to 2.5 mg/ml at 1 h and decreased to 2.1 mg/ml at 8 h after injection. Similarly, mean plasma DOX concentrations increased initially from 0.4 mg/ml at 10 min to 0.53 mg/ml at 1 h and decreased to 0.36 mg/ml at 8 h after injection. Mean plasma drug-to-lipid

ratios did not change significantly from 0.21 mg/mg over the investigated time period indicating that DOX was essentially not released from liposomes and liposomes remained in circulation for the investigated time period of 8 h (Figure 85).

At 1 h after NTSL-DOX administration, the highest lipid concentrations were found in the spleen (0.16 mg/g) and the liver (0.12 mg/g), the two RES organs, and in the lung (0.1 mg/g) while minor concentrations found in the kidneys, the heart. Only background levels were found in the (thigh) muscle. Mean lipid concentrations increased over the 8 h time period in the spleen (0.5 mg/g) and the liver (0.26 mg/g) but decreased or stayed relatively constant in other organs (Figure 86A).

At 1 h after NTSL-DOX administration, approximately 98% of the total lipid dosage was found in plasma and approximately 5% was found in the liver. The mean percentage of the total lipid dosage in plasma decreased to approximately 81% after 8 h and increased to approximately 11% in the liver. The mean percentage of the total lipid dosage in other organs at 1 h or 8 h after administration was less than 1% except for kidneys at 8 h after administration where approximately 1.4% of total lipid was found (Table 9).

Mean DOX concentrations were the highest at 1 h after NTSL-DOX administration also in the spleen (0.04 mg/g) and the liver (0.04 mg/g), but high concentrations were also found in the kidneys (0.05 mg/g). Lower DOX concentrations were found in the heart, the lung and very low levels were found the muscle. Mean DOX concentrations increased over the 8 h time period in the spleen (0.1 mg/g), the liver (0.08 mg/g), and the kidneys (0.06 mg/g) but decreased or stayed relatively levels in other organs (Figure 86B).

At 1 h after NTSL-DOX administration approximately 94% of the total DOX dosage was found in plasma and approximately 9% was found in the liver. The mean percentage of the total DOX dosage in plasma decreased to approximately 64% after 8 h and increased to approximately 15% in the liver. The mean percentage of the total DOX dosage in other organs was less than 1% except for kidneys after 1 h or 8 h where approximately 3% or 6%, respectively, was found (Table 9).

Mean drug-to lipid ratios, an indication of DOX retention, were highest at 1 h and 8 h after administration in the kidneys (1.1 mg/mg and 0.84 mg/mg) and the heart (0.9 mg/mg and 0.91 mg/mg) followed by the liver (0.36 mg/mg and 0.3 mg/mg), the spleen (0.26 mg/mg and 0.19 mg/mg), the lung (0.2 mg/mg and 0.31 mg/mg). Mean drug-to-lipid ratios were not calculated for LTSL-DOX in muscle because they were artificially high because of extremely low lipid concentration in this tissue (Figure 86C).

LTSL containing MPPC were loaded with DOX at a drug-to-lipid ratio of 0.05 mg/mg by the titration method (see section 3.7.) and injected into adult female Rag2-M mice at a dosage of 20 mg DOX/kg. Three mice were sacrificed at 1 min, 10 min, 20 min, 30 min, 1 h, 2 h, 4 h, or 8 h after LTSL-DOX injection, respectively, blood was collected into EDTA-coated microtainers by cardiac puncture, and their major organs were harvested and frozen at a temperature of -20°C until later analysis. Plasma lipid and DOX concentrations were determined by scintillation counting and fluorescence spectroscopy, respectively.

Mean plasma lipid concentrations decreased significantly after LTSL-DOX injection from 9 mg/ml at 10 min to 4.6 mg/ml at 2 h and 2.1 mg/ml at 8 h. Mean plasma DOX concentrations decreased more rapidly after injection from 0.46 mg/ml at 1 min to

0.06 mg/ml at 10 min to 0.01 mg/ml at 30 min. Mean plasma drug-to-lipid ratios decreased from 0.053 mg/mg at 1 min to 0.007 mg/mg at 10 min to 0.001 mg/mg at 30 min indicating that DOX was released rapidly from liposomes after injection (Figure 87).

At 1 h after administration, the highest lipid concentrations were found in the liver (0.92 mg/g) while minor concentrations found in the lung (0.29 mg/g), the spleen (0.27 mg/g), the kidneys (0.17 mg/g), the heart (0.07 mg/g), and the muscle (0.01 mg/g). Mean lipid concentrations increased over the 8 h time period primarily in the liver (4 mg/g) and to some extend in the spleen (0.66 mg/g) but decreased or stayed relatively constant at low levels in other organs (Figure 88A).

At 1 h after LTSL-DOX administration approximately 68% of the total lipid dosage was found in plasma and approximately 13% was found in the liver. The mean percentage of the total lipid dosage in plasma decreased to approximately 23% after 8 h and increased to approximately 53% in the liver. The mean percentage of the total lipid dosage in other organs was equal or less than 1% at 1 h or 8 h after injection (Table 10).

Mean DOX concentrations were the highest at 1 h after LTSL-DOX administration in the liver (0.6 mg/g) and the kidneys (0.6 mg/g) and lower DOX concentrations were found in the heart (0.22 mg/g), the lung (0.12 mg/g), and the spleen (0.12 mg/g). Very low levels were found in the muscle (0.04 mg/g). Mean DOX concentrations decreased over the 8 h time period in the kidneys (0.47 mg/g) and the liver (0.34 mg/g) and stayed at relatively constant levels or decreased slightly in other organs (Figure 88B).

At 1 h after LTSL-DOX administration approximately 0.4% of the total DOX dosage was found in plasma, approximately 50% was found in the liver, and

approximately 20% was found in the kidneys. The mean percentage of the total DOX dosage in plasma stayed at these low levels after 8 h and increased to approximately 27% in the liver and to approximately 15% in the kidneys. The mean percentage of the total DOX dosage in other organs was approximately 1% at 1 h or 8 h after injection (Table 10).

Mean drug-to lipid ratios, an indication of DOX retention, were highest at 1 h and 8 h after administration in the kidneys (3.5 mg/mg and 2.7 mg/mg) and the heart (3.1 mg/mg and 1.2 mg/mg) followed by the liver (0.66 mg/mg and 0.09 mg/mg), the spleen (0.43 mg/mg and 0.15 mg/mg), and the lung (0.43 mg/mg and 0.42 mg/mg). Mean drug-to-lipid ratios were not calculated for LTSL-DOX in muscle because they were artificially high because of extremely low lipid concentration in this tissue (Figure 88C).

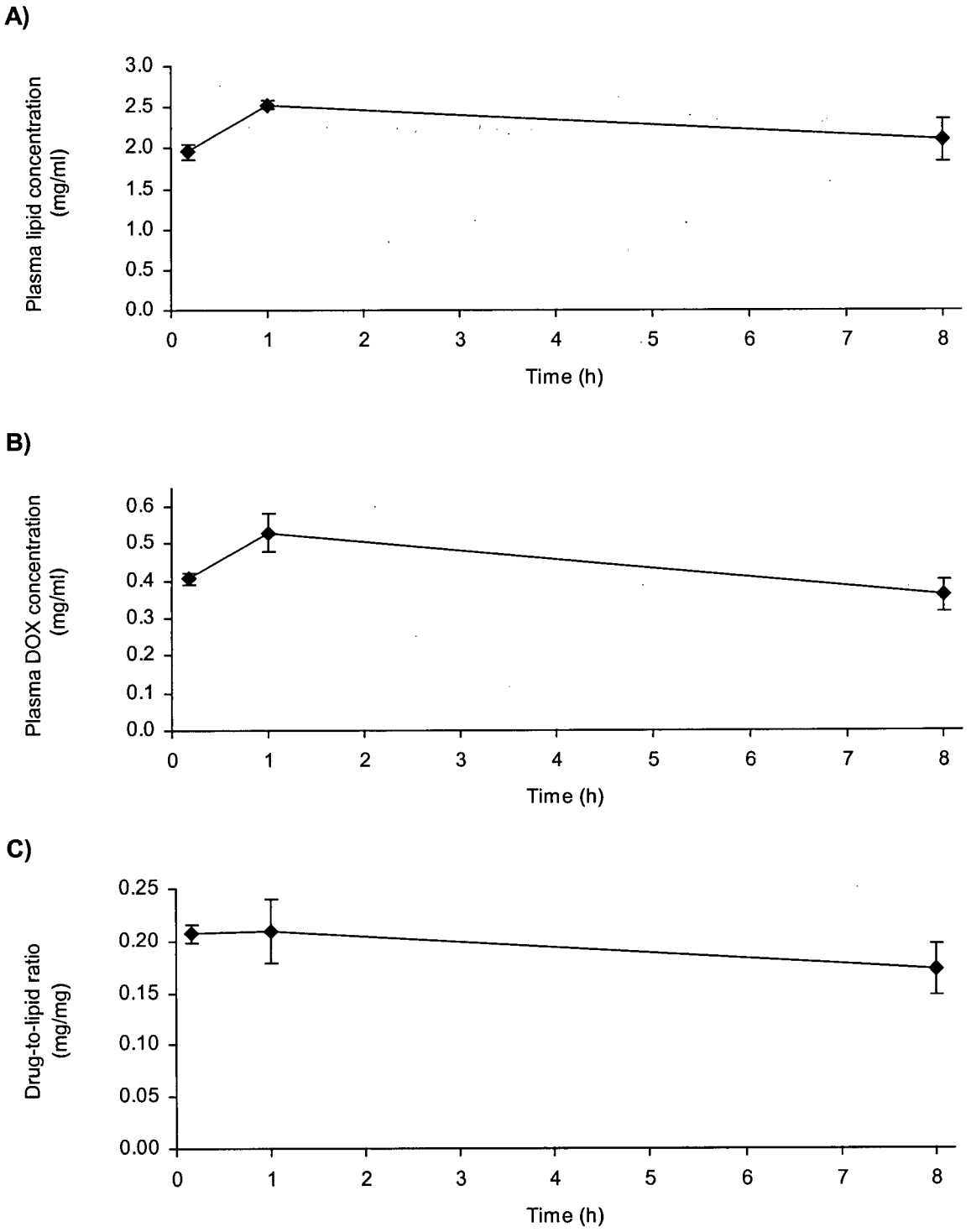

Figure 85: Plasma time profiles of NTSL-DOX for (A) lipid, (B) DOX, and (C) the drug-to-lipid ratio in adult female Balb/c mice. Error bars indicate the standard error of mean values (n = 3).

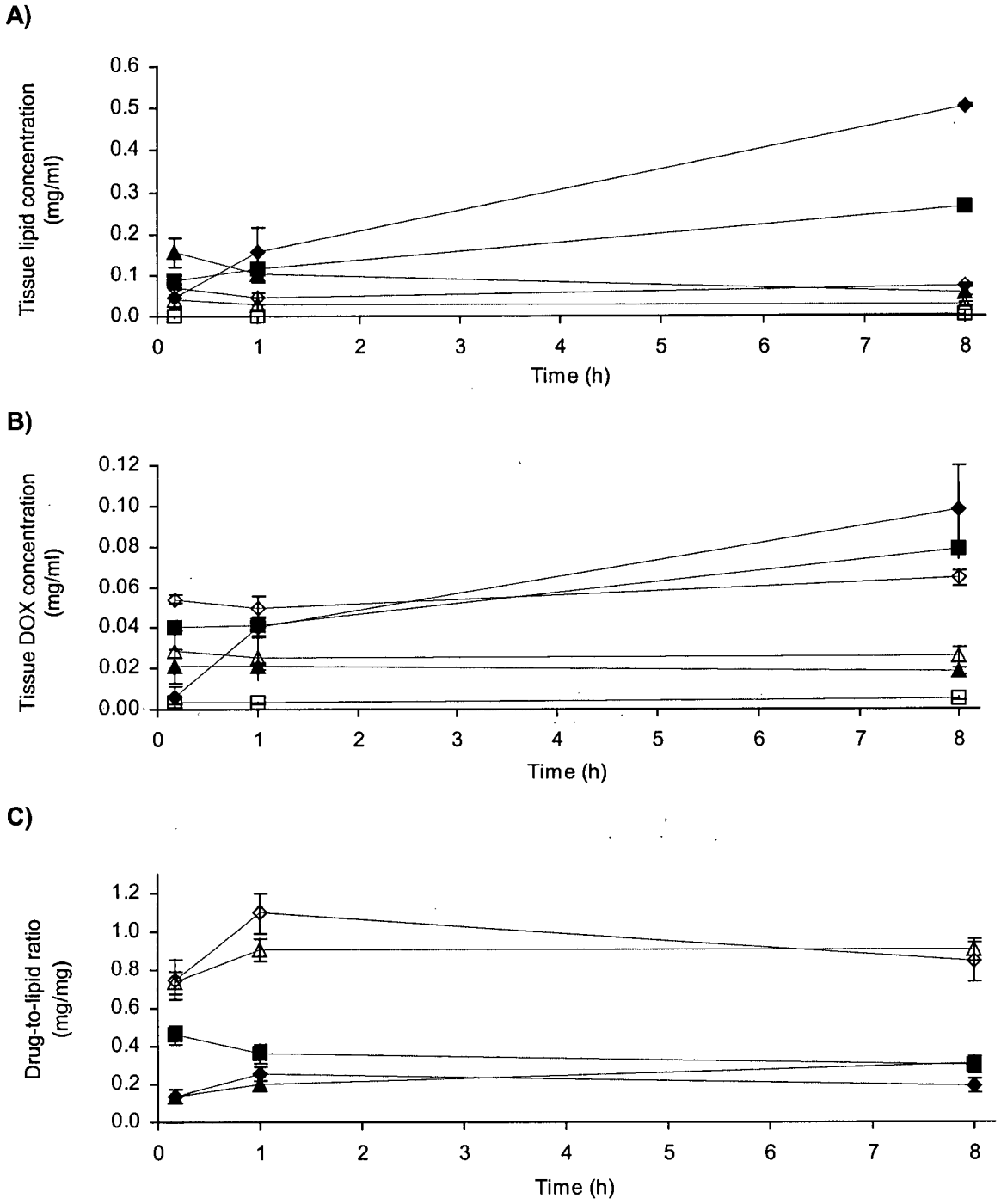

Figure 86: Tissue distribution time profiles of NTSL-DOX for (A) lipid, (B) DOX, and (C) the drug-to-lipid ratio in adult female Balb/c mice. ◆ = spleen, ◇ = kidney, △ = heart, ▲ = lung, ■ = liver, □ = muscle. Error bars indicate the standard error of mean values (n = 3).

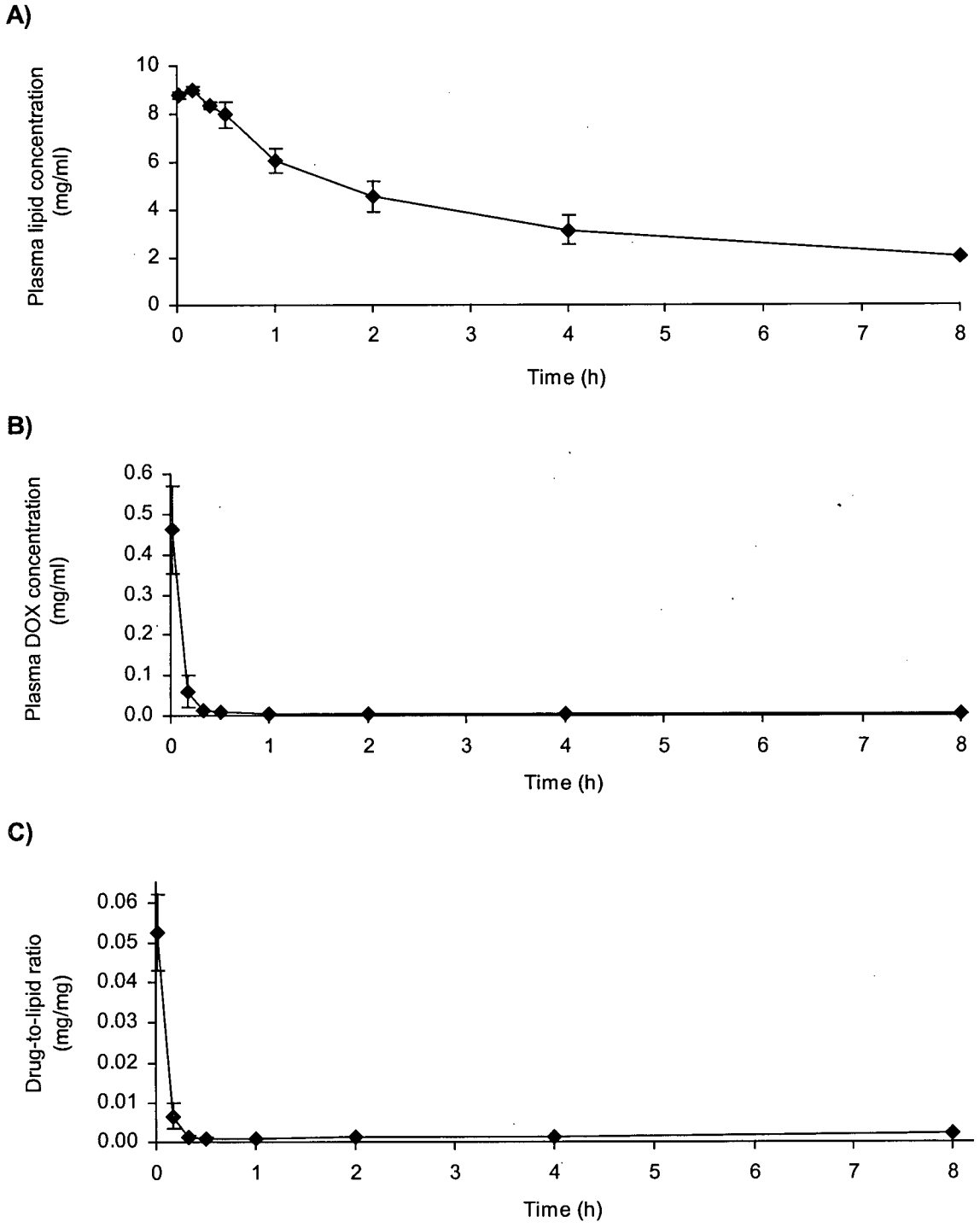

Figure 87: Plasma time profiles of LTSL-DOX containing MPPC for (A) lipid, (B) DOX, and (C) the drug-to-lipid ratio in adult female Balb/c mice. Error bars indicate the standard error of mean values (n = 3).

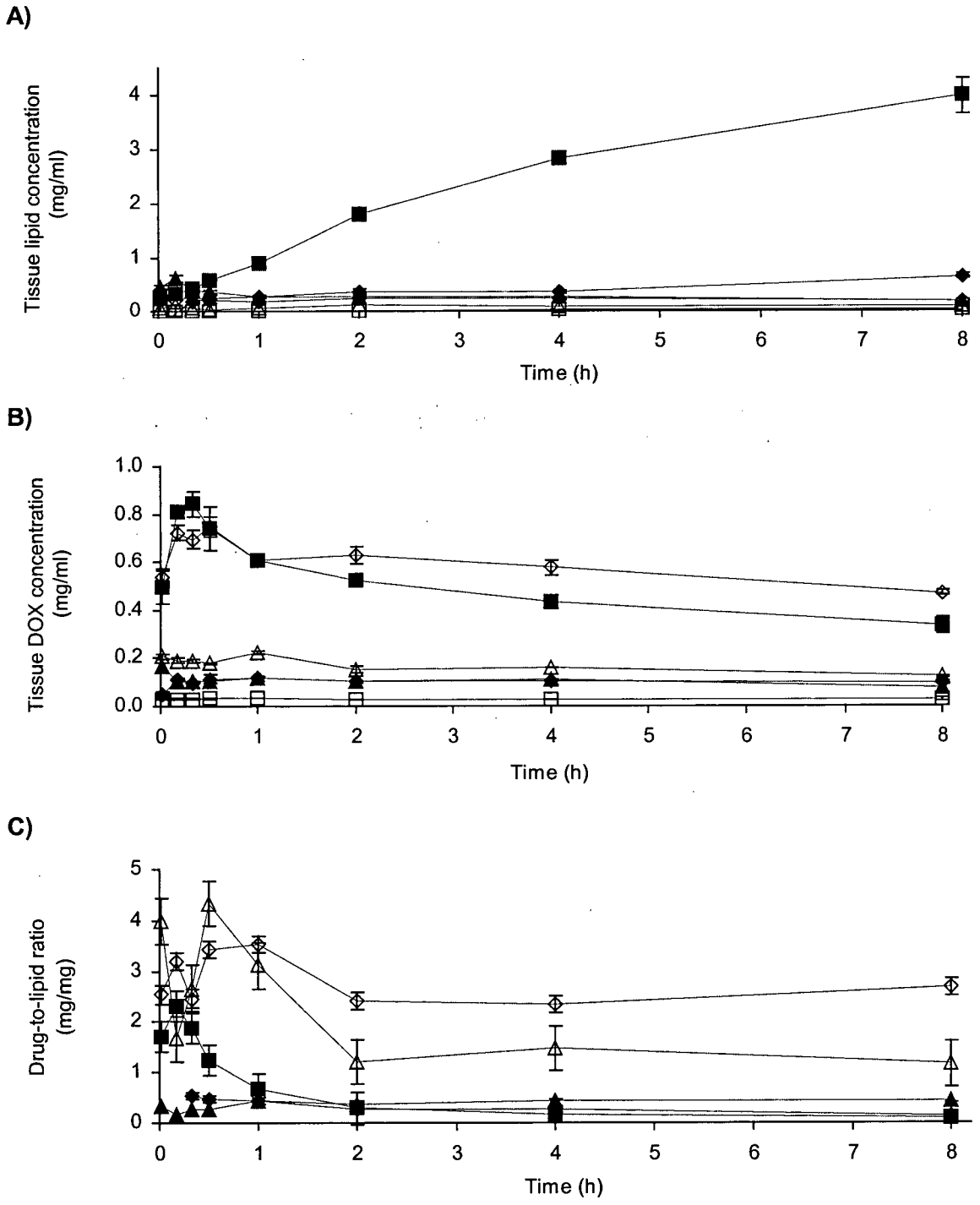

Figure 88: Tissue distribution time profiles of LTSL-DOX containing MPPC for (A) lipid, (B) DOX, and (C) the drug-to-lipid ratio in adult female Balb/c mice. ◆ = spleen, ◇ = kidney, △ = heart, ▲ = lung, ■ = liver, □ = muscle. Error bars indicate the standard error of mean values (n = 3).

Table 9: Tissue distribution of lipid and DOX at 1 h and 8 h after *i.v.* injection of NTSL-DOX at a dosage of 16.6 mg DOX/kg to adult female Balb/c mice.

	Mean percentage of total dose (SEM)			
	Lipid		*DOX*	
	1 h (n = 3)	*8 h (n = 3)*	*1 h (n = 3)*	*8 h (n = 3)*
Plasma	97.8 (2.0)	81.1 (10.0)	93.6 (9.0)	63.8 (8.9)
Liver	5.3 (0.9)	11.3 (1.3)	8.8 (0.9)	15.4 (3.0)
Spleen	0.2 (0.1)	0.5 (0.1)	0.2 (0.03)	0.4 (0.01)
Lung	0.7 (0.1)	0.4 (0.1)	0.6 (0.04)	0.6 (0.0)
Heart	0.2 (0.1)	0.2 (0.0)	0.7 (0.01)	0.7 (0.2)
Kidney	0.8 (0.3)	1.4 (0.3)	3.3 (1.2)	5.7 (1.5)
Muscle	-	-	0.1 (0.01)	0.1 (0.04)
Total	104.9 (2.2)	94.8 (8.2)	107.3 (9.1)	86.3 (4.4)

Table 10: Tissue distribution of lipid and DOX at 1 h and 8 h after *i.v.* injection of LTSL-DOX containing MPPC at a dosage of 20 mg DOX/kg to adult female Balb/c mice.

	Mean percentage of total dose (SEM)			
	Lipid		*DOX*	
	1 h *(n = 3)*	*8 h* *(n = 3)*	*1 h* *(n = 3)*	*8 h* *(n = 3)*
Plasma	68.4 (1.5)	23.2 (0.3)	0.4 (0.04)	0.3 (0.01)
Liver	12.6 (1.6)	52.6 (5.6)	50.3 (4.6)	27.2 (4.6)
Spleen	0.1 (0.01)	0.2 (0.0)	0.2 (0.03)	0.2 (0.03)
Lung	0.6 (0.06)	0.43 (0.1)	1.5 (0.05)	1.1 (0.2)
Heart	0.1 (0.03)	0.2 (0.0)	2.3 (0.1)	1.3 (0.04)
Kidney	1.0 (0.3)	0.9 (0.1)	20.2 (1.5)	14.5 (0.7)
Muscle	-	-	0.4 (0.1)	1.2 (0.5)
Total	82.8 (4.1)	77.6 (5.3)	75.3 (5.3)	45.7 (4.4)

4.4.2 Plasma time profiles of lipid and DOX after *i.v.* injection of LTSL-DOX, TSL-DOX, or NTSL-DOX into mice

LTSL containing MPPC, TSL, and NTSL were loaded with DOX at a drug-to-lipid ratio of 0.05 mg/mg for LTSL and TSL or at 0.2 mg/mg for NTSL by the titration method (see section 3.7.). DOX-loaded liposomes were injected into adult female Rag2-M mice at a dosage of 20 mg DOX/kg. Mice were sacrificed and blood was collected into EDTA-coated microtainers by cardiac puncture at 1 h, 4 h, 24 h, and 48 h after NTSL-DOX injection or at 10 min, 20 min, 30 min, 1 h, 2 h, 4 h, and 8 h after TSL-DOX or LTSL-DOX injection. Plasma lipid and DOX concentrations were determined by scintillation counting and fluorescence spectroscopy, respectively.

After NTSL-DOX injection, mean plasma lipid concentrations decreased slowly from 2.8 mg/ml at 1 h to 1.6 mg/ml at 24 h but did not decrease further at 48 h after injection. Similarly, mean plasma DOX concentrations decreased from 0.45 mg/ml at 1 h to 0.26 mg/ml at 24 h but did not decrease further at 48 h after injection. Mean plasma drug-to-lipid ratios did not change significantly from 0.15 mg/mg over the investigated time period of 24 h (Figure 89). Pharmacokinetic parameters were not calculated for NTSL-DOX because DOX elimination from plasma did not follow first order kinetics.

After TSL-DOX injection, mean plasma lipid concentrations decreased significantly from 9.7 mg/ml at 10 min to 7.7 mg/ml at 2 h to 0.9 mg/ml at 4 h. Mean plasma DOX concentrations decreased more rapidly from 0.45 mg/ml at 10 min to 0.05 mg/ml at 2 h after injection. Mean plasma drug-to-lipid ratios decreased from 0.046 mg/mg at 10 min to 0.006 mg/mg at 2 h after injection (Figure 90). Pharmacokinetic parameters are presented in Table 11.

Plasma time profiles for lipid and DOX after LTSL-DOX injection were similar to those of after TSL-DOX injection. After LTSL-DOX injection, mean plasma lipid concentrations decreased significantly from 9.2 mg/ml at 10 min to 7.6 mg/ml at 2 h to 1 mg/ml at 4 h after injection. Mean plasma DOX concentrations decreased more rapidly from 0.4 mg/ml at 10 min to 0.1 mg/ml at 2 h after injection. Mean plasma drug-to-lipid ratios decreased from 0.042 mg/mg at 10 min to 0.014 mg/mg at 2 h after injection (Figure 91). Pharmacokinetic parameters of the LTSL-DOX formulation were in the same order of magnitude as those of TSL-DOX but $AUC_{0h\text{-}4h}$ and $AUMC_{0h\text{-}4h}$ values, mean residence time (MRT), volume of distribution at steady state (V_{ss}), and half-life ($t_{½}$), were slightly elevated (Table 11).

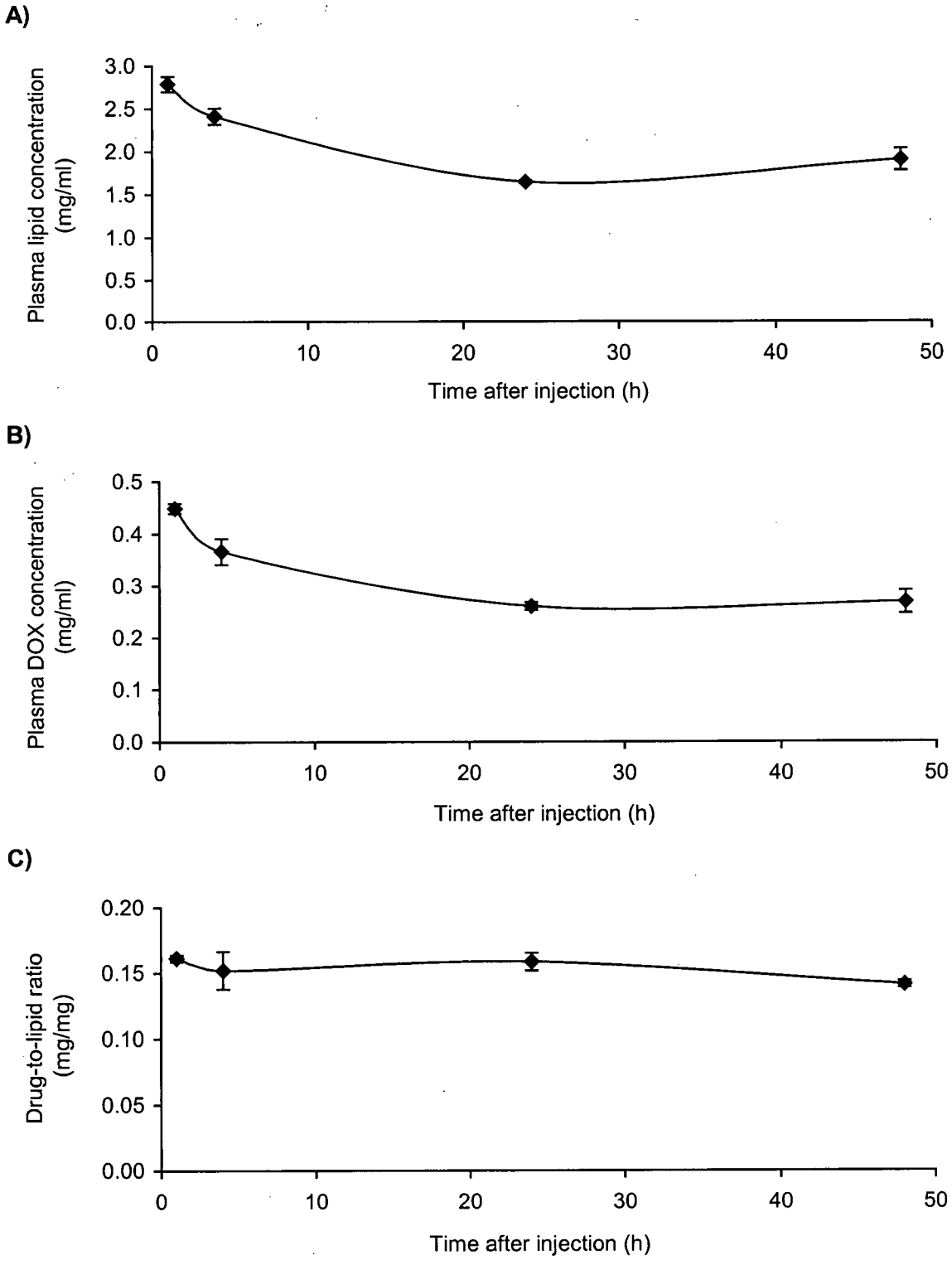

Figure 89: Plasma time profiles of NTSL-DOX for (A) lipid, (B) DOX, and (C) the drug-to-lipid ratio in adult female Rag2-M mice. Error bars indicate the standard error of mean values (n = 3).

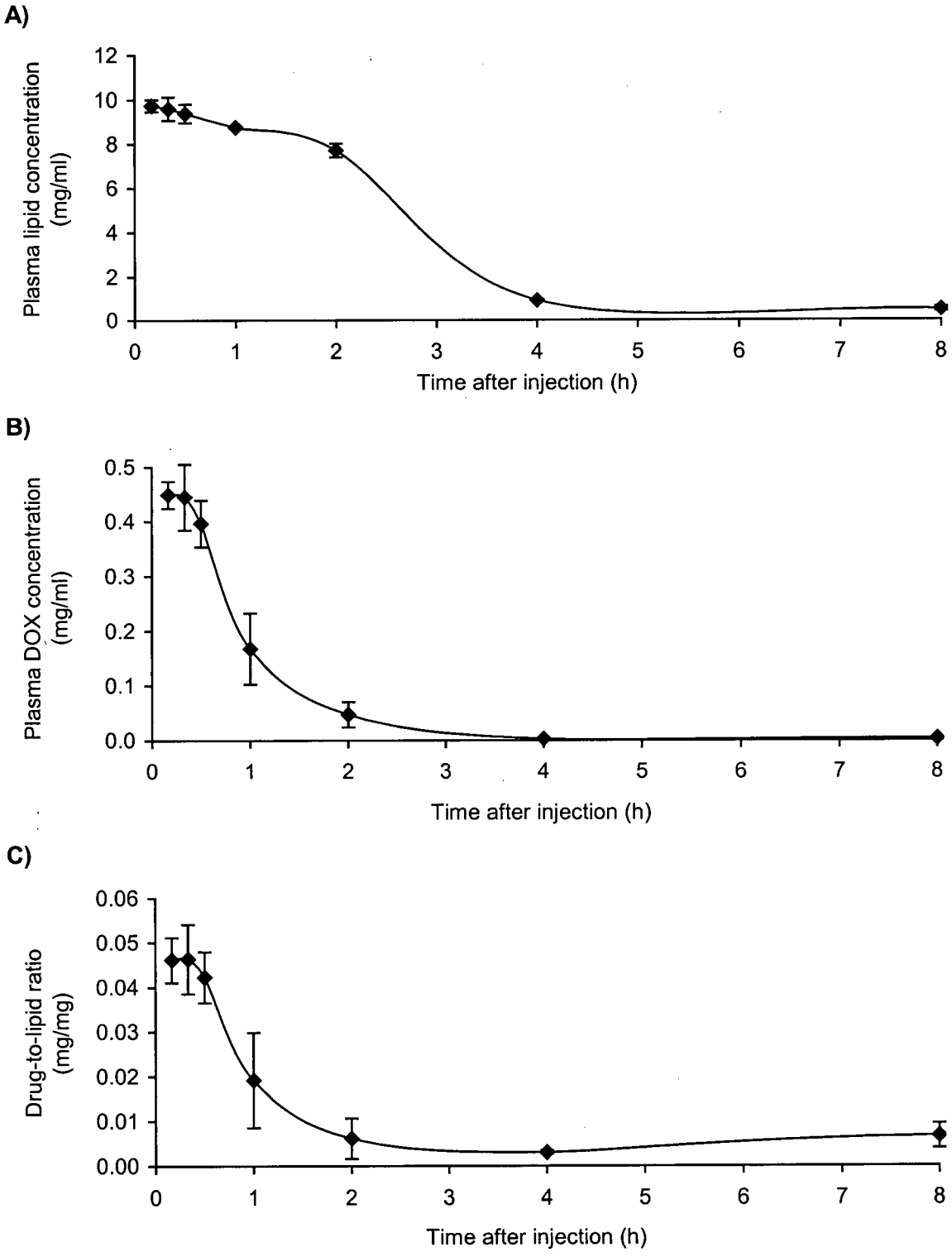

Figure 90: Plasma time profiles of TSL-DOX for (A) lipid, (B) DOX, and (C) the drug-to-lipid ratio in adult female Rag2-M mice. Error bars indicate the standard error of mean values (n = 3).

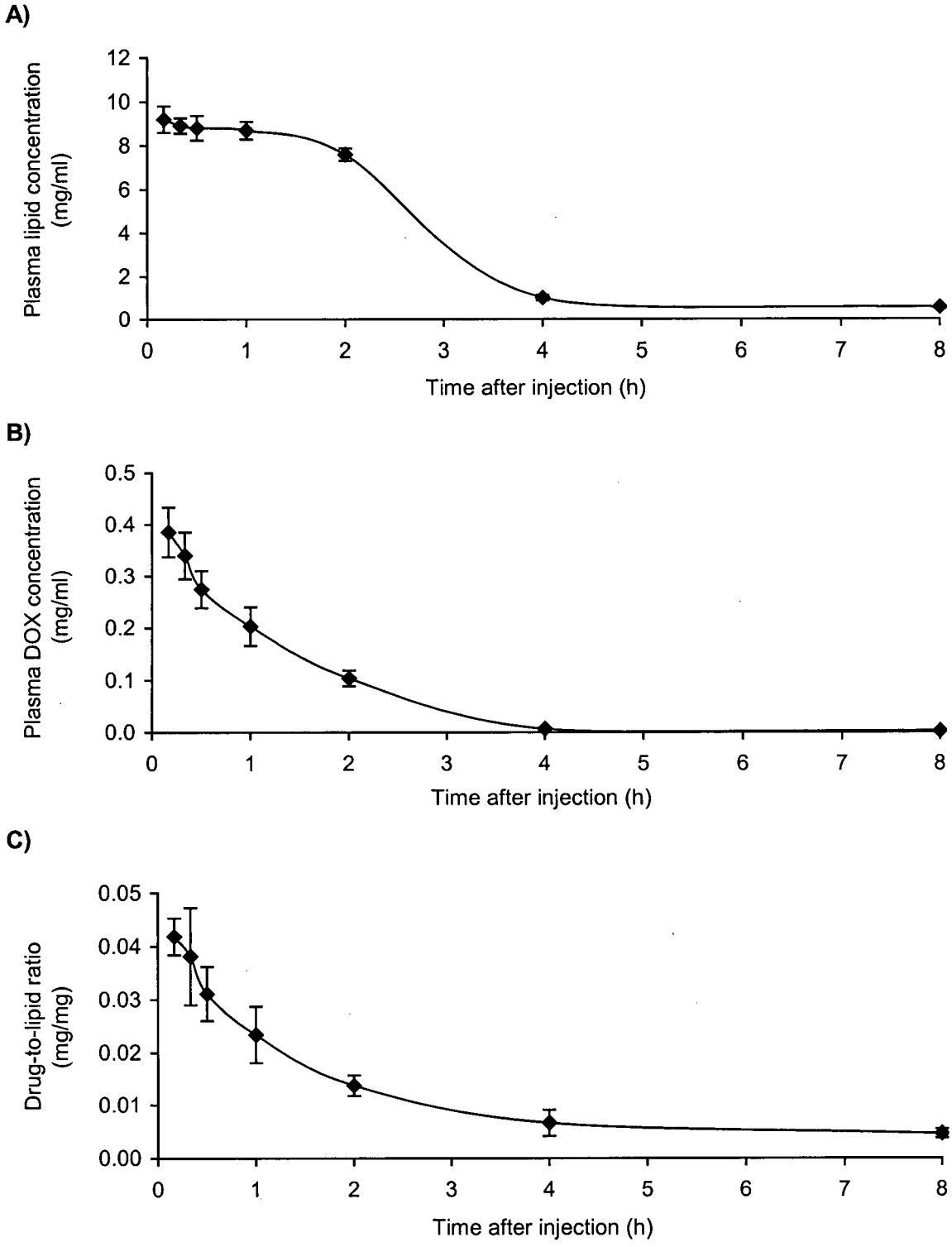

Figure 91: Plasma time profiles of LTSL-DOX containing MPPC for (A) lipid, (B) DOX, and (C) the drug-to-lipid ratio in adult female Rag2-M mice. Error bars indicate the standard error of mean values (n = 3).

Table 11: Pharmacokinetic parameters of TSL-DOX and LTSL-DOX in adult female Rag2-M mice. The area under the curve (AUC_{0h-4h}), area under the moment curve ($AUMC_{0h-4h}$), mean residence time (MRT), elimination rate constant (k), half-life ($t_{½}$), total body clearance (Cl), and volume of distribution at steady state (V_{ss}), were determined by non-compartmental analysis using the WinNonlin software program. The last four time points except the 8 h time points of Figures 100B and 101B were used for the estimation of the terminal elimination phase since the 8 h time points were thought to represent background values. AUC_{0h-4h} and $AUMC_{0h-4h}$ were calculated using the linear trapezoidal rule. MRT_{0h-4h} was estimated as the ratio of $AUMC_{0h-4h}$ and AUC_{0h-4h}. Cl was calculated as the ratio of the $Dose_{i.v}$ and the AUC_{0h-4h}. V_{ss} was calculated as $Dose_{i.v}$ / [$AUMC_{0h-4h}$ / AUC_{0h-4h}^2]. k was calculated from the slope of the line of best fit for the values associated with the terminal portion of the plasma concentration time curve (0.5 h - 4 h). $t_{½}$ was calculated as 0.693/k. R^2 = goodness of fit for the terminal elimination phase.

	TSL-DOX	LTSL-DOX
AUC_{0h-4h}	0.52 mg h / ml	0.56 mg h / ml
$AUMC_{0h-4h}$	0.38 mg h^2 / ml	0.57 mg h^2 / ml
MRT_{0h-4h}	0.74 h	1 h
Cl	0.77 ml / h	0.7 ml / h
V_{ss}	0.58 ml	0.73 ml
k	1.4 h^{-1}	1.1 h^{-1}
$t_{½}$	0.5 h	0.6 h
R^2	0.999	0.969

4.4.3 Body temperatures of mice as a response to stress

It was hypothesized that the difference in *in vivo* DOX retention between TSL-DOX or LTSL-DOX and that of NTSL-DOX as well as the differences in drug retention observed after LTSL-DOX injection into mice on different days were caused by an increased and variable body temperature in mice as a response to stress [204, 208]. As a contributing factor, mice were positioned briefly under a heat lamp prior to injection in order to dilate the tail veins and to gain easier access to blood vessels. Thus, the thermal response of mice to stress induced by the treatment procedure was assessed by measuring the body temperature with a rectal probe in mice that either positioned under a heat lamp and in those that were not positioned under a heat lamp.

The mean body temperature of female non-heated Rag2-M mice was 37.1°C. The maximum body temperature of an individual mouse in this group was 37.6°C. When placed under a heat lamp for 2 min the mean body temperature increased significantly ($p < 0.01$) to 38.5°C. The increase in body temperature was significantly greater ($p < 0.01$) when mice were placed under the heat lamp for 5 min (39.4°C). The maximum body temperature of an individual mouse in this group was 39.9°C. Mean body temperatures did not change significantly when mice were returned to their cages after 30 min regardless whether mice had been exposed to the heat lamp or not (Table 12).

The mean body temperature of male non-heated Rag2-M mice was 38.2°C and thus at a significantly greater temperature ($p < 0.05$) than that of female mice. The maximum body temperature of an individual male mouse in this group was 38.7°C. When placed under a heat lamp for 2 min or 5 min the mean body temperature did not change significantly. The maximum body temperature of an individual mouse in these groups was 39°C (Table 12).

Table 12: Mean body temperatures of male and female Rag2-M mice. Mice were either placed under a heat lamp or not placed under a heat lamp for 2 min or 5 min and their rectal temperature was recorded immediately and again after 30 min. [a] = $p < 0.01$ versus no heat; [b] = $p < 0.01$ versus no heat after 30 min; [c] = $p < 0.01$ versus no heat in female mice; [d] = $p < 0.05$ versus no heat in female mice after 30 min; [e] = $p < 0.01$ versus 2 min under heat lamp; [f] = $p < 0.01$ versus 2 min under heat lamp after 30 min.

	Mean body temperature (°C) (SEM)	
	Female mice (n = 8)	*Male mice (n = 3)*
No heat	37.1 (0.58)	38.2 (0.2) [c]
No heat after 30 min	37.3 (0.1)	38.2 (0.19) [d]
2 min under heat lamp	38.5 (0.1) [a]	38.5 (0.21)
2 min under heat lamp after 30 min	38.4 (0.12) [b]	38.5 (0.18)
5 min under heat lamp	39.4 (0.15) [a, e]	38.6 (0.11)
5 min under heat lamp after 30 min	39.4 (0.17) [b, f]	38.5 (0.14)

Since body temperatures in mice were affected by the treatment, in subsequent drug retention and efficacy experiments the mice's tail veins were dilated by placing the tail in a water bath at a temperature of 45°C prior to injection instead of placing mice under a heat lamp. Although the mean body temperature in female mice was not elevated when the heat lamp was not used, the elevated body temperature in male mice that were not placed under the heat lamp indicated that stress induced by handling mice alone was sufficient to cause hyperthermia. Therefore, all mice were tranquilized or anesthetized

and their body temperatures were monitored constantly and regulated in a mouse incubator in subsequent drug retention and efficacy experiments, because the individual stress level in mice could not be assessed or controlled (see section 3.17.2). Representative body temperature time profiles of mice in the mouse incubator tranquilized with acepromazine or anesthetized with ketamine/xylazine are shown in Figure 92.

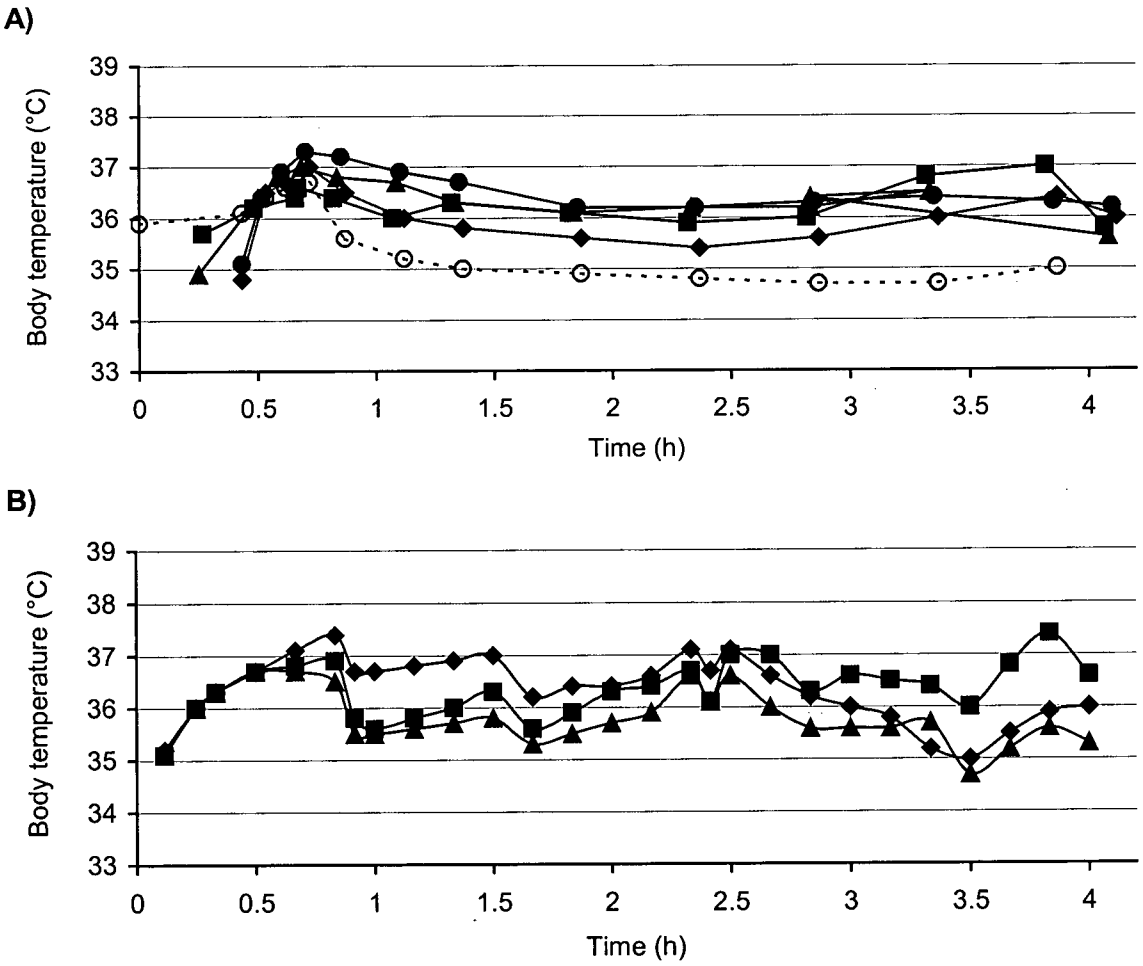

Figure 92: Individual body temperature time profiles of adult female Balb/c mice in the mouse incubator tranquilized with (A) acepromazine at a *s.c.* dosage of 6 mg/kg or (B) anesthetized with ketamine/xylazine at an initial *i.p.* dosage of 80/20 mg/kg followed by a maintenance dose of 40/10 mg/kg at 30 min after the initial dose. The dashed line in (A) indicates the chamber temperature.

4.4.4 Plasma time profiles of lipid and DOX after *i.v.* injection of LTSL-DOX into temperature controlled mice

LTSL containing MSPC were loaded with DOX at a drug-to-lipid ratio of 0.05 mg/mg by the buffer exchange method (see section 3.7). Adult female Balb/c mice were tranquilized for 4 h with acepromazine at a dosage of 6 mg/kg by *s.c.* injection. LTSL-DOX were injected into mice at a dosage of 16 mg DOX/kg after mice were tranquilized and their body temperatures were stabilized in the mouse incubator at a temperature of 36°C ± 1.5°C. Mice were sacrificed and blood was collected into EDTA-coated microtainers by cardiac puncture at 10 min, 30 min, 1 h, 2 h, 3 h, and 4 h after treatment. Lipid and DOX plasma levels were determined by scintillation counts and fluorescence spectroscopy, respectively.

In contrast to plasma lipid concentrations determined previously after *i.v.* injection of LTSL-DOX into non temperature controlled mice (Figure 91A), plasma lipid concentrations in tranquilized, temperature controlled mice were at approximately 10 mg/ml and did not change significantly over the investigated time period (Figure 93A). Plasma DOX concentrations were slightly higher at 0.6 mg/ml at 10 min, 0.3 mg/ml at 1 h, and 0.14 mg/ml at 2 h (Figure 93B) in comparison to those in non temperature controlled mice (Figure 91B). Mean plasma drug-to-lipid ratios were at 0.06 mg/mg at 10 min, 0.03 mg/mg at 1 h, and 0.01 mg/mg at 2 h (Figure 93C). Pharmacokinetic parameters after LTSL-DOX injection in tranquilized, temperature controlled mice (Table 13) were in the same order of magnitude as those in non temperature controlled mice (Table 11). However, in temperature controlled mice $AUC_{0h\text{-}4h}$, $AUMC_{0h\text{-}4h}$, and k values were slightly elevated, $MRT_{0h\text{-}4h}$ and $t_{½}$ values were slightly decreased, and Cl and V_{ss} values were decreased by approximately 50%.

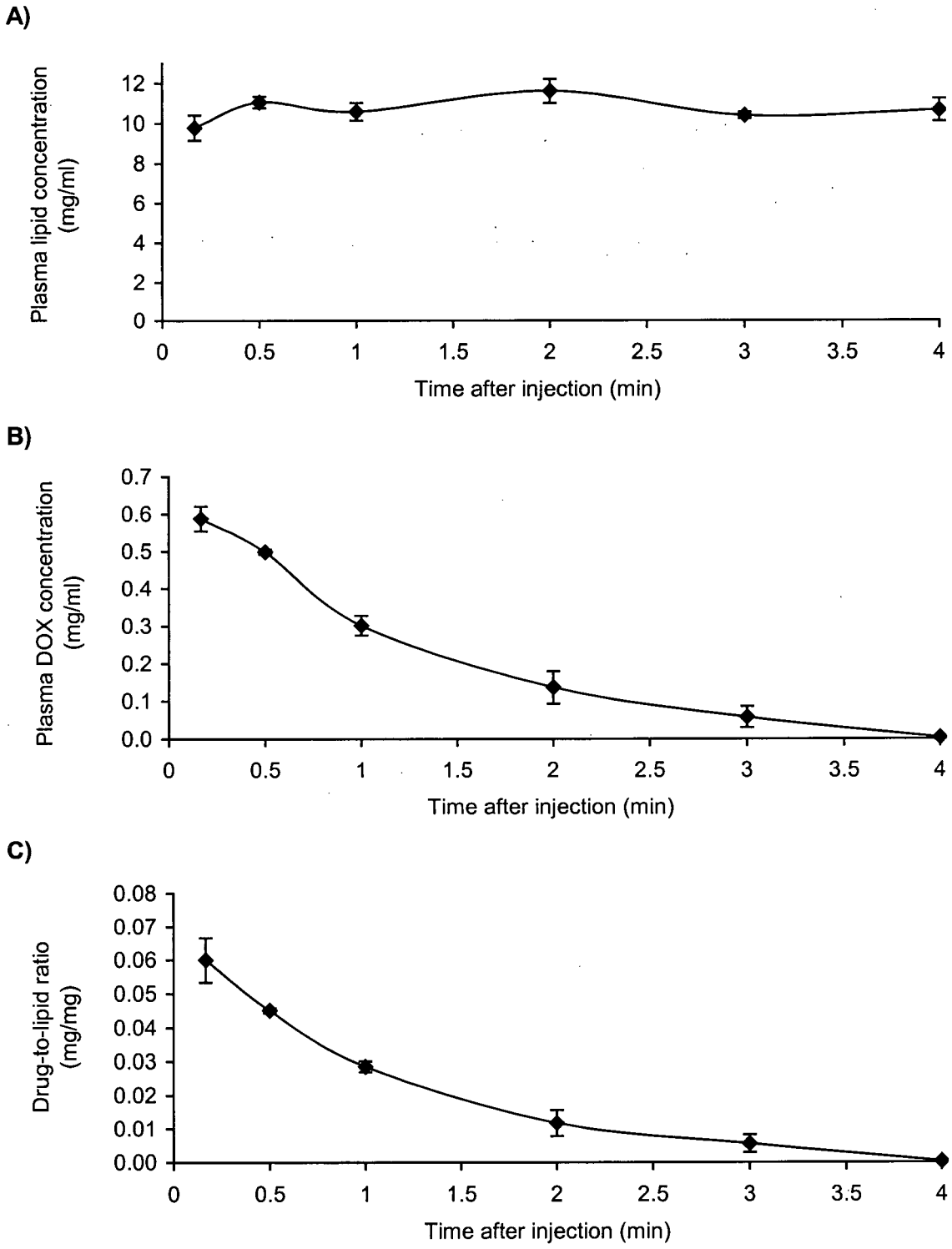

Figure 93: Plasma time profiles of LTSL-DOX containing MSPC for (A) lipid, (B) DOX, and (C) the drug-to-lipid ratio in temperature controlled adult female Balb/c mice. Error bars indicate the standard error of mean values (n = 3).

Table 13: Pharmacokinetic parameters of LTSL-DOX in euthermic temperature controlled adult female Balb/c mice. Pharmacokinetic parameters were determined by non-compartmental analysis using the WinNonlin software program. The last five time points of Figures 108B were used for the estimation of the terminal elimination phase. AUC_{0h-4h} and $AUMC_{0h-4h}$ were calculated using the linear trapezoidal rule. MRT_{0h-4h} was estimated as the ratio of $AUMC_{0h-4h}$ and AUC_{0h-4h}. Cl was calculated as the ratio of the $Dose_{i.v}$ and the AUC_{0h-4h}. V_{ss} was calculated as $Dose_{i.v}$ / [$AUMC_{0h-4h}$ / AUC_{0h-4h}^2]. k was calculated from the slope of the line of best fit for the values associated with the terminal portion of the plasma concentration time curve (0.5 h - 4 h). $t_{½}$ was calculated as 0.693/k. R^2 = goodness of fit for the terminal elimination phase.

	LTSL-DOX
AUC_{0h-4h}	0.83 mg h / ml
$AUMC_{0h-4h}$	0.81 mg h^2 / ml
MRT_{0h-4h}	0.97 h
Cl	0.38 ml / h
V_{ss}	0.38 ml
k	1.3 h^{-1}
$t_{½}$	0.54 h
R^2	0.919

4.4.5. Time dependence of LTSL, TSL, and NTSL thermosensitivity after *i.v.* injection into mice

It has been shown previously that phospholipids can exchange out of liposomes into the serum and from there into cell membranes or high density lipoproteins (HDL) after *in vivo* exposure [88, 89]. Since lysolipids have been shown to adsorb and desorb from liposomes [140] LTSL were hypothesized to loose their superior thermosensitive properties in comparison to TSL if lysolipids would leave the LTSL membrane after *i.v.* injection. To test this hypothesis, LTSL-DOX, TSL-DOX or NTSL-DOX were injected into mice and the thermosensitivity of liposomes was determined after *in vivo* exposure.

LTSL containing MPPC, TSL, and NTSL were loaded with DOX at a drug-to-lipid ratio of 0.05 mg/mg for LTSL and TSL or at 0.2 mg/mg for NTSL by the titration method (see section 3.7). DOX-loaded liposomes were injected into adult female Rag2-M mice at a dosage of 20 mg DOX/kg for LTSL-DOX and TSL-DOX, or at a dosage of 16.6 mg/kg for NTSL-DOX. Mice were sacrificed and blood was collected into EDTA-coated microtainers by cardiac puncture at 10 min, 20 min, 30 min, and 60 min after injection. Blood from three mice was pooled, placed on ice, and plasma was separated from blood cells at a temperature of 4°C in a centrifugal field of 350 g for 15 min. Plasma samples were split in half. One half was incubated for 30 min at a temperature of 37°C the other half was incubated for 10 min at a temperature of 45°C. Liposomes not injected into mice served as a control. Doxorubicin released from liposomes was removed from plasma on a Sephadex G-50 spin column in a centrifugal field of 680 g for 2 min. Lipid and DOX plasma levels were determined by scintillation counts and fluorescence spectroscopy, respectively. The percentage of DOX released from liposomes after incubation at a temperature of 45°C was calculated relative to that of

plasma incubates at a temperature of 37°C.

After *in vivo* exposure of TSL for 10 min or 20 min the mean relative percentage of DOX released was 68%. After *in vivo* exposure for 30 min or 60 min the mean relative percentage of DOX released from TSL decreased to 54% (Figure 94A).

The relative percentage of DOX released from LTSL that were not injected into mice was 91% after heating to a temperature of 42°C relative to that of LTSL heated to 37°C. After *in vivo* exposure for 10 min, 20 min, 30 min, or 60 min, the relative percentage of DOX released from LTSL decreased to 74%, 57%, 48%, and 48%, respectively (Figure 94B).

After *in vivo* exposure of NTSL for 60 min, DOX was not released from liposomes after heating to a temperature of 42°C (data not shown).

Results indicate that the superior drug release properties of LTSL in comparison to TSL were gradually lost after increasing residence time in the mice's blood circulation.

A)

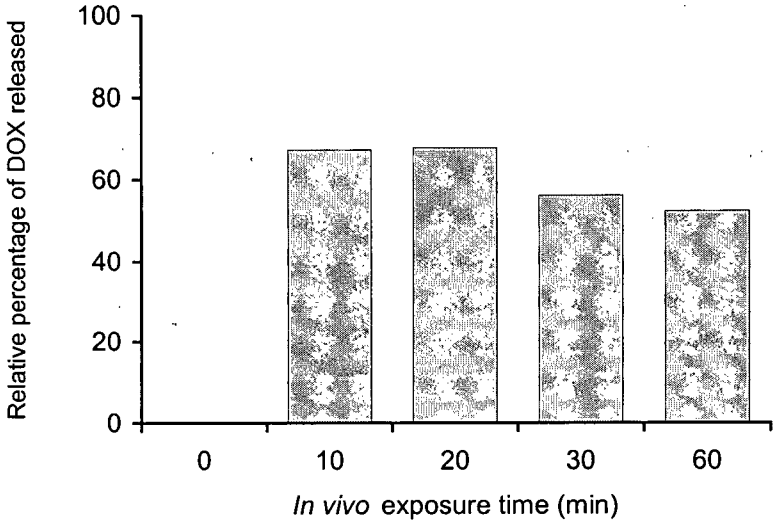

B)

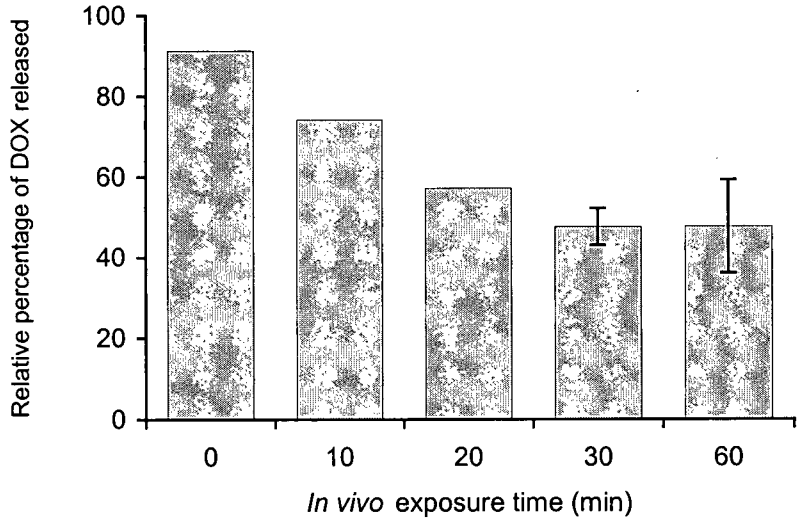

Figure 94: Thermosensitivity of (A) TSL-DOX and (B) LTSL-DOX containing MPPC recovered from plasma after *i.v.* injection into adult female Rag2-M mice. Values represent the percentage of DOX released after heating recovered plasma to a temperature of 45°C for 10 min relative to that of plasma heated to 37°C. "0 min" refers to LTSL that were not injected into mice. Plasma samples were pooled from three mice. Plasma samples in (A) after *in vivo* exposure of 30 min and 60 min, were collected from two separate experiments conducted on two different days. Error bars indicate the standard deviation.

4.4.6. Time and temperature dependence of LTSL thermosensitivity after *i.v.* injection into temperature controlled euthermic and hyperthermic mice

To investigate whether the loss of LTSL thermosensitivity was dependent on the mice's body temperature LTSL-DOX were injected into tranquilized euthermic or hyperthermic mice and the thermosensitivity of liposomes was determined after *in vivo* exposure.

LTSL containing MSPC were loaded with DOX at a drug-to-lipid ratio of 0.05 mg/mg by the buffer exchange method (see section 3.7). Adult female Balb/c mice were tranquilized for 4 h with acepromazine at a dosage of 6 mg/kg by *s.c.* injection. LTSL-DOX were injected into mice at a dosage of 10 mg DOX/kg after mice were tranquilized and their body temperatures were stabilized in the mouse incubator at a temperature of either 37°C or 40°C. This lower dosage of DOX was chosen because mice in the hyperthermia group showed signs of toxicity at a dosage of 20 mg DOX/kg. Euthermic mice were sacrificed and blood was collected into EDTA-coated microtainers by cardiac puncture at 10 min, 30 min, 1 h, 2 h, 4 h, or 8 h after injection. Hyperthermic mice were sacrificed and blood was collected at 5 min, 10 min, 15 min, 30 min, 45 min, or 1 h after injection. Plasma was separated from blood cells at a temperature of 4°C in a centrifugal field of 350 g for 15 min. Aliquots of plasma were maintained at a temperature of 4°C or heated to 50°C for 10 min and DOX released from liposomes in plasma was separated on Sephadex G-50 spin columns. Lipid and DOX plasma levels were determined by scintillation counts and fluorescence spectroscopy, respectively. Liposomes that were not injected into mice, heated and separated on a Sephadex G-50 spin column and liposomes that were not injected and not heated but to which the detergent OGP was added served as positive controls.

Body temperatures of tranquilized mice decreased initially after acepromazine injection to temperatures as low as 33.5°C. After placing mice in the mouse incubator, temperatures increased to the desired set temperature of 37°C or 40°C after approximately 20 min and were stable within 0.5 of a degree throughout the experiment. After injection of LTSL-DOX, body temperatures decreased briefly but increased back to the set temperature typically within 5-10 min (Figures 95 and 96). Euthermic mice were placed back in their cages after 1-1.5 h in the mouse incubator and cages were placed in a cage incubator heated to a temperature of 36°C. The body temperature in these mice was not further monitored and mice remained tranquilized for 4 h after acepromazine injection.

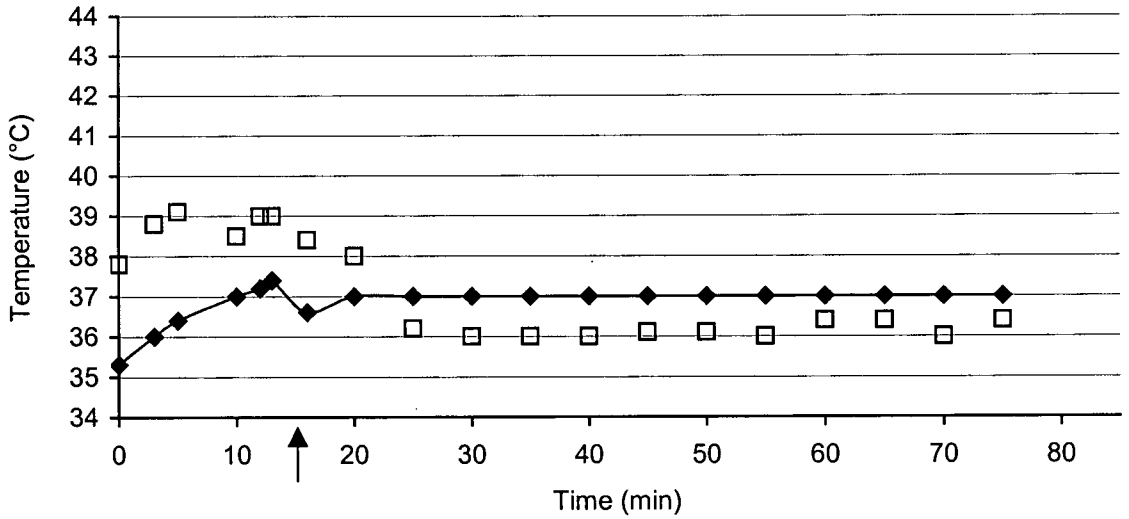

Figure 95: Representative diagram of the chamber temperature of the mouse incubator (□) and the body temperature of an adult female Balb/c mouse tranquilized with acepromazine at a dosage of 6 mg/kg (◆). The body temperature was maintained at 37°C. The arrow indicates the time point of LTSL-DOX injection.

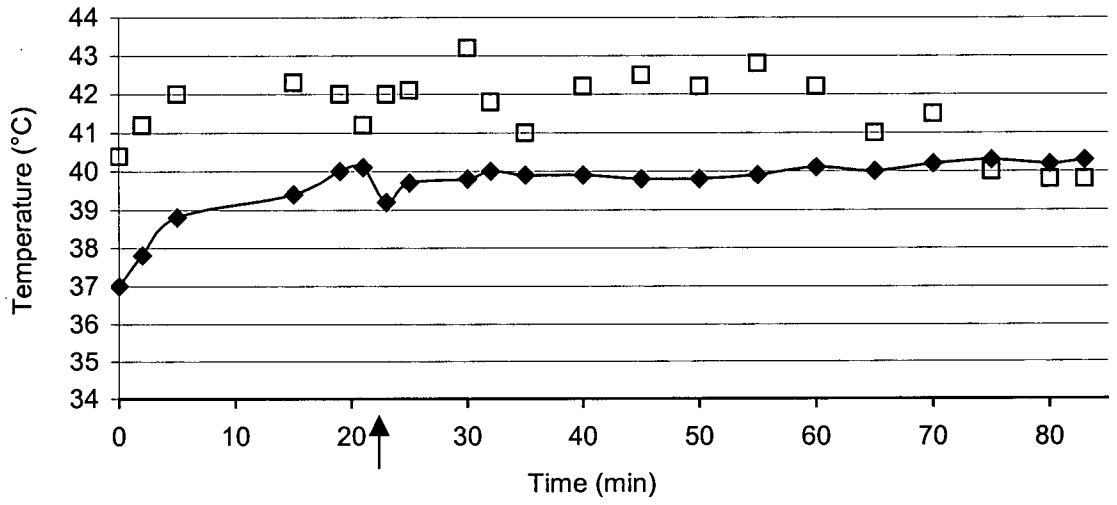

Figure 96: Representative diagram of the chamber temperature of the mouse incubator (□) and the body temperature of an adult female Balb/c mouse tranquilized with acepromazine at a dosage of 6 mg/kg (◆). The body temperature was maintained at 40°C. The arrow indicates the time point of LTSL-DOX injection.

In control liposomes approximately 80-90% of DOX was released after heating. LTSL that remained in the circulation of euthermic mice for up to 1 h after injection also released more than 80% of their DOX content after heating. LTSL that remained in circulation for 4 h or 8 h released approximately 50% of their DOX content after heating (Figure 97A) indicating that the thermosensitivity of LTSL decreased significantly when LTSL remained in plasma for time periods longer than 1 h.

LTSL that remained in the circulation of hyperthermic mice for 5-60 min released, on average, approximately 50% of their DOX content after heating (Figure 97B). The release of DOX from LTSL that remained in the circulation of hyperthermic mice for 10 min, 30 min, or 60 min was significantly less ($p < 0.05$) than that from LTSL that remained in the circulation of euthermic mice at these time points.

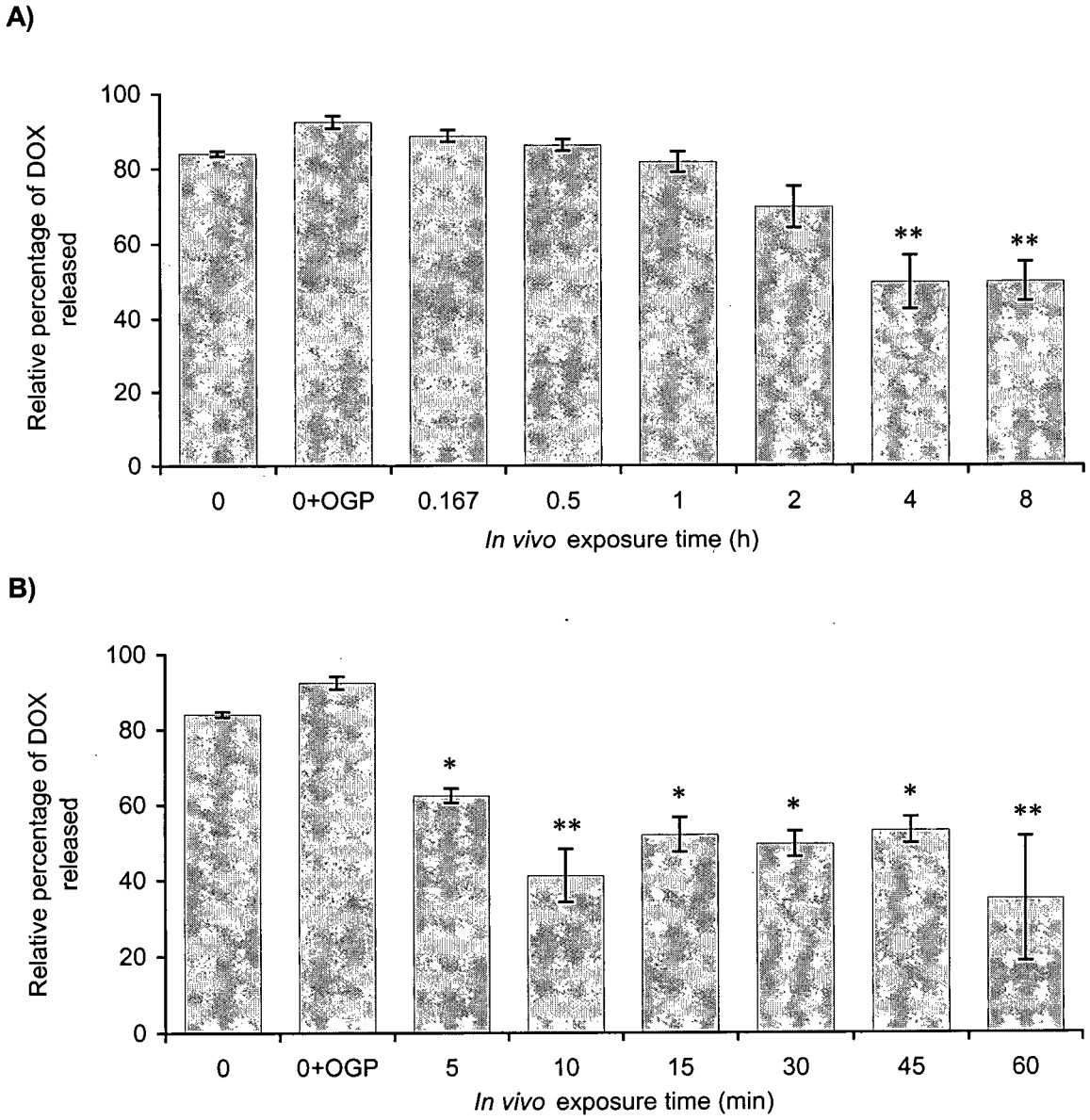

Figure 97: Thermosensitivity of LTSL-DOX containing MSPC recovered from plasma after *i.v.* injection into adult female Balb/c mice with a body temperature of (A) 37°C or (B) 40°C. Values represent the percentage of DOX released after heating plasma for 10 min to a temperature of 50°C relative to that of unheated plasma. 0 = liposomes not injected; 0 + OGP = liposomes not injected and not heated after addition of the detergent OGP. Error bars indicate the standard error of mean values (n = 3). * = $p < 0.05$ versus 0; ** = $p < 0.01$ versus 0.

4.4.7. DOX retention and lysolipid redistribution between the cellular blood fraction and plasma after *i.v.* injection of LTSL-DOX into temperature controlled euthermic and hyperthermic mice.

LTSL containing MSPC were labeled with ^{14}C-MPPC and ^{3}H-CHE at an activity ratio of 0.9 dpm/dpm and loaded with DOX at a drug-to-lipid ratio of 0.05 mg/mg by the buffer exchange method (see section 3.7.). Adult female Balb/c mice were tranquilized for 4 h with acepromazine at a dosage of 6 mg/kg by s.c. injection. LTSL-DOX were injected into mice at dosage of 10 mg DOX/kg after mice were tranquilized and their body temperatures were stabilized in a mouse incubator at of either 37°C or 40°C. Euthermic mice were sacrificed and blood was collected into EDTA-coated microtainers by cardiac puncture at 10 min, 30 min, 1 h, 2 h, 4 h, or 8 h after injection. Hyperthermic mice were sacrificed and blood was collected at 5 min, 10 min, 15 min, 30 min, 45 min, or 1 h after injection. Plasma was separated from blood cells at a temperature of 4°C in a centrifugal field of 350 g for 15 min. Aliquots of plasma and the cellular blood fraction containing primarily blood cells but also small amounts of plasma were maintained at a temperature of 4°C. The amount of DOX in plasma was determined by fluorescence spectroscopy. The amount of lipid and lysolipid in plasma and the cellular blood fraction was determined by scintillation counts.

The mean ratios of lysolipid and total lipid indicated by the ^{14}C-MPPC / ^{3}H-CHE ratios in euthermic mice injected with LTSL-DOX were approximately 40-50% higher in the cellular blood fraction than those in plasma. At 10 minutes after injection, mean lysolipid/lipid ratios decreased from an initial ratio of 0.9 dpm/dpm to 0.42 dpm/dpm in the cellular blood fraction or to 0.33 dpm/dpm in plasma. After 1 h in circulation, ratios decreased to 0.31 dpm/dpm in the cellular blood fraction or to 0.23 dpm/dpm in plasma.

After 2 h in circulation, ratios decreased further to 0.22 dpm/dpm in the cellular blood fraction or to 0.14 dpm/dpm in plasma at approximately the same rate. Mean lysolipid/lipid ratios did not decrease significantly any further at 4 h or 8 h after injection (Figure 98).

In hyperthermic mice injected with LTSL-DOX, mean lysolipid/lipid ratios were approximately twice as high in the cellular fraction than in plasma (Figure 99). At 10 minutes after injection, mean lysolipid/lipid ratios decreased from an initial ratio of 0.9 dpm/dpm to 0.33 dpm/dpm in the cellular blood fraction or to 0.2 dpm/dpm in plasma. After 1 h in circulation, ratios decreased further to 0.17 dpm/dpm in the cellular blood fraction or to 0.1 dpm/dpm in plasma at approximately the same rate (Figure 99).

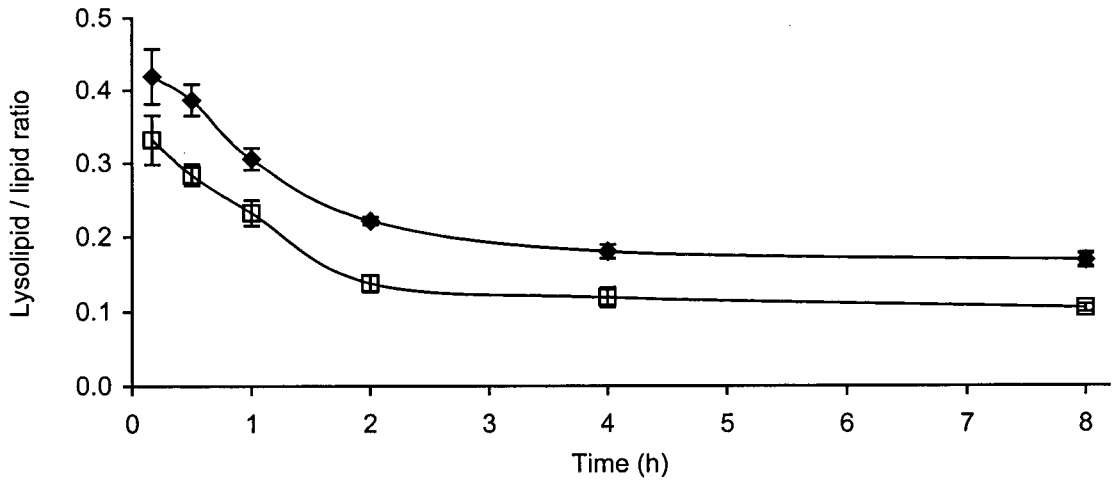

Figure 98: Lysolipid/lipid ratios determined as the ^{14}C-MPPC / ^{3}H-CHE ratios in the cellular blood fraction (◆) or in plasma (□) after injection of LTSL-DOX containing MSPC into adult female Balb/c mice with a body temperature of 37°C. The initial lysolipid/lipid ratio of the LTSL formulation was 0.9. Error bars indicate the standard error of mean values (n = 3).

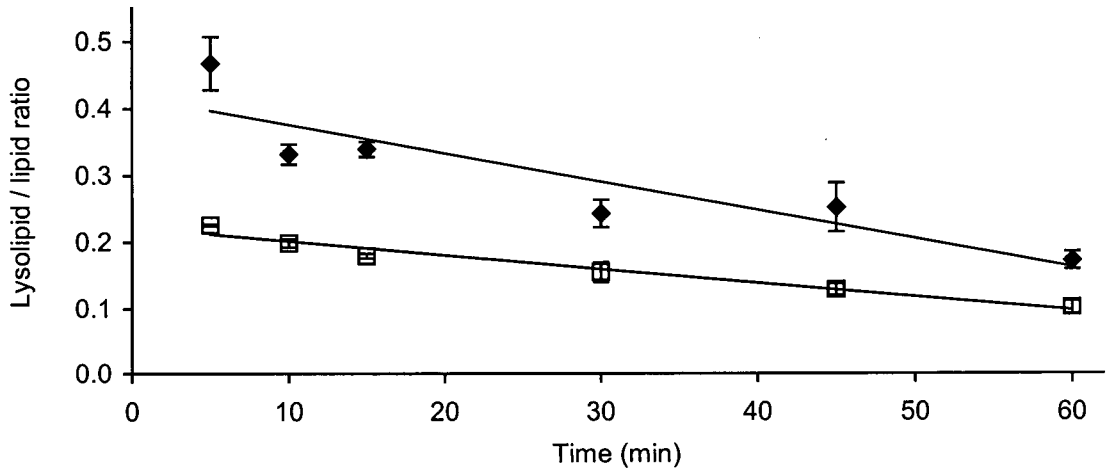

Figure 99: Lysolipid/lipid ratios determined as the ^{14}C-MPPC / ^{3}H-CHE ratios in the cellular blood fraction (◆) or in plasma (□) after injection of LTSL-DOX containing MSPC into adult female Balb/c mice with a body temperature of 40°C. The initial lysolipid/lipid ratio of the LTSL formulation was 0.9. Error bars indicate the standard error of mean values (n = 3).

Plasma time profiles for lipid, DOX, and the drug-to-lipid ratio after *i.v.* injection of LTSL-DOX containing MSPC into tranquilized, euthermic mice were similar to those determined previously (section 4.4.4.) and those of LTSL-DOX containing MPPC in non-temperature controlled mice (section 4.4.2). Mean lipid plasma concentrations decreased from 5.5 mg/ml at 10 min to 5.1 mg/ml at 2 h and 1.6 mg/ml at 8 h after injection. Mean DOX plasma concentrations decreased more rapidly immediately after injection from 0.26 mg/ml at 10 min to 0.02 mg/ml at 2 h after injection. Mean drug-to-lipid ratios decreased from 0.047 mg/mg at 10 min to 0.004 mg/mg at 2 h after injection (Figure 100).

Pharmacokinetic parameters after *i.v.* injection of LTSL-DOX containing MSPC into tranquilized, temperature controlled mice (Table 14) were in the same order of magnitude as those determined previously (Table 13) and those after *i.v.* LTSL-DOX injection into non temperature controlled mice (Table 11). The AUC_{0h-4h} and $AUMC_{0h-4h}$ values were lower because of the lower administered dose of DOX. MRT_{0h-4h}, Cl, and V_{ss} values were between those determined previously and those in non-temperature controlled mice. The k value was slightly lower and the $t_{½}$ value was slightly higher than those determined previously.

Plasma time profiles for lipid, DOX and drug-to-lipid ratio after *i.v.* injection of LTSL-DOX containing MPPC into tranquilized, hyperthermic mice were similar to those of LTSL-DOX containing MPPC in non temperature controlled mice in the tissue distribution study (section 4.4.1). Mean lipid plasma concentrations stayed relatively constant over the investigated time period of 1 h at approximately 5-6 mg/ml. Mean DOX plasma concentrations, however, decreased rapidly immediately after injection from 0.06 mg/ml at 10 min to 0.02 mg/ml at 1 h after injection. Mean drug-to-lipid ratios decreased from 0.01 mg/mg at 10 min to 0.003 at 1 h after injection (Figure 100).

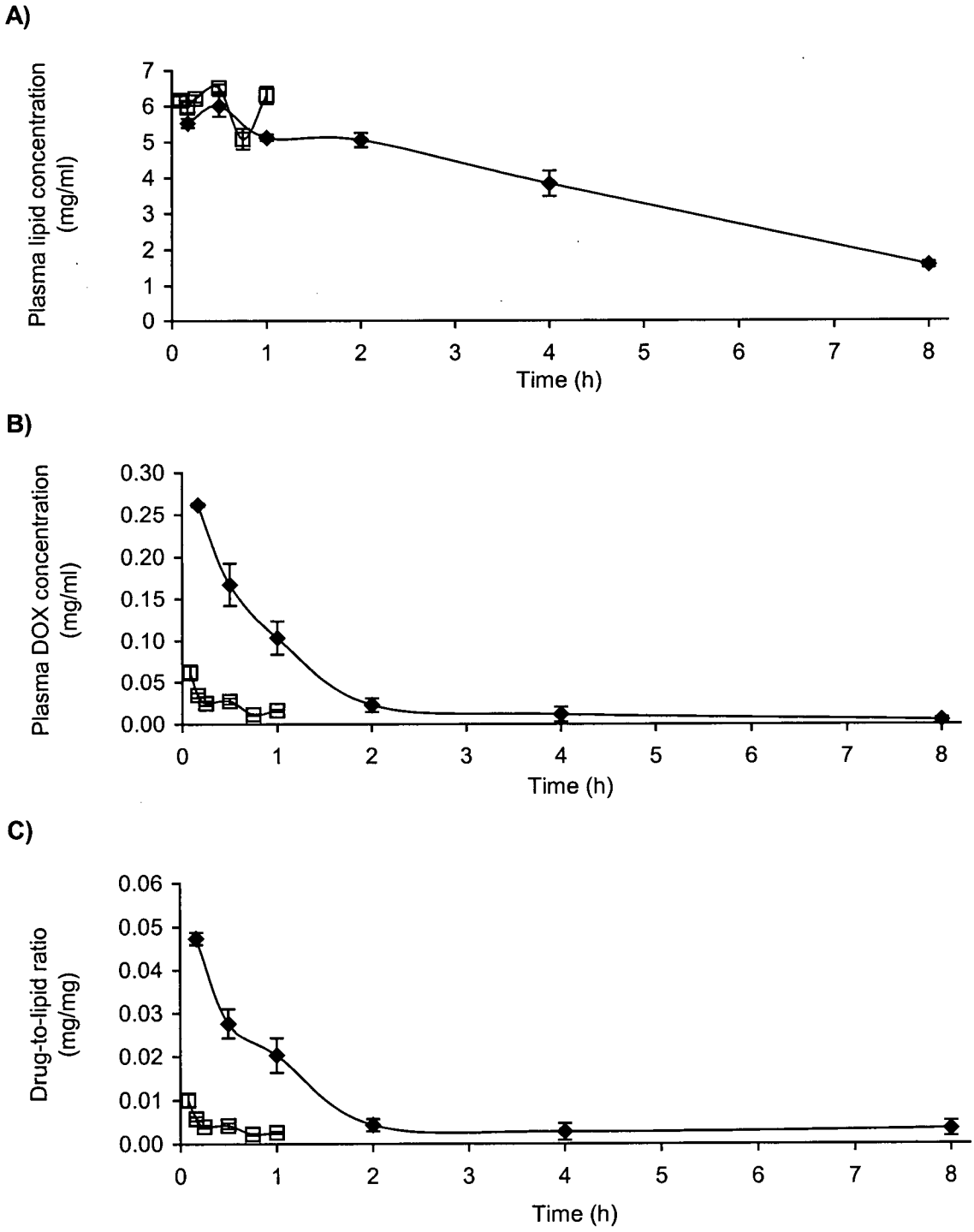

Figure 100: Plasma time profiles of LTSL-DOX for (A) lipid, (B) DOX, and (C) the drug-to-lipid ratio in adult female Balb/c mice with a body temperature of 37°C (◆) or 40°C (□). Error bars indicate the standard error of mean values (n = 3).

Table 14: Pharmacokinetic parameters of LTSL-DOX and in temperature controlled euthermic adult female Balb/c mice. Pharmacokinetic parameters were determined by non-compartmental analysis using the WinNonlin software program. The last five time points of Figures 112B were used for the estimation of the terminal elimination phase. $AUC_{0h\text{-}4h}$ and $AUMC_{0h\text{-}4h}$ were calculated using the linear trapezoidal rule. $MRT_{0h\text{-}4h}$ was estimated as the ratio of $AUMC_{0h\text{-}4h}$ and $AUC_{0h\text{-}4h}$. Cl was calculated as the ratio of the $Dose_{i.v}$ and the $AUC_{0h\text{-}4h}$. V_{ss} was calculated as $Dose_{i.v}$ / [$AUMC_{0h\text{-}4h}$ / $AUC_{0h\text{-}4h}^2$]. k was calculated from the slope of the line of best fit for the values associated with the terminal portion of the plasma concentration time curve (0.5 h - 4 h). $t_{½}$ was calculated as 0.693/k. R^2 = goodness of fit for the terminal elimination phase.

	LTSL-DOX
$AUC_{0h\text{-}4h}$	0.28 mg h / ml
$AUMC_{0h\text{-}4h}$	0.22 mg h^2 / ml
$MRT_{0h\text{-}4h}$	0.8 h
Cl	0.69 ml / h
V_{ss}	0.68 ml
k	0.81 h^{-1}
$t_{½}$	0.86 h
R^2	0.888

4.4.8. Time profiles of lipid and DOX after incubation of LTSL-DOX with whole blood, plasma, or buffer

To test the hypothesis that the presence of cellular membrane pools was responsible for the desorption of lysolipids from LTSL as observed in section 4.4.7., LTSL-DOX were incubation with whole blood, plasma or buffer

LTSL containing MSPC were loaded with DOX at a drug-to-lipid ratio of 0.05 mg/mg by the buffer exchange method (see section 3.7.). LTSL-DOX (0.2 mg DOX) was added to 1 ml of freshly obtained whole blood or plasma from adult female Balb/c mice or to HBS to match concentrations after LTSL-DOX injection into mice and the mixture was incubated at a temperature of 37°C. The amounts of DOX encapsulated in LTSL that were incubated with whole blood, plasma, or HBS were determined by fluorescence spectroscopy at 5 min, 10 min, 30 min, 1 h, 2 h, and 4 h by removing unencapsulated DOX on a Sephadex G-50 column.

The plasma time profiles for lipid, DOX, and the drug-to-lipid ratio after incubation of LTSL-DOX with whole blood were similar to those determined previously after *i.v.* injection of LTSL-DOX into tranquilized, euthermic mice (sections 4.4.4. and 4.4.7.). Lipid concentrations in plasma separated after incubation of LTSL-DOX with whole blood stayed relatively constant over the investigated time period of 4 h, except for a small initial decrease. Plasma DOX concentrations and drug-to-lipid ratios decreased from an initial value of 0.22 mg/ml and 0.046 mg/mg, respectively, to 0.08 mg/ml and 0.016 mg/mg, respectively, at 1 h after incubation. Plasma DOX concentrations and drug-to-lipid ratios did not decrease to levels as low as those determined previously and stayed, on average, at 0.08 mg/ml and 0.015 mg/mg, respectively, at incubation times of 1 h to 4 h (Figure 101). After incubation of LTSL-DOX with plasma or buffer, lipid

concentrations, DOX concentrations, and drug-to-lipid ratios remained relatively constant at their initial values (Figures 102 and 103).

These results indicate that DOX was released form LTSL when incubated at physiological temperatures in the presence of blood cells but not when LTSL-DOX was incubated with plasma or buffer.

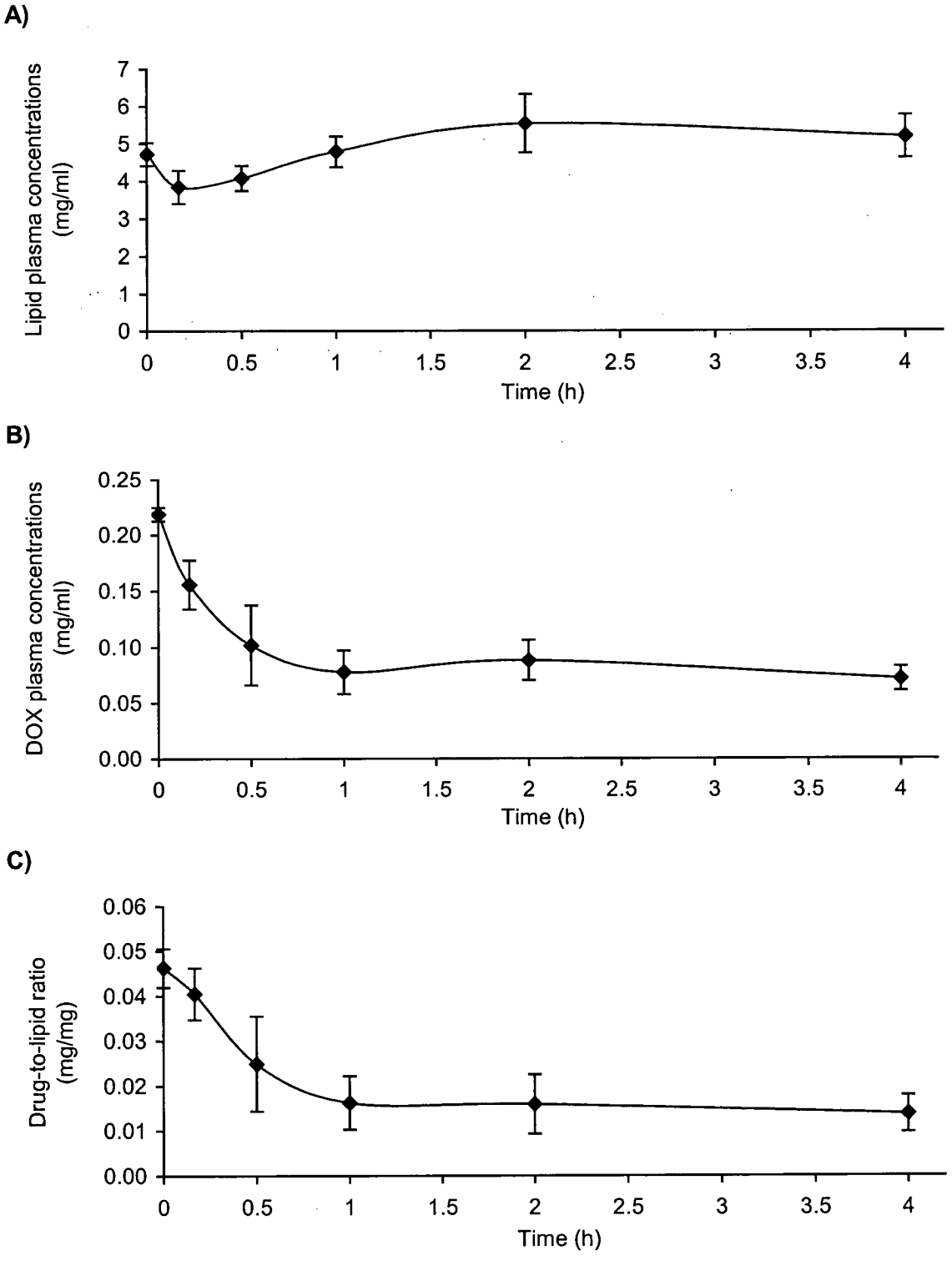

Figure 101: Plasma time profiles of LTSL-DOX for (A) lipid, (B) DOX, and (C) the drug-to-lipid ratio incubated with whole blood from adult female Balb/c mice. Error bars indicate the standard error of mean values (n = 3).

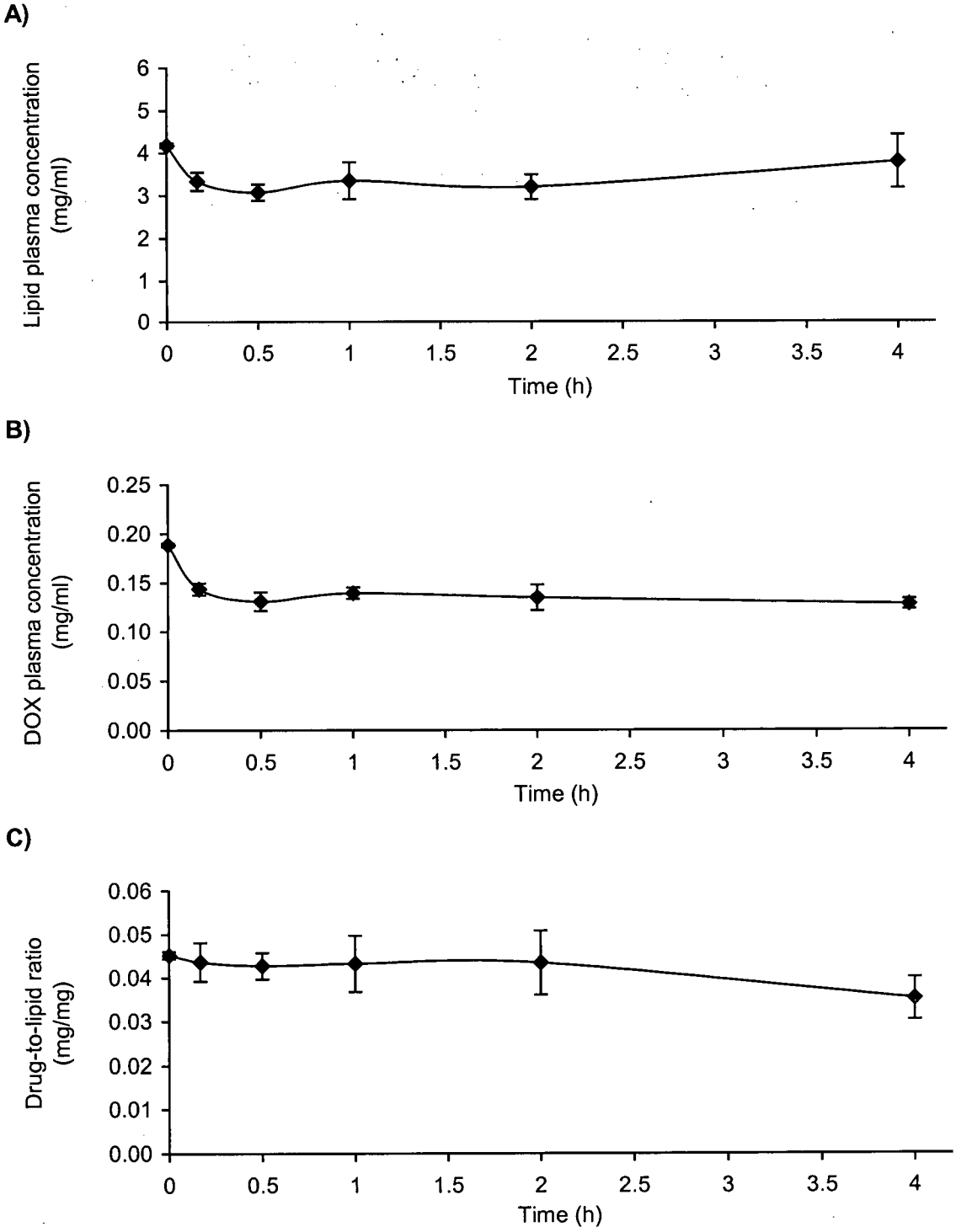

Figure 102: Plasma time profiles of LTSL-DOX for (A) lipid, (B) DOX, and (C) the drug-to-lipid ratio incubated with plasma from adult female Balb/c mice. Error bars indicate the standard error of mean values (n = 3).

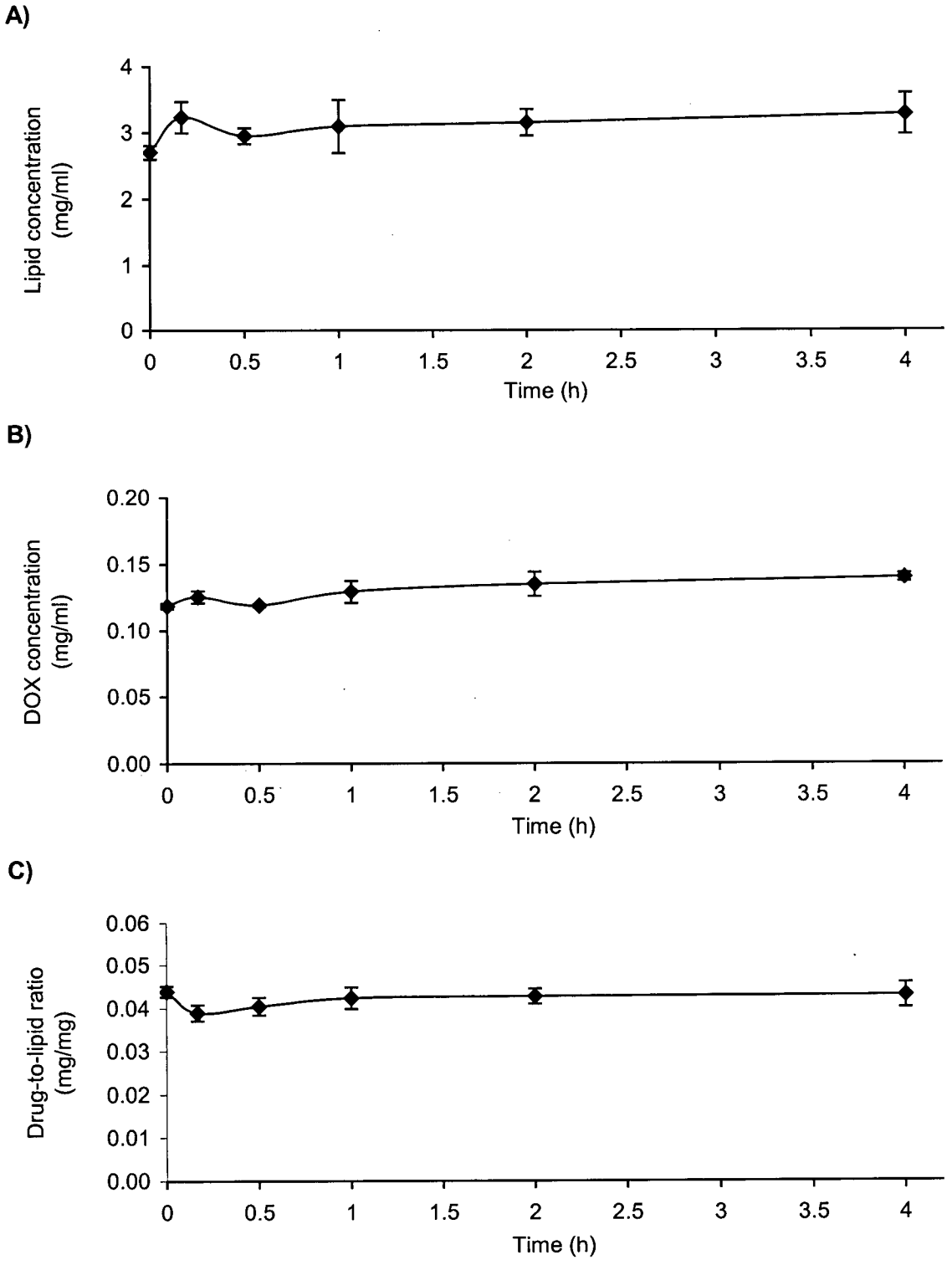

Figure 103: Plasma time profiles of LTSL-DOX for (A) lipid, (B) DOX, and (C) the drug-to-lipid ratio incubated with HBS. Error bars indicate the standard error of mean values (n = 3).

4.4.9. Plasma lysolipid concentrations in the cellular blood fraction and plasma after incubation of LTSL-DOX with whole blood

LTSL containing MSPC were labeled with ^{14}C-MPPC and ^{3}H-CHE at an activity ratio of 0.6 dpm/dpm and loaded with DOX at a drug-to-lipid ratio of 0.05 mg/mg by the buffer exchange method (see section 3.7.). LTSL-DOX (0.2 mg DOX) was added to 1 ml of freshly obtained whole blood or plasma from adult female Balb/c mice or to HBS to match concentrations after LTSL-DOX injection into mice and the mixture was incubated at a temperature of 37°C. The lysolipid/lipid ratio in whole blood, plasma separated from whole blood, plasma, and HBS was determined at 5 min, 10 min, 30 min, 1 h, 2 h, and 4 h by scintillation counting after removing free ^{14}C-MPPC on a Sephadex G-50 column. When free ^{14}C-MPPC was added to a Sephadex G-50 spin column, the amount of radioactivity in the eluent was 0.25% of the initial activity, indicating that the radiolabel is retained by the Sephadex G-50 column.

The lysolipid/lipid ratios of LTSL-DOX in whole blood, plasma, or HBS did not change significantly over the investigated time period of 4 h. In plasma separated from whole blood, the lysolipid/lipid ratio decreased significantly ($p < 0.01$) after 5 min by approximately 22% but ratios did not change significantly thereafter (Figure 104).

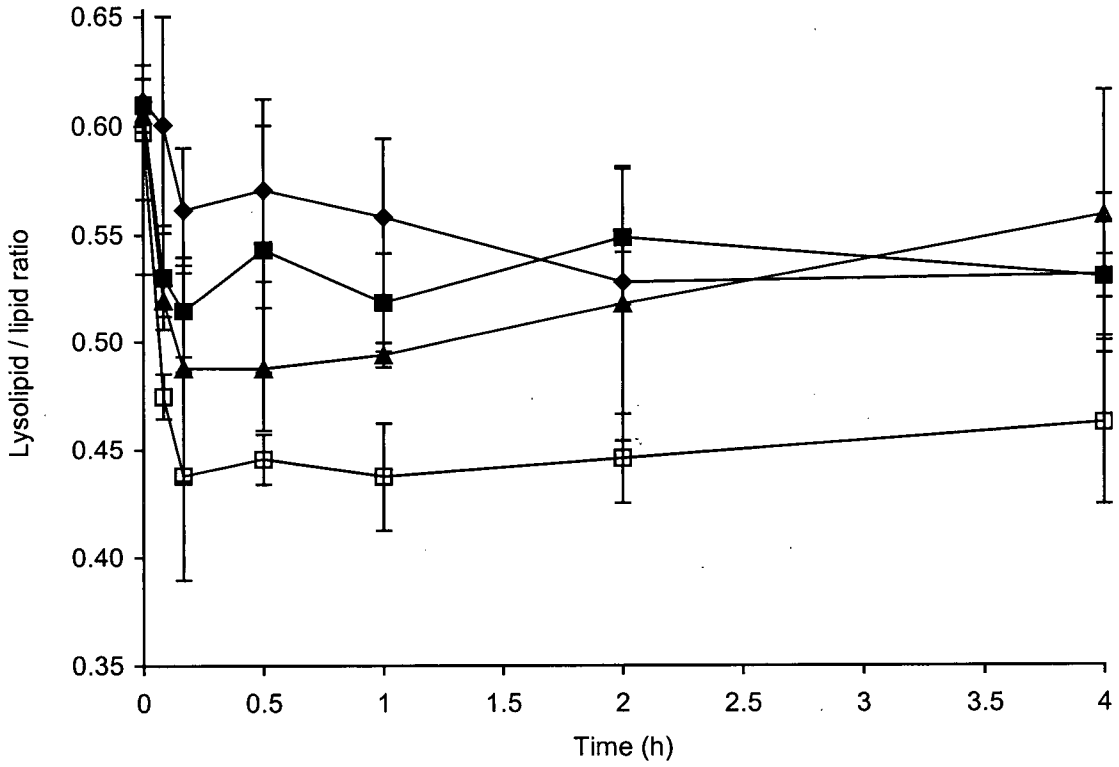

Figure 104: Lysolipid/lipid ratios after incubating LTSL-DOX with whole blood or plasma from adult female Balb/c mice or with HBS at a temperature of 37°C in whole blood (◆), plasma separated from whole blood (□), plasma (■), or HBS (▲). Error bars indicate the standard error of mean values (n = 3).

4.5. Efficacy of LTSL-DOX in MDR tumor bearing mice

LTSL-DOX treatment exhibited improved efficacy as compared to treatment with DOX-loaded traditional TSL or free DOX in combination with mild hyperthermia against DOX-sensitive FaDu tumors in mice [1]. Thus, a pilot study was undertaken to test if LTSL-DOX treatment would also result in a significant improvement in efficacy in mice as compared to treatment with free DOX in combination with mild hyperthermia against MDR human breast cancer tumors over expressing PGP.

Body temperatures of Rag2-M mice anesthetized with ketamine/acepromazine at a dosage of 100/2.5 mg/kg bearing MDA435/LCC6^{MDR1} were adjusted to temperatures equal or less than 37°C in the mouse incubator (see section 3.16.8 and 3.16.9.). Tumors of one half of all mice were heated using a fiberoptic light source and tumor temperatures were measured with a hypodermic needle probe inserted into the center of the tumor. After tumor temperatures were stabilized at 41°C, three tumor-bearing mice per treatment group were administered with free DOX at a dosage of 5 mg/kg or with LTSL-DOX at a dosage of 5 mg DOX/kg by a single *i.v.* bolus injection via the tail vein. Tumors were maintained at a temperature of 41°C for 1 h after injection. Tumors of the other half of mice were not treated with hyperthermia. Control mice received saline by *i.v.* injection and the tumor hyperthermia treatment. Tumor volumes were measured every day or every other day for one month.

Mean tumor temperatures of all mice that received the localized tumor hyperthermia treatment were at 41.3°C (STD = 1.1) (Figure 105). Tumor temperatures were easy to adjust and, except when the light source had to be readjusted, the tumor set temperature could be maintained with high precision (STD = 0.05-0.25 for individual

mice). Body temperatures of mice were relatively stable throughout the hyperthermia treatment period and never exceeded temperatures greater than 36.5°C (Figure 105).

At four days after treatment, mean tumors volumes of mice treated with DOX in combination with hyperthermia were significantly greater than those of mice in all other treatment groups ($p < 0.05$) because one tumor in this treatment group grew exceptionally large. At 18 days after treatment, the mouse bearing this tumor had to be terminated since the tumor had grown into the muscle underneath the skin, which explains the kink in the growth curve of the treatment group of mice that treated with DOX in combination with hyperthermia. For the same reason, one mouse that received LTSL-DOX but no hyperthermia treatment had also to be terminated at day 13 after treatment. At nine and fourteen days after treatment, mean tumors volumes of mice in the control group were significantly greater than those of mice treated with DOX alone or treated with LTSL-DOX in combination with hyperthermia ($p < 0.01$ at nine days and $p < 0.05$ at fourteen days). Starting at eighteen days after treatment, mean tumors volumes of mice in the control group were significantly greater than those of mice in all other treatment group until the end of the study at day 32 after treatment ($p < 0.05$). Mean tumor volumes of mice in all treatment groups were not significantly different from each other during the investigated time period (Figure 106). There was no difference in body weight between mice treated with saline, LTSL-DOX, or free DOX with or without tumor hyperthermia treatment during the investigated time period.

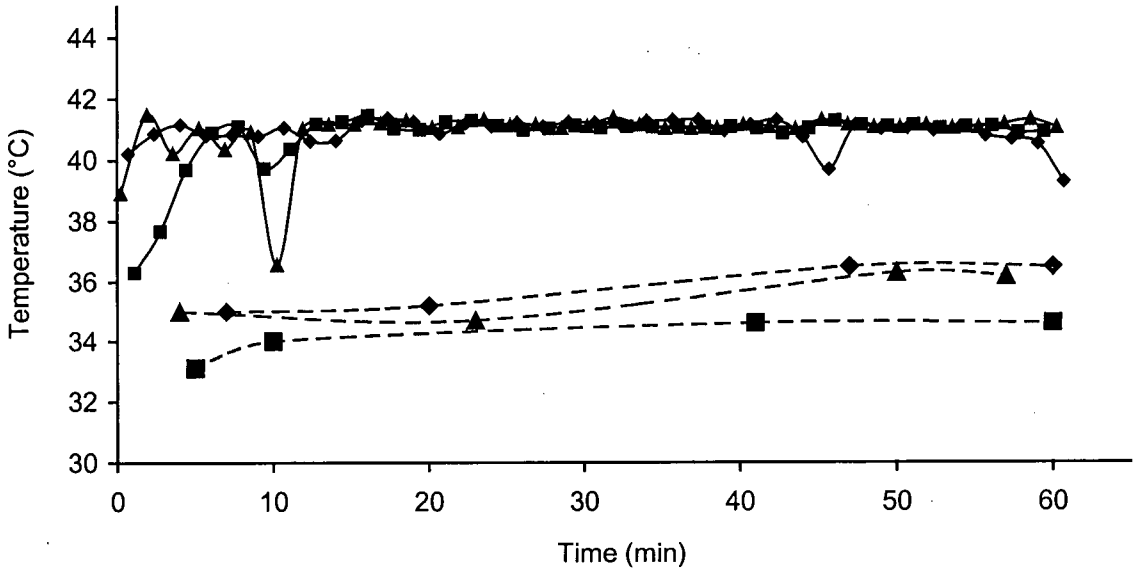

Figure 105: Representative diagram of individual body temperatures (dashed lines) and tumor temperatures (solid lines) of three adult female Rag2-M mice anesthetized with ketamine/acepromazine at a dosage of 100/2.5 mg/kg bearing subcutaneous MDA435/LCC6^{MDR1} human breast cancer tumors.

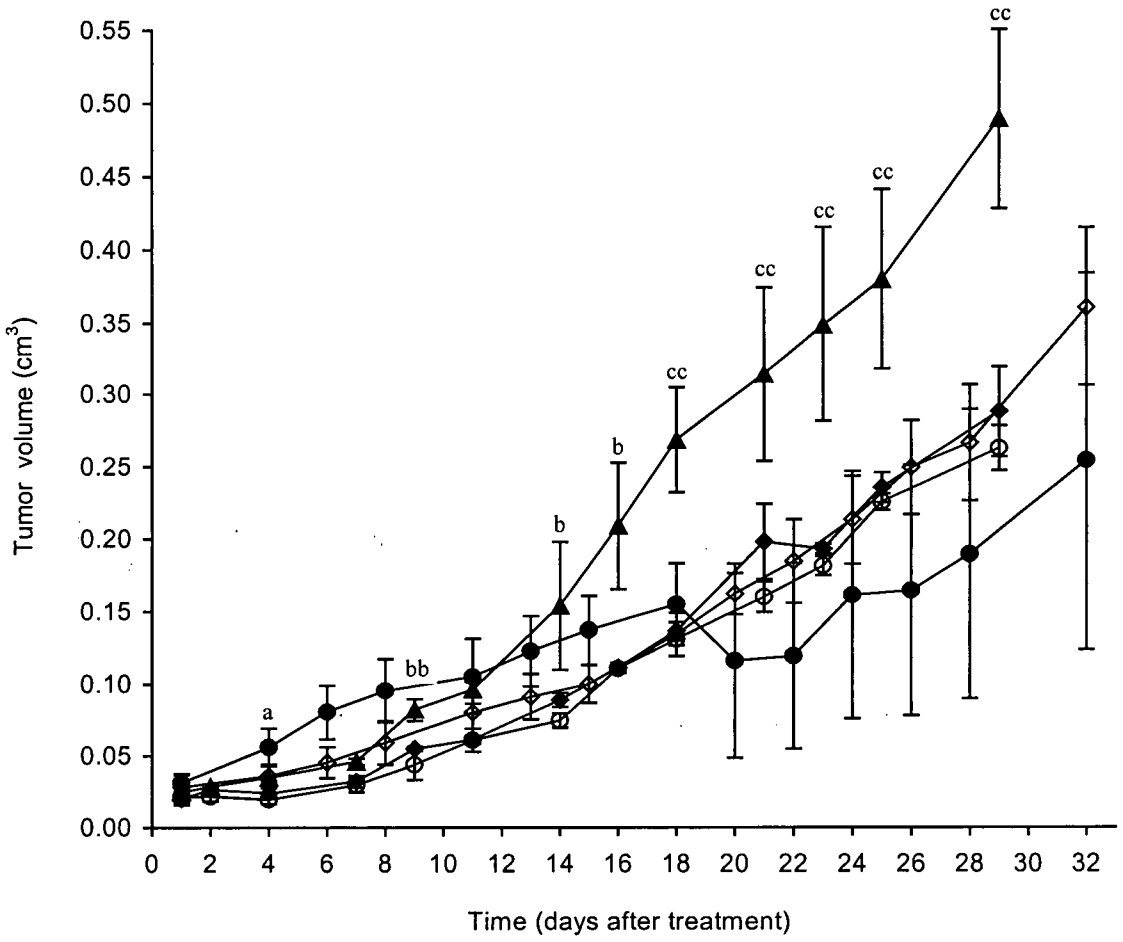

Figure 106: Efficacy of treatment with free DOX (○●) and LTSL-DOX at a dosage of 5 mg/kg (◇◆) alone (open symbols) or in combination with localized tumor hyperthermia (41°C) (closed symbols) in female Rag2-M mice bearing MDA435/LCC6^{MDR1} tumors anesthetized with ketamine/acepromazine at a dosage of 100/2.5 mg/kg. Control mice received saline and the hyperthermia treatment (▲). a = mean tumor volumes after DOX + hyperthermia treatment were significantly different from all other treatments, $p < 0.05$. b = mean tumor volumes after DOX and LTSL-DOX + hyperthermia treatment were significantly different from control, $p < 0.05$, bb = $p < 0.01$. cc = mean tumor volumes after any treatment were significantly different from control, $p < 0.01$. Error bars indicate the standard error of mean values with n = 3 except for mice that received free DOX in combination with hyperthermia starting at day 18 and for mice that received LTSL-DOX in without hyperthermia starting at day 13 where n = 2.

5. DISCUSSION

Part I

Membrane dynamics such as domain formation, lateral phase separation, and accumulation of lysolipids in the membrane due to phospholipid hydrolysis and their impact on liposome stability and behavior can largely be circumvented by incorporation of cholesterol into the liposome membrane. The impact of the effects of membrane dynamics in cholesterol-containing liposomes is then only minor. However, temperature-triggered drug release can only be achieved with cholesterol-free liposomal drug formulations. Therefore, membrane dynamics in LTSL had to be characterized and controlled to ensure consistent drug encapsulation and drug release properties of this formulation and furthermore to lay the basis for an improved LTSL formulation with more favorable drug retention properties *in vivo*. Although the T_C values of the lysolipids used in this thesis were 23°C apart, no difference in drug loading or drug release characteristics *in vitro* or *in vivo* could be detected between LTSL containing MPPC and LTSL containing MSPC [13]. Therefore, in the following discussion the two formulations were not distinguished from each other and discussed together as LTSL.

5.1. DOX encapsulation into LTSL

Previous studies on LTSL characterized drug release *in vitro* [13] and *in vivo* [209] and have demonstrated superior efficacy of this formulation in comparison to traditional liposomal DOX formulations [1]. In section 4.1., encapsulation conditions of DOX into LTSL were determined in order to develop an effective and reproducible pH-gradient driven loading procedure. The temperature dependency for DOX encapsulation (Figure 39) demonstrated that efficient drug encapsulation into LTSL could be obtained

at temperatures a few degrees below the T_C of LTSL, which was determined at 40.1°C in LTSL containing MPPC and at 42°C in LTSL containing MSPC (Table 5). At temperatures between 34°C and 37°C, DOX encapsulation efficiencies were greater than 90% when incubated for 20 min at a drug-to-lipid ratio of 0.05 mg/mg. At temperatures below the pre-transition temperature (T_C') of LTSL, which was determined previously at 34°C [13], DOX encapsulation efficiencies decreased with decreasing temperature consistent with reduced permeability of phospholipid membranes in gel ($L_{\beta'}$) phase. However, higher drug encapsulation efficiencies at temperatures below T_C' can be achieved at longer incubation times (data not shown).

DSC thermograms of LTSL containing MPPC may suggest that a dramatic decrease in drug encapsulation would correlate with the onset of the phase transition between the ripple ($P_{\beta'}$) phase and the liquid-crystalline (L_α) phase at a temperature of 40°C. At this temperature, the membrane permeability increases dramatically when membrane areas in $P_{\beta'}$ phase and L_α phase co-exist [121] and the liposomal membrane becomes permeable to protons, which rapidly dissipates the pH gradient across the membrane. However, the onset of decreased drug uptake as well as the onset of drug release was approximately three degrees below the T_C of LTSL, at temperatures close to 38°C or 39°C, respectively. This early onset of drug release and decreased drug encapsulation suggests that grain boundary regions between gel phase plates enriched in lysolipids with a lower T_C than that of the bulk phospholipid undergo phase transition at lower temperatures than the T_C of the bulk membrane.

DOX encapsulation efficiencies of LTSL decreased rapidly at temperatures above 38°C and were, on average, at 17.4% (Figure 39). These encapsulation efficiencies were

similar to those achieved with liposomes not bearing a pH gradient suggesting that these baseline encapsulation efficiencies represents the proportion of DOX that is not encapsulated inside the liposome but instead membrane-associated. Results from section 4.1. of this thesis clearly demonstrate that the encapsulation efficiency of LTSL is highly dependent on the incubation temperature in contrast to that in NTSL, which can be loaded over a wider temperature range below and above their T_C [78].

A surprising observation within this set of experiments was that maximum DOX encapsulation into LTSL was limited to drug-to-lipid ratios in the range of 0.05 mg/mg to 0.08 mg/mg (Figures 40 and 41). In contrast, DOX can be loaded into NTSL at drug-to-lipid ratios of up to 0.5 mg/mg [210]. The pH gradient in LTSL was still greater than two units after encapsulating DOX at drug-to-lipid ratios of 0.05 mg/mg, 0.1 mg/mg, or 0.2 mg/mg indicating that pH gradient dissipation was not responsible for limited DOX uptake (Table 6). Thus, the reason for the limited DOX loading capacity of LTSL remains to be determined. However, recent results from our laboratory have shown that quantitative DOX encapsulation efficiencies could be achieved at a drug-to-lipid ratio of 0.2 mg/mg when DOX was encapsulated into LTSL for 20 min at a temperature of 37°C using a manganese ion gradient instead of a pH gradient. This suggests that the complexation of DOX inside the liposomes may be responsible for the difference between the two loading procedures, which is currently investigated by another student in our laboratory in a separate Ph.D. project.

The dependence of DOX encapsulation efficiency on the MPPC membrane content was investigated, because storage of liposomes, typically in citrate buffer, pH 4, will, over time, lead to accumulation of MPPC in the liposomal membrane as a result of

acid-catalyzed DPPC hydrolysis. Results indicate that the loading efficiency of LTSL decreased proportionally to the percentage of MPPC added to the liposomal membrane but DOX could be quantitatively encapsulated into LTSL at a drug-to-lipid ratio of 0.05 mg/mg and a MPPC content of 15 mol% or less (Figure 42). The loading efficiency of LTSL is therefore dependent on the percentage of MPPC in the membrane with an upper limit of approximately 15 mol% to maintain suitable trapping efficiencies in good agreement with previous findings [142].

Incorporation of MPPC at maximally 10 mol% in the LTSL membrane has been shown to result in maximal drug release rates [13]. The hydrolysis rate in TSL was at approximately 2 mol% per month at pH 4 and a temperature of 4°C (Table 8), which compares well with literature values [125]. Thus, LTSL containing 10 mol% MPPC should not be stored refrigerated for more than 2.5 month under the described conditions in order to maintain optimal loading efficiencies. The reason for the decreased DOX uptake at increasing MPPC concentrations remains, however, to be fully elucidated.

5.2. DOX release from LTSL

Results from section 4.2. of this thesis have shown that DOX was released from LTSL at a minimum temperature of 39°C, approximately 3°C below the main melting phase transition temperature (Figures 46 and 47). It was postulated previously that the release mechanism from LTSL is based on pre-melting of grain boundaries in gel phase phospholipid membranes and it was speculated that lysolipids were then enabled to leave the membrane creating structural defects, through which encapsulated drugs could rapidly permeate [14]. However, this hypothesis can be rejected since radiolabeled lysolipid did not dissociate from LTSL after phase transition (Figure 84) but DOX was

released readily after cycling liposomes through their T_C (Figures 43, 46, and 47).

At temperatures of 41°C and 42°C, permeability coefficients of LTSL were calculated at 6.31 x 10^{-9} cm/sec and 3.33 x 10^{-8} cm/sec, respectively. In comparison, the permeability coefficient of TSL at 42°C was at 2.84 x 10^{-10} cm/sec and compares well to a literature value of 2.32 x 10^{-10} cm/sec as determined for DPPC/dicetylphosphate liposomes (molar ratio: 95:5) with ^{3}H glucose as the trapped marker [207]. The maximum permeability coefficient of LTSL at a temperature 42°C was determined to be approximately 100 times greater than that of TSL at this temperature and this might even be an underestimation because of the temperature equilibration time delay of the assay (Table 7, Figure 48). Since approximately 17.4% of DOX was determined to be membrane associated (Figure 39), the initial release of approximately 85% at various temperatures reflects the total liposome content. Therefore, drug release from LTSL after phase transition can be assumed to be complete and almost instantaneous, a remarkable feature unsurpassed by any other known drug release mechanism. The velocity of drug release cannot be explained by a membrane permeation process and strongly indicates that a different release mechanism in LTSL as compared with TSL is responsible for this effect.

5.3. Release mechanisms of LTSL

Cryo-TEM images of LTSL revealed that the appearance of 100 nm cholesterol-free phospholipid liposomes below their T_C was generally spherical with a faceted surface (Figures 43A, 50, and 62), as reported previously by other research groups [8, 211]. The origin of this polyhedral morphology stems likely from the presence of individual gel-phase plates separated by grain boundaries. Grain boundary formation occurs in the gel

phase of phospholipid membranes when the temperature is decreased from values above to values below the T_C of the membrane [62, 66]. Upon cooling, initially multiple gel phase nuclei form in the unordered liquid-crystalline membrane. These nuclei with a high degree of order grow in size as the temperature decreases until eventually the entire membrane is in the gel phase state. The degree of disorder within the gel-phase membrane is highest at domain-separating boundaries (grain boundaries) because the lattice orientation of gel-phase domains is different in each domain [66]. The T_C at grain boundary areas is lower than that of membrane domains and thus, phospholipids at grain boundaries melt at temperatures a few degrees below the T_C of the bulk lipid [118, 119].

Grain boundaries with a high degree of defects are predispositioned to accommodate a high membrane curvature. Consequently, liposomes with grain boundaries are likely to adopt a polyhedral shape with flat, highly ordered gel-phase domains intersected by boundary regions with a higher degree of disorder and curvature. The degree of curvature at boundary regions increases with decreasing liposome size in response to increasing bending forces and can be annealed by increasing the temperature above the T_C of the liposome membrane [212]. Previous results [211] and results presented in this thesis indicate that the morphology of liposomes below T_C is dependent on the liposome size. This difference in liposome morphology may reflect the difference in strength of membrane bending forces or the fact that the faceted structure may not be apparent in cryo-TEM images because the angles between bilayer plates increase with increasing liposome size.

Lysolipids have been shown to segregate from the bulk lipid by lateral phase separation [214-216]. Lateral phase separation during and after phase transition and the

existence of lipid domains spanning the inner and the outer leaflet of the liposome [129, 134] has been observed for binary phospholipid mixtures in giant unilamellar vesicles using fluorescent lipid probes [131, 132, 213], atomic force microscopy [133], and infrared spectroscopy [135]. This segregation of membrane components has been distinguished from classical lateral lipid phase separation and named lateral lipid domain formation and was shown to be dependent on the degree of bilayer curvature and thus on the liposome size [217]. To determine whether lysolipids accumulate in grain boundaries, PHDA dimerization and the associated shift in the fluorescence emission spectrum was used as an indication of lateral phase separation. The dimer (excimer) to monomer (E/M) ratio and thus the frequency of dimer formation increased with increasing temperature since PHDA monomers experience a higher mobility in membranes at higher temperatures as a result of increased membrane fluidity and increased Brownian motion (Figure 79). In thermosensitive liposomes, the mobility of PHDA decreases abruptly at T_C during phase transition and does not decrease any further when the gel-phase membrane is cooled below T_C in contrast to non-thermosensitive liposomes, in which the PHDA mobility decreases linearly with decreasing temperature beyond the T_C of its bulk lipid (Figure 79). The PHDA E/M ratios in NTSL were lower than those in TSL and LTSL because in the presence of cholesterol the membrane is less fluid at temperatures above its T_C. Although the fluidity is greater in the cholesterol-containing membrane below T_C in comparison to cholesterol-free membranes, the amount of dimers formed in TSL and LTSL at temperatures above T_C is fixed after phase transition. Proteins, detergents [63, 218] fluorescence markers [144] and PEG-lipids [109] have been shown to accumulate in corners and edges (grain boundaries) of

polygonal vesicles and stabilize defect structures. Thus, PHDA molecules likely accumulate in grain boundaries in TSL and LTSL but not in NTSL, where grain boundaries are not present and PHDA molecules are distributed homogeneously throughout the latter liposome membrane. At elevated temperatures below the T_C of TSL and LTSL, the E/M ratio increased over time in TSL and LTSL but not in NTSL (Figure 80). This finding indicates that additives to the bulk membrane component are not only segregated during phase transition as discussed above but also accumulate over time in these membrane regions. The driving force for this effect is the lower free energy state of the membrane when pure DPPC plates exist with a high degree of structural order and a minimum amount of structural defects. This state can be achieved when lysolipids and PEG-lipids accumulate at grain boundaries and adopt micelle-like aggregates in highly curved membrane regions, which also releases membrane bending stress. The electrostatic repulsion of negatively charged PEG-lipids has thereby been reported as being low in comparison to the steric repulsion of PEG molecules [109, 223].

In addition to lysolipid and PEG-lipid accumulation in grain boundaries and lateral domain formation, DPPC hydrolysis also increases lysolipid content in the membrane and thus the lysolipid grain boundary content over time. Cryo-TEM analysis revealed that a small to moderate amounts of membrane discs were generated in freshly prepared LTSL after cycling liposomes through their T_C (Figures 43, 49, and 50) but these liposomes could be conditioned to completely disintegrate into discs under various storage conditions and storage times (Figures 52-67). The common factor that correlates with the time point at which disc formation readily occurs is a lysolipid membrane content of values greater than 10 mol%. At this concentration, disc formation as

observed in cryo-TEM image analysis is correlated with a change in particle size from approximately 100 nm to 30-40 nm as determined by QELS. Discs were not formed in TSL when hydrolysis led to lysolipid concentration less than 10 mol%. In LTSL, addition of 5 mol% of each of the hydrolysis products MPPC and palmitic acid did not cause a change in particle size after T_C cycling as determined by QELS, but cryo-TEM analysis revealed that the majority of liposomes had disintegrated into membrane discs after T_C cycling. These discs were larger than 30-40 nm in size, a phenomenon also observed when lysolipids had accumulated to concentrations greater then approximately 30 mol% under various storage conditions of TSL (Figures 58, 63, 74, and 75). The total amount of DPPC hydrolysis products necessary to generate these larger fused membrane discs could not be elucidated but it has been shown clearly in section 4.3. of this thesis that the size of discs generated after cycling partially hydrolyzed TSL through their T_C increases with increasing amounts of hydrolysis products.

The incongruity between QELS particle size determinations and cryo-TEM analysis was likely caused by the insensitivity of the QELS apparatus to small changes in the average particle size when only a small number of discs were present in the sample. Furthermore, QELS is unable to differentiate between liposomes and discs with a similar size distribution. Thus, the change in average liposome size is a useful indication that disc formation was a major event in the liposomal preparation but if no change in particle size is indicated by QELS analysis, results have to be confirmed by cryo-TEM image analysis. The observation that disc formation after T_C cycling could not be observed in LTSL without PEG-lipid (Figure 51) stresses the role of this lipid component on the disc formation process. The thermodynamically most favoured aggregate structure in aqueous

solutions of PEG-lipids as well as in solutions of lysolipids is the spherical micelle (see section 1.2.1.). Since theoretical considerations and evidence presented in this thesis support the hypothesis that these micelle-forming membrane components accumulate at grain boundaries and grain boundaries melt prior to the bulk lipid, PEG-lipids and lysolipids likely adopt a micelle-like conformation within the bilayer upon phase transition. This conformational change of the membrane structure would allow for open liposome structures to exist because the rim of the phospholipid membrane is then stabilized.

The fact that membrane discs were not observed in LTSL without DSPE-PEG_{2000} (Figure 51) suggests that DSPE-PEG_{2000} is needed to sterically stabilize open liposome structures and prevent their re-closure or fusion with other membranes. Disc formation during liposome preparation has previously been described and the amount of PEG-lipids that can be incorporated into the liposome membrane without forming discs was shown to be limited to approximately 10 mol% for DSPE-PEG_{2000} [84]. This limit was dependent on the chain length of the PEG-moiety but is independent of the main phospholipid species in the membrane [84]. Above a PEG_{2000}-lipid concentration of 10 mol%, the liposome membrane is destabilized and membrane discs rather than liposomes are formed during the preparation process [84]. Even at lower PEG-lipid concentrations in the membrane drug retention is often compromized and it has been hypothesized that the formation of transient membrane pores is responsible for this effect [219]. In the absence of PEG-lipids, mixtures of phospholipids and detergents (molar ratio: 10/3.2) have been shown to form stacked membrane discs and these stacked discs can refuse and form vesicles after sonication [220].

PEG-lipids can exist in a phospholipid bilayer in two different conformations, the so-called "mushroom" and "brush"- regimes [221]. In the mushroom regime, the PEG polymer is randomly coiled and has the size

$$R_F = a\,N^{3/5} \qquad \textit{(Equation 27)}$$

where R_F = Flory dimension, a = monomer size (0.35 nm), and N = degree of polymerization. In the brush regime, the PEG polymer has the size

$$L = a\,N\,(a/D)^{2/3} \qquad \textit{(Equation 28)}$$

where L = maximum extension length, D = distance between PEG-lipid molecules.

The PEG moiety of PEG-lipids is in mushroom regime when D is greater than the R_F [109]. The limiting concentration for the mushroom regime is approximately 10 mol% for PEG_{750} and 3 mol% for PEG_{2000}. At higher PEG-lipid concentrations, when the D is less than R_F, PEG molecules are forced to stretch into the brush regime and reach their maximal extension length (Figure 107).

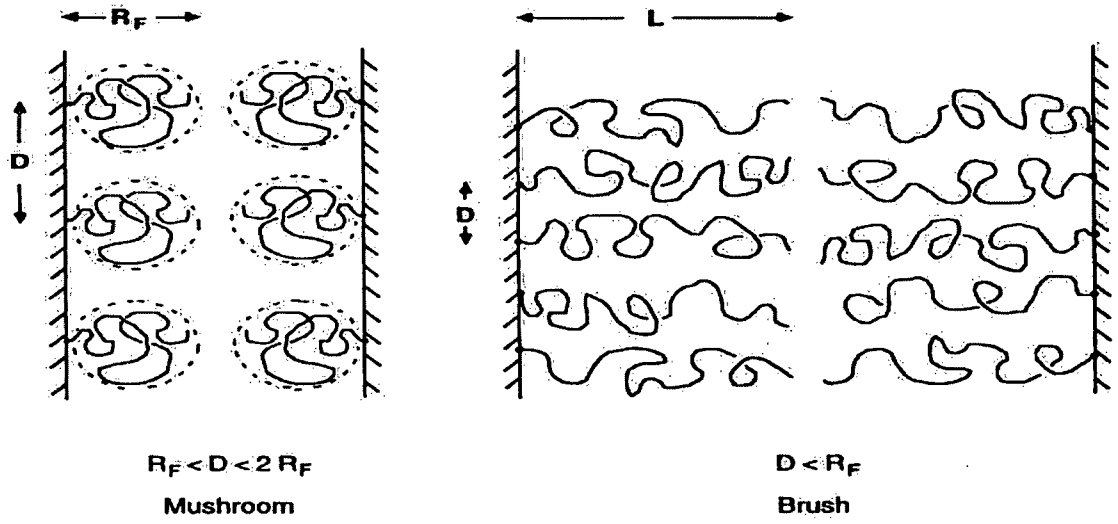

Figure 107: Schematic representation of the two major conformations of PEG-lipid molecules. R_F = Flory dimension, D = distance between PEG-lipid molecules, L = maximum extension length (adapted from [109]).

The liposome formulation used in the present thesis contains PEG-lipids at a concentration of 4 mol%. At this concentration PEG-lipids are primarily in the mushroom conformation. If PEG-lipids are accumulated at phase boundaries, their local concentration will exceed 4 mol% and the PEG moiety of the molecule will be stretched into the brush conformation. Extension of PEG molecules at grain boundaries introduces stress to the membrane in addition to the membrane bending stress. As discussed above, grain boundaries will melt first during transition from the gel to the liquid-crystalline phase of the membrane. During phase transition the membrane coherence weakens and the polymer elastic energy stored in the stretched conformation of the PEG-lipids as well as the energy stored in the curved membrane can be released when the membrane disintegrates into discs. In disc-shaped membranes, the accessible volume for the PEG-polymer increases at the rim of the disc and the disc itself does not possess curvature (Figure 108). This transformation would be predicted to be energetically more favorable than the transformation proposed earlier by Hristova and Needham [222, 223], who proposed that membrane stresses introduced by PEG-brush formation could be released by adaptation of cylindrical micelle or spherical micelle conformations of PEG molecules. These structures, however, possess highly curved surfaces with considerable stress. Thus, it seems thermodynamically favorable that cholesterol-free mixed phospholipid membranes containing PEG_{2000}-lipids disintegrate into discs at temperatures a few degrees below the T_C of the membrane when lateral phase separation has occurred even at PEG-lipid membrane concentrations less than those necessary to force the PEG polymer into the brush regime when randomly distributed throughout the liposome.

Further support for the concept of disc formation in cholesterol-free liposomes

after T_C cycling stems from the fact that the E/M ratios in TSL and NTSL decreased proportionally to the decrease in particle size after cycling liposomes through their T_C (Figures 82 and 83) indicating separation of PHDA enriched membrane regions after T_C cycling and disc or pore formation. This is corroborated by the fact that DSC thermograms captured the disc formation event when TSL were partially hydrolyzed and lysolipids had accumulated in grain boundaries at concentrations greater than 10 mol%.

It should be pointed out, however, that a force that works against lateral phase separation of PEG-lipids and lysolipids in the liposome membrane is the decrease in mixing entropy. In the discussion of factors leading to disc formation in liposome membranes, this force has to be considered small in comparison to polymer stretching energy and membrane bending energy. Results in section 4.3. of this thesis support the hypothesis that in small (100 nm) LTSL, micelle-forming membrane components such as PEG-lipids and lysolipids accumulate in 100 nm liposomes at grain boundaries and occupy structural defects in the membrane. Liposomes with PEG-lipids and lysolipids accumulated at grain boundaries are thermodynamically metastable and conformational changes of the aggregate structure such as the formation of pores and discs that are able to release these stresses are thermodynamically favored. The formation of membrane discs has been shown extensively in this thesis, but no evidence for pore formation has been presented. Pore formation as a drug release mechanism has been shown previously as a consequence of liposome membrane interaction with surfactants [224, 225], lysolipids [140], PEG-lipid [219], or drug [226]. Thus, pore formation as a drug release mechanism in LTSL would be consistent with the presented results and derived concepts.

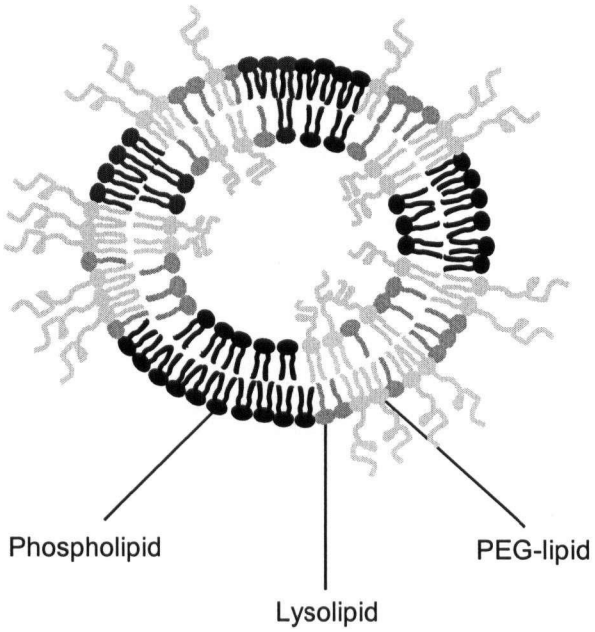

Figure 108: Schematic representation of a mixed liposome membrane in which lateral phase separation has occurred.

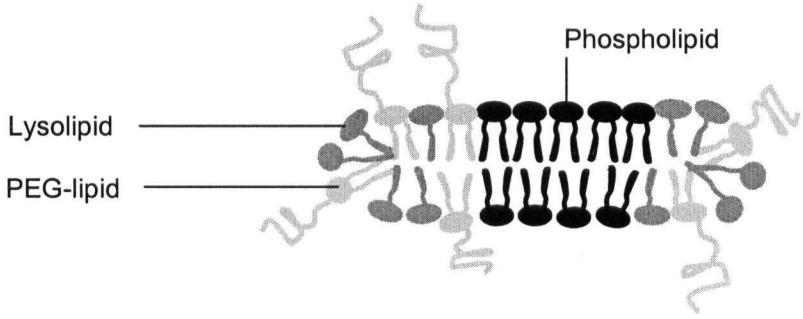

Figure 109: Schematic representation of a mixed membrane disc.

In summary, a number of results presented in this thesis indicate that the presence of both membrane components, DSPE-PEG_{2000} and MPPC or MSPC, is a necessary condition to generate a significant proportion of membrane discs after cycling LTSL

through their T_C. The presence of PEG-lipids and lysolipids in the liposome membrane, especially if segregated into grain boundaries, facilitate the temperature-triggered formation of membrane pores, liposome openings, and the disintegration of liposomes into membrane discs. Cholesterol-free liposomes containing 4 mol% DSPE-PEG_{2000} are stable at a size of 100 nm at lysolipid membrane concentrations up to approximately 15 mol%. At lysolipid concentrations of approximately 10 mol%, drug is released presumably through membrane pores formed in grain boundaries where lysolipid and PEG lipid have accumulated. Above a concentration of 10 mol%, drug is released by disintegration of the liposome membrane into discs (Figure 123). It should be noted that in freshly prepared LTSL, only a moderate number of liposomes disintegrated into discs after heating liposomes to temperatures close to or above their T_C but disc formation only occurred readily after multiple T_C cycles or in partially hydrolyzed liposomes after one T_C cycle. However, drug was released from fresh or partially hydrolyzed LTSL within seconds of heating liposomes to temperatures 3°C below their T_C. Consequently, although disc formation occurs in LTSL, it is unlikely to be directly responsible for the release of drug upon heating of freshly prepared LTSL. However according to the proposed model, membrane domains enriched in the bulk phospholipid surrounded by grain boundaries enriched in micelle-forming membrane components regions must form as precursors for discs. If concentrations of micelle-forming membrane components in grain boundaries are not sufficient to stabilize a disc, the model predicts that during phase transition membrane pores are formed which appear to be a sufficiently high enough failure of the membrane integrity to allow rapid efflux of entrapped contents.

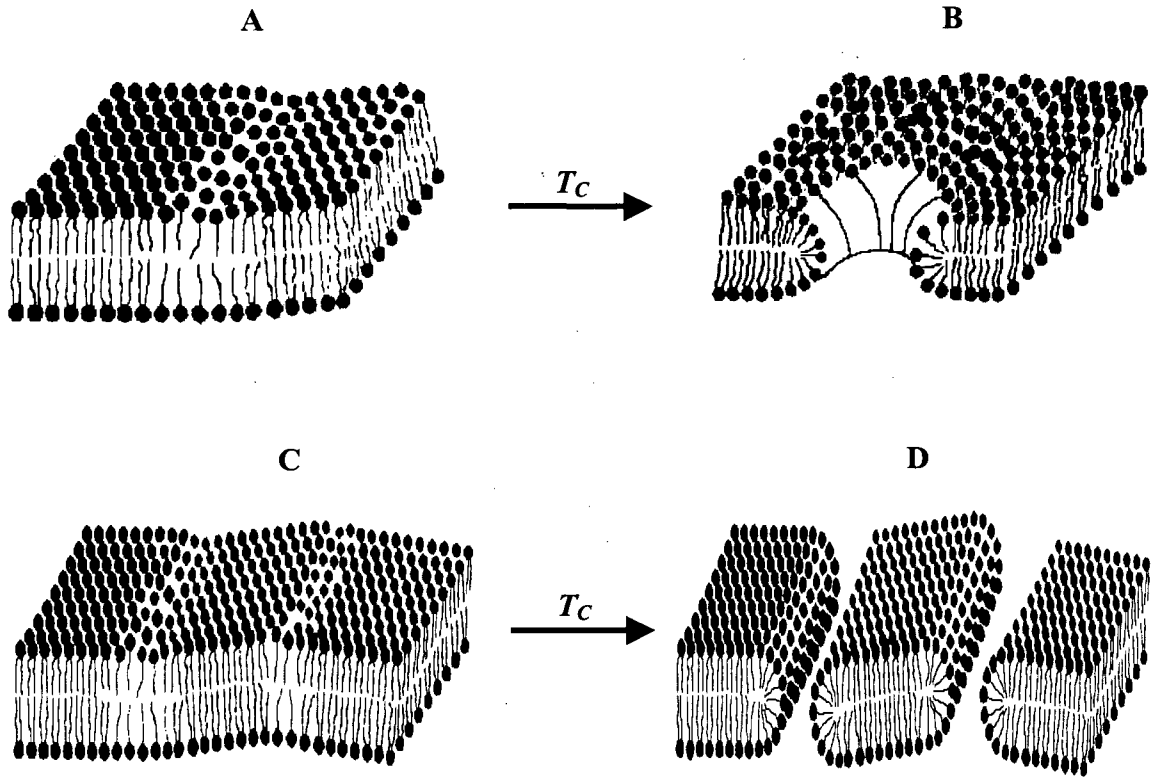

Figure 110: Schematic representation of proposed drug release mechanisms in LTSL. (A, C) Accumulation of micelle-forming lipids at grain boundaries; (B) Pore formation during phase transition; (D) Disc formation during phase transition. PEG-lipids are not included in the drawing, T_C = phase transition temperature.

Part II

5.4. DOX and lysolipid retention of LTSL *in vivo*

After NTSL-DOX injection into mice, liposomes accumulated over the course of 8 h primarily in the spleen and the liver and DOX accumulated primarily in the spleen, kidneys, and the liver. After LTSL-DOX injection into mice, liposomes accumulated over the course of 8 h primarily in the liver and DOX accumulated primarily in the kidneys and the liver. The mean percentage of the total DOX dose 1 h after injection of

LTSL-DOX in comparison to NTSL-DOX was 234 times less in plasma and six times greater in liver and kidneys, four times greater in muscle, three times greater in heart, and 2.5 times greater in the lung. In addition, 25% of the total dose was not accounted for at 1 h after LTSL-DOX injection, probably due to DOX metabolism and excretion, whereas 100% of the dose was recovered from major organs after NTSL-DOX injection.

Plasma concentration-time profiles of DOX after injection of TSL-DOX (Figure 90B), LTSL-DOX containing MPPC (Figure 91B) or LTSL-DOX containing MSPC (Figures 93B and 100B) were similar regardless of the mice's strain or body temperature. The mean plasma half-life of DOX after LTSL-DOX injection was 0.67 h (SEM: 0.1; n = 3). Typically at approximately 4 h after LTSL-DOX injection, plasma DOX concentrations reached baseline levels in contrast those after NTSL-DOX injection, which decreased by only 40% at 48 h after injection (Figure 89B). One exception to this pattern was observed in the tissue distribution study (section 4.4.1.) where plasma DOX concentrations after LTSL-DOX injection decreased exceptionally fast and DOX concentrations reached baseline levels at approximately 20 min after injection (Figure 87B). The body temperature of mice in this study was not controlled and it can be speculated that the body temperature might have been elevated in this study since plasma-time profiles of DOX after LTSL-DOX injection were similar when the mice's body temperatures were elevated to 40°C (Figure 100B).

These results indicate that the presence of lysolipids in cholesterol-free liposomes did not influence liposomal DOX retention *in vivo* since plasma-time profiles of TSL-DOX and LTSL-DOX were in the same order of magnitude. The relatively poor drug retention properties of TSL and LTSL *in vivo* as a result of the absence of cholesterol in

the liposome membrane might be caused by preferential adsorption and integration of plasma proteins into grain boundaries or by interactions of membrane areas unprotected by PEG-lipids with biological membranes.

A somewhat surprising finding in section 4.4.7. of this thesis was the velocity of lysolipid dissociation from LTSL after injection into mice. The lysolipid/lipid ratio in plasma decreased to approximately 36% of the initial value at 10 min after LTSL-DOX injection into euthermic mice, decreased further to 26% at 1 h, and stayed at 15% at 2-8 h after injection (Figure 98). In hyperthermic mice the lysolipid/lipid ratio in plasma decreased even more rapidly to approximately 26% of the initial value at 10 min after injection of LTSL-DOX into hyperthermic mice and continued to decrease to approximately 11% at 1 h after injection (Figure 99). Since plasma lipid levels stayed relatively constant for at least 2 h after LTSL injection (Figures 91A, 93A, and 100A) the decrease in the lysolipid/lipid ratio reflects the elimination of lysolipids from plasma. The fact that the lysolipid/lipid ratio was higher in the cellular blood fraction than in plasma further suggests that lysolipids integrate into biological membranes after dissociation from liposomes until an equilibrium is reached. This conclusion is supported by lysolipid/lipid ratios (Figure 104) after incubation of LTSL-DOX with whole blood, which mirror *in vivo* results, in contrast to those after incubation of LTSL-DOX with plasma (Figure 102) or with buffer (Figure 103). The lysolipid/lipid ratio after incubation with whole blood was 28% of the initial value at 10 min, which was 78% of the value obtained *in vivo*. The lysolipid/lipid ratio did not decrease any further at longer incubation times (Figure 104) in contrast to results obtained *in vivo*, where the lysolipid/lipid ratio decreased to 15% of the initial value at 2 h after injection (Figure 98).

Similarly, DOX plasma concentrations after incubation of LTSL-DOX with whole blood (Figure 101) did not decrease any further after 1 h in contrast to results obtained *in vivo* (Figures 91B, 93B, and 100B). The reason for this difference may be based on the quantitive limitation of biological membrane pools and plasma proteins in the *ex vivo* experiment since biological membranes can take up lysolipids from plasma and plasma proteins can integrate into liposomes. The consequence of lysolipids leaving LTSL after *in vivo* administration is that their superior drug release characteristics are lost after injection and drug release characteristics of LTSL are then similar to those of TSL. At 10 min after injection of LTSL-DOX into mice, whose body temperatures were not thermally controlled, the thermosensitivity of LTSL was indistinguishable from that of TSL (Figure 94). The thermosensitivity of LTSL injected into thermally controlled hyperthermic mice decreased rapidly after injection (Figure 97). In euthermic mice however, close to 80% of the DOX content of LTSL was released upon heating plasma to a temperature of 50°C for 10 min after 1 h of *in vivo* exposure (Figure 97A) when lysolipid concentrations were at approximately at 25% of their original value (Figure 98). This incongruity is likely a reflection of the thermosensitivity assay conditions. Heating times of less than 10 min would have likely emphasized the changes in thermosensitivity of LTSL since a significant amount of the liposomal content is expected to be released form TSL in the absence of lysolipids when heated to a temperature of 50°C for 10 min.

DOX and lysolipid retention properties of LTSL *in vivo* characterized in the second part of the present thesis emphasize that an effective thermosensitive liposomal drug formulation should not only possess ideal drug retention and release characteristics *in vitro*, but these properties have to be maintained after *in vivo* exposure for, ideally, 1-2

days after injection to ensure functionality after tumor accumulation [104-106]. Consequently, LTSL-DOX treatment requires that the localized tumor hyperthermia treatment must be applied during or immediately after LTSL-DOX injection and therefore relies on the release of DOX from LTSL as liposomes pass through heated tumor blood vessels. This may compromise the potential advantages of liposomal drug delivery because extravasation and selective accumulation of LTSL in tumor tissue will not occur to a substantial extent during this time period. DOX release from LTSL will then primarily target the tumor vasculature since DOX has been shown to pass barely beyond the outer cell layer of experimental tumors or multicellular spheroids [227].

5.5. Efficacy of LTSL-DOX against MDR tumors

Results of the LTSL-DOX efficacy pilot study (section 4.5.) confirm concerns based on DOX and lysolipid retention properties after *in vivo* exposure. When Rag2-M mice bearing MDA435/LCC6^{MDR1} tumors were treated with saline, free DOX, or LTSL-DOX and half of the tumors were heated to 41°C for 1 h after injection, mean tumor volumes in all treatment groups were significantly smaller than those in the control group (saline + tumor hyperthermia). However, mean tumor volumes in all treatment groups were not significantly different from each other during the investigated time period regardless whether tumors were exposed to hyperthermia or not (Figure 106). These results are not too surprising considering that the mean plasma half-life of DOX after LTSL-DOX injection into euthermic mice was 0.67 h and the fact that the lysolipid concentration in LTSL was approximately at a quarter of its original value 1 h after administration (Figure 98).

Efficacy results in Rag2-M mice bearing MDA435/LCC6^{MDR1} tumors obtained in experiments presented in this thesis contrast efficacy results presented previously in NCr athymic nude mice bearing human squamous FaDu tumors derived from a hypopharyngeal tumor [1]. In that study, tumors were 0.03-0.1 cm^3 in size before treatment and were inoculated in the mice's hind leg. Mice were anesthetized for at least 1 h with phenobarbital via *i.p.* injection at a dosage of 80 mg/kg. Tumors were heated by placing the tumor bearing leg in a water bath heated to a temperature of 43°C, but tumor temperatures were not monitored. Injection with LTSL-DOX containing MPPC in combination with mild hyperthermia resulted in complete regressions of 11 out of 11 tumor lasting up to 60 days post-treatment. Treatment with a traditional thermosensitive liposomal DOX formulation composed of DPPC/hydrogenated soy phosphatidylcholine (HSPC)/Cholesterol/DSPE-PEG_{2000} (molar ratio: 100:50:30:6) or a non-thermosensitive liposomal DOX formulation resulted in only a moderate growth delay [1]. The dosage of animals in that study and that used in experiments presented in this thesis were both at 5 mg DOX/kg.

This impressive increase in efficacy with LTSL in comparison to TSL obtained by Needham and coworkers [1] was achieved despite the fact that DOX was poorly retained in LTSL after *in vivo* exposure as revealed in the present thesis. The difference in efficacy between LTSL and TSL in that previous study may be partially explained by the choice of the TSL formulation since it contains considerable amounts of cholesterol, which increases DOX retention after incubation with human plasma but compromizes its thermosensitivity [228].

The difference in efficacy of LTSL-DOX between results observed previously in

FaDu tumors [1] and those presented in this thesis in MDA435/LCC6^{MDR1} tumors is most likely caused by the choice of the tumor model. Since a dramatic response to the LTSL-DOX treatment in combination with hyperthermia was observed in DOX-sensitive FaDu tumors it was hypothesized that the treatment may also be effective in DOX-insensitive MDA435/LCC6^{MDR1} tumors if DOX could be delivered to the tumor in large enough quantities. Efficacy results similar to those presented in this thesis have been obtained in MDA435/LCC6^{MDR1} tumors implanted into Rag2-M mice that were treated with free DOX or with DOX encapsulated into various non-thermosensitive liposomal DOX formulations at a dosage of 7.5 or 5 mg/kg, respectively. The efficacy of the treatment could be increased by *p.o.* administration of the MDR modulator Valspodar prior to DOX-treatment [229]. Although the hyperthermia treatment of solid MDR tumors may have increased DOX exposure to tumor cells or tumor endothelial cells as compared to free DOX administration in the efficacy study presented in this thesis, LTSL treatment did not overcome MDR in MDA435/LCC6^{MDR1} tumors. It remains to be determined if increasing the dosage of LTSL-DOX treatment to 10 mg/kg or 15 mg/kg and increasing the drug-to-lipid ratio in LTSL may be sufficient to overcome MDR in MDA435/LCC6^{MDR1} tumors.

6. CONCLUSIONS

In this thesis, encapsulation and release parameters of a LTSL formulation of the antineoplastic anticancer drug DOX were determined and the pharmacokinetic performance of the LTSL-DOX formulation was evaluated after injection into mice. Correlation of specific physicochemical properties of the LTSL-DOX formulation with its *in vitro* and *in vivo* behavior provided insight into the mechanisms whereby LTSL release encapsulated DOX upon exposure to hyperthermia.

DOX could be encapsulated into LTSL up to a drug-to-lipid ratio of 0.05 mg/mg by titrating the exterior citrate buffer to pH 7.5 using sodium carbonate or 0.08 mg/mg using the buffer exchange method when incubated for at least 30 min at a temperature between 34°C and 37°C. The incubation temperature was a few degrees below the T_C of LTSL and the loading limits were not caused by a depletion of the pH gradient across the LTSL membrane. Encapsulation efficiencies in LTSL were dependent on MPPC membrane concentrations with an upper limit of 15 mol% for quantitative DOX encapsulation at a drug-to-lipid ratio of 0.05 mg/mg. MPPC was generated in TSL and LTSL upon storage in a pH and temperature dependent manner with a hydrolysis rate of approximately 2% per month at pH 4 and a temperature of 4°C. Therefore, it is recommended that LTSL containing 10 mol% MPPC should not be stored refrigerated for more than 2.5 month at pH 4 and a temperature of 4°C in order to maintain optimal loading efficiencies.

Under *in vitro* conditions, DOX was not released from LTSL at temperatures of 37°C or 38°C and at temperatures of 41°C or 42°C DOX was released at an approximately 100-times greater rate in comparison to DOX release of from TSL. One

focus of this thesis was to identify the reason for this difference in the drug release rates between TSL and LTSL and to determine the molecular and structural basis of the drug release mechanism. It was found that the presence of both lysolipids and PEG lipids in the liposome membrane was a necessary condition for instant drug release from LTSL. Accumulation of these micelle-forming membrane components in grain boundaries due to lateral phase separation, segregation of membrane components, and hydrolysis up to approximately 10 mol% lead presumably to the formation of membrane pores by stabilizing the rim of open liposome structures after increasing the membrane temperature to values close to its T_C. Accumulation of lysolipids beyond 10 mol% lead increasingly to the formation of membrane discs. The extent of disc formation in LTSL after T_C cycling depended on the degree of DPPC hydrolysis and thus on storage conditions, i.e. on pH, temperature, and time. It was concluded that structural changes in the LTSL membrane leading to pore and disc formation were responsible for a catastrophic failure of the membrane as a drug barrier when LTSL were cycled through the T_C of the liposome membrane. Results obtained in this thesis could not support a previous hypothesis stating that the release mechanism from LTSL after phase transition was based on lysolipids leaving the membrane creating structural defects through which encapsulated drugs rapidly permeate.

Drug retention properties of the LTSL-DOX formulation were remarkably different after *in vivo* exposure from *in vitro* conditions. The mean half-life of DOX after LTSL-DOX injection into mice of was 0.67 h, which was similar to that of TSL-DOX (0.5 h). Lysolipids dissociated rapidly from LTSL after injection into mice and redistributed into cellular blood components and arguably other membrane pools. As a

consequence, the superior drug release characteristics of LTSL in comparison to TSL were gradually lost after injection into mice.

LTSL-DOX treatment of mice bearing MDR tumors in combination with tumor hyperthermia did not improve the efficacy of DOX in comparison to LTSL-DOX treatment without hyperthermia or with free drug with or without hyperthermia. The reason is likely a consequence of poor DOX retention *in vivo* in LTSL and the choice of the DOX insensitive MDR tumor model. From these results it is concluded that LTSL-DOX in its present formulation is not suited for the treatment of MDR tumors. However, if *in vivo* drug retention problems could be resolved, the LTSL-DOX formulation or LTSL formulations of other chemotherapeutic agents bear the potential to improve efficacy and decrease side effects of anticancer drugs for a variety of solid tumors including MDR tumors.

7. FUTURE EXPERIMENTS

Results obtained from experiments described in this thesis project suggest that improvements in *in vivo* drug retention for the LTSL-DOX formulation could potentially improve efficacy when combined with localized tumor hyperthermia. One solution to this problem may be the encapsulation of a different drug instead of DOX into LTSL. One such drug may be cisplatin, which has been shown previously to be better retained in liposomes *in vivo* [2]. In addition, LTSL could also be loaded with multiple cytotoxic agents affecting tumor cells in different states of their cell cycle and by different mechanisms simultaneously. This combination therapy may increase the efficacy of the treatment in comparison to administration of several cytotoxic agents in different rounds of chemotherapy.

One feature of the current LTSL formulation is the rapid dissociation of lysolipids from LTSL after *i.v.* injection into mice. To address this problem, the use of different micelle-forming membrane components instead of MSPC should be examined in order to achieve better retention in the DPPC/DSPC-PEG membrane after *in vivo* exposure while preserving the favorable membrane and aggregate properties of MSPC and MPPC. These lipids may be lysolipids with a longer acyl chain as the membrane anchor (C_{20}-C_{24}) or a phospholipid with a short (C_4-C_8) and a long (C_{16}-C_{24}) acyl chain. In perhaps a more elegant approach, the use of LTSL prepared with an asymmetric distribution of membrane components could circumvent the exchange and redistribution of membrane components after *in vivo* exposure. In this approach, LTSL would be prepared with no or minimum amounts of PEG-lipids. Liposomes would then be dialyzed maybe in the presence of a membrane sink to remove MSPC from the outer liposome leaflet, since a

flip-flop of MSPC from the inner liposome leaflet to the outer leaflet is a rare and energy-dependent process. Different PEG-lipids with various polymer lengths ($PEG_{300-5000}$) could then be exchanged only into the outer leaflet of liposome membranes, by adding PEG-lipids to the outside buffer. As a result, liposomes would contain MSPC only at the inner liposome leaflet and PEG-lipids only at the outer leaflet. PEG-lipids with different polymer chain lengths and different lipid anchors could be allowed to integrate into the outer liposome membrane until an equilibrium is reached. Thus, lysolipids may be prevented from leaving the LTSL membrane and incorporation of membrane proteins may prevented more efficiently since the density of PEG-lipids in the membrane may thereby be increased. It remains, however, to be tested if these asymmetric LTSL retain their favorable instantaneous drug release characteristics and gain improved drug retention properties after *in vivo* exposure.

Finally, the concept of pore formation in LTSL at lysolipid membrane concentrations of up to 10 mol% mentioned in several sections of this thesis is thus far largely speculative. To collect evidence to support this concept, freshly prepared LTSL should be encapsulated with molecules of different sizes, such as lactose, dextrans, and proteins. After heating LTSL through their T_C, the released molecule species should be identified to investigate whether results confirm the pore formation hypothesis in LTSL and to estimate the pore size base on the size of the released molecule species.

8. REFERENCES

1 D. Needham, G. Anyarambhatla, G. Kong, M.W. Dewhirst (2000) A new temperature-sensitive liposome for use with mild hyperthermia: characterization and testing in a human tumor xenograft model. *Cancer Res* **60:** 1197-1201.

2 S. Bandak, D. Goren, A. Horowitz, D. Tzemach, A. Gabizon (1999) Pharmacological studies of cisplatin encapsulated in long-circulating liposomes in mouse tumor models. *Anticancer Drugs* **10:** 911-920.

3 R.K. Jain (1994) Barriers to drug delivery in solid tumors. *Sci Am* **271:** 58-65.

4 J.D. Minna, G.A. Higgins, E.J. Glatstein (1982) in Cancer: Principles and Practice of Oncology (DeVita Jr. V.T., Hellman S., and Rosenberg S.A., eds.), pp. 396-458, J. B. Lippincott Company, Philadelphia, Toronto.

5 B.A. Chabner, C.E. Meyers (1982) in Cancer: Principles and Practice of Oncology (DeVita Jr. V.T., Hellman S., and Rosenberg S.A., eds.), pp. 156-197, J. B. Lippincott Company, Philadelphia, Toronto.

6 A.G. Gilman, P. Taylor, A.S. Nies (1990) Goodman and Gilman's The Pharmacological Basis of Therapeutics, 8th ed., Pergamon Press, New York, Oxford, Beijing, Frankfurt, Sao Paulo, Sydney, Tokyo, Toronto.

7 D.S. Alberts, D.J. Garcia (1997) Safety aspects of pegylated liposomal doxorubicin in patients with cancer. *Drugs* **54:** 30-35.

8 D.D. Lasic (1993) Liposomes: From Physics to Applications, Elsevier, Amsterdam, London, New York, Tokyo.

9 P.G. Tardi, L.M. Ickenstein, M.B. Bally, L.D. Mayer (2002) in Cancer Drug Discovery and Development: Tumor Targeting in Cancer Therapy (Pagé, M., ed.), pp. 119-135, Humana Press Inc., Totowa, NJ.

10 M.J. Parr, D. Masin, P.R. Cullis, M.B. Bally (1997) Accumulation of liposomal lipid and encapsulated doxorubicin in murine Lewis lung carcinoma: the lack of beneficial effects by coating liposomes with poly(ethylene glycol). *J Pharmacol Exp Ther* **280:** 1319-1327.

11 Y. Barenholz (1998) in Application of Liposomes (Lasic and Papahadjopoulos, eds.), pp. 545-565, Elsevier Sciences B.V.

12 G. Kong, M.W. Dewhirst (1999) Hyperthermia and liposomes. *Int J Hyperthermia* **15:** 345-370.

13 G.R. Anyarambhatla, D. Needham (1999) Enhancement of the phase transition permeability of DPPC liposomes by incorporation of MPPC: A new temperature-sensitive liposome for use with mild hyperthermia. *J Liposome Res* **9:** 491-506.

14 D. Needham, M.W. Dewhirst (2001) The development and testing of a new temperature-sensitive drug delivery system for the treatment of solid tumors. *Adv Drug Delivery Rev* **53:** 285-305.

15 L.M.G. van Golde, V. Tomasi, L.M. van Deenen (1967) Determination of molecular species of lecithin from erythrocytes and plasma. *Chem Phys Lipids* **1:** 282-293.

16 F. Krafft (1896) Über eine Theorie der colloïdalen Lösungen. *Ber Dtsch Chem Ges* **29:** 1334-1344.

17 E. Gorter, F. Grendel (1924) On bimolecular layers of lipoids on the chromocytes of the blood. *J Exp Med* **41:** 439-443.

18 A.D. Bangham, M.M. Standish, J.C. Watkins (1965) Diffusion of univalent ions across the lamella of swollen phospholipids. *J Mol Biol* **13:** 238-252.

19 G. Sessa, W. G. (1968) Phospholipid spherules (liposomes) as a model for biological membranes. *J Lipid Res* **9:** 310-318.

20 C. Huang (1969) Studies on phosphatidylcholine vesicles. Formation and physical characteristics. *Biochemistry* **8:** 344-352.

21 T.D. Madden (1997) in Principles of Medical Biology (Bittar, E.E. and Bittar, N., eds.), Vol. 7A, pp. 1-17, JAI Press Inc., Greenwich, Conn.

22 M.B. Bally, H. Lim, P.R. Cullis, L.D. Mayer (1998) Controlling the drug delivery attributes of lipid-based drug formulations. *J Liposome Res* **8:** 299-335.

23 F. Yuan, M. Leunig, S.K. Huang, D.A. Berk, D. Papahadjopoulos, R.K. Jain (1994) Microvascular permeability and interstitial penetration of sterically stabilized (stealth) liposomes in a human tumor xenograft. *Cancer Res* **54:** 3352-3356.

24 D. Lichtenberg, Y. Barenholz (1988) Liposomes: preparation, characterization, and preservation. *Methods Biochem Anal* **33:** 337-462.

25 G. Blume, G. Cevc (1990) Liposomes for the sustained drug release in vivo. *Biochim Biophys Acta* **1029:** 91-97.

26 J.M. Brown, A.J. Giaccia (1998) The unique physiology of solid tumors: opportunities (and problems) for cancer therapy. *Cancer Res* **58:** 1408-1416.

27 S. Kohn, J.A. Nagy, H.F. Dvorak, A.M. Dvorak (1992) Pathways of macromolecular tracer transport across venules and small veins. Structural basis for the hyperpermeability of tumor blood vessels. *Lab Invest* **67:** 596-607.

28 R.K. Jain (1987) Transport of molecules in the tumor interstitium: A review. *Cancer Res* **47:** 3039-3051.

29 R.K. Jain (1988) Determinants of tumor blood flow: A review. *Cancer Res* **48:** 2641-2658.

30 P.R. Cullis, M.J. Hope (1985) in Biochemistry of Lipids and Membranes (Vance, D.E. and Vance, J.E., eds.), pp. 25-72, The Benjamin Cummings Publishing Company, Inc., Menlo Park, California.

31 Y. Barenholz, T.E. Thompson (1980) Sphingomyelins in bilayers and biological membranes. *Biochim Biophys Acta* **604:** 129-158.

32 R.H. Michell, M.J. Wakelam (1994) Second messengers. Sphingolipid signaling. *Curr Biol* **4:** 370-373.

33 J. Ohanian, V. Ohanian (2001) Sphingolipids in mammalian cell signaling. *Cell Mol Life Sci* **58:** 2053-2068.

34 R. Kolesnick, Z. Fuks (1995) Ceramide: a signal for apoptosis or mitogenesis? *J Exp Med* **181:** 1949-1952.

35 R.N. Kolesnick, M. Kronke (1998) Regulation of ceramide production and apoptosis. *Annu Rev Physiol* **60:** 643-665.

36 T. Okazaki, T. Kondo, T. Kitano, M. Tashima (1998) Diversity and complexity of ceramide signalling in apoptosis. *Cell Signal* **10:** 685-692.

37 M.D. Houslay, K.K. Stanley (1982) Dynamics of Biological Membranes. Influence on Synthesis, Structure, and Function, John Wiley & Sons, Chichester, New York, Brisbane, Toronto, Singapore.

38 C. Tanford (1972) Micelle shape and size. *J Phys Chem* **76:** 3020-3024.

39 J.N. Israelachvili, S. Marcelja, R.G. Horn (1980) Physical principles of membrane organization. *Q Rev Biophys* **13:** 121-200.

40 P.R. Cullis, D. Fenske, M.J. Hope (1996) in Biochemistry of Lipids, Lipoproteins, and Membranes (Vance, D.E. and Vance, J.E., eds.), pp. 1-33, Elsevier Science BV.

41 M.C. Woodle, D. Papahadjopoulos (1989) in Methods in Enzymology, Vol. 171, (Fleischer, S. and Packer, L., eds.), pp. 193-217, Academic Press, Inc., New York, San Francisco, London.

42 G. Gregoriadis (1991) Overview of liposomes. *J Antimicrob Chemother* **28:** 39-48.

43 M.J. Hope, M.B. Bally, L.D. Mayer, A.S. Janoff, P.R. Cullis (1986) Generation of multilamellar and unilamellar phospholipid vesicles. *Chem Phys Lipids* **40:** 89-107.

44 L.D. Mayer, M.J. Hope, P.R. Cullis, A.S. Janoff (1985) Solute distributions and trapping efficiencies observed in freeze-thawed multilamellar vesicles. *Biochim Biophys Acta* **817:** 193-196.

45 Y. Barenholz, S. Amselem, D. Lichtenberg (1979) A new method for preparation of phospholipid vesicles (liposomes) - French press. *FEBS Lett* **99:** 210-214.

46 S. Batzri, E.D. Korn (1973) Single bilayer liposomes prepared without sonication. *Biochim Biophys Acta* **298:** 1015-1019.

47 R.A. Parente, B.R. Lentz (1984) Phase behavior of large unilamellar vesicles composed of synthetic phospholipids. *Biochemistry* **23:** 2353-2362.

48 T.D. Madden (1986) Current concepts in membrane protein reconstitution. *Chem Phys Lipids* **40:** 207-222.

49 F. Szoka, Jr., D. Papahadjopoulos (1978) Procedure for preparation of liposomes with large internal aqueous space and high capture by reverse-phase evaporation. *Proc Natl Acad Sci U S A* **75:** 4194-4198.

50 F. Szoka, Jr., D. Papahadjopoulos (1980) Comparative properties and methods of preparation of lipid vesicles (liposomes). *Annu Rev Biophys Bioeng* **9:** 467-508.

51 M.J. Hope, M.B. Bally, G. Webb, P.R. Cullis (1985) Production of large unilamellar vesicles by a rapid extrusion procedure. Characterization of size distribution, trapped volume and ability to maintain a membrane potential. *Biochim Biophys Acta* **812:** 55-65.

52 L.D. Mayer, M.J. Hope, P.R. Cullis (1986) Vesicles of variable sizes produced by a rapid extrusion procedure. *Biochim Biophys Acta* **858:** 161-168.

53 H.M. Burt, J.K. Jackson (1988) Monosodium urate monohydrate crystal induced changes in membrane fluidity: A fluorescence polarization study. *J Rheumatol* **15:** 1144-1151.

54 R.M. Weis (1991) Fluorescence microscopy of phospholipid monolayer phase transition. *Chem Phys Lipids* **57:** 227-239.

55 H.H. Mantsch, R.N. McElhaney (1991) Phospholipid phase transitions in model and biological membranes as studied by infrared spectroscopy. *Chem Phys Lipids* **57:** 213-226.

56 A. Watts, P.J. Spooner (1991) Phospholipid phase transitions as revealed by NMR. *Chem Phys Lipids* **57:** 195-211.

57 R.N. McElhaney (1982) The use of differential scanning calorimetry and differential thermal analysis in studies of model and biological membranes. *Chem Phys Lipids* **30:** 229-259.

58 W.W. Wendlandt, P.K. Gallagher (1981) in Thermal Characterization of Polymeric Materials (Turi, E.A., ed.), pp. 46-67, Academic Press, New York, London, Paris, San Diego, San Francisco, Sao Paulo, Sydney, Tokyo, Toronto.

59 B.G. McFarland, H.M. McConnell (1971) Bent fatty acid chains in lecithin bilayers. *Proc Natl Acad Sci U S A* **68:** 1274-1278.

60 M.J. Janiak, D.M. Small, G.G. Shipley (1976) Nature of the thermal pretransition of synthetic phospholipids: dimyristolyl- and dipalmitoyllecithin. *Biochemistry* **15:** 4575-4580.

61 R.P. Rand, D. Chapman, K. Larsson (1975) Tilted hydrocarbon chains of dipalmitoyl lecithin become perpendicular to the bilayer before melting. *Biophys J* **15:** 1117-1124.

62 A.G. Lee (1977) Lipid phase transitions and phase diagrams I. Lipid phase transitions. *Biochim Biophys Acta* **472:** 237-281.

63 E. Sackmann, D. Rüppel, C. Gebhardt (1980) in Liquid Crystals of One- and Two-Dimensional Order (Helfrich, W. and Heppke, G., eds.), Vol. 11, pp. 309-326, Springer-Verlag, Berlin, Heidelberg, New York.

64 T. Heimburg (2000) A model for the lipid pretransition: Coupling of ripple formation with the chain-melting transition. *Biophys J* **78:** 1154-1165.

65 P.C. Haegele, W. Pechold (1970) Struktur- und Konformationsberechnung in Polymeren. *Kolloid Z Z Polym* **241:** 977-985.

66 A.G. Lee (1975) Functional properties of biological membranes: A physical-chemical approach. *Prog Biophys Mol Biol* **29:** 5-56.

67 P.G. Barton, F.D. Gunstone (1975) Hydrocarbon chain packing and molecular motion in phospholipid bilayers formed from unsaturated lecitins. Synthesis and properties of sixteen positional isomers of 1,2-dioctadecenoyl-sn-glycero-3-phosphorylcholine. *J Biol Chem* **250:** 4470-4476.

68 D. Marsh (1990) CRC Handbook of Lipid Bilayers, CRC Press, Boca Raton, Ann Arbor, Boston.

69 L. Finegold, M.A. Singer (1991) Cholesterol-multilipid interactions in bilayers. *Chem Phys Lipids* **58:** 169-173.

70 H. Hauser (1991) Effect of inorganic cations on phase transitions. *Chem Phys Lipids* **57:** 309-325.

71 J.R. Trudell, D.G. Payan, J.H. Chin, E.N. Cohen (1974) Pressure-induced elevation of phase transition temperature in dipalmitoylphosphatidylcholine bilayers. An electron spin resonance measurement of the enthalpy of phase transition. *Biochim Biophys Acta* **373:** 436-443.

72 P.R. Cullis, M.J. Hope, M.B. Bally, T.D. Madden, L.D. Mayer (1983) in Liposomes (Ostro, M.J., ed.), pp. 39-72, Marcel Dekker, Inc., New York, Basel.

73 G. Storm, J.A. Crommelin (1998) Liposomes: quo vadis? *PSTT* **1:** 19-31.

74 A.S. Janoff (1992) Lipids, liposomes, and rational drug design. *Lab Invest* **66:** 655-658.

75 C. Ouyang, E. Choice, J. Holland, M. Meloche, T.D. Madden (1995) Liposomal cyclosporine. Characterization of drug incorporation and interbilayer exchange. *Transplantation* **60:** 999-1006.

76 E. Choice, D. Masin, M.B. Bally, M. Meloche, T.D. Madden (1995) Liposomal cyclosporine. Comparison of drug and lipid carrier pharmacokinetics and biodistribution. *Transplantation* **60:** 1006-1011.

77 D.D. Lasic. (1993) Liposomes: From Physics to Applications, Elsevier, Amsterdam, London, New York, Tokyo.

78 L.D. Mayer, T.D. Madden, M.B. Bally, P.R. Cullis (1993) in Liposome Technology (Gregoriadis, G., ed.), Vol. II, 2nd ed., pp. 27-44, CRC Press, Boca Raton, Ann Arbor, London, Tokyo.

79 G. Haran, R. Cohen, L.K. Bar, Y. Barenholz (1993) Transmembrane ammonium sulfate gradients in liposomes produce efficient and stable entrapment of amphipathic weak bases. *Biochim Biophys Acta* **1151:** 201-215.

80 L.D. Mayer, M.B. Bally, P.R. Cullis (1986) Uptake of adriamycin into large unilamellar vesicles in response to a pH gradient. *Biochim Biophys Acta* **857:** 123-126.

81 X. Li, D.J. Hirsh, D. Cabral-Lilly, A. Zirkel, S.M. Gruner, A.S. Janoff, W.R. Perkins (1998) Doxorubicin physical state in solution and inside liposomes loaded via a pH gradient. *Biochim Biophys Acta* **1415:** 23-40.

82 H.J. Lim, D. Masin, T.D. Madden, M.B. Bally (1997) Influence of drug release characteristics on the therapeutic activity of liposomal mitoxantrone. *J Pharmacol Exp Ther* **281:** 566-573.

83 G. Gregoriadis, C. Davis (1979) Stability of liposomes *in vivo* and *in vitro* is promoted by their cholesterol content and the presence of blood cells. *Biochm Biophys Res Com* **89:** 1287-1293.

84 K. Edwards, M. Johnson, G. Karlsson, M. Silvander (1997) Effect of polyethyleneglycol-phospholipids on aggregate structure in preparations of small unilamellar liposomes. *Biophys J* **73:** 258-266.

85 M. Silvander, M. Johnsson, K. Edwards (1998) Effects of PEG-lipids on permeability of phosphatidylcholine/cholesterol liposomes in buffer and in human serum. *Chem Phys Lipids* **97:** 15-26.

86 A.R. Nicholas, M.J. Scott, N.I. Kennedy, M.N. Jones (2000) Effect of grafted polyethylene glycol (PEG) on the size, encapsulation efficiency and permeability of vesicles. *Biochim Biophys Acta* **1463:** 167-178.

87 J.H. Senior (1987) Fate and behavior of liposomes in vivo: a review of controlling factors. *Crit Rev Ther Drug Carrier Syst* **3:** 123-193.

88 G. Scherphof, F. Roerdink, M. Waite, J. Parks (1978) Disintegration of phosphatidylcholine liposomes in plasma as a result of interaction with high-density lipoproteins. *Biochim Biophys Acta* **542:** 296-307.

89 G. Scherphof, B. Van Leeuwen, J. Wilschut, J. Damen (1983) Exchange of phosphatidylcholine between small unilamellar liposomes and human plasma high-density lipoprotein involves exclusively the phospholipid in the outer monolayer of the liposomal membrane. *Biochim Biophys Acta* **732:** 595-599.

90 C. Kirby, J. Clarke, G. Gregoriadis (1980) Cholesterol content of small unilamellar liposomes controls phospholipid loss to high density lipoproteins in the presence of serum. *FEBS Lett* **111:** 324-328.

91 C. Kirby, G. Gregoriadis (1980) The effect of the cholesterol content of small unilamellar liposomes on the fate of their lipid components in vitro. *Life Sci* **27:** 2223-2230.

92 S.C. Semple, A. Chonn, P.R. Cullis (1996) Influence of cholesterol on the association of plasma proteins with liposomes. *Biochemistry* **35:** 2521-2525.

93 R.D. Klausner, R. Blumenthal, T. Innerarity, J.N. Weinstein (1985) The interaction of apolipoprotein A-I with small unilamellar vesicles of L-alpha-dipalmitoylphosphatidylcholine. *J Biol Chem* **260:** 13719-13727.

94 T.M. Allen, P. Williamson, R.A. Schlegel (1988) Phosphatidylserine as a determinant of reticuloendothelial recognition of liposome models of the erythrocyte surface. *Proc Natl Acad Sci U S A* **85:** 8067-8071.

95 A.J. Schroit, J. Madsen, R. Nayar (1986) Liposome-cell interactions: in vitro discrimination of uptake mechanism and in vivo targeting strategies to mononuclear phagocytes. *Chem Phys Lipids* **40:** 373-393.

96 A. Chonn, S.C. Semple, P.R. Cullis (1992) Association of blood proteins with large unilamellar liposomes in vivo. Relation to circulation lifetimes. *J Biol Chem* **267:** 18759-18765.

97 D.R. Absolom (1986) Opsonins and dysopsonins: an overview. *Methods Enzymol* **132:** 281-318.

98 G. Poste, C. Bucana, A. Raz, P. Bugelski, R. Kirsh, I.J. Fidler (1982) Analysis of the fate of systematically administered liposomes and implications for their use in drug delivery. *Cancer Res* **42:** 1412-1422.

99 J. Freise, W.H. Muller, C. Brolsch, F.W. Schmidt (1980) "*In vivo*" distribution of liposomes between parenchymal and non parenchymal cells in rat liver. *Biomedicine* **32:** 118-123.

100 G. Gregoriadis, B.E. Ryman (1972) Fate of protein-containing liposomes injected into rats. An approach to the treatment of storage diseases. *Eur J Biochem* **24:** 485-491.

101 B.M. Altura (1980) Reticuloendothelial cells and host defense. *Adv Microcirc* **9:** 252-294.

102 K.J. Hwang (1987) in Liposomes: From Biophysics to Therapeutics (Ostro, M.J., ed.), pp. 109-156, Marcel Dekker, Inc., New York and Basel.

103 C.D. Oja, S.C. Semple, A. Chonn, P.R. Cullis (1996) Influence of dose on liposome clearance: critical role of blood proteins. *Biochim Biophys Acta* **1281:** 31-37.

104 F.M. Muggia (1997) Clinical efficacy and prospects for use of pegylated liposomal doxorubicin in the treatment of ovarian and breast cancers. *Drugs* **54:** 22-29.

105 A. Gabizon, F. Martin (1997) Polyethylene glycol-coated (pegylated) liposomal doxorubicin: Rationale for use in solid tumors. *Drugs* **54:** 15-21.

106 T.M. Allen, C. Hansen (1991) Pharmacokinetics of stealth versus conventional liposomes: effect of dose. *Biochim Biophys Acta* **1068:** 133-141.

107 T.M. Allen, C. Hansen, J. Rutledge (1989) Liposomes with prolonged circulation times: factors affecting uptake by reticuloendothelial and other tissues. *Biochim Biophys Acta* **981:** 27-35.

108 D. Needham, D.V. Zhelev, T.J. McIntosh (1999) in Liposomes: Rational Design (Janoff A.S., ed.), pp. 13-62, Marcel Dekker, Inc., New York, Basel.

109 A.K. Kenworthy, K. Hristova, D. Needham, T.J. McIntosh (1995) Range and magnitude of the steric pressure between bilayers containing phospholipids with covalently attached poly(ethylene glycol). *Biophys J* **68:** 1921-1936.

110 D.D. Lasic, F.J. Martin, A. Gabizon, S.K. Huang, D. Papahadjopoulos (1991) Sterically stabilized liposomes: a hypothesis on the molecular origin of the extended circulation times. *Biochim Biophys Acta* **1070:** 187-192.

111 T.M. Allen (1994) Long-circulating (sterically stabilized) liposomes for targeted drug delivery. *Trends Pharmacol Sci* **15:** 215-220.

112 D. Papahadjopoulos, T.M. Allen, A. Gabizon, E. Mayhew, K. Mattahay, S.K. Huang, K.-D. Lee, M.C. Woodle, D.D. Lasic, C. Redemann, F.J. Martin (1991) Sterically stabilized liposomes: improvements in phamacokinetics and antitumor therapeutic efficacy. . *Proc Natl Acad Sci U S A* **88:** 11460-11464.

113 A. Gabizon, D. Papahadjopoulos, (1988) Liposome formulations with prolonged circulation time in blood and enhanced uptake by tumors. *Proc Natl Acad Sci U S A* **85:** 6949-6953.

114 C. Allen, N. Dos Santos, R. Gallagher, G.N. Chiu, Y. Shu, W.M. Li, S.A. Johnstone, A.S. Janoff, L.D. Mayer, M.S. Webb, M.B. Bally (2002) Controlling the physical behavior and biological performance of liposome formulations through use of surface grafted poly(ethylene glycol). *Biosci Rep* **22:** 225-250.

115 S.A. Johnstone, D. Masin, L. Mayer, M.B. Bally (2001) Surface-associated serum proteins inhibit the uptake of phosphatidylserine and poly(ethylene glycol) liposomes by mouse macrophages. *Biochim Biophys Acta* **1513:** 25-37.

116 A.G. Lee (1974) Clusters in lipid bilayers and the interpretation of thermal effects in biological membranes. *Biochemistry* **13:** 3699-3705.

117 G.E. Beltz, D.M. Lipkin (2000) A dislocation model for the directional anisotropy of grain boundary fracture. *Mater Res Soc Bull* **25:** 21-26.

118 O.G. Mouritsen, M.J. Zuckermann (1987) Model of interfacial melting. *Phys Rev Lett* **58:** 389-392.

119 O.G. Mouritsen (1991) Theroretical models of phospholipid phase transitions. *Chem Phys Lipids* **57:** 179-194.

120 O.G. Mouritsen, K. Jorgensen (1997) Small-scale lipid-membrane structure: simulation versus experiment. *Curr Opin Struct Biol* **7:** 518-527.

121 D. Papahadjopoulos, K. Jacobson, S. Nir, T. Isac (1973) Phase transitions in phospholipid vesicles. Fluorescence polarization and permeability measurements concerning the effect of temperature and cholesterol. *Biochim Biophys Acta* **311:** 330-348.

122 D. Marsh, A. Watts, P.F. Knowles (1976) Evidence for phase boundary lipid. Permeability of Tempo-choline into dimyristoylphosphatidylcholine vesicles at the phase transition. *Biochemistry* **15:** 3570-3578.

123 C.S. Smith (1964) Structure, substructure, and superstructure. *Rev Mod Phys* **36:** 524-530.

124 M. Grit, W.J. Underberg, D.J. Crommelin (1993) Hydrolysis of saturated soybean phosphatidylcholine in aqueous liposome dispersions. *J Pharm Sci* **82:** 362-366.

125 J.A. Zhang, J. Pawelchak (2000) Effect of pH, ionic strength and oxygen burden on the chemical stability of EPC/cholesterol liposomes under accelerated conditions. Part 1: Lipid hydrolysis. *Eur J Pharm Biopharm* **50:** 357-364.

126 M. Grit, D.J.A. Crommelin (1993) Chemical stability of liposomes: implications for their physical stability. *Chem Phys Lipids* **64:** 3-18.

127 A.G. Lee (1977) Lipid phase transitions and phase diagrams II. Mixtures involving lipids. *Biochim Biophys Acta* **472:** 285-345.

128 E. Sackmann, T. Feder (1995) Budding, fission and domain formation in mixed lipid vesicles induced by lateral phase separation and macromolecular condensation. *Mol Membr Biol* **12:** 21-28.

129 J. Korlach, P. Schwille, W.W. Webb, G.W. Feigenson (1999) Characterization of lipid bilayer phases by confocal microscopy and fluorescence correlation spectroscopy. . *Proc Natl Acad Sci U S A* **96:** 8461-8466.

130 L. Cruzeiro-Hansson, J.H. Ipsen, O.G. Mouritsen (1989) Intrinsic molecules in lipid membranes change the lipid-domain interfacial area: cholesterol at domain interfaces. *Biochim Biophys Acta* **979:** 166-176.

131 L.A. Bagatolli, E. Gratton (2000) A correlation between lipid domain shape and binary phospholipid mixture composition in free standing bilayers: a two-photon fluorescence microscopy study. *Biophys J* **79:** 434-447.

132 L.A. Bagatolli, E. Gratton (2000) Two-photon fluorescence microscopy of coexisting lipid domains in giant unilamellar vesicles of binary phospholipid mixtures. *Biophys J* **78:** 290-305.

133 T. Kaasgaard, O.G. Mouritsen, K. Jorgensen (2002) Lipid domain formation and ligand-receptor distribution in lipid bilayer membranes investigated by atomic force microscopy. *FEBS Lett* **515:** 29-34.

134 P.F. Almeida, W.L. Vaz, T.E. Thompson (1992) Lateral diffusion and percolation in two-phase, two-component lipid bilayers. Topology of the solid-phase domains in-plane and across the lipid bilayer. *Biochemistry* **31:** 7198-7210.

135 K. Jørgensen, A. Klinger, R.L. Biltonen (2000) Nonequilibrium lipid domain growth in the gel-fluid two-phase region of a $DC_{16}PC$-$DC_{22}PC$ lipid mixture investigated by Monte Carlo computer simulation, FT-IR, and fluorescence spectroscopy. *J Phys Chem B* **104:** 11762-11773.

136 W.H. Moolenaar (2000) in Lysophospholipids and Ricanoids in Biology and Pathophysiology (Goetzl, E.J. and Lynch, K.R., eds.), pp.1-10, Vol. 905, Annals of the York Academy of Sciences, New York.

137 J. Lutz, A.J. Augustin, L.J. Jäger, D. Bachmann, M. Brandl (1995) Acute toxicity and depression of phagocytosis in vivo by liposomes: Influence of lysophosphatidylcholine. *Life Sci* **56:** 99-106.

138 D.V. Zhelev (1998) Material property characteristics for lipid bilayers containing lysolipid. *Biophys J* **75:** 321-330.

139 D.V. Zhelev (1996) Exchange of Monooleoylphosphatidylcholine with single egg phosphatidylcholine vesicle membranes. *Biophys J* **71:** 257-273.

140 D. Needham, D.V. Zhelev (1995) Lysolipid exchange with lipid vesicle membranes. *Ann Biomed Eng* **23:** 287-298.

141 Y. Lee, S.I. Chan (1977) Effect of lysolecithin on the structure and permeability of lecithin bilayer vesicles. *Biochemistry* **16:** 1303-1309.

142 M. Grit, D.J. Crommelin, (1992) The effect of aging on the physical stability of liposome dispersions. *Chem Phys Lipids* **62:** 113-122.

143 M. Laradji, O.G. Mouritsen, S. Toxvaerd, M.J. Zuckermann (1994) Molecular dynamics simulations of phase separation in the presence of surfactants. *Phys Rev E Stat Phys Plasmas Fluids Relat Interdiscip Topics* **50:** 1243-1252.

144 L.M.S. Loura, A. Fedorov, M. Prieto (1996) Resonance energy transfer in a model system of membranes: application to gel and liquid crystalline phases. *Biophys J* **71:** 1823-1836.

145 K. Inoue, T. Kitagawa (1974) Effect of exogenous lysolecithin on liposomal membranes. Its relation to membrane fluidity. *Biochim Biophys Acta* **363:** 361-372.

146 T. Kitagawa, K. Inoue, S. Nojima (1976) Properties of liposomal membranes containing lysolecithin. *J Biochem* **79:** 1123-1133.

147 H.J. Lim, D. Masin, N.L. McIntosh T.D. Madden, M.B. Bally, (2000) Role of drug release and liposome-mediated drug delivery in governing the therapeutic activity of liposomal mitoxantrone used to treat human A431 and LS180 solid tumors. *J Pharmacol Exp Ther* **292:** 337-345.

148 L.D. Mayer (1998) Future developments in the selectivity of anticancer agents: Drug delivery and molecular target strategies. *Cancer Metastasis Rev* **17:** 211-218.

149 J. Connor, L. Huang (1986) pH-sensitive liposomes as an efficient and target-specific carrier for antitumor drugs. *Cancer Res* **46:** 3431-3435.

150 G. Klein (1968) Tumor-specific transplantation antigens: G. H. A. Clowes memorial lecture. *Cancer Res* **28:** 625-635.

151 M.W. Dewhirst, E. Jones, T. Samulski, Z. Vujaskovic, C. Li, L. Prosnitz. (1999) in Cancer Medicine, Vol. 6, pp. 623-636.

152 S.B. Field, N.M. Bleehen (1979) Hyperthermia in the treatment of cancer. *Cancer Treat Rev* **6:** 63-94.

153 R.P. Hill, J.W. Hunt (1987) in The Basic Science of Oncology (Tannock, I.F. and Hill, R.P., eds.), pp. 337-357, Pergamon Press, New York, Oxford, Beijing, Frankfurt, Sao Paulo, Sydney, Tokyo, Toronto.

154 C.W. Song, M.S. Kang, J.G. Rhee, S.H. Levitt (1980) Effect of hyperthermia on vascular function in normal and neoplastic tissues. *Ann N Y Acad Sci* **335:** 35-47.

155 C.W. Song (1984) Effect of local hyperthermia on blood flow and microenvironment: a review. *Cancer Res* **44:** 4721s-4730s.

156 O. Meyer, D. Kirpotin, K. Hong, B. Sternberg, J.W. Park, M.C. Woodle, D. Papahadjopoulos (1998) Cationic liposomes coated with polyethylene glycol as carriers for oligonucleotides. *J Biol Chem* **273:** 15621-15627.

157 J. Landry, P. Chretien, D. Bernier, L.M. Nicole, N. Marceau, R.M. Tanguay (1982) Thermotolerance and heat shock proteins induced by hyperthermia in rat liver cells. *Int J Radiat Oncol Biol Phys* **8:** 59-62.

158 M.P. Law (1982) Prospects for hyperthermia in cancer therapy. *Radiography* **48:** 209-219.

159 J.R. Bertino, C.D. Kowal, M.E. Klein, J. Dombrowski, E. Mini (1984) Perfusion and Systemic Hyperthermia-Chemotherapy. *Front Radiat Ther Oncol* **18:** 162-170.

160 R.A. Vertrees, A. Bidani, D.J. Deyo, W. Tao, J.B. Zwischenberger (2000) Venovenous perfusion-induced systemic hyperthermia: hemodynamics, blood flow, and thermal gradients. *Ann Thorac Surg* **70:** 644-652.

161 M.W. Dewhirst, D.A. Sim (1984) The utility of thermal dose as a predictor of tumor and normal tissue responses to combined radiation and hyperthermia. *Cancer Res* **44:** 4772s-4780s.

162 S. Jacobsen, P.R. Stauffer, D.G. Neuman (2000) Dual-mode antenna design for microwave heating and noninvasive thermometry of superficial tissue disease. *IEEE Trans Biomed Eng* **47:** 1500-1509.

163 P.R. Stauffer, F. Rossetto, M. Leoncini, G.B. Gentilli (1998) Radiation patterns of dual concentric conductor microstrip antennas for superficial hyperthermia. *IEEE Trans Biomed Eng* **45:** 605-613.

164 P.S. Swift, P.R. Stauffer, P.D. Fries, S. Kaleta-Michaels, T. Murray, P.K. Sneed, T.L. Phillips, D.H. Char (1990) Microwave hyperthermia for choroidal melanoma in rabbits. *Invest Ophthalmol Vis Sci* **31:** 1754-1760.

165 V. Sathiaseelan, L. Leybovich, B. Emami, P. Stauffer, W. Straube (1991) Characteristics of improved microwave interstitial antennas for local hyperthermia. *Int J Radiat Oncol Biol Phys* **20:** 531-539.

166 C.J. Diederich, W.H. Nau, E.C. Burdette, I.S. Bustany, D.L. Deardorff, P.R. Stauffer (2000) Combination of transurethral and interstitial ultrasound applicators for high-temperature prostate thermal therapy. *Int J Hyperthermia* **16:** 385-403.

167 C.J. Diederich, P.R. Stauffer, D. Bozzo (1994) An improved bolus configuration for commercial multielement ultrasound and microwave hyperthermia systems. *Med Phys* **21:** 1401-1403.

168 M.H. Gaber, N.Z. Wu, K. Hong, S.K. Huang, M.W. Dewhirst, D. Papahadjopoulos (1996) Thermosensitive liposomes: extravasion and release of contents in tumor microvasculature networks. *Int J Rad Oncol Biol Phys* **36:** 1177-1187.

169 S. Unezaki, K. Maruyama, N. Takahashi, M. Koyama, T. Yuda, A. Suginaka, M. Iwatsuru (1994) Enhanced delivery and antitumor activity of doxorubicin using long-circulating thermosensitive liposomes containing amphipathic polyethylene glycol in combination with local hyperthermia. *Pharm Res* **11:** 1180-1185.

170 Y. Zou, M. Yamagishi, I. Horikoshi, M. Ueno, X. Gu, R. Perez-Soler (1993) Enhanced therapeutic effect against liver W256 carcinoma with temperature-sensitive liposomal adriamycin administered into the hepatic artery. *Cancer Res* **53:** 3046-3051.

171 J.N. Weinstein, R.L. Magin, M.B. Yatavin, D.S. Zaharko (1979) Liposomes and local hyperthermia: selective delivery of methotrexate to heated tumors. *Science* **204:** 188-191.

172 K. Iga, N. Hamaguchi, Y. Igari, Y. Ogawa, H. Toguchi, T. Shimamoto (1989) Heat-specific drug release of large unilamellar vesicle as hyperthermia-mediated targeting delivery. *Int J Pharmaceut* **57:** 1989.

173 J.E.F. Reynolds (1989) Martindale The Extra Phaarmacopoeia, 29th ed., The Pharmaceutical Press, London.

174 H.G. Keizer, H.M. Pinedo, G.J. Schuurhuis, H. Joenje (1990) Doxorubicin (Adriamycin): A critical review of free radical-dependent mechanisms of cytotoxicity. *Pharm Ther* **47:** 219-231.

175 J. Bouma, J.H. Beijnen, A. Bult, W.J.M. Underberg (1986) Anthracycline antitumor agents. *Pharm Weekbl Sci* **8:** 109-133.

176 Y. Barenholz, S. Amselem, D. Goren, R. Cohen, D. Gelvan, A. Samuni, E.B. Golden, A. Gabizon (1993) Stability of liposomal doxorubicin formulations: problems and prospects. *Med Res Rev* **13:** 449-491.

177 X. Li, D. Cabral-Lilly, A.S. Janoff, W.R. Perkins (2000) Complexation of internalized doxorubicin into fibre bundles affects its release rate from liposomes. *J Liposome Res* **10:** 15-27.

178 C.P. Association (1995) Compendium of pharmaceuticals and specialities, Vol. 13, CK Productions, Toronto.

179 R.H. Blum, S.K. Carter (1974) Adriamycin. A new anticancer drug with significant clinical activity. *Ann Intern Med* **80:** 249-259.

180 A. Andersen, H. Holte, L. Slordal (1999) Pharmacokinetics and metabolism of doxorubicin after short-term infusions in lymphoma patients. *Cancer Chemother Pharmacol* **44:** 422-426.

181 C.K. van Kalken, H.M. Pinedo, G. Giaccone (1991) Multidrug resistance from the clinical point of view. *Eur J Cancer* **27:** 1481-1486.

182 G. Bradley, P.F. Juranka, V. Ling (1988) Mechanism of multidrug resistance. *Biochim Biophys Acta* **948:** 87-128.

183 J. Mattern, M. Volm (1993) Multiple pathway drug resistance. *Int J Oncol* **2:** 557-561.

184 A.L. Harris, D. Hochhauser (1992) Mechanisms of multidrug resistance in cancer treatment. *Acta Oncol* **31:** 205-213.

185 J.A. Kellen (1995) Alternative Mechanisms of Multidrug Resistance in Cancer, Birkhäuser, Boston, Basel, Berlin.

186 A.T. Fojo, K. Ueda, D.J. Slamon, D.G. Poplack, M.M. Gottesman, I. Pastan (1987) Expression of a multidrug-resistance gene in human tumors and tissues. . *Proc Natl Acad Sci U S A* **84:** 265-269.

187 H.S. Chan, G. DeBoer, P.S. Thorner, G. Haddad, B.L. Gallie, V. Ling (1994) Multidrug resistance. Clinical opportunities in diagnosis and circumvention. *Hematol Oncol Clin North Am* **8:** 383-410.

188 S.P. Cole, G. Bhardwaj, J.H. Gerlach, J.E. Mackie, C.E. Grant, K.C. Almquist, A.J. Stewart, E.U. Kurz, A.M. Duncan, R.G. Deeley (1992) Overexpression of a transporter gene in a multidrug-resistant human lung cancer cell line. *Science* **258:** 1650-1654.

189 K.J. Laidler, J.H. Meiser (1982) Physical Chemistry, The Behjamin/Cummings Publishing Company Inc., Menlo Park, Reading, London, Amsterdam, Don Mills, Sydney.

190 I. Johnson, D (1996) in Handbook of Fluorescence Probes and Research Chemicals (Spence, M.T.Z., ed.), 6 ed., pp. 1-4, Molecular Probes, Inc., Eugene, OR.

191 J.R. Bellare, H.T. Davis, L.E. Scriven, Y. Talmon (1988) Controlled environment vitrification system: An improved sample preparation technique. *J Elec Micros Tech* **10:** 87-111.

192 J. Dubochet, M. Adrian, J.-J. Chang, J.-C. Homo, J. Lepault, A.W. McDowall, P. Schultz (1988) Cryo-electron microscopy of vitrified specimens. *Quart Rev Biophys* **21:** 129-228.

193 M. Almgren, K. Edwards, G. Karlsson (2000) Cryo transmission electron microscopy of liposomes and related structures. *Colloids Surf B Biointerfaces* **174:** 3-21.

194 M.B. Bally, L.D. Mayer, M.J. Hope, R. Nayar (1993) in Liposome Technology (Gregoriadis, G., ed.), Vol. III, 2nd ed., pp. 27-41, CRC Press, Boca Raton, Ann Arbor, London, Tokyo.

195 P.R. Harrigan, M.J. Hope, T.E. Redelmeier, P.R. Cullis (1992) Determination of transmembrane pH gradients and membrane potentials in liposomes. *Biophys J* **63:** 1336-1345.

196 P.R. Cullis, M.B. Bally, T.D. Madden, L.D. Mayer, M.J. Hope (1991) pH gradients and membrane transport in liposomal systems. *Trends Biotechnol* **9:** 268-272.

197 L.D. Mayer, P.R. Cullis, M.B. Bally (1994) The use of transmembrane pH gradient-driven drug encapsulation in the pharmacodynamic evaluation of liposomal doxorubicin. *J Liposome Res* **4:** 529-553.

198 M.B. Lande, J.M. Donovan, M.L. Zeidel (1995) The relationship between membrane fluidity and permeabilities to water, solutes, ammonia, and protons. *J Gen Physiol* **106:** 67-84.

199 H. Schieren, S. Rudolph, M. Finkelstein, P. Coleman, G. Weissmann (1978) Comparison of large unilamellar vesicles prepared by a petroleum ether vaporization method with multilamellar vesicles: ESR, diffusion and entrapment analyses. *Biochim Biophys Acta* **542:** 137-153.

200 Y. Barenholz, T. Cohen, E. Haas, M. Ottolenghi (1996) Lateral organization of pyrene-labeled lipids in bilayers as determined from the deviation from equilibrium between pyrene monomers and excimers. *J Biol Chem* **271:** 3085-3090.

201 P.K. Vinson (1987) in Proceedings of the 45th Annual Meeting of the Electron Microscopy Society of America (Bailey, G.W., ed.), pp. 644-645, San Francisco Press, San Francisco.

202 D. Plumb, C (2002) Veterinary Drug Handbook, 4 ed., Iowa State Press, Ames, IO.

203 T.J.J. Zethof, J.A.M. van der Heyden, J.T.B.M. Tolboom, B. Olivier (1994) Stress-induced hyperthermia in mice: a methodological study. *Physiol Behav* **55:** 109-115.

204 T.J. Zethof, J.A. Van der Heyden, J.T. Tolboom, B. Olivier (1995) Stress-induced hyperthermia as a putative anxiety model. *Eur J Pharmacol* **294:** 125-135.

205 J.H. Ferguson, G.E. Folk, Jr. (1970) The critical thermal minimum of small rodents in hypothermia. *Cryobiology* **7:** 44-46.

206 F. Leonessa, D. Green, T. Licht, A. Wright, K. Wingate-Legette, J. Lippman, M.M. Gottesman, R. Clarke (1996) MDA435/LCC6 and MDA435/LCC6MDR1: ascites models of human breast cancer. *Br J Cancer* **73:** 154-161.

207 G.J. Bresseleers, H.L. Goderis, P.P. Tobback (1984) Measurement of the glucose permeation rate across phospholipid bilayers using small unilamellar vesicles. Effect of membrane composition and temperature. *Biochim Biophys Acta* **772:** 374-382.

208 J.A.M. van der Heyden, T.J.J. Zethof, B. Olivier (1997) Stress-induced hyperthermia in singly housed mice. *Physiol Behav* **62:** 463-470.

209 G. Kong, G. Anyarambhatla, W.P. Petros, R.D. Braun, O.M. Colvin, D. Needham, M.W. Dewhirst (2000) Efficacy of liposomes and hyperthermia in a human tumor xenograft model: importance of triggered drug release. *Cancer Res* **60:** 6950-6957.

210 L.D. Mayer, L.C.L. Tai, D.S.C. Ko, D. Masin, R.S. Ginsberg, P.R. Cullis, M.B. Bally (1990) Characterization of liposomal systems containing doxorubicin entrapped in response to pH gradients. *Biochim Biophys Acta* **1025:** 143-151.

211 M. Andersson, L. Hammarström, K. Edwards (1995) Effect of bilayer phase transitions on vesicle structure and its influence on the kinetics of virologen reduction. *J Phys Chem* **99:** 14531-14538.

212 R. Lawaczeck, M. Kainosho, S.I. Chan (1976) The formation and annealing of structural defects in lipid bilayer vesicles. *Biochim Biophys Acta* **443:** 313-330.

213 S. Pedersen, K. Jørgensen, T.R. Bækmark, O.G. Mouritsen (1996) Indirect evidence for lipid-domain formation in the transition region of phospholipid bilayers by two-probe fluorescence energy transfer. *Biophys J* **71:** 554-560.

214 W.R. Burack, A.R.G. Dibble, M.M. Allietta, R.L. Biltonen (1997) Changes in vesicle morphology induced by lateral phase separation modulate phospholipase A_2 activity. *Biochemistry* **36:** 10551-10557.

215 W.R. Burack, Q. Yuan, R.L. Biltonen (1993) Role of lateral phase separation in the modulation of phospholipase A2 activity. *Biochemistry* **32:** 583-589.

216 W.R. Burack, R.L. Biltonen (1994) Lipid bilayer heterogeneities and modulation of phospholipase A2 activity. *Chem Phys Lipids* **73:** 209-222.

217 B.R. Lentz, Y. Barenholz, T.E. Thompson (1976) Fluorescence depolarization studies of phase transitions and fluidity in phospholipid bilayers. Two-component phosphatidylcholine liposomes. *Biochemistry* **15:** 4529-4537.

218 D. Rüppel, E. Sackmann, (1983) On defects in different phases of two-dimensional lipid bilayers. *J Phys* **44:** 1025-1034.

219 M. Silvander, K. Edwards (1996) A method to detect leakage of DNA intercalators through liposome membranes. *Anal Biochem* **242:** 40-44.

220 P. Fromherz, C. Röcker, D. Rüppel (1986) From discoid micelles to spherical vesicles. The concept of edge activity. *Faraday Discuss Chem Soc* **81:** 39-48.

221 P.G. deGennes (1987) Polymers at an interface: a simplified view. *Adv Coll Inter Sci* **27:** 189-209.

222 K. Hristova, D. Needham (1995) Phase behavior of a lipid/polymer-lipid mixture in aqueous medium. *Macromolecules* **28:** 991-1002.

223 K. Hristova, A. Kenworthy, T.J. McIntosh (1995) Effect of bilayer composition on the phase behavior of liposomal suspensions containing poly(ethylene glycol)-lipids. *Macromolecules* **28:** 7693-7699.

224 K. Edwards, M. Almgren (1990) Kinetics of surfactant-induced leakage and growth of unilamellar vesicles. *Prog Col Poly Sci* **82:** 190-197.

225 K. Edwards, M. Almgren (1992) Surfactant-induced leakage and structural change of lecithin vesicles: Effect of surfactant headgroup size. *Langmuir* **8:** 824-832.

226 C.L. Weakliem, G. Fujii, J.-E. Chang, A. Ben-Shaul, W.M. Gelbart (1995) Effect of tension on pore formation in drug-containing vesicles. *J Phys Chem* **99:** 7694-7697.

227 R.E. Durand (1990) Slow penetration of anthracyclines into spheroids and tumors: atherapeutic advantage? *Cancer Chemother Pharmacol* **26:** 198-204.

228 M.H. Gaber, K. Hong, S.K. Huang, D. Papahadjopoulos (1995) Thermosensitive sterically stabilized liposomes: formulation and *in vitro* studies on mechanism of doxorubicin release by bovine serum and human plasma. *Pharm Res* **12:** 1407-1416.

229 R. Krishna, M. St-Louis, L.D. Mayer (2000) Increased intracellular drug accumulation and complete chemosensitization achieved in multidrug-resistant solid tumors by co- administering valspodar (PSC 833) with sterically stabilized liposomal doxorubicin. *Int J Cancer* **85:** 131-141.